

Fall 2013

Development Of A Field-Portable Miniature Mass Spectrometer Designed For In-Situ Analysis And Ion Trap Miniaturization

Paul Isaac Hendricks
Purdue University

Follow this and additional works at: https://docs.lib.purdue.edu/open_access_dissertations



Part of the [Analytical Chemistry Commons](#)

Recommended Citation

Hendricks, Paul Isaac, "Development Of A Field-Portable Miniature Mass Spectrometer Designed For In-Situ Analysis And Ion Trap Miniaturization" (2013). *Open Access Dissertations*. 150.
https://docs.lib.purdue.edu/open_access_dissertations/150

PURDUE UNIVERSITY
GRADUATE SCHOOL
Thesis/Dissertation Acceptance

This is to certify that the thesis/dissertation prepared

By Paul Isaac Hendricks

Entitled **DEVELOPMENT OF A FIELD-PORTABLE MINIATURE MASS SPECTROMETER
DESIGNED FOR IN-SITU ANALYSIS AND ION TRAP MINIATURIZATION**

For the degree of Doctor of Philosophy

Is approved by the final examining committee:

R. Graham Cooks

Chair

Peter T. Kissinger

John P. Denton

Timothy Zwier

To the best of my knowledge and as understood by the student in the *Research Integrity and Copyright Disclaimer* (Graduate School Form 20), this thesis/dissertation adheres to the provisions of Purdue University's "Policy on Integrity in Research" and the use of copyrighted material.

Approved by Major Professor(s): R. Graham Cooks

Approved by: R. E. Wild

Head of the Graduate Program

9/30/2013

Date

DEVELOPMENT OF A FIELD-PORTABLE MINIATURE MASS SPECTROMETER
DESIGNED FOR *IN-SITU* ANALYSIS AND ION TRAP MINIATURIZATION

A Dissertation

Submitted to the Faculty

of

Purdue University

by

Paul Isaac Hendricks

In Partial Fulfillment of the

Requirements for the Degree

of

Doctor of Philosophy

December 2013

Purdue University

West Lafayette, Indiana

To Krista G. Hendricks, my best friend and wife, there could have been no better partner
for this incredible experience.

ACKNOWLEDGEMENTS

If, at the beginning of my thesis work, somebody were to tell me how much I would need to rely on others in order to finish this journey I would not have believed them. I use the phrase ‘rely on others’ generally as there are many challenges associated with the pursuit of a Ph.D. Mentorship and guidance attributed to the research and academic components of the program are obviously large and important, however, of equal magnitude are the emotional, psychological, and interpersonal components that constitute the remainder of the experience. I have found that it is inside these ‘soft’ experiences that we learn about ourselves (and others) and we learn these lessons in ways that are not predictable. I have been blessed; with very few exceptions those who have helped me along my path afforded generosity, kindness, and patience throughout my time as a graduate student – To them I am forever grateful and hope that when it is my time to act as a mentor, confidant, or friend I may do justice to the standard they have set.

First, I would like to thank Professor R. Graham Cooks for allowing me the opportunity to join Aston Labs. His work ethic and passion for science is fierce which serves as a reminder that one’s scientific development does not end upon obtaining a doctoral degree, but rather it begins. The quality and quantity of publications, awards, and scientific achievements that are held by Prof. Cooks do much to inspire personal as well as professional excellence. Moreover, the culture of the laboratory is one of

camaraderie where high character people work together to accomplish high quality science. I am grateful for the experience of having worked with Prof. Cooks and to have been able to walk in the footsteps of the students before me.

One of my most surprising conversations I have had was with Dr. Robert J. Noll on the topic of Big Ten football. While I am likely to forget, this conversation educated me to not pass judgment on how astute scientific professionals can be on the topic of collegiate athletics, or any other topic for that matter. I want to express my sincere appreciation for your open door policy and the willingness talk through an idea or problem and to lend your perspective. Your insights routinely offered a fresh perspective that challenged me scientifically to complete more meaningful experiments, to be diligent in data reduction, and to consider multiple points of view in the critique of my own work. Thank you again and best of luck in your endeavors as a Sycamore.

As a returning student myself I have some perspective on how challenging it is to return to academics. Jason, your decision to return to school and the fortitude you demonstrated by completing your bachelors degree made us all proud. Through the years you have been an outstanding resource for all of the chemistry students who had marginal understanding of electrical circuits and poor technique when it came to soldering, taping, shrink wrapping, etc. Thank you for your patience and willingness to educate us in methods of troubleshooting, operation of electronic test and measurement equipment, circuit layout, and parts selection. Hopefully we were able to teach you some chemistry and theory of ion trap operation.

A special thank you to Dr. Jake Shelley and Dr. Jon Dagleish for their camaraderie in the completion of the backpack instrument; this was by far the best team I

have been a part of and to this day I am surprised at how much we learned what we were able to accomplish. In the future there will undoubtedly be MS instrumentation, reminiscent of the backpack unit, which will surface in airports, border checkpoints, mobile crime labs, and the like. Many people will get credit for this advancement. We, however, will know that work completed on the backpack project was of the initial discoveries which clearly demonstrated that chemical analysis of this type was possible and was completed by a group of focused colleagues between the hours of 12 pm and 12 am, day-in and day-out, for the months of January, February, March, and April in 2012. Thank you again, it was a pleasure to work with the two of you.

The ability to communicate technical concepts and ideas is a major part of the doctorate program. When involved with research that is heavily weighted in instrumentation an additional dimension is added whereby this same communication needs to span multiple, different, disciplines. I would like to thank Frank Boudreau, Matthew Kirleis, and Matthew McNicholas for being excellent engineers and for all of their help on the Mini instrument projects.

I would like to thank many of the current lab members with whom I have the pleasure of working with, roomed with, and had the opportunity to talk science over a few cold beers. These interactions do much to stimulate scientific thinking in a relaxed environment and critique what new research is hot and what is not. In no particular order Josh Wiley, Kevin Kerian, Alan Jarmusch, Zane Baird, Ryan Espy, Chris Pulman, Ryan Bain, Shi Choong, Dr. Xin Li, Anyin Li, Mike Wleklinski, Xin Yan, Cederic D'Hue, and Dr. Christina Ferreira have all been influential and I am grateful for the time we have had together. I am optimistic that one day our paths will again cross.

I would like to thank the administrative assistants of the lab Brandy McMasters, Sarah Johnson, and Leann Herndon. You are awesome and do much to make sure we get our orders placed, get reimbursed, get paid, get our reports done (and sent), and get our publications submitted. Thank you for taking on this thankless job and having a positive attitude all the while- OK, most of the while.

I would like to thank all of the former students and post doctoral students who did their part to establish projects, resources, and the culture of the lab. The following list of names is necessarily incomplete as it could only contain of those with whom I have had overlap during my time at Aston Labs. Thank you to Dr. Ewa Sokol, Dr. Santosh Soparawalla, and Dr. Jonell Smith for introducing me to the Mini. Thank you to Dr. Richard Perry, Dr. Scott Smith, Dr. Marcela Nefliu and Dr. Demian Ifa for critical discussion of the research presented by visiting speakers. Thank you to Dr. Dahlia Campbell, Dr. Sheran Oradu, Dr. Abraham Bad-Tawiah, Dr. Guangtao Li, Dr. Jobin Cyriac, Dr. Chunping Wu, Dr. Fatkhulla Tadjimukhamedov, Dr. Jeffery Maas, Dr. Nathan Sanders, and Dr. Sameer Kothari for discussions on chemistry, instrumentation, and correct lab practices.

I would like to thank the collaborating group Biomedical Engineering group for their assistance in the instrumentation development projects. In particular I would like to thank Prof. Zheng Ouyang and Tsung-Chi Chen for their help on the backpack and Mini 12 instruments.

Last I would like to thank my wife, immediate family, and friends who allowed me to be selfish and pursue my interest in science. Though I will try, I will never be able to fully repay this debt. —Paul Isaac Hendricks 9/12/2013

TABLE OF CONTENTS

	Page
LIST OF TABLES	x
LIST OF FIGURES	xi
ABSTRACT.....	xxiii
PUBLICATIONS.....	xxv
CHAPTER 1. AUTONOMOUS <i>IN-SITU</i> ANALYSIS AND REAL-TIME CHEMICAL DETECTION: NEW MASS SPECTROMETER CONCEPTS, INSTRUMENTATION DEVELOPMENT, AND PERFORMANCE.....	1
1.1 Introduction	1
1.2 Integration of a Low Temperature Plasma Ion Source.....	5
1.2.1 Background	5
1.2.2 Co-axial LTP Source Development and Characterization.....	11
1.2.3 Thermographic and Schlieren Imaging of co-axLTP	14
1.2.3.1 Thermographic Imaging.....	14
1.2.3.2 Schlieren Imaging	15
1.2.4 Co-Axial LTP and Mini-S Instrument Performance.....	16
1.2.5 Power Consumption, RF Voltage, and Batteries	18
1.3 Instrument Hardware	21
1.3.1 Backpack Assembly.....	21
1.3.2 Hand-held Head Unit: Ion Introduction, Mass Analyzer, Detector, and Connections.....	21
1.3.3 Vacuum System	23
1.3.3.1 Vacuum Manifold Characterization.....	24
1.3.3.2 Vacuum Bellows Characterization	26
1.4 Instrument Control Electronics and Software	27
1.4.1 Printed Circuit Board Design and Fabrication.....	28
1.4.2 Instrument Control Software and Firmware	29
1.4.2.1 Firmware	29
1.4.2.2 RF Generation.....	29
1.4.2.3 Digital Feedback Control	31

	Page
1.4.2.4 Frequency Tuning	33
1.4.2.5 SWIFT Isolation.....	33
1.4.3 Software	34
1.4.3.1 Advanced User Interface.....	34
1.4.3.2 Novice User Interface	35
1.4.3.3 Automated Startup and Shutdown	35
1.4.3.4 Automated Mass Calibration	36
1.4.3.5 Data Acquisition and Results Reporting.....	36
1.5 Conclusion.....	38
1.6 References	40
 CHAPTER 2. APPLICATION OF MINIATURE MASS SPECTROMETERS FOR THE CHARACTERIZATION OF TISSUE TYPES VIA LIPID PROFILES..... 84	
2.1 Introduction	84
2.2 Lipid Analysis and Biological Tissue Characterization	85
2.3 Materials and Methods	88
2.4 Results and Discussion.....	88
2.5 Conclusion.....	91
2.6 References	92
 CHAPTER 3. PERFORMANCE OF A LOW VOLTAGE ION TRAP AND ALTERNATIVE MATERIALS FOR ION TRAP FABRICATION 100	
3.1 Introduction	100
3.2 1/3 Size Stainless Steel RIT	102
3.2.1 Materials and Method	102
3.2.2 Results and Discussion	105
3.2.2.1 MS Performance	105
3.2.2.2 Mass Selective Ion Ejection.....	107
3.2.2.3 Tandem MS Performance	107
3.3.1 PCB Fabrication.....	109
3.3.2 Characterization	110
3.3 1/2 Size PCB RIT	111
3.4 Conclusions	113
3.5 References	115
 CHAPTER 4. DEVELOPMENT OF A MINIATURE RECTILINEAR ION TRAP ARRAY WITH INDEPENDENTLY CONTROLLED CHANNELS 141	
4.1 Introduction	141
4.2 Materials and Methods	145

	Page
4.2.1	Fabrication: PCB-Stereolithography Apparatus Technology, Metallization, Channel Isolation.....
	145
4.2.2	Instrumentation: Control Electronics (LCQ), Pumping System, Operational Pressure, and Voltage Amplitudes
	147
4.3	Results and Discussion
	149
4.3.1	Channel Control
	149
4.3.1.1	Bias Tee & Operational Amplifiers
	149
4.3.2	Performance
	154
4.3.2.1	Mass Resolution and Mass Range
	154
4.3.2.2	Tandem MS- Single Channel Data
	156
4.3.2.3	Multi-channel Signal Response
	157
4.4	Conclusions
4.5	References
	162
APPENDIX CHAPTER 3.....	186
VITA.....	210

LIST OF TABLES

Table	Page
1.1 Power draw response for each of the main components of the Mini-S instrument; also reference figures 21 – 23.	45
1.2 Mini-S instrument systems located in the backpack.	46
1.3 Mini-S instrument systems located on the handheld head-unit.....	47
1.4 LED indicators on the handheld head-unit of the Mini-S instrument	48
3.1 Comparison of RIT mass analyzers constructed at different dimensions and with different materials	119
4.1 Internal distance between X and Y-electrode pairs in the ion trap array. Measurements were taken for all 8 ion traps in the X-Y plane at the top of the ion trap array; NanoForm™ 15120 was used as the SLA resin. Measurements taken in 2010 reflect the dimensions when the device was initially fabricated. ΔX and ΔY are the absolute values of the differences between the design dimension and the measured dimension. 2011 measurements were taken roughly 12 months after the device had been fabricated, under constant vacuum, and subjected to high amplitude RF. It is noteworthy to mention that the magnitude of the dimensional variation between the measurements taken in 2010 and 2011 differ by more than 100 μm for almost all traps and were completed the same microscope and measurement methods.	166

LIST OF FIGURES

Figure	Page
1.1 Top) Computer aided design (CAD) rendering of the Mini-S instrument and location of the instrument systems. Bottom A&B) Photograph of the fully assembled and operational Mini-S mass spectrometer outfitted with handheld head unit containing the mass analyzer and detection circuit, geometry-independent co-axLTP source, pressure transducer, and flexible vacuum bellows.....	49
1.2 Schematic image of the DBDI source developed by X. R. Zhang et al.; image adapted from reference 33.....	50
1.3 A) Schematic of the components that comprise the LTP source and operation of the LTP ion source. B) Image of the LTP discharge (inside the source) and plasma afterglow (outside the source). Note surface temperatures that are exposed to the plasma afterglow do not exceed 30 °C with low power inputs. Figures A and B were adapted from reference 25.....	50
1.4 Image adapted from reference 43; schematic of the components for a LTP array and a close-up image of LTP array interfaced to a DPAI on a miniaturized instrument.....	51
1.5 A) Photograph of the 7 probe LTP array with 6.5 mm outer electrodes. B & C) Photographs of the 7 probe LTP array installed on a Mini-S system. Note the bright emission which is indicative of high power-density plasma.	52
1.6 RF discharge on the inlet capillary used to ground the center conductor of the LTP probe.....	52
1.7 A) Full scan MS for TNT operated with a He discharge at 40 ml/min. B) Full scan MS for RDX operated using Air at 40 ml/min as the plasma gas. C) RDX ion signal (m/z 284) as a function of LTP power. The trend demonstrates improved desorption and ionization as the LTP power is increased, which is likely due to increased surface heating.....	53

Figure	Page
1.8 A & C) Miniaturized single probe co-axial LTP design and probe form factor. B) Plasma density produced by the miniaturized probe. NOTE: This design does NOT consist of an array of LTP probes.....	54
1.9 A) Thermographic images of surface temperatures generated from the single probe co-axLTP source; glass slide used as a surface stimulant. Input powers range from 14.0 to 2.6 W and surface to sample distance of 1 – 5mm. All images are on the same temperature scale of 30 to 80° C. B) maximum temperatures (From A) plotted as a function of source to sample distance of 1- 10 mm.....	55
1.10 Maximum temperature of the glass surface as a function of the source-to- sample distance for the two coaxial LTP configurations, array (blue) and non- array (black).	56
1.11 Diagram of the Schlieren imagining setup used to visualize the helium interaction with the sample and gas sampling of the DAPI valve. The co- axLTP source is placed inside the collimated light path where differences in refractive index between He and the ambient air can be visualized and captured with the high speed camera.	57
1.12 Schlieren image of helium-co-axLTP on aMini 12 development instrument. Operational conditions are 500 ml/min He flow rate and ~ 3W input power. Due to the buoyancy of helium in air, helium in the afterglow region which makes contact with the sample surface is dispersed at distances of 5mm.	58
1.13 Detection of drugs of abuse using the coax-LTP interfaced to the Mini-S. A) Tandem MS of cocaine ($2\mu\text{g}/\text{cm}^2$) detected directly from human skin. B) Tandem MS of 3,4-methylenedioxy-N-methylamphetamine (MDMA), also known as ecstasy, ($10\mu\text{g}/\text{cm}^2$) detected directly from the inside corners of a cardboard box. C) Tandem Ms of methamphetamine ($10\mu\text{g}/\text{cm}^2$) detected directly from an organic chemistry book cover.....	59
1.14 Detection of explosives from glass. All three compounds are detected at quantities of $1\mu\text{g}/\text{cm}^2$ or less. A) detection of trinitrotoluene note the appearance of a pattern formed by m/z 226[M-H] ⁻ and m/z 197 [M-NO] ⁻ . B) Cyclotrimethylenetrinitramine (RDX) is present as a nitrate attachment at m/z $284 [\text{M+NO}_3]^-$. C) Pentaerythritol tetranitrate (PETN) this spectrum shows the appearance of both the molecular radical m/z 316 M [•] and the nitrate adduct m/z $378 [\text{M+NO}_3]^-$ however, under these operating conditions the adduct formation is typically the dominate species.....	60

Figure	Page
1.15 Chemical warfare agent (CWA) simulants. A) Tandem MS of Mipafox ($1\mu\text{g}/\text{cm}^2$) detected from latex. B) Tandem MS of dimethyl methylphosphonate (DMMP) ($1\mu\text{g}/\text{cm}^2$) detected from cotton fibers. C) Full scan MS of a mixture of triethyl phosphate (TEP), tripropyl phosphate (TPP), tributyl phosphate (TBP) 1000ppm from cotton fibers.....	61
1.16 nESI mass spectrum of $[\text{PEG}+\text{Na}]^+$ acquired on the Mini-S instrument to demonstrate the maximum detectable mass-to-charge range of the instrument at 930 amu. The PEG sample was a mixture of PEG oligomers at μM concentrations. Also demonstrated is the mass resolution for the instrument which is $\sim 1 - 2$ amu at FWHM across the mass range.	62
1.17 A) DAPI valve assembled with the ion introduction and transfer capillaries and the conductive rubber tubing. See table 3 for details for assembly P/Ns. B) Black trace is the manifold pressure as measured from the analog output of the pressure transducer for three consecutive DAPI pulses. Blue highlights indicate the maximum pressure of the manifold (~ 100 mTorr) during introduction of ions and neutrals from atmosphere; red highlights indicate the pressure of the manifold during mass analysis ($\sim 10 - 1$ mTorr). Note that for each of the three scans the base pressure of the manifold does not return to the 10×10^{-6} Torr. This is due to the reduced efficiency of the turbo pump operating in helium (supplied from the LTP source and introduced to the manifold during the DAPI pulse) rather than air.....	63
1.18 Three scan average of $1\mu\text{g}/\text{cm}^2$ ketamine, m/z 237 $[\text{M}+\text{H}]^+$. Sample was ionized with LTP, 80 ml/min He, 500 V _{p-p} @ 30kHz (>1W). FWHM values ions are ~ 1 amu across the mass range, X+2 isotope is visible with 9.5% valley and 42% intensity relative to the monoisotopic mass. In addition to the $[\text{M}+\text{H}]^+$ species ketamine undergoes fragmentation to lose methyl amine [mass 31 Da] resulting in m/z 207 which also carries the chlorine creating a chemical footprint in the full MS scan.....	64
1.19 Three scan average of $1\mu\text{g}/\text{cm}^2$ TNT, m/z 226 $[\text{M}-\text{H}]^-$. Sample was ionized with LTP, Sample was ionized with LTP, 80 ml/min He, 500 V _{p-p} @ 30kHz (>1W). FWHM values are ~ 0.6 amu and the presence of m/z 226 and 227 are visible as the $[\text{M}-\text{H}]^-$ and molecular radical ions M^\cdot . 1 amu separation with a 58.5% valley at abundances of approximagine 1:1.....	65
1.20 Left) nESI full scan mass spectrum of cocaine m/z 304 $[\text{M}+\text{H}]^+$ at 100ppm. MS/MS of m/z 304 → 182 demonstrating the characteristic loss of benzoic acid. Right MS/MS/MS of m/z 304 → 182 → 150 and 122 demonstrating the consecutive loss of MeOH and CO.	66

Figure	Page
1.21 A) Initial start-up of the power-distribution board for 400 ms. An instantaneous current draw of ~6 A occurred when the instrument was first plugged in, consuming ~144 W during this short period of time. The power then settled to a baseline power draw of ~24 W. B) Current spike upon turning on the rough pump. C) Power draw upon enabling the turbo pump. Note the current draw during this period is similar to that upon initially plugging in the battery indicating that most of the initial power draw is due to the turbo. D) Power draw upon enabling the on-board LTP supply in negative mode; instantaneous power exceeds 150 W. Note: the current probe produces a 100 mV signal per Ampere consumed and the instrument has an input voltage of 24 V.....	67
1.22 Side-by-side plots of the power consumption, RF voltage amplitude, and operating pressures for the Mini-S (A) cumulative instrument power consumption, (B), main RF voltage amplitude, and (C) manifold pressure curves for three consecutive scans. Manifold pressure increase is due to actuation of the DAPI valve (15 – 25 ms) during ion injection into the mass analyzer. Ramp in RF voltage amplitude is due to mass-selective instability scan during mass analysis.....	68
1.23 A) Power profile during an analytical scan, maximum available RF is used to analyze ions up to m/z 930. B) Power profile during an analytical scan with RF amplitude limited to analyzing ions up to m/z 550. The source voltage is not on during this time. Although the difference in peak-power draw between the two scan functions was 58 W (156 W versus 98 W) the battery life for each mode of operation was approximately the same (~90 min).	69
1.24 Battery-life profile for lithium polymer (Li-Po) batteries obtained from Tenergy (Fremont, Ca, US) (725g, 5000 mAh, item no. 31428). Instrument could be operated for approximately 200 minutes, battery charge < 22 V.....	70
1.25 A & B) Images of the fully assembled backpack case and the weight of all the components; 20.77 lbs. The backpack is made of two components providing access to the electronics and vacuum system. Table 2 contains the full list of instrument systems contained in the backpack unit and additional details related to the components.....	71
1.26 Hand-held head unit containing the mass analyzer, ion detector assembly, electrical connections, ion introduction, and pressure transducer.....	72

Figure	Page
1.27 Pressure profiles of the vacuum manifold recorded directly from the pressure transducer demonstrate the pumping performance of two Mini 11.5 and the Mini-S manifold A under conditions of air, continuous helium, 17 ms pulse of Helium, and 77 ms pulse of Helium. Each pressure trace is an average of the pressure recordings for 5 consecutive 17ms DAPI pulses.	73
1.28 Pressure-time profiles for the Mini 11.5 and Mini-S manifold B for four configurations and in the presence of helium and air as the buffering gas.	74
1.29 Image adapted from reference 4, fabrication layout images of the analogy board (left) and the digital board (left). The digital board contains 8 layers and 457 individual components. Tables 2 and 3 details the other boards used on the Mini-S instrument.....	75
1.30 Images adapted from reference 4. A) Block diagram of the Mini-S and Mini 12 instrument systems and high level interpretation of the electronic signal connections. B) Details of the electronic signal paths for the FPGA, DSP, and shared random access memory (SRAM).	76
1.31 Images adapted from reference 4. A) Error associated with the RF amplitude ramp during mass analysis for the analog feedback control used on the Mini 11.5 instrument. B) Same plot as A, but with the Mini 12 digital controller. Notice that the magnitude of the RF error is substantially smaller over the entire RF ramp as compared to the analog control. C) Mass drift over time for the digital controller implemented on the Mini 12 compared to the analog implementation on the 11.5.	77
1.32 Open view of the RF coil box used to amplify the RF voltage amplitude. Note the use of a 20pF tuning capacitor in parallel with the RF resonant circuit. The tuning capacitor was used to manually adjust the resonate frequency of the circuit to 1 MHz by adding or removing capacitance.	78
1.33 Application of SWIFT for ion isolation. A) Time domain SWIFT waveform calculated by the software based on the specified frequency notch. Waveform is applied to the X-electrodes a total of 4 times while the ions are stored inside the ion trap. Frequency notch is 277 to 292 kHz which corresponds to a mass isolation notch of <i>m/z</i> 301 – 310. B) Yellow trace is the RF waveform acquired from the RF amplifier board. Blue trace is the AC voltage applied to the X-electrodes acquired from the AC amplifier board. C) Mass spectrum after the isolation waveform has been applied; inside the notch cocaine (10ppb) <i>m/z</i> 304 [M+H] ⁺ and cocaine-d3 (50ppb) <i>m/z</i> 307 [M+H] ⁺ are isolated.	79

Figure	Page
1.34 Advanced user interface for the Mini-S and Mini 12 instruments adapted from reference 4. This interface is used for setting the voltage control operation and timing for all of the instrument devices which includes the mass analyzer, ion detection circuit, source voltage, ion introduction, and data acquisition. In addition all of the instrument ADCs, the RF frequency, and the RF PID controller are also tuned through this interface. The central display allows for the viewing of acquired data, a graphical view of the instrument method, i.e. voltage amplitudes with respect to time, and the visualization of the SWIFT notch in both frequency and time domains.	80
1.35 Novice user interface (NUI) that allows control of the Mini-S instrument. This interface was developed with research partners at JHU/APL and was designed to work on top of the advanced user interface by executing previously generated scan tables. The NUI is designed to be used with the library search feature however, other functionality necessary for instrument operation such as control of the vacuum system during start up and shutdown, data review, manual switch of polarities, and the ability sweep the RF frequency are also available.....	81
1.36 Fully assembled Mini-S instrument installed on a mannequin with active LEDs (green) on the hand-held unit indicating the instrument system status as ‘ready for analysis’.....	82
1.37 Decision flow chart for data acquisition results reporting for the color LEDs.	83
2.1 A) Image and dimensions of the Mini 12 mass spectrometer fully assembled with the touch screen PC computer and the paper spray cartridge tray installed. B) Mini 12 instrument chassis. The placement of the electronics is visible on the top half of the instrument and the vacuum system, manifold and inlet to the mass spectrometer is on the bottom. C) Details of the mass analyzer, 5 x 4 mm rectilinear ion trap (RIT) and the electron multiplier / dynode assemble which comprise the ion detection system.....	94
2.2 Modifications to the Mini 12 RF circuit which increased the voltage from 5.5 kV _{p-p} to 7.8 kV _{p-p} . The anticipated maximum detectable mass-to-charge at the increased voltage amplitude was 1300 amu. The voltage rating of the RF cable and connections were the limiting factor in extending the voltage amplitude further.	95
2.3 nESI mass spectrum of PEG oligomers obtained on the Mini 12 instrument as demonstration of the increased mass range.....	96

Figure	Page
2.4 Full scan mass spectrum of gray matter (~ 100 µg) sampled directly from mouse brain tissue with TS and analyzed on a Mini 12 mass spectrometer. The mass range <i>m/z</i> 700 to 900 is the target range for biological lipid analysis. Inside this mass range the relevant phospholipids used in tissue characterization can be clearly identified. Common lipids are listed in the figure and are designated in the mass spectrum with an asterisks.	97
2.5 Left) Optical image of mouse brain tissue slice, grid spacing is 2 mm. The small circles across the mouse brain tissue are regions that have been sampled with the TS probe is spot represents ~100 µg of material that has been removed. Right top) grey matter sampled from the cerebral cortex Right bottom) White matter sampled from the hippocampus. Notice that for the two regions the relative intensity of PS 18:0 / 22:6 is lower for white matter relative to grey matter and also the occurrence of ST 24:1. Both of these differences are expected physiologically and are measured here with a Mini 12 mass spectrometer.	98
2.6 PLS-DA analysis of the grey and white matter mass spectra acquired with a Mini 12 MS. The statistical tool used to complete the processing was a 3 rd party online application http://www.metaboanalyst.ca/MetaboAnalyst/faces/Home.jsp . Largest sources of difference between the two samples were for <i>m/z</i> 888.5 corresponding to ST 24: 1 and <i>m/z</i> 885 corresponding to PI 18:0 / 20:4, fitting well with the physiological differences between white and grey matter of brain tissue.....	99
3.1 Computer aided design (CAD) model of the miniature RIT trapping electrodes and ceramic spacers. The ceramic spacers (white) ensure proper alignment of the trapping electrodes (gray) and act as electrical insulators.....	120
3.2 A) Optical image of the X-Y plane of the 1/3 rd scaled ion trap note the position of the X and Y- electrodes which have X ₀ and Y ₀ dimensions of 1.66 and 1.33mm respectively. B & C) Images of the fully assembled ion trap mounted to its holder and positioning of the electron multiplier along the ion ejection slit on the X-axis; A US dime (17.91 mm) is used for scale.....	121
3.3 Scan function used to operate the miniaturized RIT. During experiments in which no ion isolation or activation were conducted amplitudes and time segments for SWIFT and CID were set to zero.....	122
3.4 SIMION modeling of 1/3 rd size stainless steel ion trap. Electrode structures were used to calculate the expansion coefficient for the quadrupole (A2) component of the electric field.....	123

Figure	Page
3.5 Visualization of the electric fields for 1/3 rd size RIT calculated from the SIMION potential array. Top) Field in the X-Y plane; Middle) Field in the X-Z plane; Bottom) Field in the Y-Z plane.	124
3.6 Electric field in the X-Y plane; Note: due to symmetry only ¼ of the entire filed (represented by this grid) is required for the calculation of the expansion coefficients.	125
3.7 Nano-electrospray ionization of PEG oligomers 1-2 Th (FWHM) at concentrations of 10 µM to 100 µM in 1x10 ⁻³ M NaOH. RF voltage amplitude scan from 68 V _{0-p} to 610 V _{0-p} , using resonance ejection at 358 kHz with the AC amplitude ramped from 340 mV _{p-p} to 1.1 V _{p-p} throughout the analytical scan.	126
3.8 Full scan performance of the 1/3 rd size RIT for PEG oligomers across the mass range. Note that FWHM values are approximately 1-2 amu across the mass range.	127
3.9 Selective ejection of <i>m/z</i> 305 (n = 6) by application of dipolar supplementary AC excitation voltage applied to the X-electrodes; freq 142 kHz, 130 mV _{p-p} , 50 ms.	128
3.10 Ion frequency map: Solid line indicates the calculated secular ion frequencies. Points indicate frequencies determined experimentally through selective ion resonant ejection.	129
3.11 Cocaine after A) 200 mV _{p-p} activation B) 220 mV _{p-p} activation C) 230 mV _{p-p} activation D) 250 mV _{p-p} activation. All activation experiments were initiated at a pressure of 20 mtorr and at 10µg/ml concentration.	130
3.12 Figures A – C show the conversion of the production <i>m/z</i> 182 from the parent <i>m/z</i> 304 as the collision energy is increased.	131
3.13 Precursor <i>m/z</i> 304, □, and product ion <i>m/z</i> 182, ■, intensity vs. AC amplitude; Right axis) Fragmentation efficiency, ▲,(Fragment ion intensity/ Total intensity).	132
3.14 Collisional induced dissociation (CID) mass spectrum of Bradykinin obtained on the 1/3 rd RIT; activation q_z = 0.206, AC amplitude 220 mV, manifold pressure 15 mTorr, activation 30 ms.	133
3.15 Composite figure of the 1/3 rd stainless steel RIT demonstrating the X ₀ and Y ₀ dimensions, PEG spectrum, position of the detector, operating voltages and pressures, as well as tandem MS capability.	134

Figure	Page
3.16 Full size (5 x 4 mm) RIT fabricated with FR-4. A) Aspect image of a fully assembled RIT. Note the entrance aperture on the right side of the image which is used for axial injection of ions and the ion ejection slit on the left which is used for radial ejection of ions during mass analysis. B) Side view of the 5 x 4 mm RIT with a clearer image of the ion ejection slit. C) Monolithic construction of the PCB RIT. all six electrodes and the support base are fabricated simultaneously.....	135
3.17 1/3 rd scaled RIT PCB. A & B) Aspect and top, respectively, images of the miniaturized PCB RIT; this mass analyzer has the same $X_0 \times Y_0 \times Z$ dimensions as the 1/3 rd scaled stainless steel RIT.....	136
3.18 Nano-electrospray ionization of $[PEG+Na]^+$ oligomers ~ 1 Th (FWHM) for low mass ion and increases to ~ 2 Th for high mass ions. Concentrations of 10 μM to 100 μM in 1×10^{-3} M NaOH. RF voltage amplitude scan from 312 V_{0-p} to 3345 V_{0-p} , using resonance ejection at 409 kHz ($q_z = 0.887$)with the AC amplitude $2V_{p-p}$ to $18V_{p-p}$ throughout the analytical scan.....	137
3.19 Tandem MS of MRFA acquired using full size PCB RIT	138
3.20 RF and DC waveforms used to complete mapping of the first region of ion stability for the PCB RIT. Notice there are two pairs of RF and DC waveforms applied. The first is used to isolate m/z 91 at the stability region apex and the second is used to reposition the ion packet corresponding to m/z 91 to determine boundaries of the stability region.....	139
3.21 Map of the first region of stability as acquired with the PCB RIT. The boundary of the stability region was determined to be when the s/n of m/z 91 was equal to 1	140
4.1 A) Base PCB substrate B) Pattered substrate that contains the electrical pads for all RF and DC connections to the array electrodes C) SLA build on PCB surface, gray pillars represent layer by layer construction of the electrodes D) Finished integration of SLA and PCB E) Gold plated array F) Electrode isolation is completed by laser ablation.	167
4.2 Eight channel rectilinear ion trap array with independently isolated electrodes arranged in a circular pattern around a single centralized detector. Electrical connections to each electrode are milled into the PCB substrate. Each channel is designed to be 1.66 x 1.33 x 16.66 mm in the X_0 Y_0 and Z directions, entire footprint measures 77 x 90 x 32 mm. Note the US dime (17.91 mm diameter) as a scale reference.	168

Figure	Page
4.3 A) Bias T circuit schematic used to control the DC voltage applied to the Y-electrodes during operation of the ion trap. B&C) Position of the Mathieu operational parameter ‘ <i>a</i> ’ in relation to the first stability region. Note because of the implementation of an external switch, the ‘ <i>a</i> ’ parameter can be adjusted in real time and without interference to the applied RF.....	169
4.4 Spectra for individual channels, 10 µg/ml MRFA, <i>m/z</i> 524.3 [M+H] ⁺ . All spectra have the same normalization to show the relative intensities for each channel. All channels are operated with the same RF and AC waveforms. Special attention should be made to the difference in performance between channel 4 and channel 7 demonstrating the contrast between the best performing and worst performing traps in the array.	170
4.5 50 µg/ml MRFA, <i>m/z</i> 524.3 [M+H] ⁺ , Red trace is the spectrum acquired with all channels in the array being acquired simultaneously. Blue trace is the summation of signal acquired from channels 1 through 8 independently and then summed to total trace. Note Red and blue traces are conceptually the same.	171
4.6 Polyethylene glycol (PEG) in concentrated NaOH to form [M+Na] ⁺ adducts. Simultaneous operation of all eight channels in the array, smaller peaks that are reminiscent of a bi and tri modal distribution are due to dimensional variation between ion trap channels.	172
4.7 A) Circuit schematic of the PA85 operational amplifier used to drive a single channel of the ion trap array. B) OrCAD rendering of the RF circuit, two drive circuits are side by side. C) Assembled multi-channel RF drive circuit for the array.....	173
4.8 Effect of pulse duration on mass assignment and peak resolution for 50 µg/ml MRFA, <i>m/z</i> 524.3 [M+H] ⁺ . For a 50 ms pulse duration FWHM values are approximately 5 amu while reducing the duration to 20 ms improved the resolution approximately 2 amu. 15 ms was tested to verify that no further improvements were obtained by continuing to reduce the pulse duration.	174
4.9 50 µg/ml MRFA, <i>m/z</i> 524.3 [M+H] ⁺ , fully optimized source conditions resulting in FWHM values on the order of 1 amu for both +1 and +2 charge states.....	175
4.10 PEG oligimers ranging from 50 to 500 µM in solution with concentrated NaOH, [M+Na] ⁺ , at intervals of 44 amu across the mass range.	176

Figure	Page
4.11 56 μM of equine myoglobin (17 kDa), detection of the charge state envelope from +26 to +14 is detectable at RF voltages of 1.2 kV _{p-p} . By way of comparison the source spray voltage was 1.6 kV _{DC}	177
4.12 Scan function used to execute tandem MS, red trace represents AC and blue trace represents the pressure inside the manifold. A) SWIFT isolation of parent ion at <i>m/z</i> 267 at sub mTorr pressures. B) Excitation for CAD, pressure increase is due to a second DAPI pulse increasing the manifold pressure to 25 mTorr. C) AC ramp during mass analysis.....	178
4.13 Tandem MSMS of atenolol, <i>m/z</i> 267. Fragment ions at <i>m/z</i> 225 and 250 are indicative of propene and NH ₃ losses. Red trace at <i>m/z</i> 190 is indicative of the calculated LMCO based upon the amplitude of the applied RF during CAD. Fragment ions below this value are not detected.	179
4.14 <i>N,N</i> -Diethyl-meta-toluamide (DEET) fragment <i>m/z</i> 119 and monomer <i>m/z</i> 192 and respectively A) Ion traps 1 and 4 driven independently using the multi-channel operational amplifier circuits described in the text. Most apparent is the DEET monomer ejecting from trap 1 just before trap 4. B) q_z values for all ions in trap 1 have been increased by increasing the amplitude of the RF waveform. Ions eject at roughly the same time for the two channels. C) Further increase of the RF waveform amplitude causes ions from trap 1 to eject after trap 4.....	180
4.15 4 ion trap channels operating simultaneously using individually calibrated RF waveforms. nanoESI mass spectrum of caffeine (<i>m/z</i> 195), propranolol (<i>m/z</i> 260), and cocaine (<i>m/z</i> 304) each at 33 ug/ml.....	181
4.16 A) Single channel B) Multi-channel Gaussian fits to propranolol [M+H] ⁺ signal to define the limits of integration. The area between the low <i>m/z</i> (L1 & L4) and the high <i>m/z</i> (H1& H4) define ~95% of the peak area based upon the fit. <i>m/z</i> values inside this boundary are the limits of integration from which the peak area was calculated.	182
4.17 Signal response due to one or four channels for propranolol and atenolol. Increased sensitivity obtained by operating multiple channels in parallel. Response was linear from 100 ng/ml to 1400 ng/ml and had good linearity over this range as represented by the R ² values; 0.982 and 0.97 for one and four channels respectively. Slopes increased from 3.145×10^8 to 8.709×10^8 for one versus four channels.	183

Figure	Page
4.18 Relative contribution for each channel in the array for the composite spectrum. Note that not all channels contribute equally to the analyte response and that not all channels have the same resolution performance. Resonance ejection parameters were tuned for channel 4 and used for all other channels (only one AC signal was available on the LCQ instrument). Recalibrated RF waveforms helped to adjust ion ejection points but did not improve resolution.	184
4.19 Independently controlled RF waveforms allow mass analysis to be completed for any ion trap channel at any time point. The above figure shows an atmospheric pressure chemical ionization (APCI) mass spectrum of DEET from ion trap 1 and 4, but each ion trap channel was scanned at two different time points, i.e. ion trap 1 was scanned first and upon completion the detector was left on to collect the ion signal from trap 4 in which the RF amplitude (from an independent waveform) was scanned. While it was not necessary to scan ion trap 4 following ion trap 1, any element in the array could be scanned in any order, this demonstrated that ions continued to remain trapped in adjacent traps that were not scanned after the first RF ramp. The mass scales from each ion trap are the same and there is no relevance to the difference in peak heights for the <i>m/z</i> 119 and 192 ions.	185

ABSTRACT

Hendricks, Paul Isaac. Ph.D., Purdue University, December 2013. Development of A Field-Portable Miniature Mass Spectrometer Designed for *In-Situ* Analysis and Ion Trap Miniaturization. Major Professor: Robert G. Cooks.

Chemical analysis by mass spectrometry has become the gold standard due to the sensitivity, selectivity, and short analysis times that are afforded by the method. Advances in miniaturized vacuum systems, mass analyzers, electronics, and ionization sources have allowed for the development of field-portable mass spectrometers. The performance of portable instruments has received much attention for their utility in the detection of illicit drugs, explosives, environmental contaminants, therapeutic drugs, and more recently, biological tissues. Furthermore, detection of the aforementioned compounds can be completed at atmospheric pressures and in the presence of complex matrices and sample surfaces when used in conjunction with ambient ionization sources. The work contained in this thesis is a summary of investigations that touch on different themes which further the advancement of miniaturized mass spectrometer instrumentation.

Chapter 1 details the development and performance characterization of a wearable, backpack-portable, miniature mass spectrometer- the Mini-S. Based on earlier versions, the Mini-S instrument has miniaturized electronics, vacuum system, mass analyzer, and ion detection system. Additionally, a key to achieving chemical analysis on time scales

relevant for *in-situ* detection and real-time analysis is the coupling of ambient ionization to miniature instruments. Also included in chapter 1 is the development of a co-axial low temperature plasma (LTP) probe as an ambient desorption / ionization (ADI) source. Chapter 2 extends the work in chapter 1 with the introduction of the Mini 12 mass spectrometer and application of touch spray for the characterization of tissues based upon detected lipid profiles.

Rectilinear ion traps (RITs) are a subset of linear ion traps (LITs) that utilize planar instead of hyperbolic electrodes to generate a quadrupolar field to confine gas phase ions. The simplified geometry of planar electrodes has the advantage of being easier to fabricate which reduces fabrication cost and they are easier to scale to miniaturized dimensions. Chapter 3 details the performance of a 1/3rd scaled RIT (1.66 x 1.33 mm) fabricated with stainless steel and introduces the fabrication of RITs with the printed circuit board (PCB) material and tooling. The performance of a full size (5 x 4 mm) PCB-RIT is also detailed.

A method used to offset the reduced ion capacity associated with dimensional miniaturization of the mass analyzer is parallel operation of multiple ion traps, i.e. ion trap array. Chapter 4 details the fabrication and operation of an eight-channel array of 1/3rd scale rectilinear ion traps (RITs) constructed monolithically with stereolithography apparatus (SLA). Each ion trap channel inside the array is independently isolated and can be controlled with a unique set of RF and DC voltages. Bias tee networks and dedicated operational amplifiers were used to improve the overall spectral quality of the device as a compensation for dimensional variation of individual ion trap channels. In this work it was also demonstrated that any given ion trap channel could be scanned at any time point.

PUBLICATIONS



Short communication

Performance of a low voltage ion trap

Paul Hendricks^a, Jason Duncan^a, Robert J. Noll^a, Zheng Ouyang^b, R. Graham Cooks^{a,*}^aDepartment of Chemistry, Purdue University, West Lafayette, IN 47907, United States^bWeldon School of Biomedical Engineering, Purdue University, West Lafayette, IN 47907, United States

ARTICLE INFO

Article history:

Received 20 April 2011

Received in revised form 12 May 2011

Accepted 16 May 2011

Available online 26 May 2011

Keywords:

Mass analyzer

Quadrupole ion trap

Rectilinear ion trap

Miniature ion trap

Portable mass spectrometry

Portable instrumentation

External ion generation

Atmospheric pressure interface

Discontinuous atmospheric pressure

interface (DAPI)

Tandem MS

ABSTRACT

Reduced power operation of a mass analyzer with minimum loss of spectral resolution and mass range is desirable in portable instruments. Miniaturizing quadrupole-based ion traps can be especially worthwhile since the RF amplitude necessary for mass analysis scales with the square of the analyzer dimensions. The performance of a miniature, stainless steel, rectilinear ion trap (RIT) with dimensions of $1.66\text{ mm} \times 1.43\text{ mm}$ (x_0 and y_0 respectively) is characterized by sampling externally generated ions and performing mass analysis without benefit of differential pumping to simulate conditions in a miniature system. This system is capable of detecting analyte ions of up to m/z 1250 at operating voltages of $610V_{0,p}$ (drive frequency of 1.105 MHz), and with spectral resolution on the order of 2 Th (FWHM) across the entire mass range. The ability to acquire structural information through tandem MS is also demonstrated.

© 2011 Elsevier B.V. All rights reserved.

1. Introduction

Demand for *in situ* detection of specific compounds at the parts-per-billion (ppb) and parts-per-million (ppm) levels is one of the factors driving the development of portable mass spectrometers [1–5]. The ability to successfully miniaturize and/or simplify the geometry of instrument components, particularly the electronics, vacuum system, and mass analyzer [6,7] is the key to this development. Quadrupole ion trap mass analyzers are well suited for use in portable instruments due to their ability to operate at elevated pressures (10^{-2} to 10^{-3} Torr), relaxing the vacuum system requirements, and the ability to use a single mass analyzer for tandem MS experiments. Additionally, ion traps, especially those with electrodes of simple geometry such as the cylindrical ion trap [8] (CIT) and the rectilinear ion trap [7] (RIT), are more easily scaled to mini [9–11] and micro [12–15] dimensions than other mass analyzer types.

RITs are simplified linear ion trap mass analyzers consisting of planar electrodes, *viz.* two end caps, and pairs of Y-electrodes and

X-electrodes, respectively. At the usual size scale the optimized, dimensions are $5\text{ mm} \times 4\text{ mm}$ nominally (one-half the distance between opposing X and Y-electrodes) [7]. This device has been well characterized and utilized as the mass analyzer in portable instruments for in-field applications [16–19]. Since the operating voltage scales as the square of the dimensions of the trapping electrodes, and power scales to the square of the RF amplitude, greatly reduced power requirements needed for portable instruments can be achieved by size reduction [10].

RIT mass analyzers have previously been fabricated with nearly the same geometry as used in this work and they have given peak widths of approximately 1.5–2 Th (FWHM) [20,21]. However, these earlier experiments did not employ small total MS systems, and notably they did not suffer from the limited pumping capabilities characteristic of handheld MS systems. In this work a miniaturized, steel, RIT was characterized in a single stage manifold, without ion optics or specialized buffer gas, and under pressure conditions comparable to those of a portable mass spectrometer utilizing a discontinuous atmospheric pressure interface (DAPI) to sample externally generated ions [22–24]. The performance of a miniaturized, steel, RIT analyzer ($1.66\text{ mm} \times 1.43\text{ mm}$ for x_0 and y_0 respectively; 1/3rd the scale of the usual RIT dimensions) operated at pressures expected for a portable instrument is characterized and evaluated in this study.

* Corresponding author. Tel.: +1 765 494 5263; fax: +1 765 494 9421.
E-mail address: cooks@purdue.edu (R.G. Cooks).

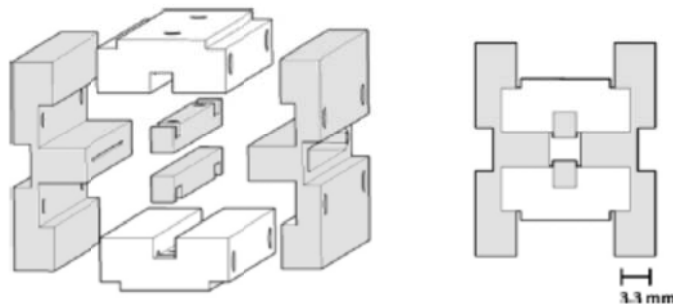


Fig. 1. Computer aided design (CAD) model of the miniature RIT trapping electrodes and ceramic spacers. The ceramic spacers (white) ensure proper alignment of the trapping electrodes (gray) and act as insulators.

2. Materials and methods

Machining of the electrodes (304 stainless steel) was executed using computer numerical control (CNC) followed by hand polishing of the inner electrode surfaces to a mirror finish. Precision cut Macor ceramic established the inter-electrode distances and formed the insulating spacers between adjacent electrodes (Fig. 1). Analyzer assembly was completed by hand. Upon final assembly the average gap spacing (distance between adjacent X and Y-electrodes) was 0.590 mm, and the trapping dimensions (distance between opposing X and Y-electrode pairs) were 1.66 mm and 1.43 mm respectively. These measurements were made using an optical microscope (SmartScope MVP 300, Optical Gauging Products, Inc.) and are accurate to $\pm 1 \mu\text{m}$. The length of the ion trap (z-dimension) and the dimensions of the ion ejection slits in the X-electrodes were measured to be 40 mm and $0.33 \text{ mm} \times 25 \text{ mm}$, respectively, as measured with a micrometer (Mitutoyo, CD-6 BS). As in all linear ion traps, the z-dimension of this device is critical to the ion trapping volume but does not impact the generation of a quadrupolar field in the x-y plane. A confining force is however, established in the z-dimension by applying a DC potential to the end cap electrodes.

Mass calibration and experimental determination of the upper limit of the m/z range was determined using polyethylene glycol (PEG) in methanol/water (1:1 by vol.) at concentrations ranging from $10 \mu\text{M}$ to $100 \mu\text{M}$. The PEG mix was prepared from seven oligomers with average molecular weights ranging from approximately 100 to 600 (Sigma-Aldrich, Inc.) all used without further

purification or modification. PEG was selected for its ability to produce singly charged, sodiated adducts in the presence of sodium salts. Ions generated by nano-ESI were pulsed into the vacuum manifold using a discontinuous atmospheric pressure interface (DAPI) [22–24]. This ion introduction interface is comprised of a controllable, short duration valve (ASCO Scientific, Florham Park, NJ) with a conductive rubber capillary as the seating material (Simolex Rubber Corp., Plymouth, MI). When the DAPI valve is open, gas phase neutrals and the ions generated in the ambient environment are passed to the low pressure (base pressure $\sim 10^{-4}$ to 10^{-5} Torr) vacuum manifold that contains the mass analyzer. Once the DAPI valve is closed, the introduced ions are trapped while neutral gas phase molecules are pumped away. This decreases the operating pressure of the ion trap, and allows the electron multiplier (Photonics, Magnum 5903) to be turned on. In the scan function implemented for these experiments (Fig. 2), the DAPI valve was opened to the atmosphere for 50 ms and then closed for the duration of the pump down and mass scan period, which was approximately 2000 ms. The stainless steel ion introduction capillary was aligned co-axially with the aperture in the ion trap front end cap and positioned such that there was a 1 mm gap between the two components. This allowed gating of the ions into the trap using the front end cap voltage and it avoided perturbation of the quadrupolar field by inserting the capillary directly between the X and Y electrodes.

A laboratory built system that utilized LCQ Duo (Thermo Fisher Scientific, San Jose, CA) electronics and LCQ Duo Tune 1.0 software/Ion Trap Control Language interface was used for electronic

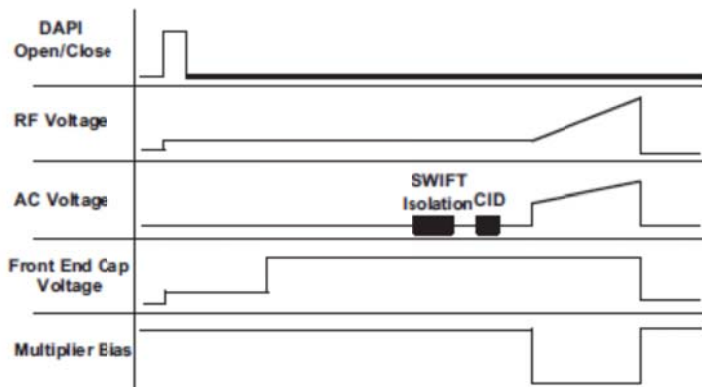


Fig. 2. Scan function used to operate the miniaturized RIT. During experiments in which no ion isolation or activation was conducted amplitudes and time segments for SWIFT and CID were set to zero.

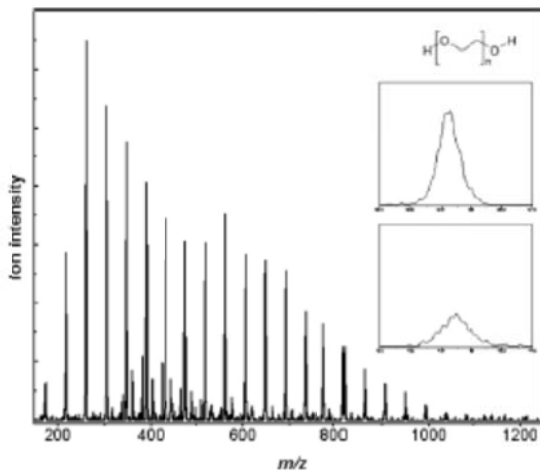


Fig. 3. Nano-electrospray ionization of PEG oligomers 2 Th (FWHM) at concentrations of 10–100 μM in 1×10^{-3} M NaOH. RF voltage amplitude scan from $68 \text{ V}_{0,\text{p}}$ to $610 \text{ V}_{0,\text{p}}$, using resonance ejection at 358 kHz with the AC amplitude ramped from $340 \text{ mV}_{\text{p-p}}$ to $1.1 \text{ V}_{\text{p-p}}$ throughout the analytical scan.

timing and control. The vacuum consisted of a TSQ7000 manifold with single stage pumping. A BocEdwards E2M30 ($30 \text{ m}^3/\text{h}$) rotary vane pump at the front and a Pfeifer 260 turbo molecular pump (210 L/s) backed by a second BocEdwards E2M40 ($40 \text{ m}^3/\text{h}$) was necessary to accommodate the large vacuum manifold. The performance was specifically de-tuned to achieve pressures in the ion trap similar to those given by miniature systems. After the DAPI valve was closed, ending the 50 ms ion sampling pulse, the front end cap was held at 1.8 V for 150 ms to allow the ions in the sample volume to transfer completely out of the 200 mm introduction capillary and into the ion trap. Next, the front end cap was raised to 15 V, and the rear end cap continued to be held at 25 V. Ions were allowed to cool for 500 ms while the manifold pressure dropped from its peak pressure of $\sim 75 \text{ mTorr}$ to $\sim 15 \text{ mTorr}$, at which point the RF (drive frequency 1.105 MHz) amplitude was scanned from $68 \text{ V}_{0,\text{p}}$ to $610 \text{ V}_{0,\text{p}}$ at a rate of 833.3 Th/s, thus completing the analytical mass scan (Fig. 2). The scan rate in this work is slower than that used in typical operation of full size RITs (10,000 Th/s) and was done to maximize mass spectral resolution. Resonance ejection was implemented by applying a dipolar supplementary RF to the x-electrodes at a frequency of 358 kHz ($q_x = 0.77$) and its amplitude was ramped linearly from $340 \text{ mV}_{\text{p-p}}$ to $1.1 \text{ V}_{\text{p-p}}$ throughout the analytical scan.

3. Results and discussion

3.1. MS performance

The trapping voltage (depth of the effective potential well) for the miniature RIT was optimized by increasing the RF amplitude several volts at a time until the m/z distribution of the PEG sample was detected. A trapping voltage of $68 \text{ V}_{0,\text{p}}$ (low mass cutoff $\sim m/z$ 140) was determined experimentally to be the minimum voltage necessary to detect ions of up to m/z 1250. These ions covered the entire mass range and were separated by intervals of 44 Th (Fig. 3). The peak RF voltage necessary for completing an analytical scan over this mass range was $610 \text{ V}_{0,\text{p}}$ and spectral resolution was on the order of 2 Th FWHM at m/z 305, which increased with m/z .

By way of comparison the Mini 11, a portable mass spectrometer that uses a full size RIT, is limited by the available RF voltage

($2250 \text{ V}_{0,\text{p}}$) to a maximum m/z of 700 when operated at $\sim 1 \text{ MHz}$ [25]. Under the operating conditions described in Section 2, the miniaturized RIT is capable of detecting m/z of 900 at $448 \text{ V}_{0,\text{p}}$. The two systems give comparable mass resolution. The miniaturized RIT mass analyzer, when tested on a laboratory scale instrument, exhibits the necessary performance characteristics in terms of resolution, mass range, and operating voltage. It therefore should be recognized that the operational parameters for an ion trap do not depend on whether it is installed in a laboratory scale or a miniaturized instrument making the prospect of using such a mass analyzer in a portable instrument highly attractive. To further support the feasibility of using a 1/3rd size RIT in a portable instrument the method of ion introduction in the present study is similar to that expected for a portable instrument also utilizing a DAPI source. It is anticipated that operational pressure for the laboratory scale and the portable instrument will be sufficiently similar to avoid a significant decrease in performance of the mass analyzer.

The DAPI source provides a method for sampling charged analytes at atmospheric pressure while satisfying the vacuum requirements of the mass spectrometer. We note, however, the somewhat inefficient use of the sample since the duty cycle (open time vs. overall cycle period) of the DAPI is just a few percent. Another drawback is that the mass analyzer is operated at pressures that are an order of magnitude or more above the optimal working pressure of 10^{-3} Torr. This together with mechanical imperfections contributes to peak broadening. The results obtained here are consistent with the performance anticipated for a device of this geometry, scale, and operation inside the pressure range achieved using a DAPI source.

3.2. Mass selective ion ejection

Frequencies which correlate with effective ion ejection were measured by applying supplementary, low amplitude AC to the X-electrodes during the ion trapping phase of the scan function. Ions of a selected m/z were resonantly excited and ejected from the ion trap by controlling the frequency, amplitude, and time of the applied AC. Typical time and amplitude values ranged from 50 to 100 ms and 100 to $200 \text{ mV}_{\text{p-p}}$.

An approximate determination of the ejection frequency for an ion of a particular m/z ratio can be made by monitoring the frequency at which the ion disappears from the mass spectrum (Figs. 4 and 5). Repeating this experiment for the most abundant ions in the sample, allows a plot of the ejection frequency versus m/z to be constructed. The results (Fig. 5) demonstrate that the ejection frequencies for a given m/z are in close agreement with the calculated secular frequency and follow the theoretical trend attributable to the inverse relationship between q_x and m/z .

3.3. Tandem MS performance

The protonated cocaine molecule, m/z 304, fragments to give m/z 182 by elimination of benzoic acid [26,27]. Also observable, although in lower abundance, is a competing fragmentation pathway in which benzaldehyde is lost from the protonated molecule, forming an ion of m/z 198. Conditions under which both fragmentation pathways are observed can be particularly useful for chemical profiling experiments used to identify pure compounds and/or compound metabolites using known fragmentations [28]. Cocaine was isolated through the application of a stored waveform inverse Fourier transform (SWIFT) [29] function for 450 ms, followed by activation at $q_x = 0.36$ ($\sim 147 \text{ kHz}$) for 30 ms at amplitudes of approximately $200 \text{ mV}_{\text{p-p}}$. DAPI, as previously described, allows introduction of both analyte ions and neutral molecules into

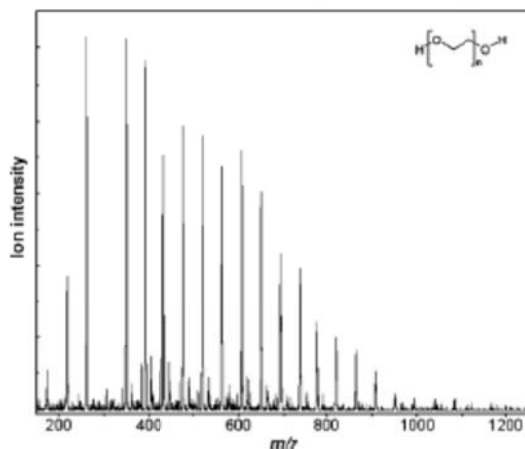


Fig. 4. Selective ejection of m/z 305 ($n=6$) by application of dipolar supplementary AC excitation voltage applied to the X-electrodes; freq 142 kHz, 130 mV_{p-p}, 50 ms.

the vacuum manifold and consequently the mass analyzer. The manifold pressure for CID was optimized at 20 mTorr, where the neutral molecules introduced during the DAPI pulse serve as the buffer gas during these experiments.

To optimize MS/MS performance the AC amplitude was varied from 200 to 250 mV_{p-p} by increments of approximately 10 mV_{p-p} (Fig. 6). The maximum fragmentation efficiency was found to be 9.1% (Fig. 7). The mechanisms by which ions are activated in CID and by which they are resonantly ejected from the ion trap are similar. Excitation energy is supplied using a supplementary AC applied in resonance with the ion secular frequency. Considering that the pseudopotential well depth is proportional to the magnitude of the applied RF, the well for a miniaturized RIT is shallower than its full-size counterpart by approximately a factor of nine (due to the three-fold reduction in physical size). Under these conditions resonance ejection increasingly competes with activation and results in poor fragmentation efficiency. In this experiment over 90% of the precursor ions are lost prior to dissociation.

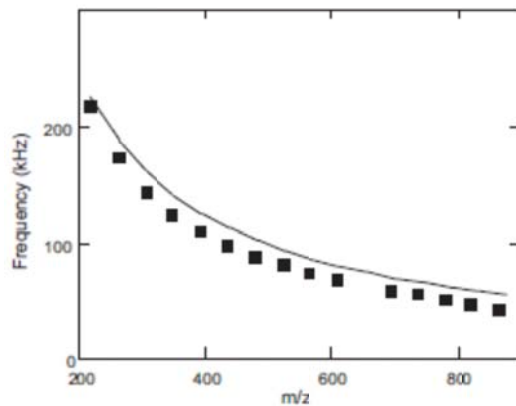


Fig. 5. Ion frequency map: solid line indicates the calculated secular ion frequencies. Points indicate frequencies determined experimentally through selective ion resonant ejection.

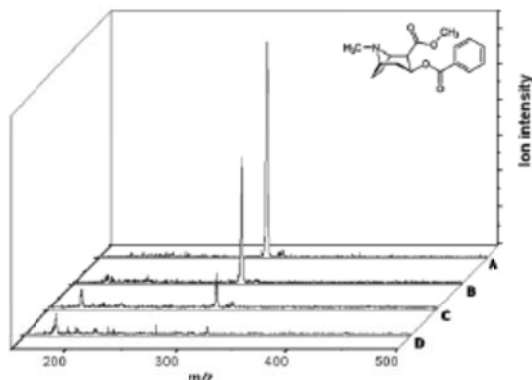


Fig. 6. Cocaine after (A) 200 mV_{p-p} activation, (B) 220 mV_{p-p} activation, (C) 230 mV_{p-p} activation, and (D) 250 mV_{p-p} activation. All activation experiments were initiated at a pressure of 20 mTorr and at 10 µg/ml concentration.

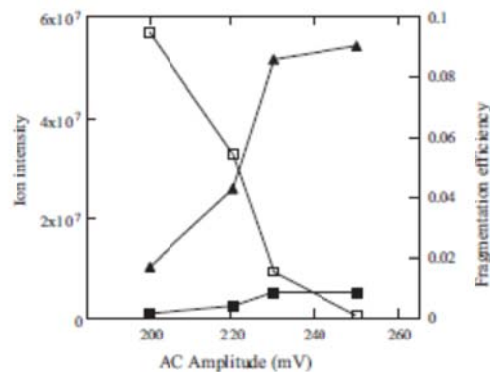


Fig. 7. (Left axis) Precursor m/z 304, \square , and product ion 182, \blacksquare , intensity vs. AC amplitude; (right axis) fragmentation efficiency, \blacktriangle (fragment ion intensity/total intensity).

4. Conclusions

The mass range, spectral quality, tandem MS capabilities, and operating voltages of a miniaturized RIT make it an attractive mass analyzer for use in portable mass spectrometers. It also serves as a method for evaluation of ion traps in other areas of research namely, even more miniaturized devices, traps made of electrodes fabricated using new technologies/materials, traps with novel electrode geometries, and ion trap arrays [9,21,30–32]. In addition, at this scale (and smaller) the RF amplitude necessary to complete mass analysis over a range of approximately 100–500 Th, suitable for the detection of most standard organic compounds, is within the range of commercially available operational amplifiers. A "direct drive" approach to RF control would offer the benefit of ion trap operation without the use of specially designed inductance coils, thus simplifying the design and construction of field portable mass spectrometers.

Acknowledgements

The authors thank Frank Boudreau, and Jeff Maas for engineering support and technical discussions.

This work was supported by Thermo Fisher Scientific and NSF award #CHE0848650.

References

- [1] A. Keil, H. Hernandez-Soto, R.J. Noll, M. Fico, L. Gao, Z. Ouyang, R.G. Cooks, Monitoring of toxic compounds in air using a handheld rectilinear ion trap mass spectrometer, *Analytical Chemistry* 80 (2008) 734–741.
- [2] C.C. Mulligan, D.R. Juster, R.J. Noll, N.L. Sanders, B.C. Laughlin, R.G. Cooks, Direct monitoring of toxic compounds in air using a portable mass spectrometer, *Analyst* 131 (2006) 556–567.
- [3] L.S. Riter, Y. Peng, R.J. Noll, G.E. Patterson, I. Aggerholm, R.G. Cooks, Analytical performance of a miniature cylindrical ion trap mass spectrometer, *Analytical Chemistry* 74 (2002) 6154–6162.
- [4] J.N. Smith, A. Keil, J. Likens, R.J. Noll, R.G. Cooks, Facility monitoring of toxic industrial compounds in air using an automated, fieldable, miniature mass spectrometer, *Analyst* 135 (2010) 994–1003.
- [5] J.N. Smith, A.D. Keil, R.J. Noll, R.G. Cooks, Ion/molecule reactions for detecting ammonia using miniature cylindrical ion trap mass spectrometers, *Analyst* 136 (2011) 120–127.
- [6] E.R. Badman, R. Graham Cooks, Miniature mass analyzers, *Journal of Mass Spectrometry* 35 (2000) 659–671.
- [7] Z. Ouyang, G. Wu, Y. Song, H. Li, W.R. Plass, R.G. Cooks, Rectilinear ion trap: concepts, calculations, and analytical performance of a new mass analyzer, *Analytical Chemistry* 76 (2004) 4595–4605.
- [8] R.F. Bonner, J.E. Fulford, R.E. March, G.F. Hamilton, The cylindrical ion trap. Part I. General introduction, *International Journal of Mass Spectrometry and Ion Physics* 24 (1977) 255–269.
- [9] D.E. Austin, Y. Peng, B.J. Hansen, I.W. Miller, A.L. Rockwood, A.R. Hawkins, S.E. Tolley, Novel ion traps using planar resistive electrodes: implications for miniaturized mass analyzers, *Journal of the American Society for Mass Spectrometry* 19 (2008) 1435–1441.
- [10] G.E. Patterson, A.J. Guymon, L.S. Riter, M. Everly, J. Griep-Raming, B.C. Laughlin, Z. Ouyang, R.G. Cooks, Miniature cylindrical ion trap mass spectrometer, *Analytical Chemistry* 74 (2002) 6145–6153.
- [11] Z. Zhu, C. Xiong, G. Xu, H. Liu, X. Zhou, R. Chen, W.-P. Peng, Z. Nie, Characterization of bioparticles using a miniature cylindrical ion trap mass spectrometer operated at rough vacuum, *Analyst* (2011).
- [12] M.G. Blain, L.S. Riter, D. Cruz, D.E. Austin, G.Wu, W.R. Plass, R.G. Cooks, Towards the hand-held mass spectrometer: design considerations, simulation, and fabrication of micrometer-scaled cylindrical ion traps, *International Journal of Mass Spectrometry* 236 (2004) 91–104.
- [13] A. Chaudhary, F. vanAmerom, R.T. Short, Development of microfabricated cylindrical ion trap mass spectrometer arrays, *Journal of Microelectromechanical Systems* 18 (2009) 442–448.
- [14] D. Cruz, J.P. Chang, M. Fico, A.J. Guymon, D.E. Austin, M.G. Blain, Design, microfabrication, and analysis of micrometer-sized cylindrical ion trap arrays, *Review of Scientific Instruments* 78 (2007) 015107.
- [15] J. Moxom, P.T.A. Reilly, W.B. Whitten, J.M. Ramsey, Analysis of volatile organic compounds in air with a micro ion trap mass analyzer, *Analytical Chemistry* 75 (2003) 3739–3743.
- [16] G. Huang, W. Xu, M.A. Vishal-Onufraik, Z. Ouyang, R.G. Cooks, Direct analysis of melamine in complex matrices using a handheld mass spectrometer, *Analyst* 135 (2010) 705–711.
- [17] A. Keil, N. Talaty, C. Janleit, R.J. Noll, L. Gao, Z. Ouyang, R.G. Cooks, Ambient mass spectrometry with a handheld mass spectrometer at high pressure, *Analytical Chemistry* 79 (2007) 7734–7739.
- [18] N.L. Sanders, E. Sokol, R.H. Perry, G.M. Huang, R.J. Noll, J.S. Duncan, R.G. Cooks, Hand-held mass spectrometer for environmentally relevant analytes using a variety of sampling and ionization methods, *European Journal of Mass Spectrometry* 16 (2010) 11–20.
- [19] E. Sokol, K.E. Edwards, K. Qian, R.G. Cooks, Rapid hydrocarbon analysis using a miniature rectilinear ion trap mass spectrometer, *Analyst* 133 (2008) 1064–1071.
- [20] M. Fico, J.D. Maas, S.A. Smith, A.B. Costa, Z. Ouyang, W.J. Chappell, R.G. Cooks, Circular arrays of polymer-based miniature rectilinear ion traps, *Analyst* 134 (2009) 1338–1347.
- [21] M. Fico, M. Yu, Z. Ouyang, R.G. Cooks, W.J. Chappell, Miniaturization and geometry optimization of a polymer-based rectilinear ion trap, *Analytical Chemistry* 79 (2007) 8076–8082.
- [22] L. Gao, R.G. Cooks, Z. Ouyang, Breaking the pumping speed barrier in mass spectrometry: discontinuous atmospheric pressure interface, *Analytical Chemistry* 80 (2008) 4026–4032.
- [23] L. Gao, G. Li, Z. Nie, J. Duncan, Z. Ouyang, R.G. Cooks, Characterization of a discontinuous atmospheric pressure interface. Multiple ion introduction pulses for improved performance, *International Journal of Mass Spectrometry* 283 (2009) 30–34.
- [24] W. Xu, N. Charipar, M.A. Kirleis, Y. Xia, Z. Ouyang, Study of discontinuous atmospheric pressure interfaces for mass spectrometry instrumentation development, *Analytical Chemistry* 82 (2010) 6584–6592.
- [25] L. Gao, Q. Song, G.E. Patterson, R.G. Cooks, Z. Ouyang, Handheld rectilinear ion trap mass spectrometer, *Analytical Chemistry* 78 (2006) 5994–6002.
- [26] P. Wang, M.G. Bartlett, Collision-induced dissociation mass spectra of cocaine, and its metabolites and pyrolysis products, *Journal of Mass Spectrometry* 33 (1998) 961–967.
- [27] S.A. McLuckey, D.E. Goeringer, G.L. Glish, Collisional activation with random noise in ion trap mass-spectrometry, *Analytical Chemistry* 64 (1992) 1455–1460.
- [28] R.W. Kondrat, G.A. McClusky, R.G. Cooks, Multiple reaction monitoring in mass spectrometry/mass spectrometry for direct analysis of complex mixtures, *Analytical Chemistry* 50 (1978) 2017–2021.
- [29] S. Guan, A.G. Marshall, Stored waveform inverse Fourier transform (SWIFT) ion excitation in trapped-ion mass spectrometry: theory and applications, *International Journal of Mass Spectrometry and Ion Processes* 157–158 (1996) 5–37.
- [30] A.T. Clare, L. Gao, B. Brkic, P.R. Chalker, S. Taylor, Linear ion trap fabricated using rapid manufacturing technology, *Journal of the American Society for Mass Spectrometry* 21 (2010) 317–322.
- [31] J.D. Maas, P.J. Hendricks, O. Zheng, R.G. Cooks, W.J. Chappell, Miniature monolithic rectilinear ion trap arrays by stereolithography on printed circuit board, *Journal of Microelectromechanical Systems* 19 (2010) 951–960.
- [32] M. Yang, T.-Y. Kim, H.-C. Hwang, S.-K. Yi, D.-H. Kim, Development of a palm portable mass spectrometer, *Journal of the American Society for Mass Spectrometry* 19 (2008) 1442–1448.

Miniature Monolithic Rectilinear Ion Trap Arrays by Stereolithography on Printed Circuit Board

Jeffrey Daniel Maas, *Student Member, IEEE*, Paul Isaac Hendricks, Zheng Ouyang,
R. Graham Cooks, and William Johnson Chappell, *Senior Member, IEEE*

Abstract—This paper reports the creation and characterization of monolithic arrays of miniature rectilinear ion traps (RIT) with common electronic packaging materials. Miniature ion traps benefit from a lower operating voltage as their dimensions decrease. Their integration into circuit board materials facilitates smaller and more integrated sensor systems. Arrays of ion traps provide a larger ion trap storage volume to increase sensitivity lost from size reduction. A new technique, integrating stereolithography-produced ion traps on planar rigid substrates, makes possible the 3-D isolation techniques for more complex monolithic structures. A description of the fabrication process is included. Performance-limiting metrics of the mass analyzer, such as geometrical and electrical deviations, are analyzed to determine their magnitudes for design improvement. The integration of the array with the PCB replaces complex wiring schemes with traces routed within existing multilayer substrates. The substrate can serve as the integration platform for an entire mass spectrometer in a package. [2009-0332]

Index Terms—Mass spectrometer, monolithic, rectilinear ion trap (RIT), stereolithography, 3-D isolation.

I. INTRODUCTION

AMONG the challenges facing modern society is our ability to extend awareness beyond the capabilities of our natural senses. The ability to monitor trace levels of molecules is important in the manufacture of electronics [1], food processing, and pharmaceuticals [2], to name a few examples. It is also useful in the detection of chemical warfare agents, criminal investigation, and pharmaceutical analysis [3], [4]. One of the most useful tools used in these analytical studies is the mass spectrometer. The development of the mass spectrometer over the last century has provided us with large mass range measuring capabilities and high specificity in molecular ion detection [5]. A mass spectrometer system separates chemical species according to their mass-over-charge ratios, hereafter referred to as m/z . Obtaining the mass of a molecule is useful

in deriving its chemical formula and thereby its identity. Mass spectrometers have been commercially available for several decades, albeit almost all are prohibitively large for *in situ* applications [6].

Several applications would benefit from hand-portable chemical-monitoring capabilities. Among these are inline process monitoring and fieldable substance detection [7], aiding local law enforcement in the battle against illicit drugs [8], and improving public safety through chemical warfare agent and explosives detection [7], [9]. Miniature mass spectrometers are governed by additional figures of merit over their full size counterparts. In a full size commercial mass spectrometer, resolving capability and the ability to detect over a wide mass range are highly desirable. However, in portable systems, it is also important to have lower power consumption and be of a small size and weight [5], [10].

A significant means for miniaturizing the mass spectrometer is through reducing the size of one of its primary components, the mass analyzer. This has a cascade effect and allows reduction in the size of other system components. The miniaturization of the mass analyzer began with magnetic-field-based [11] and ion-storage-type [12] mass analyzers in the early 1990s. This led to an interest in reducing the size of several different mass analyzers [7]. More recent miniaturization strategies utilize alternative fabrication strategies, such as rapid manufacturing stereolithography [13] and digital light processing [14], microfabrication [15]–[18], low temperature cofired ceramic [19], and printed circuit board [20] in order to fabricate ion traps and ion trap arrays. A benefit of miniature mass analyzers is the lower operating potential required for generating a given electric field strength [21] of a larger analyzer. Additionally, lower operating potential leads to lower power consumption and smaller size requirements of the miniature mass spectrometer system.

This paper illustrates a process for the creation of monolithic arrays of miniature-sized ion-trap-type mass analyzers (Fig. 1). The substrate provides a circuit platform for integrating this sensor into a more complete package.

The ion trap is one type of mass analyzers used in many commercial mass spectrometers. Ion traps are employed in the separation of ionized molecules of interest, analytes, by their m/z values. In an ion trap, the balance of forces is described by a second-order differential equation, which governs the movement of a charged molecule within an electric field. The solution to this differential equation reveals stability regions, defined by a few key parameters, in which ions with a range of m/z values may be trapped in stable orbits within the device,

Manuscript received December 30, 2009; revised February 26, 2010; accepted March 24, 2010. Date of publication May 24, 2010; date of current version July 30, 2010. This work was supported by the National Science Foundation under Sensors and Sensor Networks Grant SST-0528948 Thermo Scientific Instruments, Inc. Subject Editor R. R. A. Syms.

J. D. Maas and W. J. Chappell are with the Electrical Engineering Department, Purdue University, West Lafayette, IN 47907 USA (e-mail: jmaas@purdue.edu; chappell@purdue.edu).

P. I. Hendricks and R. G. Cooks are with the Chemistry Department, Purdue University, West Lafayette, IN 47907 USA (e-mail: phendricks@purdue.edu; cooks@purdue.edu).

Z. Ouyang is with the Biomedical Engineering Department, Purdue University, West Lafayette, IN 47907 USA (e-mail: ouyang@purdue.edu).

Color versions of one or more of the figures in this paper are available online at <http://ieeexplore.ieee.org>.
Digital Object Identifier 10.1109/JMEMS.2010.2048554

CHAPTER 1. AUTONOMOUS *IN-SITU* ANALYSIS AND REAL-TIME CHEMICAL DETECTION: NEW MASS SPECTROMETER CONCEPTS, INSTRUMENTATION DEVELOPMENT, AND PERFORMANCE

1.1 Introduction

Mass spectrometry has become a preferred method for chemical analysis because of the selectivity, sensitivity, speed of analysis, and wide applicability to diverse classes of chemical compounds. Not surprisingly, portable mass spectrometers are highly attractive for in-field use for the ability to complete chemical analyses at the location from which the sample(s) were obtained. Relative to the traditional practice of collecting samples in the field and then shipping those samples to a centralized laboratory for analysis, portable mass spectrometers offer greatly reduced time, cost, and effort necessary to complete the analysis. Although miniaturized and portable instruments have reduced performance relative to laboratory based instruments, this is offset for applications which have a critical dependence on the time to obtain results rather than on obtaining the lowest levels of detection, highest mass resolution, or greatest mass accuracy. The mass spectrometer(s) detailed in this work have been developed to achieve *in-situ* and in-field analysis for a diverse range of chemical compounds and a special emphasis has been made to the reduction of raw MS data to information that is represented by a series of colored LEDs.

Advancements in ion introduction,[1-3] digital electronics,[4-6] and miniaturized vacuum systems[2, 7, 8] have improved the performance of portable mass spectrometers. Current field portable instruments have parts-per-million (ppm) to parts-per-billion (ppb) detection limits, mass ranges suitable for standard organic molecules (m/z 600, or greater), unit mass resolution, and are capable of tandem MS[9]. These instruments have been developed commercially[8, 10-13] and academically[3, 14-16] and used for the detection of explosives, illicit drugs, biological warfare agents[17], food adulterants, pesticides, toxic industrial compounds (TICs), and even for select clinical applications.[18-20] Notably, ambient ionization methods have been developed for applications that overlap with those of portable mass spectrometers and have demonstrated excellent performance when compared to data from liquid and gas chromatography.

Ambient ionization methods[21] have become increasingly popular because they allow selective ionization of a wide range of chemical analytes in the presence of complex matrices without sample or surface preparation. Although these sources have been mainly characterized on laboratory based instruments they have shown reduced analysis time through the elimination of traditional sample preparation, separation, and preconcentration procedures. Furthermore, ambient ionization sources typically have simple designs and are easily coupled to the mass spectrometer inlet. All of these developments are complementary to portable mass spectrometers and contribute to the goal of realizing *in-situ* and real-time chemical analysis with a field-portable mass spectrometer.

Despite advances and commercialization of both portable instrumentation and ambient ionization methods their use, especially for in-field applications, has not become

widespread. An interesting question can therefore be posed, have advances in ambient ionization and portable mass spectrometer instrumentation come together in a manner that allow relevant compounds to be analyzed quickly, accurately, and interpreted by non-scientists? A number of challenges specific to this inquiry were considered as the design criteria for the development of the Mini-S (backpack) and thereafter the Mini 12 (desktop) miniature mass spectrometers.

- Direct sampling of ions generated at atmospheric pressures
- Detection of both positively and negatively charged species
- Integration of the ionization source with the ion inlet
- Ionization source that requires no optimization
- Sampling from surfaces with complex geometries and matrices
- Stability of the system electronics
- Low operational power
- Automated instrument operation and data acquisition
- Automated chemical library searching and data interpretation

Built on the Mini 10 and 11 platforms,[14, 22] the Mini-S and Mini12 utilize similar mechanical and turbo molecular pumps, discontinuous atmospheric pressure interfaces (DAPI),[2, 3] rectilinear ion traps (RIT)[23] mass analyzers, as well as the multipliers and dynode assemblies for detection of positive and negative ion species[24]. Performance of the miniaturized vacuum system with limited pumping capabilities is offset by short time durations of high ion/neutral conductance into the vacuum manifold from atmosphere by utilization of DAPI - a key enabler for instrumentation that is constrained by size, weight, and power. Although DAPI reduces the instrument duty cycle to approximately two percent because of its pulsed operation, the benefits of

sampling ions generated at atmospheric pressure and in sufficient quantities to afford relevant sensitivities (ppm to ppb) offset this drawback.

Because externally generated ions can be sampled at atmospheric pressures, ambient ionization sources such as low temperature plasma (LTP),[25] paper spray (PS),[26, 27] and desorption electrospray ionization (DESI)[28, 29] in addition to more general ionization sources, e.g. nano-electrospray (nESI)[30] and atmospheric pressure chemical ionization (APCI),[31] and others can be successfully coupled to the miniaturized instrument. Compatibility with a range of different ionization sources expands the classes of chemical compounds that can be analyzed relative to systems that are restricted to membrane-inlet sampling or solid-phase micro-extraction (SPME) columns and therefore greatly expands the utility this portable mass spectrometer.

In this work, the Mini-S was designed as a wearable instrument that allows for maximum portability and greatest flexibility to complete *in-situ* analysis. This system consumes an average of 65 W and can be operated on battery power for 1.5 hrs. The instrument form factor is comprised of two sections; a wearable backpack unit housing the heaviest components of the instrument (i.e. the vacuum system, electronic control boards, batteries, and plasma discharge gas) and a separate handheld head unit which contains the mass analyzer, ion detection circuit, sample inlet, and integrated plasma-based ion source, fig. 1.1. The LTP source is co-axial to the ion transport capillaries (co-axLTP) and mass analyzer and is designed specifically for geometry-independent sampling of target analytes directly from surfaces that have complex matrices and heat sensitive surfaces (i.e. human fingers, cloth, and cardboard) at levels as low as 2 $\mu\text{g}/\text{cm}^2$.

Data reduction and the reporting of chemical information specific to the sample was also considerable initiative to this project. A novice user interface (NUI) and library search software were developed in conjunction with research partners at JHU/APL to aid in instrument operation, data acquisition / reduction, and results interpretation. With this software instrument operations such as start-up, pump down, and data acquisition are reduced to automated procedures that are initiated via a click button in the NUI. In addition, data is automatically interpreted via a library search algorithm that compares MS and MSMS data against a user configurable library, and can automatically switch between positive and negative polarity during data acquisition. Results from the library search are displayed in the NUI which details the matched compounds and in addition green, yellow, and red LEDs are present on the handheld unit to act as a visual indicator of the detected threat level and instrument status.

1.2 Integration of a Low Temperature Plasma Ion Source

1.2.1 Background

The primary ion source used on the Mini-S instrument is LTP which belongs to a larger category of plasma ionization sources known as dielectric barrier discharge sources (DBDs). When used as ion sources DBDs have the following general characteristics (i) simple electrode configurations, (ii) low temperatures, (iii) ability to sustain a discharge at atmospheric pressures, (iv) can work with a variety of discharge gasses such as helium, nitrogen, and argon, and (v) have low power requirements.[32] The earliest industrial application of DBDs was for the production of ozone and used for water and surface

sterilization. More recently however, DBDs have found utility in analytical chemistry because they can ionize diverse classes of chemical compounds through soft ionization processes. Moreover, DBDs have demonstrated the ability to selectively ionize target analytes in the presence of complex backgrounds and matrices without need for sample preparation or surface conditioning and therefore belong to the larger, more general, category of ambient ionization sources.[21]

DBDs differentiate themselves from other plasma sources because an AC voltage, as opposed to DC, is used for plasma generation (due to the use of a dielectric) and therefore has different chemical / electrical properties that influence the characteristics of the plasma such as temperature, electron density, and reagent ion species generation. Three of the most prominent DBDs that have demonstrated analytical utility are LTP developed by this lab, dielectric barrier discharge ionization (DBDI) developed by X. R. Zhang,[33] and plasma-assisted desorption / ionization (PADI) developed by M. McCoustra.[34] Of the three, only PADI operates at high frequency RF (<13 MHz @ 200-500 V_{p-p}, >5 W) while DBDI and LTP operate at much lower frequencies and are typically ~20 kHz (3500 – 4500 V_{p-p}, 5 – 30 W) and ~2.5 to 35 kHz (2500 to 5000 V_{p-p}, >3 W) respectively.

Differences between DBDI and LTP sources exist in the arrangement of the source electrodes with respect to the sample and inlet of the mass spectrometer. In the case of DBDI the high voltage electrode is a hollow metal needle, supplying the discharge gas, and is positioned over top of a counter electrode with the dielectric barrier and sample (the sample alone may serve as the dielectric barrier) in between the two

electrodes. When the discharge occurs the sample is inside the discharge region and is in direct contact with the ionizing species generated by the plasma, fig 1.2.

The electrode configuration for a LTP source is different from DBDI in that the electrodes are arranged concentrically around a glass or quartz dielectric. The outer electrode is the HV electrode and the inner electrode (surrounded by the glass or quartz dielectric) is the counter electrode which is typically at ground. In this arrangement the discharge occurs through the dielectric, between the two electrodes, and in the presence of the discharge gas, fig 1.3. All of the electrons, ions, excited neutrals, and neutral molecules generated during the formation of the plasma (and shortly thereafter) are pushed out of the source discharge region via positive discharge gas pressure and toward the sample surface where they interact with the sample. This region of the plasma is referred to as the plasma afterglow.

The LTP source design eliminates the need to have a counter electrode and dielectric underneath the sample in order to generate a discharge. This greatly improves the flexibility of analyzing compounds directly from surfaces without having to disturb the sample or make provisions for surfaces which are geometrically complex. This in combination with the fact that positive and negatively charged ions can be generated with roughly the same source conditions and there is no requirement for additional solvents or chemical reagents needed to affect analyte ionization was the basis for using LTP on the Mini-S instrument. Although the configuration of the LTP probe that was eventually coupled to the Mini-S instrument is different than LTP sources that have been previously investigated,[25, 35-37] general characteristics such as operational frequency, input voltages / operating powers, electrode distances, material of the dielectric barrier,

discharge gas, and gas flow rates remained relatively the same. Thus the same processes that were thought to affect ionization in previous work with LTP are assumed.

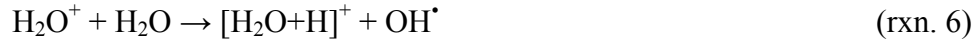
The field of study pertaining to creation and characterization of plasmas and subsequent analyte ionization are both large and complex. While it is not the purpose of this text to provide a comprehensive analysis of this area of study it would be incomplete if the major processes involved in plasma formation and the formation of analyte ions were not introduced.

As previously discussed the LTP is a DBD ion source that is operated at atmospheric pressure. These sources are referred to as having a pulsed operation because an AC waveform is utilized to generate a breakdown (discharge) across the dielectric barrier. Breakdown occurs when the electric field across the dielectric barrier gap exceeds the threshold necessary to induce an electrical breakdown. The breakdown threshold between the electrodes is dependent upon the (i) dielectric material and thickness, (ii) distance between electrodes, and (iii) discharge gas.[32, 38] This process occurs approximately once every half cycle of the applied waveform resulting in plasma that is formed by small micro discharges that occur randomly in space and time inside the source. These discharges are responsible for generating the free electrons, ions, and excited state molecules that comprise the plasma.

Two main types of plasmas may be formed, (i) streamers which are observed as discrete breakdown events that have a filament appearance and (ii) Townsend breakdown which is characterized by a more homogenous discharge that spans the length of the electrodes. Although the physical and chemical properties of the LTP used in this work were not fully characterized, the plasma generated by the LTP exists with Townsend-like

characteristics. Therefore, literature values for maximum ion densities (10^{11} cm $^{-3}$), current density (10 - 100 mA/cm 2), as well as other properties, reported for Townsend breakdowns in helium serve as relevant estimates for understanding physical characteristics of the LTP source.[38]

An important characteristic of LTP is that analytes are exposed directly to the plasma in the open atmosphere and are thus in contact with high energy species that have relatively long life times. It has been discussed that excited helium atoms also known as helium metastables (He^* , 19.8 eV) can ionize analyte ions directly through, penning ionization (rxn. 1), or through the same processes ionize water (rxn. 2) and nitrogen (rxn. 3) from atmospheric vapors. Once ionized, water and nitrogen are subsequently involved in the reaction pathway for the formation of water clusters that contain an acidic proton which is the proton source for analyte ionization (rxn. 4 – 8).[39, 40] This cascade of chemical reactions which lead to the formation of water clusters is well known and accepted to be the same processes involved in atmospheric chemical ionization (APCI).[31, 41]





From the reaction pathways detailed above it is apparent that N_2^+ is a key intermediate in formation of reagent ions that ultimately lead to analyte ionization. Recent work by G. M. Hieftje has used time-resolved spectroscopic methods to investigate the ionic and excited state species generated in a He-LTP source. This work established He_2^+ as the dominate positive ion formed in the plasma and also acts as an energy carrier into the afterglow region of the source. Based upon the co-existence of He_2^+ and N_2 in the same spatial location, overlap in excited state energies of these species, N_2^+ rotational temperatures, and other supporting evidence, it was concluded that charge transfer from He_2^+ to N_2 (rxn. 9) , and not penning ionization via He^* , is the more prominent reaction pathway for N_2^+ formation.[39]



The authors were careful to note that this study and its finds are only valid for He plasma sources in which there is a direct interaction between the plasma and the surface sample in the presence of N_2 . Conditions in which no interactions are allowed or if the ionic species are prevented from making contact with the sample would preclude these findings from being valid.

1.2.2 Co-axial LTP Source Development and Characterization

A new LTP source configuration in which the plasma probe(s) were aligned co-axially with the ion inlet capillary was developed to allow the sampling of surfaces independently of the geometry of the ion source and sample introduction capillary of the mass spectrometer. In the case of the Mini-S instrument the ion introduction capillary is located on the hand-held head unit. During operation of the source, ionizing species from the plasma probe are in close proximity (1 - 5 mm) to both the sampling surface containing the target analyte and the introduction to the mass spectrometer. Helium, the discharge gas, is supplied at (80 – 120 ml/min) via a T-fitting that generates positive pressure inside the plasma source which causes the plasma afterglow to impinge upon the sample surface. The discharge gas is heated via Joule heating[42] inside the source and subsequently transfers thermal energy to the surface via direct contact which aids in desorption and ionization of the target analyte(s). In situations where increased surface temperatures were needed for desorption of compounds with low vapor pressures, e.g. PETN and RDX[43] (1.16×10^{-8} and 3.3×10^{-9} Torr, respectively). the operational conditions of the could be tuned to supply additional input power (~ 14 W) which increased surface temperatures to 80 °C at source-to sample-distances of 1 to 2 mm.

The first iteration of the co-axLTP source utilized arrays of LTP probes. Work with LTP arrays was pioneered by Jon Dalgleish in an effort to improve the desorption and ionization characteristics of low temperature plasma sources. Specifics related to construction and characterization of the LTP arrays are detailed in his thesis[44] however, briefly, probe construction of the first iteration of the co-axial LTP array is as follows: 6 or 7 quartz tubes (each forming a plasma probe) surround the stainless-steel ion inlet

capillary connected directly to the DAPI valve (10-cm long, 250- μm i.d.). The inlet capillary is wrapped in Kapton HV tape to isolate it from the high-voltage electrode surrounding the individual plasma probes. When fully assembled this configuration utilized an array of 6 or 7 micro LTP probes arranged concentrically around the ion inlet capillary of the mass spectrometer and were aligned along the same axis of ion introduction hence the name co-axial LTP, fig. 1.4. Extensions to this work and several iterations of the co-axial LTP probe design were necessary in order to develop a LTP probe that could withstand increased voltage amplitude inputs necessary to volatilize compounds with low vapor pressures and to simplify the probe design such that it would be acceptable for field use.

The second design modification utilized the original 6-probe coaxial LTP, previously described, except that the length of the outer, high voltage, electrode for the LTP was reduced from 30 to 6.5 mm. A shorter electrode length reduced the contact area along the grounded inlet capillary and created a more energetic discharge with increased power density. This design also had the advantage of being shorter than its predecessor, thus, lighter and more maneuverable as the instrument frontend, fig. 1.5. While it did produce high quality mass-spectral spectra for TNT and RDX, it continued to suffer the same malfunctions as its predecessor. Sustained operation of the source could not be achieved at a voltage amplitude of 6kV_{p-p} which was necessary to desorb and ionize compounds with low volatilities, fig. 1.6. The primary cause of the failure was due to the high voltage applied to the source electrode which discharged through the dielectric barrier that insulated the grounded ion inlet capillary. Two types of 3M dielectric tape were investigated as the insulating material P/N 1205 (dielectric breakdown 7500 V) and

P/N 1350F-1 (dielectric breakdown 5500 V), both exhibited the same failure over the same time period of operation. This issue in combination with the amount of time that was necessary to construct these sources (>2 hours) as well as the ability to clean a contaminated probe led to the exploration of alternative electrode configurations for the LTP probe and the use of air instead of helium as the discharge gas.

Temperature measurements of the LTP source under different operating conditions were conducted in an effort to characterize the new LTP probe design. The first of these experiments utilized the co-axial LTP array that used air instead of helium (He) as the plasma gas. The plasma generated with air was 7 - 12 °C hotter, as measured with a thermocouple than helium under similar gas flow rates and was attributed to the fact that slightly elevated input powers were necessary in order to sustain the plasma in the case of the air discharge. This increase in plasma temperature transfers more thermal energy into the surface of the sample, improving desorption. Data for RDX response at different input power levels was acquired with the Mini-S using a typical scan function that utilized a 15 -25 ms DAPI pulse widths, fig. 1.7. Increased input power corresponded to increased plasma temperature and therefore improved signal.

In an effort to develop a probe that could withstand high input powers a single LTP probe was integrated with the ion inlet capillary by suing a 42.5 mm long quartz tubing (4 mm OD, 2 mm ID) which formed the dielectric barrier and surrounded the ion inlet capillary to the mass spectrometer. The high voltage connection for the LTP is supplied to an electrode on the outside of the quartz while the ion transfer capillary continued to serve as the counter, grounded, electrode, fig. 1.8. In this configuration the discharge region is between the inside surface of the dielectric and the grounded ion inlet

capillary. The high voltage waveform applied to the LTP probe was approximately 2 kV_p - p at 27 – 33 kHz. Input powers of approximately 1 W were used for most compounds analyzed and under these conditions the ionization performance of this probe was identical to the LTP arrays. However, under conditions where increased input powers were necessary, this probe could withstand up to 14 W of input power, though when used in the high power mode the source was typically operated at ~8 W.

With the use of a thermocouple, a maximum gas temperature of 50 °C was measured for the single LTP co-axial source at 8 W of input power. This is at least 10 °C hotter than measured for the LTP arrays. This allowed helium to again be utilized as the plasma discharge gas- although either helium or air could continue to be utilized. In addition to generating increased surface temperatures at lower input powers, the new source configuration demonstrated continued ionization for both polarities (positive and negative analytes) and the signal response was more reproducible than observed with the arrays.

1.2.3 Thermographic and Schlieren Imaging of co-axLTP

1.2.3.1 Thermographic Imaging

Thermal profiles of the single co-axial LTP were characterized using a Fluke Ti40 thermographic camera (Everett, Washington, US). The thermographic image was taken from a glass slide that was used as the simulated sample surface. In this experiment a LECO HT Unique (LECO Corp. St Joseph, MI) mass spectrometer was outfitted with DAPI inlet that was combined with a co-axLTP source. The DAPI was pulsed open for

15ms and then closed for the following 2.5 seconds in order to simulate operation of the LTP on the Mini-S instrument. The glass slide was placed directly in front of the LTP to simulate a sampling surface. Distances between the source and the glass slide were varied from 1 to 10 mm and the thermographic camera was placed directly behind the glass slide at a distance of 6 in. Thermal profiles of the glass slide were taken starting with the farthest distance (10 mm) and then moved closer to the source by increments of 1 mm. At each increment the glass slide was allowed 30 sec for the temperature to equilibrate. A profile of the surface temperature was generated by repeating this process for input powers from 2 to 14 W, fig. 1.9. It was demonstrated that at input powers of ~8 W the LTP source could heat the sample surface to ~50 °C at source-to-sample distances of up to 2 mm. The same characterization was completed with the co-axLTP array. Figure 1.10 is a plot of the maximum surface temperatures obtained on the glass slide for the single probe and array LTP configurations. In this figure it is demonstrated that increased surface temperatures of approximately 5 to 10 °C over the same source-to-sample distances and operational conditions are achieved.

1.2.3.2 Schlieren Imaging

For LTP, the plasma afterglow is in direct contact with the sample surface. Helium is less dense than air, and therefore has less surface area contact with the sample surface at increasing standoff distances which potentially limits the formation of analyte ions. Additionally, the pulsed nature of the DAPI valve directly affects the sensitivity of the instrument as it is the mechanism for introducing ions to the mass spectrometer.

Because this system relies on the pressure differential between the ambient atmosphere and the vacuum manifold to sample gas phase ions, there is a limit to distance over which ions can be sampled. To characterize and visualize (i) complex gas flows at the interface of the afterglow and sample surface and (ii) sampling of ions at atmospheric conditions Schlieren imaging was utilized as an optical characterization method. This technique has been recently used to characterize other helium, plasma-based, ambient ionization sources for the same purposes.[45]

The Schlieren imaging apparatus is detailed in figure 1.11; the co-axLTP and DAPI source installed on a development version of the Mini 12 was placed inside the collimated light path. It was possible to visualize the helium gas leaving the LTP source which showed that source-to-sample distances of greater than 5 mm had significantly less interaction with the He plasma gas. Furthermore, upon actuation of the DAPI valve it was observed that the sampling of ambient gas in excess of 5 mm was no longer apparent from the Schlieren image. Thus placing an upper limit for the source-to-sample distance for which analyte ions are reliably generated and sampled the Mini-S instrument, fig. 1.12. These observations agreed well with the source-to-sample distances used in actual analysis. All of the sample analysis work completed detailed in subsequent sections was acquired with at source-to-sample distance of approximately 2 to 5 mm.

1.2.4 Co-Axial LTP and Mini-S Instrument Performance

Human fingers, paper, latex, cotton fibers, glass and other surfaces with complex geometries such as the inside corners of a box were analyzed using the co-axLTP source interfaced to the Mini-S. Illicit drugs, CWAs, and explosives at $\mu\text{g}/\text{cm}^2$ levels were

successfully detected at $\mu\text{g}/\text{cm}^2$, or lower quantities, fig 1.13 - 1.15. Helium flow rates for this analysis were approximately 0.1 LPM and input powers were typically less than 1 W. In situations where increased thermal desorption was required for low volatility compounds, e.g. PETN and RDX, input powers were increased to ~8W to aid in thermal desorption. Operation of the increased power mode was supported through the software interface and could be enabled or disabled as needed.

Normal operating parameters produced a maximum mass-to-charge range of 100 to 930 amu, using resonance ejection[46, 47], as verified using sodiated polyethylene glycol $[\text{PEG}+\text{Na}]^+$, fig. 1.16. For mass analysis, the RF amplitude was scanned at a rate of 12,000 amu/s and utilized resonance ejection at a 369kHz ($q_z = 0.81$) with the AC ramped from 700 mV to 3.0 V over the scan. Ion introduction periods were between 15 and 25 ms, during which time the vacuum manifold pressure increased to approximately 100 mTorr. After ion introduction the manifold pressure was allowed to drop to approximately 1.5 mTorr, ~ 2 s after ion injection, before initiating mass analysis fig. 1.17. Total mass spectral scan times were 2.3 s and under these operating conditions mass resolutions of 1-2 amu FWHM were obtained across the mass range as standard full MS scan performance. This resolution was sufficient to resolve the X+2 isotopic distribution of halogen containing chemical species at mass-to-charge 240 with less than a 10% valley from the baseline, fig. 1.18. It should be noted that under the best operating conditions in which the number of ions introduced into the trap was carefully controlled and with appropriately tuned RF/AC amplitudes and frequencies, the FWHM for analyte peaks can have values of ~0.6 amu, in a full MS scan. This resolution is enough to distinguish chemical species 1 amu apart with less than a 60% valley as measured from

the baseline. This is demonstrated in fig. 1.19 where the pseudomolecular ion $[M-H]^-$ and molecular $M^{\circ\circ}$ for TNT, m/z 226 and 227 respectively, are clearly resolved. The resolution does however fall with increasing mass.

A key functionality of ion trap mass analyzers is that multiple stages of tandem MS can be performed with a single analyzer.[48, 49] This functionality allows for structural characterization, increased confidence in analyte identification (via fragment ions), and enhanced detection limits by improving the signal-to-noise ratio. Multiple stages of tandem MS was performed on cocaine. Fragmentation of the protonated molecular ion m/z 304 → 182, demonstrated the loss of benzoic acid, and subsequent fragmentation of m/z 182 → 150 & 122, with the concerted loss of methanol and carbon monoxide, respectively, fig. 1.20.

1.2.5 Power Consumption, RF Voltage, and Batteries

One of the key considerations for a field-portable instrument is the amount of power that the system requires to operate. Low power requirements are valued because this typically translates to increased operation time and a reduction to the weight of the instrument by allowing for smaller and lighter components to be used. Monitoring the power consumption of the instrument during operation is therefore of interest and provides information that is of diagnostic value because it provides insight that is not accessible by monitoring the RF voltage or operating pressure alone.

Cumulative current draw for the Mini-S instrument was measured with a Fluke 80i-110s current clamp (Everett, Washington, US) placed between the AC/DC converter and the main instrument-power input. Each of the system components (e.g., diaphragm pump,

turbo pump, power distribution board, high-voltage board, etc.) was turned on sequentially to monitor the power draw for each, table 1.1 and fig. 1.21. Once under vacuum, power draw of the system was monitored during operation which included actuation of the DAPI and sample valve, utilization of the on board LTP power supply, and RF amplitudes necessary to achieve mass analysis.

Information about the performance of individual instrument components relative to system-level events, i.e. ion introduction and mass analysis, was obtained by measuring the power consumption during instrument operation. For example, the rapid increase in manifold pressure (~ 100 mTorr; 15-25 ms DAPI pulse) during ion introduction is identifiable from the increase in power consumption of the mechanical and turbo molecular pumps in response to elevated manifold pressures, fig. 1.22. During the 1.26 sec after actuation of the DAPI valve the pumping system required 4.9% more power to re-establish mTorr pressures in the manifold necessary for mass analysis. Another example is the power consumption associated with the RF. While the RF is on and ions are confined inside the electrodynamic field of the ion trap 13.5% of the total power is used by the RF system just to confine the ions. This can be compared to the power consumed by the RF system during mass analysis; upon scanning the RF amplitude necessary to eject m/z 930 (~ 6.2 kV_{p-p}) the instantaneous power consumption was 144 W, representing 58.5% of the total power. By way of comparison scanning to m/z 550, 98 W, was only 38.9%, fig. 1.23. Thus, monitoring multiple aspects of the instrument provides insight and connection between events, the timing of events, and system components that impact the instrument design.

As a requirement for autonomous operation, the Mini-S instrument needed to operate on batteries. For evaluation of the nickel-metal hydride (NiMH) batteries obtained from BaterySpace (1410 g, 4200 mAh, CU-MM105 | ID 4725) the Mini-S instrument was fully vented to the atmosphere and powered down before it was connected to a battery pack. All batteries were charged for a minimum of 8 hours and measured ~25.9 V prior to instrument testing. Table 1.1 contains details related to the comparison of vacuum pressure and power consumption during the initial startup of the instrument; once connected to a battery pack the main instrument power was turned on and the vacuum system started. The vacuum system reached pressures of $<1\text{e}10^{-5}$ Torr in ~10 min at which time analytical mass scans were run continuously for a maximum of ~80 min before the battery was depleted (< 22.3 V). During the 80 min of mass analysis all of the onboard devices were in operation, this included the voltage for the ion source, actuation of the DAPI valve for sample introduction, RF ramp for mass analysis, and the writing of mass-spectral data to the computer hard drive. It should be noted that the average power for the system during operation was 65 W regardless of the maximum mass-to-charge used in the analytical scan and the 90 min battery life was not significantly impacted by the mass to which the RF amplitude was scanned, i.e. m/z 930 or m/z 550. Additional battery technologies have also been investigated. Under similar test conditions, high discharge lithium polymer (Li-Po) batteries obtained from Tenergy (Fremont, Ca, US) (725g, 5000 mAh, item no. 31428) have demonstrated total runtimes of ~200 min, 122% longer than NiMH and are lighter by 48.6% and therefore show promise as a replacement technology, fig. 1.24.

1.3 Instrument Hardware

1.3.1 Backpack Assembly

Fully assembled, the Mini-S instrument is comprised of two major components; a wearable backpack and a handheld head unit. The backpack portion of the instrument weighs 10 kg when fully assembled and contains the heaviest components of the instrument. Table 1.2 details the Mini-S instrument systems located in the backpack. Briefly, these systems are the vacuum pumps, electronics, power, ion source gas supply, and the ion source power supply. A KNF Neuberger (Trenton, NJ) mechanical pump (5 L/min) and a Pfeiffer Vacuum HiPace10 (Nashua, NH) turbo molecular pump (10 L/s) comprise the vacuum system and are mounted to a lightweight aluminum (5052) frame (30.43 x 11.68 x 30.43 cm) which forms the backpack portion of the instrument. Integrated with the aluminum frame are provisions to mount an onboard gas regulator and miniature Helium tank (Leland Limited, Inc.; South Plainfield, NJ) for the LTP source, a dual mode on-board power supply for the LTP source, and a 24 V rechargeable battery. Also, all of the system electronics were contained in the backpack along with two fans (6.35 cm, 24 V) to ventilate the backpack unit, fig. 1.25.

1.3.2 Hand-held Head Unit: Ion Introduction, Mass Analyzer, Detector, and Connections

Development of the hand-held head unit was to allow for *in-situ* analysis of target analyte(s) directly from geometrically complex surfaces and to maintain the dexterity of a hand held device. In order to allow for the most efficient desorption, ionization, sampling,

and subsequent transfer of ions to the mass analyzer (all of which impact instrument sensitivity) the analyte, ionization source, sampling mechanism, and mass analyzer needed to be located in close proximity to each other. These requirements were satisfied by reducing the shape and size of the instrument manifold so that it could be hand-held and by development of the co-axLTP source. The mass analyzer, located inside the head unit, was linearly integrated with the source to allow for efficient introduction and transmission of ions to the mass analyzer from atmospheric pressures, fig. 1.26.

Similar to earlier iterations of Mini mass spectrometers, the Mini-S utilizes a RIT as the mass analyzer and a detector that is made up of an electron multiplier (EM) (Detector Technologies, Inc., model no. 2300) and dynode for detection of positive and negative ions.[24] The distance between the Y-electrodes of the mass analyzer and the center of the conversion dynode is 0.4 in and is consistent with dimensions implemented on previous Mini 10.5 and 11.5 instruments. The detector housing and the dynode material also remain unchanged from earlier designs. The angle of the detector was modified for the Mini-S from 50° to 90° to allow for placement inside the handheld manifold. In order to maintain the same vertical height as the ion ejection slit on the x-electrode of the mass analyzer the detector was mounted to a pedestal with a height of 1.0 cm. The head unit was constructed from aluminum (6061) (8.13 x 7.37 x 7.62 cm) and weighs 2 kg when fully assembled. Vacuum was maintained in the head-unit via a 76 cm stainless-steel vacuum bellows (Krut J. Lesker; Clairton, PA) that was connected to the vacuum system on the backpack. Details related to the components integrated with the head unit can be found in table 1.3.

It is important to note that for the Mini-S design, the RF-amplification circuit is split between the backpack, containing the inductance coil, and the head unit containing the mass analyzer. This required an unusually long cable connection between these two components to transmit the main RF signal and represented a departure from the design of typical mass spectrometers in which the mass analyzer and inductance coil are often intentionally close together in an effort to minimize capacitance associated with the amplification circuit. Taking advantage of the low capacitance of the RIT mass analyzer ($\sim 22 \text{ pF}$) and a specially designed inductance coil ($\sim 300 \mu\text{H}$), a connection from the RF coil to the mass analyzer on the head unit was made with a low-capacitance high-voltage cable (RG62/U, 44.62 pF/m). This allowed the resonate frequency of the main RF circuit to be 1MHz. Operating at 1MHz provides a balance between the dimensions and type of analyzer used, mass resolution, and mass range for voltage-limited applications.[9, 50] The RF signal connection was made with a hermetically sealed MHV connector (Pasternack Enterprises, PE4311, Irvine, Ca, US); all other electrical connections were made with 102 series Fischer connectors (Fischer Connectors, Switzerland).

1.3.3 Vacuum System

Vacuum system performance of the Mini-S manifold was characterized with different vacuum configurations, manifolds used on the Mini11.5 instrument, and in the presence of air, helium, or a mixture of the two which were used for the LTP source. The discharge gas for the plasma source is injected into the vacuum manifold along with ions during actuation of the DAPI valve and therefore has an effect on the performance of the vacuum system as the pumping speed of the turbo drops from 10 L/s in air to 6 L/s in

helium. For these characterization tests the DAPI valve was opened for 15 or 17 ms (depending upon the experiment) and then closed. During the following 2.8 seconds the vacuum system was allowed to pump out the vacuum manifold before the next DAPI pulse. Pressure was monitored directly from the analog read back on the MKS, 925C pressure transducer (Andover, Ma, US) connected directly to the manifold. Ion transfer capillaries, DAPI valve, and DAPI tubing were the same as those previously described and are detailed in table 1.3.

1.3.3.1 Vacuum Manifold Characterization

Performance of the Mini-S manifold was compared against two manifolds that were formerly used on Mini 11.5 instruments and previously demonstrated the ability to obtain pressures of 10×10^{-6} torr or lower. The three manifolds were tested using identical scan functions and under conditions of air, continuous helium at 0.1 LPM, and short, timed, pulses of helium (also at 0.1 LPM) as the discharge gas for the ions source. Each manifold tested used the same vacuum system which consisted of the rough and turbo pumps previously described which were connected to a KF40 bellows with a handle; configuration 4 in the following section. Helium was supplied through the co-axLTP ion source and during the pulsed helium experiments a control valve supplying helium to the source was actuated from the Mini-S software. In this experiment the co-axial LTP utilized an ion inlet capillary of 500 μm that was 10 cm in length. The remaining source design is consistent with that of other co-axLTP sources which have been previously described.

Two ‘pulsed gas’ experiments were conducted, one with the helium valve open for 17 ms, simultaneously with the opening of the DAPI valve, and a second in which the helium valve was open for 60 ms immediately before and then during the 17ms DAPI pulse- for a total time of 77 ms. Data shown in Figure 1.27 was generated by setting the air or helium conditions, allowing the instrument to pump down to its base pressure of 1×10^{-5} Torr, actuating the DAPI control valve for 17 ms, and then recording the system pressure from its maximum, 100×10^{-3} Torr, throughout the duration of the scan. Five consecutive scans were executed without allowing the instrument to return to base pressure. The five scans for each manifold were averaged and then plotted. As anticipated, the general performance for each manifold was better (i.e. lower pressures reached faster) for air than for helium, which is due the pumping capabilities of the turbo for the two gases (10 l/s vs. 6 l/s). Also, readily explained are the similarities between pressure curves for the 17 and 77 ms of pulsed helium to that of air and continuous helium, respectively. Because the pump down speed of the system is dependent upon the gas injected into the manifold, it can be inferred that the gas composition for the 17 ms helium pulse was primarily air while that of the 77 ms pulse was helium based upon a comparison to the respective pressure profiles of air and helium. What is not yet fully understood is the tailing off that is exhibited by the Mini-S manifold upon reaching pressures in the low mTorr pressure regime. It is suspected that this phenomenon is due to a weak vacuum seal or a damaged seal in the electrical feed through which presents itself only within this pressure range, increasing the time for the system to reach base pressure. While this performance of the Mini-S manifold is not ideal, it does not inhibit data acquisition, require further instrument development, or decrease duty cycles due to

unnecessarily long pump-down times. This instrument can be operated inside 1×10^{-3} to high 1×10^{-4} Torr pressures and deliver good analytical performance in terms of mass resolution and sensitivity. Additionally, the graph for ‘Air’ demonstrates that the pump-down speed for the Mini-S manifold from 100×10^{-3} (5.0 volts) to 1×10^{-3} Torr is comparable to the Mini 11.5 over this pressure range. Thus, the time between ion introduction until the manifold pressure is low enough that the amplitude of the RF for the mass analyzer can be scanned (<1.5 s) is roughly the same between the two manifold designs.

1.3.3.2 Vacuum Bellows Characterization

Placement of the vacuum system components plays a critical role in the efficiency of the vacuum system, i.e. time necessary for the manifold to reach mTorr pressure, and therefore feasibility of the instrument design and analysis duty cycle. Four different vacuum configurations were investigated by injecting a 15 ms pulse of air or helium into the manifold by actuation the DAPI valve and then monitoring the manifold pressure response with respect to time.

1. Manifold connected directly to the turbo and rough pump
2. Manifold connected directly to the turbo and 4-ft PFA tube (0.25" OD x 0.2" ID) connecting the turbo to the rough pump
3. 2-ft bellows with 25 mm ID between the Manifold and vacuum system
4. 2-ft bellows with 40 mm ID between the Manifold and vacuum system

Configuration 1 was established to determine the baseline performance of the Mini-S manifold. This configuration demonstrated the best pressure-time profiles in terms of needing the least amount of time to reach mTorr pressures. These results were mirrored

almost identically with configuration 2, indicating that the roughing pump used in this application (10 L/min) was large enough to successfully back up the turbo pump with the 4 ft extension and that keeping the volume of the high vacuum region small translates directly to improved pressure-time profiles. This insight led to the suggestion of a third form factor for the Mini-S instrument, one in which the turbo pump is located at or near the instrument handle. This option however, was forgone in favor of keeping the head unit small and flexible and to avoid increases to the size and, or, weight. It is planned however, that the feasibility of such a design will be investigated in the near future.

Even though implementation of 2-ft (configuration 3 and 4) bellows used to connect the turbo pump to the manifold required additional time to reach mTorr pressures and ultimately reduced the analysis duty cycle relative to configuration 1 and 2 due to the increased volume, operation of the instrument with 2-3 sec scan times was acceptable and delivered good analytical performance at 10^{-3} to high 10^{-4} Torr. Although the total volume for configuration 4 was larger than configuration 3 due to the larger diameter bellows (25 vs 40 mm) configuration 4 had a slightly better pressure-time profile due to the increased cross-sectional area. For this reason and because the KF40 bellows were significantly more flexible, when under vacuum, they were incorporated into the final design, fig. 1.28.

1.4 Instrument Control Electronics and Software

The instrument control architecture, printed circuit board (PCB) design / layout, mechanical design, and user interface software, for the Mini-S was developed at Purdue University. In particular the digital and analog board sets which form the core instrument

control for the Mini-S and Mini 12 instruments was pursued by Matt Kirleis as his thesis work.[4] He details the development of the instrument control architecture, namely the implementation of a field programmable gate array (FPGA) coupled to a digital signal processor (DSP). This digital control architecture was the key enabler for functionality such as digital RF feedback control, generation and playback of Stored Waveform Inverse Fourier Transform (SWIFT)[51] waveforms for ion isolation which were unavailable on the Mini 11[22] and 11.5 instruments. Additionally, the FPGA was programmed to function as a direct digital synthesizer (DDS) for RF and AC signal generation. Because these features are critical to the operation of all mass spectrometers and represent forward progress in the development of field portable mass spectrometers, short discussions of each of these functionalities are included in this chapter.

1.4.1 Printed Circuit Board Design and Fabrication

All of the electronic circuit designs were completed using schematic capture design software (OrCAD 16.2.0.p001; Cadence, San Jose) and transferred to a physical layout design before being sent to Sierra Circuits (Sunnyvale, CA), a commercial PCB fabrication company. Many of the electronic circuits were designed for PCBs that required multiple layers to support internal grounding planes, shielding for electronic signals, and internal connections between components on opposite sides of the PCB. The digital control board is the most dramatic example, fig. 1.29. In total, eleven different PCBs are required to complete one full board set for the Mini instruments; tables 1.2 and 1.3 detail the connectivity of the instrument PCBs and provide descriptions of individual boards.

1.4.2 Instrument Control Software and Firmware

1.4.2.1 Firmware

Mass spectrometer instrumentation is inherently complex due to the heavy integration of electronic control that is needed in order to synchronously operate multiple devices to produce a mass spectrum. Located on the digital control board is the DSP (TMS320F2835PGFA, Texas Instruments; Dallas, TX) which is used in tandem with a FPGA (Cyclone III FPGA, Altera; San Jose, CA) to manage instrument to data system communication (5 MB/s), scan function execution, data acquisition (10 Msps), direct digital synthesis (DDS) waveform generation, Stored Waveform Inverse Fourier Transform[51] (SWIFT) signal generation and playback (30 Msps), and error correction to RF amplitude linearity, fig. 1.30.

1.4.2.2 RF Generation

Main RF and supplementary AC waveform generation is completed using the FPGA programmed to operate as a DDS. Waveform generation includes frequency generation and amplitude modulation prior to the waveform being sent (30 Msps) to the DAC and subsequently on to the RF amplifier (main RF waveform) or AC amplifier (supplementary AC waveform). Waveform signals for the main RF and AC of the Mini-S were compared against the Mini11.5 to evaluate the performance of the FPGA operated as a DDS. At 1MHz (main RF) the FFT magnitude was higher, had lower total harmonic distortion (THD), and had a higher spurious free dynamic range than the Mini11.5-

indicating the generation of a high fidelity RF signal. The same characterization with similar results was obtained for the supplemental AC waveforms.

As previously discussed the RF voltage amplitude is generated by using a resonate circuit designed with a resonant frequency of 1 MHz. Resonate circuits are discussed in electrical engineering and instrumentation texts and are represented by the following equation:

$$f_{res} = \frac{1}{2\pi\sqrt{LC}} \quad (\text{eqn 1})$$

Where f_{res} is the natural oscillation frequency for the circuit, C is the total capacitance of in Farads (F) and L is the value of the inductor in Henry's (H). When used in a quadrupole mass spectrometer typically the capacitance value of the mass analyzer is the major contributor to C and the inductance coil is the major contributor to L . Because of the design of the Mini-S in which the mass analyzer is located in the hand-held head unit and the inductor is located in the backpack, the cable used to connect the RF signal from the inductor to the mass analyzer also becomes a significant contributor to the overall capacitance of the circuit. Inductor values used on the Mini-S were $\sim 310 \mu\text{H}$ and the total circuit capacitance was divided between the RF cable $\sim 45\text{pF}$ and the mass analyzer $\sim 20\text{pF}$ in order for the RF amplification circuit to have a resonant frequency at 1 MHz; tables 1.2 and 1.3 respectively.

The Mini-S RF amplifier circuit is capable of achieving a maximum output voltage of $\sim 6 \text{ kV}_{\text{p-p}}$, at 1 MHz, which corresponds to a maximum detectible mass-to-

charge of 930, fig 1.16. Given this performance the RF voltage amplitude is no longer a bottleneck to completing analysis of organic molecules such as explosives, chemical warfare agents, and illicit drugs. In fact the voltage amplitude generated for this field-portable instrument is inside the range which would be useful in the detection of biological agents, such as lipid analysis from microorganisms or lipids from tissues. Due to these findings an experimental RF circuit was created to further increase the maximum voltage output. Modifications were made to the power distribution board, RF amplifier board, and RF coil board. This circuit was implemented on a Mini 12 which could support a larger inductor because of its large form factor. Details of this investigation and demonstration of increased mass range of 100 - 1300 amu at 1 MHz is detailed in chapter 2.

1.4.2.3 Digital Feedback Control

Electronic systems include instrument state/status communication(s), event timing, waveform generation, voltage amplification, and data acquisition. Failure to execute the required process with high fidelity (e.g., carrier frequency generation, amplitude modulation, error correction, etc.) will lead to poor mass resolution, incorrect mass assignments, and truncated mass ranges. A digital feedback circuit for the main RF running a proportional, integral, differentiation (PID) controller is used in place of a traditional analog feedback circuit to maintain RF amplitude linearity during the RF ramp of the mass selective instability scan. PID controllers are described elsewhere in the literature however, briefly, these controllers are software based elements that utilize the

current (P), cumulative (I), and rate of change (D) of the error (defined as the difference between the input RF signal and the demodulated feedback RF signal) to predict the magnitude and direction of future errors in an attempt to drive the error to zero.

In the current design the modulated RF feedback signal is sampled through an ADC connected to the feedback signal line on the RF amplifier, the signal is interpolated to 40 Msps inside the FPGA, demodulated, and then corrected for errors in linearity using the PID controller (also run though the FPGA) before the corrected waveform is sent back to the DAC and RF amplifier. This strategy provides a method for error correction during periods of extended operation that may lead to mass drift caused by heat, component fatigue, or changes in the surrounding environment. When operated with the digital control enabled mass drift was measured to be 0.6 to -0.2 amu over one hour of consecutive operation. Under the same test conditions the analog feedback control implemented for the Mini11.5 had a drift range of 1.7 to -0.5 amu; fig. 1.31. Updating the feedback control parameters, or, updating the entire feedback control algorithm as opposed to making hardware modification(s) is particularly advantageous in situations where the instrument is deployed in an environment that is not immediately accessible to an operator or, if the instrument is subject to an environmental change which requires preprogrammed or continuous updates.

1.4.2.4 Frequency Tuning

A sweep of the main RF frequency can be performed from inside the Mini-S advanced user interface (UI) to determine the resonant frequency of the main RF circuit, i.e. the frequency that produces the maximum RF voltage amplitude. During the frequency sweep the instrument automatically sets the RF voltage amplitude to an intermediate value (35000 DAC units), scans the specified frequency range at the defined intervals (also specified inside the UI), and logs the frequency-amplitude response. LC-tank circuits are sensitive to stray capacitances which cause shifts in the resonant frequency of the circuit, reducing the maximum voltage amplitude that can be generated, and therefore the available mass range of the instrument. A 20 pF adjustable capacitor in parallel with the RF circuit allows small changes to the capacitance of the circuit to be made so that the instrument can be tuned to operate at precisely 1 MHz, fig. 1.32.

1.4.2.5 SWIFT Isolation

Increased processor speed and available memory relative to earlier Mini instruments, allows SWIFT waveforms to be generated with a user defined notch in the frequency domain as a part of the instrument method. This waveform is used for ion isolation as the frequency notch corresponds to an ion of a particular m/z (or range of m/z) all ions outside of the notch become resonantly excited via the applied waveform and are ejected from the ion trap or are discharged upon colliding with the electrodes of the analyzer. A time domain waveform is calculated from the defined frequency notch using up to 524288 (2^{19}) 16-bit points using the specified frequency notch and stored on the

static random-access memory (SRAM) where it is available for playback (30 Msps) in any segment(s) inside the instrument method. Additional functionality for SWIFT allows for up to four different waveforms to be defined (reduces the number of time domain points to 2^{17}) and are available for playback in any segment (as well as multiple times inside the same segment) of the instrument method.

1.4.3 Software

Instrument operation and method development for the Mini12 is supported through a graphical user interface (GUI or UI) (Visual Basic / Visual Studio 2010; Microsoft, 10.0.40219.1 SP1) developed as a part of ongoing efforts. Two UIs were created; an advanced user interface (Purdue University) for expert users needing to create and modify experimental methods and a novice user interface (in collaboration with JHU / APL; Dr. Nathan A. Hagan, Dr. Charles A. Fancher, Dr. Plamen A. Demirev, Phares J. Gray, and Jim F. Piotrowski) that facilitates instrument startup, shutdown, data acquisition, and analysis procedures for non-expert users.

1.4.3.1 Advanced User Interface

The advanced UI environment allows direct access to instrument voltages, frequencies, and event timing which are used during execution of the scan method. Access to these parameters allows for user control of the source voltage, ion sampling duration, main RF frequency and amplitude, application of the supplemental AC for ion isolation, activation, and resonance ejection, ion detection, and raw data acquisition. A

graphical display is supported for review of mass spectral data, or, as a graphical representation of the instrument method fig. 1.34. In addition, the advanced UI supports data processing and data export, mass calibration, instrument status logging, calibration of the system ADCs / DACs, and calibration of the PID controller.

1.4.3.2 Novice User Interface

The novice UI connects directly with the Mini-S instrument and initiates system status checks, automated startup routines, execution of predefined chemical analysis methods, and completion of data processing from a single user input. In the case of the Mini-S a push button trigger, mounted to the handle of the head unit, is used to initiate data acquisition and execution of the predefined data analysis workflow Analytical methods and data processing workflows include the ability to complete a series of positive, negative, or polarity switching full scans, automatic MSMS of target m/z values, library peak matching. It should be noted that the novice user interface was developed as a layered application that was designed to be installed on top of the advanced UI and is not a standalone application. No method development capabilities or the ability to tune the RF PID and instrument ADCs are available inside the novice user interface, fig. 1.35

1.4.3.3 Automated Startup and Shutdown

The startup and shutdown routines available inside the NUI are initiated via a single software button. In the case of instrument startup, the UI will connect to the instrument and turn on the rough pump, the manifold pressure is monitored by the program until it

reaches 5 Torr at which time the turbo is enabled to allow the system to reach pressures of 10×10^{-6} Torr. Once the system is inside the μ Torr range the program enables the MS system high voltage (e.g. main RF, source voltage, detection circuit, and end cap voltages) in preparation for data acquisition. Instrument shutdown is automated similarly, but in the reverse order of operations.

1.4.3.4 Automated Mass Calibration

Mass calibration can be completed using arbitrary compounds or mixtures of compounds through a user defined m/z calibrant list inside the novice UI. Once the list is defined, sample is introduced to the mass spectrometer and the calibration routine searches for the specified m/z values within 20 amu windows. If the m/z values from the calibrant list are identified in the mass spectrum the mass calibration is calculated, if no m/z are identified a warning is triggered and the user can restart or exit the routine. Parameters related to the calibration routine such as the number of identified peaks necessary to complete calibration, peak intensity thresholds, search window width, number of scans to average, etc. are specified inside a configuration file used by the NUI interface to allow for calibrant, and more generally analyte, detection optimization.

1.4.3.5 Data Acquisition and Results Reporting

Data acquisition is initiated by one of two methods; the software buttons inside the UI or the physical trigger on the instrument handle. Once data acquisition is initiated, a full MS scan is acquired, if a detected m/z from the full MS mode spectra matches a precursor ion mass to charge value defined in the library the routine will continue and

automatically load and execute a predefined tandem MS method to fragment that precursor ion. Results of the tandem MS experiment are then matched against mass to charge values of the fragment ions which pertain to the precursor ion. Search results are reported through the NUI identifying any matched compounds along with digital and physical status LEDs that turn red or green to indicate either a positive match has been made or no match has been made (see following section and table 1.4 for additional details of the LEDs status indicators). Additionally, the data acquisition routine takes advantage of the instruments ability to detect positive and negative ions and can be programmed to complete chemical analysis in only one polarity, or, alternated between the two. This functionality is also controlled by the novice user interface configuration file.

Visual status indicators are a key instrument feature for non-expert operators because they help guide data acquisition and results interpretation. As a design requirement, mass spectral information and the interpretation of that information has been automated with the use of the aforementioned novice NUI. To further complement that software package, color LEDs were mounted to the head unit, fig. 1.36 and table 1.4, which report the status of the instrument and results of the data analysis as color LEDs. Effectively reducing the decision making process to red-light, green-light, where a red-light indicates a threat has been detected and green-light indicates no threat has been detected.

The LED – chemical detection flow chart, fig. 1.37, details the behavior of the LEDs with respect to data acquisition and analysis. Briefly the process is as follows: after acquisition of MS data, if no peaks from the MS or MS/MS scan match mass-to-charge

values specified in the library, a green LED will turn on indicating to the user that it is safe to scan another location. However, if a detected peak matches an entry in the library, a yellow LED is turned on and a MS/MS scan is performed. The yellow LED alerts the operator to keep the device in the same location while the analysis is being completed. If the results from MS/MS and peak matching algorithms match against a compound in the library, a red LED is illuminated that signifies a chemical of interest has been detected. If no match is made, the green LED is illuminated and the user can proceed with analysis on another location. The remaining green LEDs on the bottom of the PCB are used to report instrument power and vacuum.

1.5 Conclusion

A new miniaturized and portable mass spectrometer, Mini-S, has been developed and can be configured for deployment in multiple configurations that target *in-situ* chemical analysis and real-time detection of illicit drugs, explosives, and pharmaceutical drugs. Implementation of new instrument design strategies, i.e. an on board FPGA in tandem with a DSP for waveform generation and RF error correction, and integration of ambient ionization source(s) with DAPI have been demonstrated to improve instrument performance and versatility while keeping the size, weight, and power consumption relatively low. Furthermore, instrument control software has been a significant portion of the development effort. In particular, the novice user interface enables autonomous data acquisition, processing, and report generation based upon pre-defined user workflows and without continued user input. Together, all the design concepts implemented for the Mini-S have produced an instrument that is highly portable, designed for *in-situ* analysis,

and may be effectively operated (i.e. decision(s) can be made) by personnel not familiar with instrumentation, chemical analysis procedures, or results interpretation.

1.6 References

1. Ouyang, Z., Gao, L., Cooks, R.G., *Discontinuous Atmospheric Pressure Interface*, U.S.P. Office, Editor. 2010, Purdue Research Foundation: US.
2. Gao, L., R.G. Cooks, and Z. Ouyang, *Breaking the Pumping Speed Barrier in Mass Spectrometry: Discontinuous Atmospheric Pressure Interface*. Analytical Chemistry, 2008. **80**(11): p. 4026-4032.
3. Gao, L., et al., *Characterization of a discontinuous atmospheric pressure interface. Multiple ion introduction pulses for improved performance*. International Journal of Mass Spectrometry, 2009. **283**(1-3): p. 30-34.
4. Kirleis, M., *FPGA RF Control for a Portable Mass Spectrometer*, in ECET. 2011, Purdue University.
5. Rafferty, D., *Driving a mass spectrometer ion trap or mass filter*. 2011, 1ST Detect Corporation: US.
6. Schaefer, R.T., et al., *Digitally synthesized high purity, high-voltage radio frequency drive electronics for mass spectrometry*. Review of Scientific Instruments, 2008. **79**(9).
7. Kline-Schoder, R., *Miniature High Vacuum Pumps for Analytical Instruments*, in *Workshop on Harsh-Environment Mass Spectrometry*. 2007: Cocoa Beach, Fl.
8. Yang, M., et al., *Development of a Palm Portable Mass Spectrometer*. Journal of the American Society for Mass Spectrometry, 2008. **19**(10): p. 1442-1448.
9. Ouyang, Z. and R.G. Cooks, *Miniature Mass Spectrometers*. Annual Review of Analytical Chemistry, 2009. **2**(1): p. 187-214.
10. Lange, F.a.L., Thomas. *Mobile Mass Spectrometer in Daily use - Experiences Made by Non-Scientific Operators*. in *Harsh Environment Mass Spectrometry*. 2011. Florida, USA.
11. Mino, W.K.J., ; Spencer, Michael; Wylde, James; Raftery, David. *Application of Tandem Mass Spectrometry In a Miniature Ion Trap MS: Measuring BTEX*. in *American Society for Mass Spectrometry*. 2012. Vancouver, CAN.
12. Contreras, J.A., et al., *Hand-Portable Gas Chromatograph-Toroidal Ion Trap Mass Spectrometer (GC-TMS) for Detection of Hazardous Compounds*. Journal of the American Society for Mass Spectrometry, 2008. **19**(10): p. 1425-1434.

13. Spaeder, T.A. and R.B. Walton, *Hapsite GC/MS analysis of low level chemical warfare agents, toxic industrial compounds and toxic industrial materials in the field by first responders*. Abstracts of Papers of the American Chemical Society, 2003. **226**: p. U128-U128.
14. Gao, L., et al., *Handheld Rectilinear Ion Trap Mass Spectrometer*. Analytical Chemistry, 2006. **78**(17): p. 5994-6002.
15. Patterson, G.E., et al., *Miniature Cylindrical Ion Trap Mass Spectrometer*. Analytical Chemistry, 2002. **74**(24): p. 6145-6153.
16. Ecelberger, S.A., et al., *Suitcase TOF: A man-portable Time-of-Flight Mass Spectrometer*. Johns Hopkins Apl Technical Digest, 2004. **25**(1): p. 14-19.
17. Smith, J.N., et al., *Facility monitoring of toxic industrial compounds in air using an automated, fieldable, miniature mass spectrometer*. Analyst, 2011. **135**(5): p. 994-1003.
18. Liu, J.J., R.G. Cooks, and Z. Ouyang, *Biological Tissue Diagnostics Using Needle Biopsy and Spray Ionization Mass Spectrometry*. Analytical Chemistry, 2011. **83**(24): p. 9221-9225.
19. Schafer, K.C., et al., *Real Time Analysis of Brain Tissue by Direct Combination of Ultrasonic Surgical Aspiration and Sonic Spray Mass Spectrometry*. Analytical Chemistry, 2011. **83**(20): p. 7729-7735.
20. Schafer, K.C., et al., *In Situ, Real-Time Identification of Biological Tissues by Ultraviolet and Infrared Laser Desorption Ionization Mass Spectrometry*. Analytical Chemistry, 2011. **83**(5): p. 1632-1640.
21. Harris, G.A., A.S. Galhena, and F.M. Fernandez, *Ambient Sampling/Ionization Mass Spectrometry: Applications and Current Trends*. Analytical Chemistry, 2011. **83**(12): p. 4508-4538.
22. Gao, L., et al., *Design and characterization of a multisource hand-held tandem mass spectrometer*. Anal Chem, 2008. **80**(19): p. 7198-205.
23. Ouyang, Z., et al., *Rectilinear Ion Trap: Concepts, Calculations, and Analytical Performance of a New Mass Analyzer*. Analytical Chemistry, 2004. **76**(16): p. 4595-4605.
24. Sanders, N.L., et al., *Detection of Explosives as Negative Ions Directly from Surfaces Using a Miniature Mass Spectrometer*. Analytical Chemistry, 2010. **82**(12): p. 5313-5316.

25. Harper, J.D., et al., *Low-Temperature Plasma Probe for Ambient Desorption Ionization*. Analytical Chemistry, 2008. **80**(23): p. 9097-9104.
26. Liu, J., et al., *Development, Characterization, and Application of Paper Spray Ionization*. Analytical Chemistry, 2010. **82**(6): p. 2463-2471.
27. Wang, H., et al., *Paper Spray for Direct Analysis of Complex Mixtures Using Mass Spectrometry*. Angewandte Chemie-International Edition, 2010. **49**(5): p. 877-880.
28. Takats, Z., et al., *Mass spectrometry sampling under ambient conditions with desorption electrospray ionization*. Science, 2004. **306**(5695): p. 471-473.
29. Takats, Z., J.M. Wiseman, and R.G. Cooks, *Ambient mass spectrometry using desorption electrospray ionization (DESI): instrumentation, mechanisms and applications in forensics, chemistry, and biology*. Journal of Mass Spectrometry, 2005. **40**(10): p. 1261-1275.
30. Wilm, M.S. and M. Mann, *Electrospray and Taylor-Cone Theory, Doles Beam of Macromolecules at Last*. International Journal of Mass Spectrometry, 1994. **136**(2-3): p. 167-180.
31. Horning, E.C., et al., *New picogram detection system based on a mass spectrometer with an external ionization source at atmospheric pressure*. Analytical Chemistry, 1973. **45**(6): p. 936-943.
32. Meyer, C., et al., *Dielectric barrier discharges in analytical chemistry*. Analyst, 2011. **136**(12): p. 2427-2440.
33. Na, N., et al., *Development of a dielectric barrier discharge ion source for ambient mass spectrometry*. Journal of the American Society for Mass Spectrometry, 2007. **18**(10): p. 1859-1862.
34. Ratchiffe, L.V., et al., *Surface analysis under ambient conditions using plasma-assisted desorption/ionization mass spectrometry*. Analytical Chemistry, 2007. **79**(16): p. 6094-6101.
35. Dagleish, J.K., et al., *Arrays of low-temperature plasma probes for ambient ionization mass spectrometry*. Rapid Communications in Mass Spectrometry, 2012. **27**(1): p. 135-142.
36. Jackson, A.U., et al., *Analysis of drugs of abuse in biofluids by low temperature plasma (LTP) ionization mass spectrometry*. Analyst, 2010. **135**(5): p. 927-933.

37. Wiley, J.S., et al., *Screening of agrochemicals in foodstuffs using low-temperature plasma (LTP) ambient ionization mass spectrometry*. Analyst, 2010. **135**(5): p. 971-979.
38. Massines, F., et al., *Recent advances in the understanding of homogeneous dielectric barrier discharges*. European Physical Journal-Applied Physics, 2009. **47**(2).
39. Chan, G.C.Y., et al., *Elucidation of Reaction Mechanisms Responsible for Afterglow and Reagent-Ion Formation in the Low-Temperature Plasma Probe Ambient Ionization Source*. Analytical Chemistry, 2011. **83**(10): p. 3675-3686.
40. Cody, R.B., *Observation of Molecular Ions and Analysis of Nonpolar Compounds with the Direct Analysis in Real Time Ion Source*. Analytical Chemistry, 2009. **81**(3): p. 1101-1107.
41. Dzidic, I., et al., *Comparison of Positive-Ions Formed in Nickel-63 and Corona Discharge Ion Sources Using Nitrogen, Argon, Isobutane, Ammonia and Nitric-Oxide as Reagents in Atmospheric-Pressure Ionization Mass-Spectrometry*. Analytical Chemistry, 1976. **48**(12): p. 1763-1768.
42. Kang, W.S., H.S. Kim, and S.H. Hong, *Gas Temperature Effect on Discharge-Mode Characteristics of Atmospheric-Pressure Dielectric Barrier Discharge in a Helium-Oxygen Mixture*. Ieee Transactions on Plasma Science, 2010. **38**(8): p. 1982-1990.
43. Ostmark, H., S. Wallin, and H.G. Ang, *Vapor Pressure of Explosives: A Critical Review*. Propellants Explosives Pyrotechnics, 2012. **37**(1): p. 12-23.
44. Dalgleish, J.K., *Developing and Characterizing Improved Low-Termperature Plasma Probes for Ambient ionization Mass Spectrometry*, in *Chemistry*. 2012, Purdue University.
45. Pfeuffer, K.P., et al., *Visualization of mass transport and heat transfer in the FAPA ambient ionization source*. Journal of Analytical Atomic Spectrometry, 2013. **28**(3): p. 379-387.
46. Charles, M.J., S.A. McLuckey, and G.L. Glish, *Competition between Resonance Ejection and Ion Dissociation During Resonant Excitation in a Quadrupole Ion-Trap*. Journal of the American Society for Mass Spectrometry, 1994. **5**(12): p. 1031-1041.
47. Goeringer, D.E., et al., *Theory of high-resolution mass spectrometry achieved via resonance ejection in the quadrupole ion trap*. Analytical Chemistry, 1992. **64**(13): p. 1434-1439.

48. Louris, J.N., et al., *Instrumentation, Applications, and Energy Deposition in Quadrupole Ion-Trap Tandem Mass-Spectrometry*. Analytical Chemistry, 1987. **59**(13): p. 1677-1685.
49. McLuckey, S.A., *Principles of collisional activation in analytical mass spectrometry*. Journal of the American Society for Mass Spectrometry, 1992. **3**(6): p. 599-614.
50. March, R.E. and J.F.J. Todd, *Quadrupole Ion Trap Mass Spectrometry*. Chemical Analysis: A Series of Monographs on Analytical Chemistry and Its Applications. 2005, Hoboken, New Jersey: John Wiley & Sons, Inc.
51. Guan, S. and A.G. Marshall, *Stored waveform inverse Fourier transform (SWIFT) ion excitation in trapped-ion mass spectrometry: Theory and applications*. International Journal of Mass Spectrometry and Ion Processes, 1996. **157-158**: p. 5-37.

Table 1.1: Power draw response for each of the main components of the Mini-S instrument; also reference figures 21 – 23.

Conditions of test setup:		
Battery PACK A: Powerizer 24V 4200mAh, NiMH Rechargeable		
Battery charge: 25.9 V when tested against DMM		
Backpack: powered off system vented to atmosphere Dual Fan operation with LTP supply		
	Volts	Watts
Battery plug-in: instantaneous response		Figure 21A
quiescent power (system on):	0.096	24.096
pressure (Torr): 4.2 e2	0.096	24.096
Rough pump on: instantaneous response		Figure 21B
2.5 e1	0.132	33.132
4.00E+00	0.128	32.128
1.80E+00	0.126	31.626
Turbo on: instantaneous response		Figure 21C
3.50E-01	0.307	77.057
2.00E-04	0.171	42.921
4.00E-05	0.169	42.419
8.00E-06	0.169	42.419
HV on: instantaneous response		N/A
	0.206	51.706
Sample valve open	0.216	54.216
On board LTP supply (negative): instantaneous response		Figure 21D
	0.288	72.288
On board LTP supply (positive)	0.241	60.491
power profile during scan (negative mode LTP ON)		Figure 22A & B

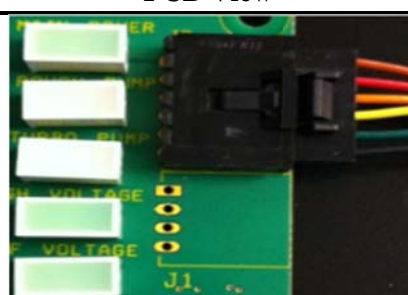
Table 1.2: Mini-S instrument systems located in the backpack.

Mini-S instrument systems located to the backpack			
System	Manufacturer	Model or P/N	Notes
Vacuum			
Mechanical pump	KNF Neuberger	MPU 1220-N84.0-9.00	5 L/min
Turbomolecular pump	Pfeiffer Vacuum	HiPace10	10 L/s
Electronics			
Digital board	Sierra Circuits	A0BME503 R0.1	Purdue University
Analog board	Sierra Circuits	A0BME502 R0.1	Purdue University
Power distribution board	Sierra Circuits	A0115501 R2	Purdue University
High voltage board	Sierra Circuits	A0115505 R4	Purdue University
RF amplifier board	Sierra Circuits	A0115503 R2.6	Purdue University
RF inductance coil	Sierra Circuits	N/A	~310 µH Mini-S ~560 µH Mini12
AC amplifier board	Sierra Circuits	A0115507 RB	Purdue University one board required for each polarity of the AC
Digital breakout board	Sierra Circuits	A0BME504 R1	Purdue University
Digital power board	Sierra Circuits	A0BME509 R0	Purdue University
Power			
Nickel metal hydride battery	Powerizer	Item No. 31428	1410g, 4200 mAh
Lithium polymer	Tenergy	CU-MM105 ID 4725	725g, 5000 mAh
Battery charge level indicator	Prototype	N/A	25.9 V = Green Led 22.3 V = Red Led
Ion source discharge gas			
Helium	Leland Limited, Inc.	P/N 49615He	2.4 g helium
Regulator	Leland Limited, Inc.	Item No. 50047-004	80 PSI max
Ion source power supply			
HV circuit with transformer	Information Unlimited	28K089	2 kVp-p low; 9.5 kVp-p high
Cooling			
24 V, 0.09A fan	Minebea-Matsushita	2408NL-05W-B59	two fans installed

Table 1.3: Mini-S instrument systems located on the handheld head-unit

Mini-S instrument systems on the handheld unit			
System	Manufacturer	Model or P/N	Notes
Mass analyzer			
Rectilinear ion trap	University Machine	5 x 4	~20 pF capacitance
RF cable		RG62/U	~45 pF Mini-S Mini 12
Ion detection circuit			
Electrom Multiplier (EM)	Detector Technologies, Inc.	2300	N/A
Dynode	Prototype	N/A	316 Stainless Steel
Current amplifier	Sierra Circuits	A0115507 RB	Purdue University
Pressure transducer			
Micro Pirani	MKS	925C; P/N 925C-11	RS232 port with analog read outs
Ion source			
Low Temperature Plasma (LTP)	Purdue University	co-axLTP	capable of sampling externally generated ions at atmospheric pressure
Ion introduction			
Discontinuous atmospheric pressure interface (DAPI)	ASCO Scientific	P/N: 390NC24330	30 PSI
Ion introduction capillaries			
External capillary (atmospheric side)	IDEX Health & Science	yellow band	508µm ID x 10cm
Internal capillary (vacuum side)	IDEX Health & Science	White band	762µm x 5cm
Rubber tubing for DAPI	Simolex	SIMST-048 x 125	conductive tubing
Instrument Status LEDs			
LED board	Sierra Circuits	A0115515 R0	Purdue University
Trigger	C&K Components	DM Series two pole rocker switch	Trigger used to initiate data acquisition

Table 1.4: LED indicators on the handheld head-unit of the Mini-S instrument

Order of indicator LEDs, BIOs numbers, and purpose.			
PCB View	Color	BIO No.	Meaning
	Green	8	Clear
	Yellow	9	Potential risk
	Red	10	Dangerous
	Green	11	Status of Switch(or TBD)
	Green	12	Status of Power(or TBD)

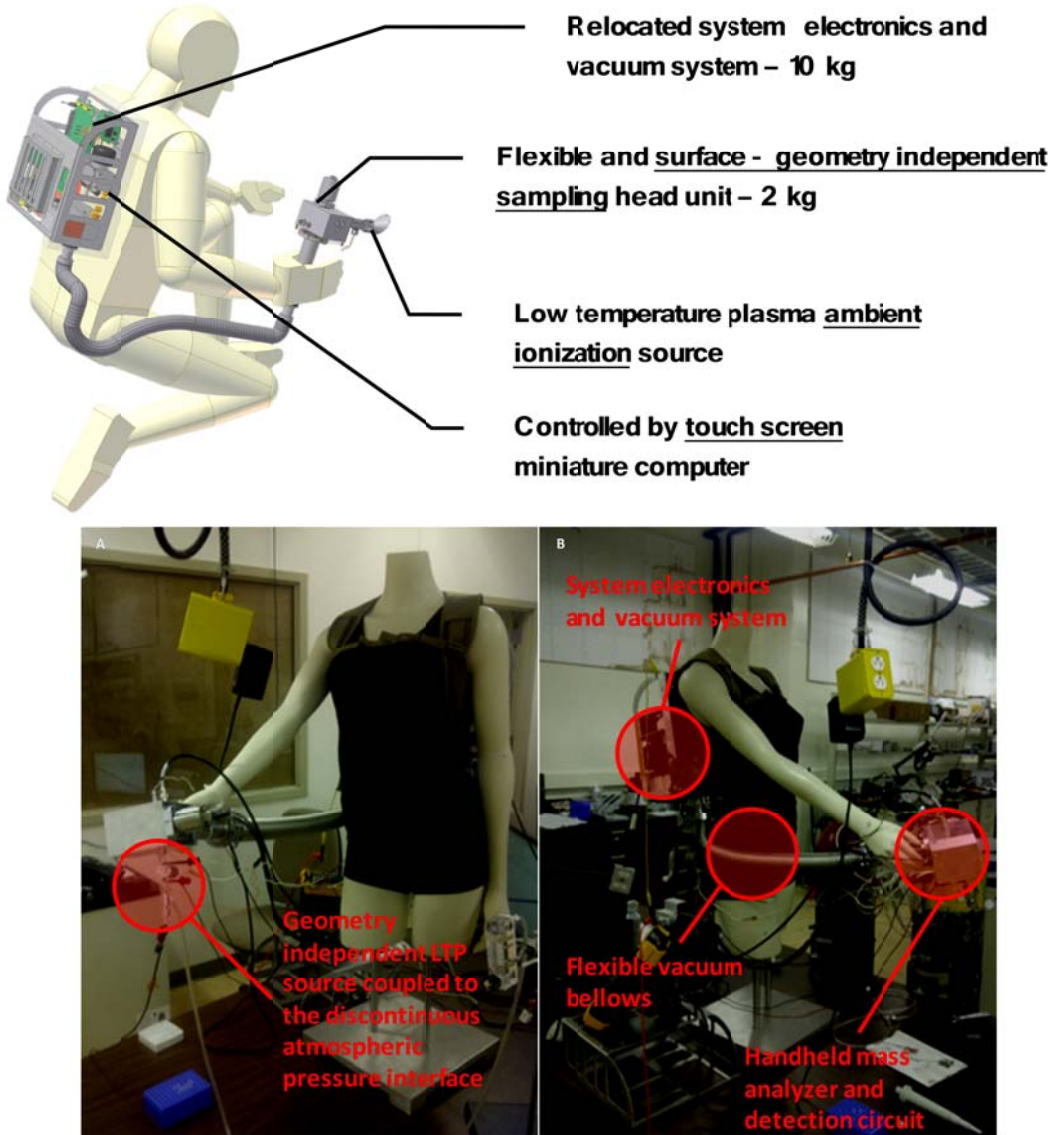


Figure 1.1: Top) Computer aided design (CAD) rendering of the Mini-S instrument and location of the instrument systems. Bottom A&B) Photograph of the fully assembled and operational Mini-S mass spectrometer outfitted with handheld head unit containing the mass analyzer and detection circuit, geometry-independent co-axLTP source, pressure transducer, and flexible vacuum bellows.

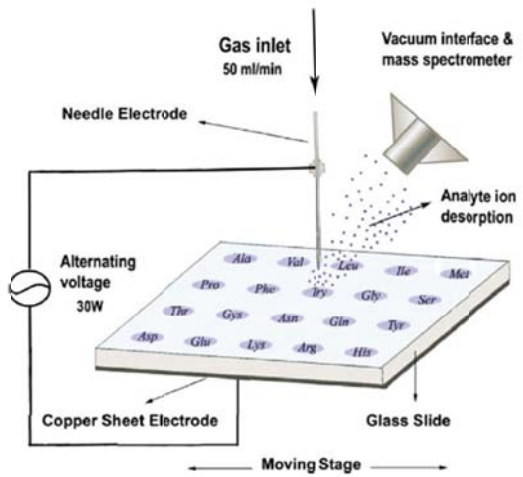


Figure 1.2: Schematic image of the DBDI source developed by X. R. Zhang et al.; image adapted from reference 33.

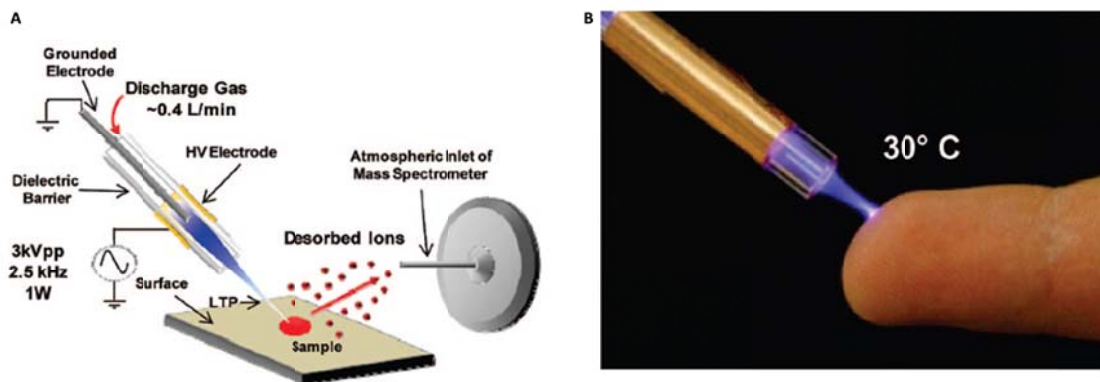


Figure 1.3: A) Schematic of the components that comprise the LTP source and operation of the LTP ion source. B) Image of the LTP discharge (inside the source) and plasma afterglow (outside the source). Note surface temperatures that are exposed to the plasma afterglow do not exceed 30 °C with low power inputs. Figures A and B were adapted from reference 25.

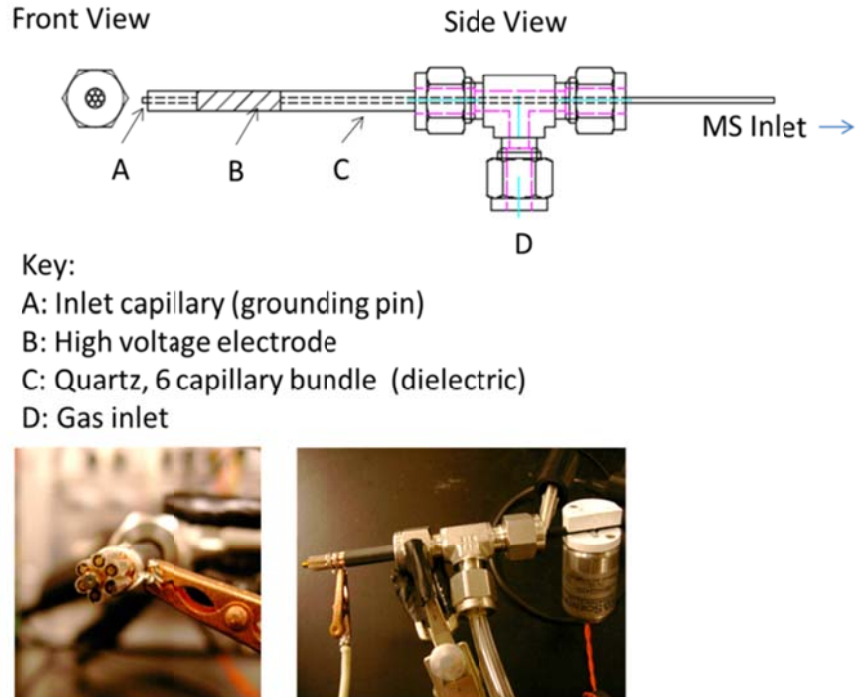


Figure 1.4: Image adapted from reference 43; schematic of the components for a LTP array and a close-up image of LTP array interfaced to a DPAI on a miniaturized instrument.



Figure 1.5: A) Photograph of the 7 probe LTP array with 6.5 mm outer electrodes. B & C) Photographs of the 7 probe LTP array installed on a Mini-S system. Note the bright emission which is indicative of high power-density plasma.



Figure 1.6: RF discharge on the inlet capillary used to ground the center conductor of the LTP probe.

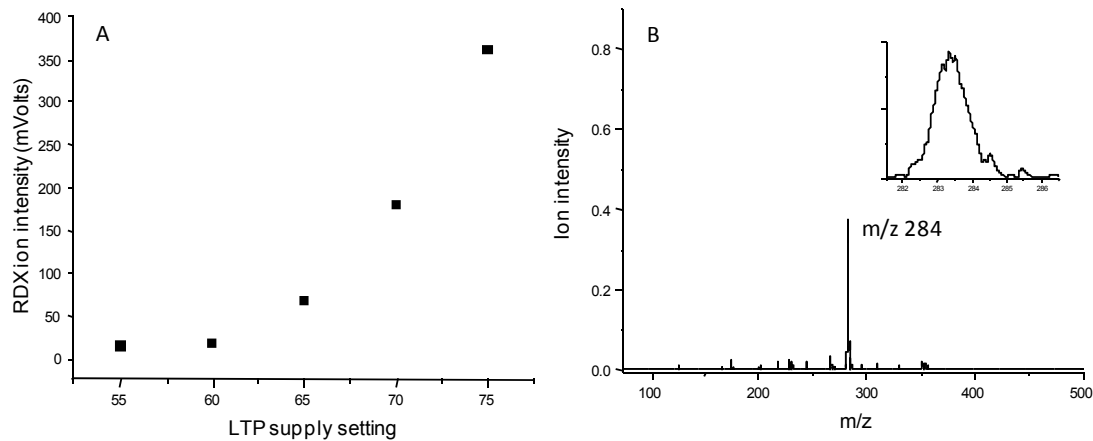


Figure 1.7: A) Full scan MS for TNT operated with a He discharge at 40 ml/min. B) Full scan MS for RDX operated using Air at 40 ml/min as the plasma gas. C) RDX ion signal (m/z 284) as a function of LTP power. The trend demonstrates improved desorption and ionization as the LTP power is increased, which is likely due to increased surface heating.

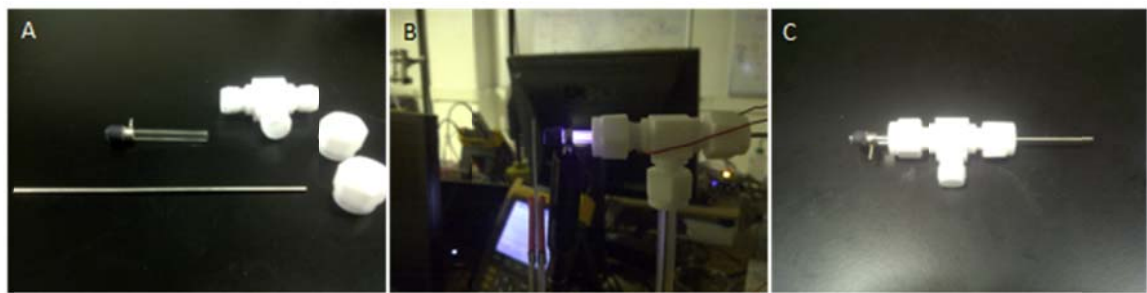


Figure 1.8: A & C) Miniaturized single probe co-axial LTP design and probe form factor. B) Plasma density produced by the miniaturized probe. NOTE: This design does NOT consist of an array of LTP probes.

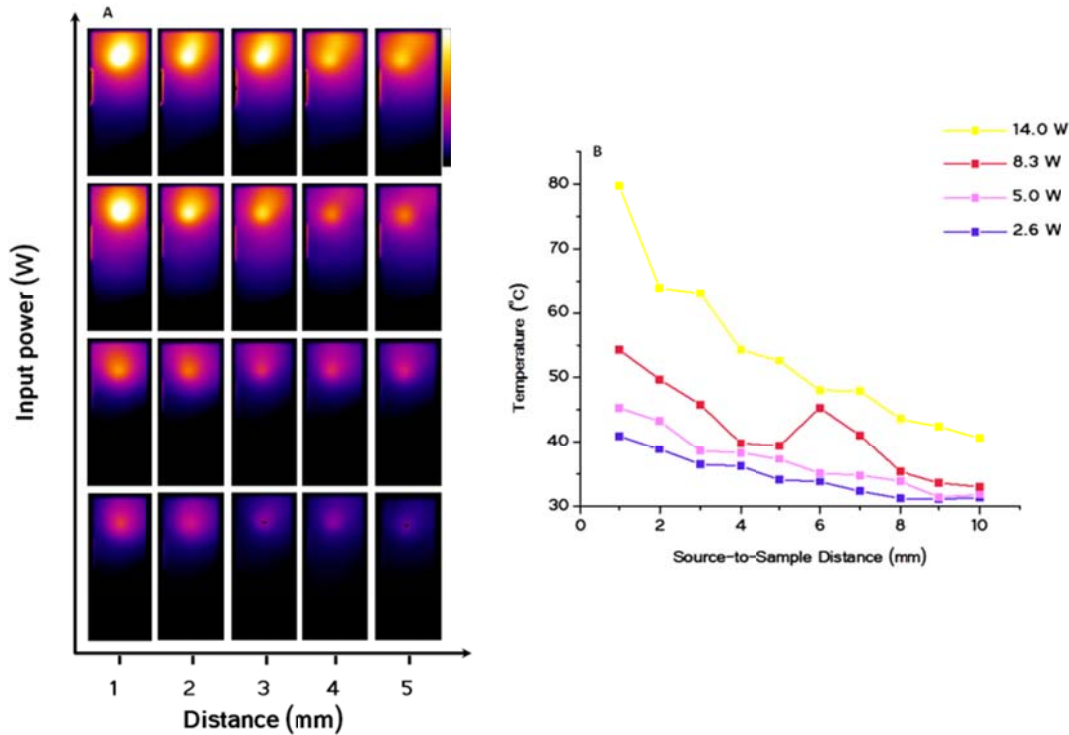


Figure 1.9: A) Thermographic images of surface temperatures generated from the single probe co-axLTP source; glass slide used as a surface stimulant. Input powers range from 14.0 to 2.6 W and surface to sample distance of 1 – 5mm. All images are on the same temperature scale of 30 to 80° C. B) maximum temperatures (From A) plotted as a function of source to sample distance of 1-10 mm.

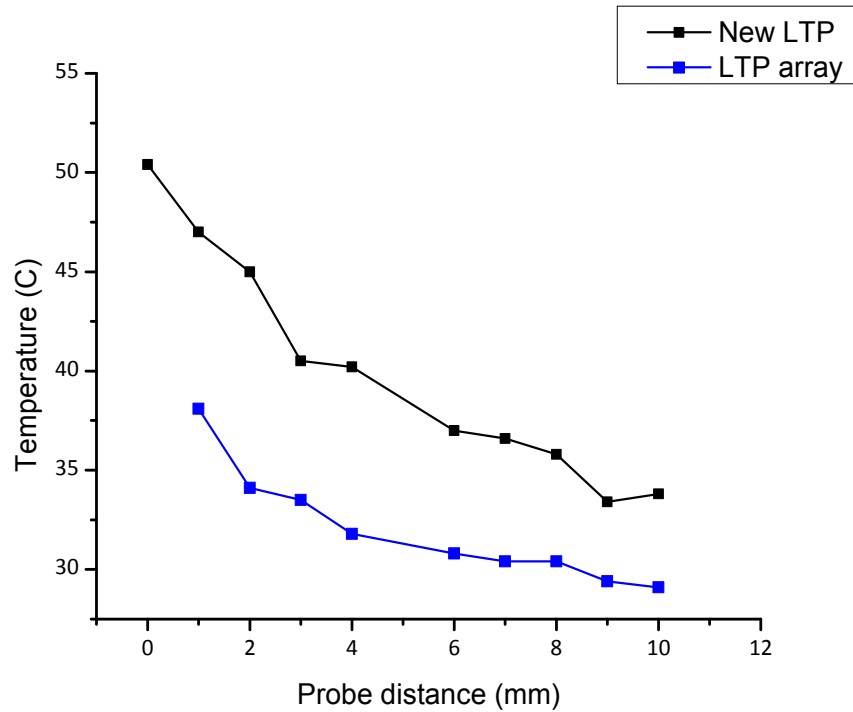


Figure 1.10: Maximum temperature of the glass surface as a function of the source-to-sample distance for the two coaxial LTP configurations, array (blue) and non-array (black).

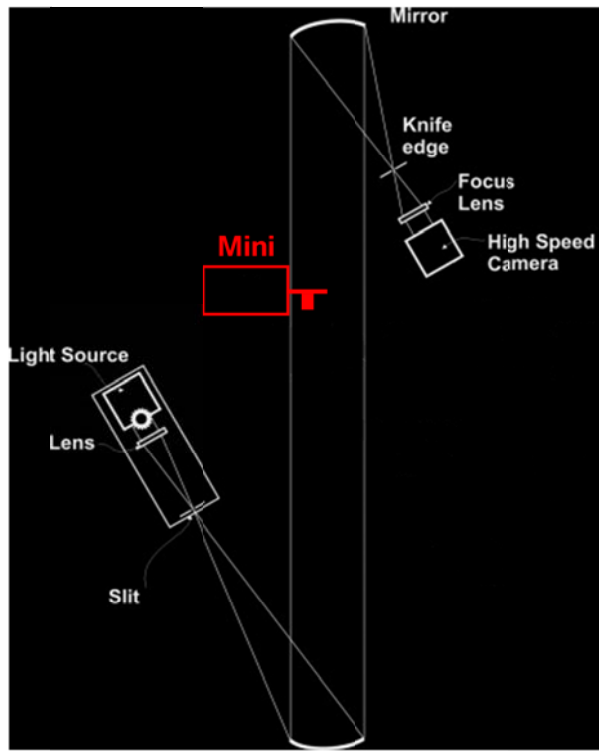


Figure 1.11: Diagram of the Schlieren imagining setup used to visualize the helium interaction with the sample and gas sampling of the DAPI valve. The co-axLTP source is placed inside the collimated light path where differences in refractive index between He and the ambient air can be visualized and captured with the high speed camera.

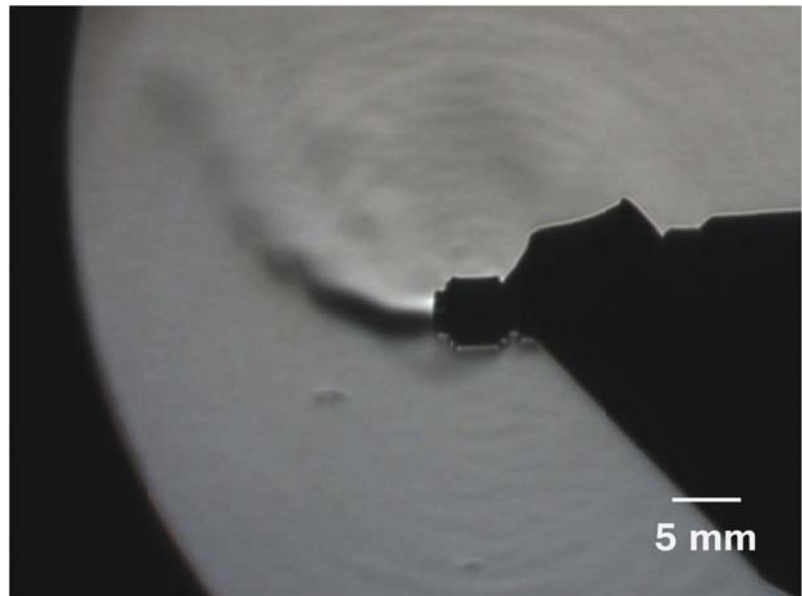


Figure 1.12: Schlieren image of helium-co-axLTP on aMini 12 development instrument. Operational conditions are 500 ml/min He flow rate and $\sim 3\text{W}$ input power. Due to the buoyancy of helium in air, helium in the afterglow region which makes contact with the sample surface is dispersed at distances of 5mm.

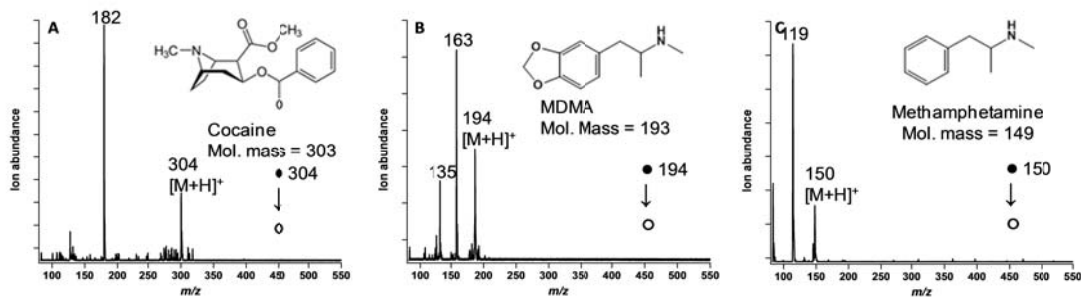


Figure 1.13: Detection of drugs of abuse using the coax-LTP interfaced to the Mini-S. A) Tandem MS of cocaine ($2\mu\text{g}/\text{cm}^2$) detected directly from human skin. B) Tandem MS of 3,4-methylenedioxy-*N*-methylamphetamine (MDMA), also known as ecstasy, ($10\mu\text{g}/\text{cm}^2$) detected directly from the inside corners of a cardboard box. C) Tandem Ms of methamphetamine ($10\mu\text{g}/\text{cm}^2$) detected directly from an organic chemistry book cover.

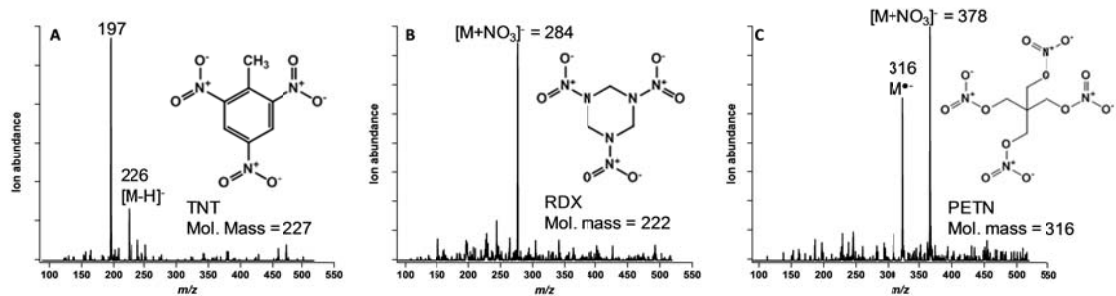


Figure 1.14: Detection of explosives from glass. All three compounds are detected at quantities of 1 $\mu\text{g}/\text{cm}^2$ or less. A) detection of trinitrotoluene note the appearance of a pattern formed by m/z 226 $[\text{M}-\text{H}]^-$ and m/z 197 $[\text{M}-\text{NO}]^-$. B) Cyclotrimethylenetrinitramine (RDX) is present as a nitrate attachment at m/z 284 $[\text{M}+\text{NO}_3]^-$. C) Pentaerythritol tetranitrate (PETN) this spectrum shows the appearance of both the molecular radical m/z 316 M^\bullet and the nitrate adduct m/z 378 $[\text{M}+\text{NO}_3]^-$ however, under these operating conditions the adduct formation is typically the dominate species.

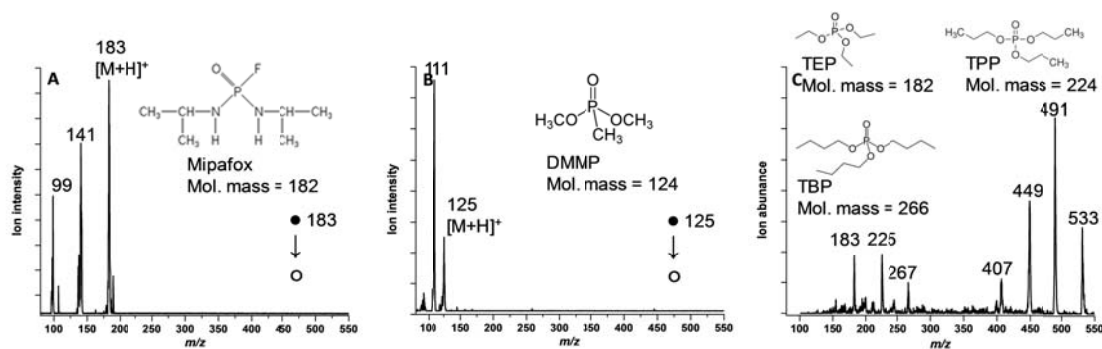


Figure 1.15: Chemical warfare agent (CWA) simulants. A) Tandem MS of Mipafox ($1\mu\text{g}/\text{cm}^2$) detected from latex. B) Tandem MS of dimethyl methylphosphonate (DMMP) ($1\mu\text{g}/\text{cm}^2$) detected from cotton fibers. C) Full scan MS of a mixture of triethyl phosphate (TEP), tripropyl phosphate (TPP), tributyl phosphate (TBP) 1000ppm from cotton fibers.

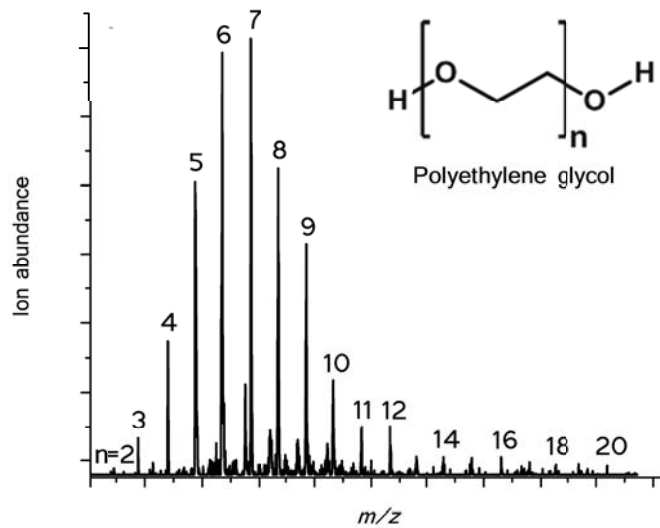


Figure 1.16: nESI mass spectrum of $[\text{PEG}+\text{Na}]^+$ acquired on the Mini-S instrument to demonstrate the maximum detectable mass-to-charge range of the instrument at 930 amu. The PEG sample was a mixture of PEG oligomers at μM concentrations. Also demonstrated is the mass resolution for the instrument which is $\sim 1 - 2$ amu at FWHM across the mass range.

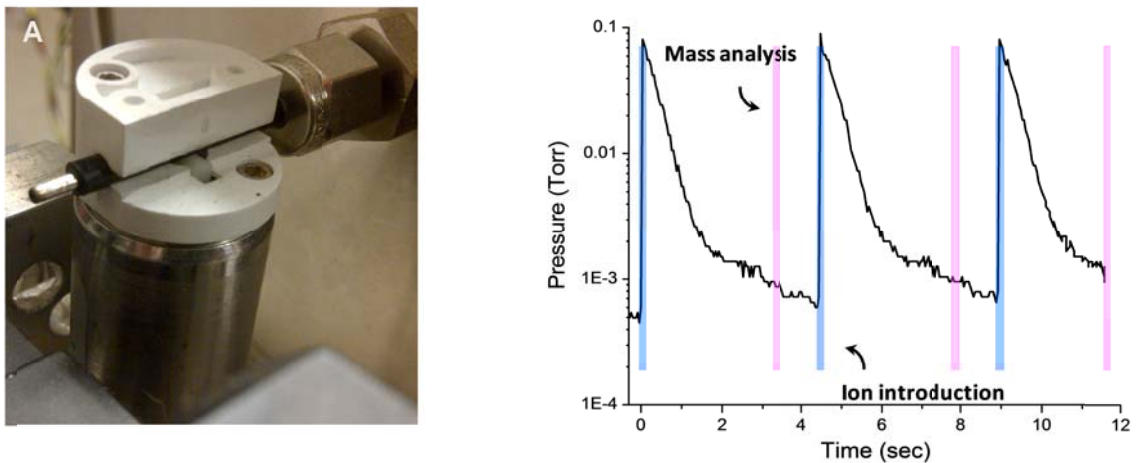


Figure 1.17: A) DAPI valve assembled with the ion introduction and transfer capillaries and the conductive rubber tubing. See table 3 for details for assembly P/Ns. B) Black trace is the manifold pressure as measured from the analog output of the pressure transducer for three consecutive DAPI pulses. Blue highlights indicate the maximum pressure of the manifold (~100 mTorr) during introduction of ions and neutrals from atmosphere; red highlights indicate the pressure of the manifold during mass analysis (~10 – 1 mTorr). Note that for each of the three scans the base pressure of the manifold does not return to the 10×10^{-6} Torr. This is due to the reduced efficiency of the turbo pump operating in helium (supplied from the LTP source and introduced to the manifold during the DAPI pulse) rather than air.

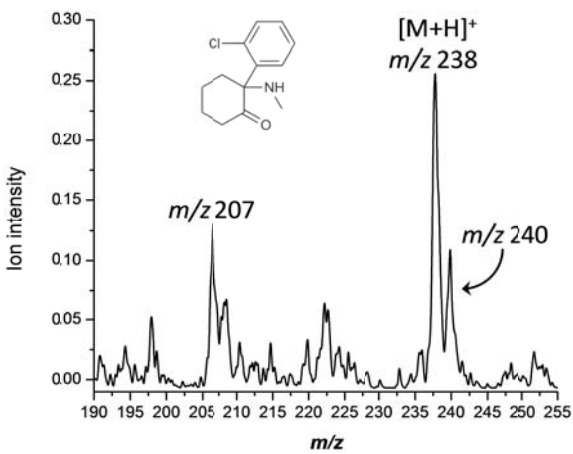


Figure 1.18: Three scan average of $1\mu\text{g}/\text{cm}^2$ ketamine, m/z 237 $[\text{M}+\text{H}]^+$. Sample was ionized with LTP, 80 ml/min He, 500 V_{p-p} @ 30kHz ($>1\text{W}$). FWHM values ions are ~1 amu across the mass range, X+2 isotope is visible with 9.5% valley and 42% intensity relative to the monoisotopic mass. In addition to the $[\text{M}+\text{H}]^+$ species ketamine undergoes fragmentation to lose methyl amine [mass 31 Da] resulting in m/z 207 which also carries the chlorine creating a chemical footprint in the full MS scan.

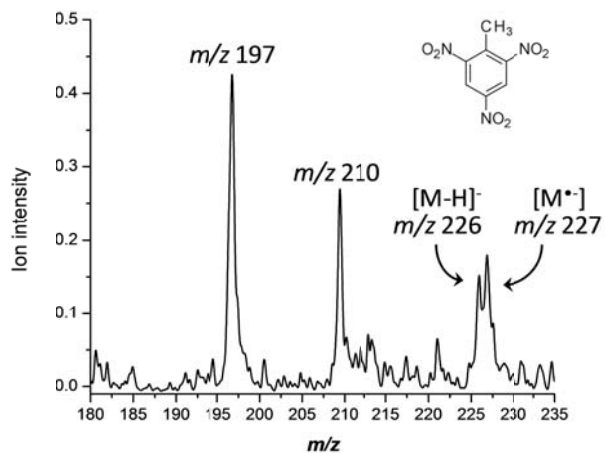


Figure 1.19: Three scan average of $1\mu\text{g}/\text{cm}^2$ TNT, m/z 226 $[\text{M}-\text{H}]^-$. Sample was ionized with LTP, Sample was ionized with LTP, 80 ml/min He, 500 V_{p-p} @ 30kHz (>1W). FWHM values are ~ 0.6 amu and the presence of m/z 226 and 227 are visible as the $[\text{M}-\text{H}]^-$ and molecular radical ions $\text{M}^{\bullet-}$. 1 amu separation with a 58.5% valley at abundances of approximaginey1:1.

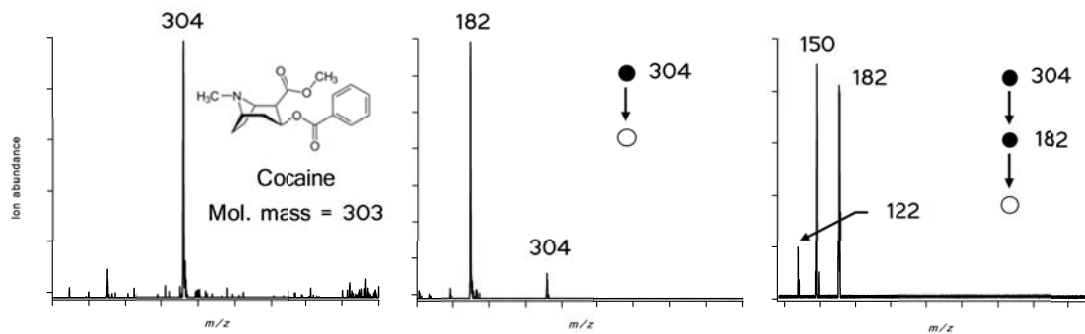


Figure 1.20: Left) nESI full scan mass spectrum of cocaine m/z 304 $[\text{M}+\text{H}]^+$ at 100ppm. MS/MS of m/z 304 → 182 demonstrating the characteristic loss of benzoic acid. Right MS/MS/MS of m/z 304 → 182 → 150 and 122 demonstrating the consecutive loss of MeOH and CO.

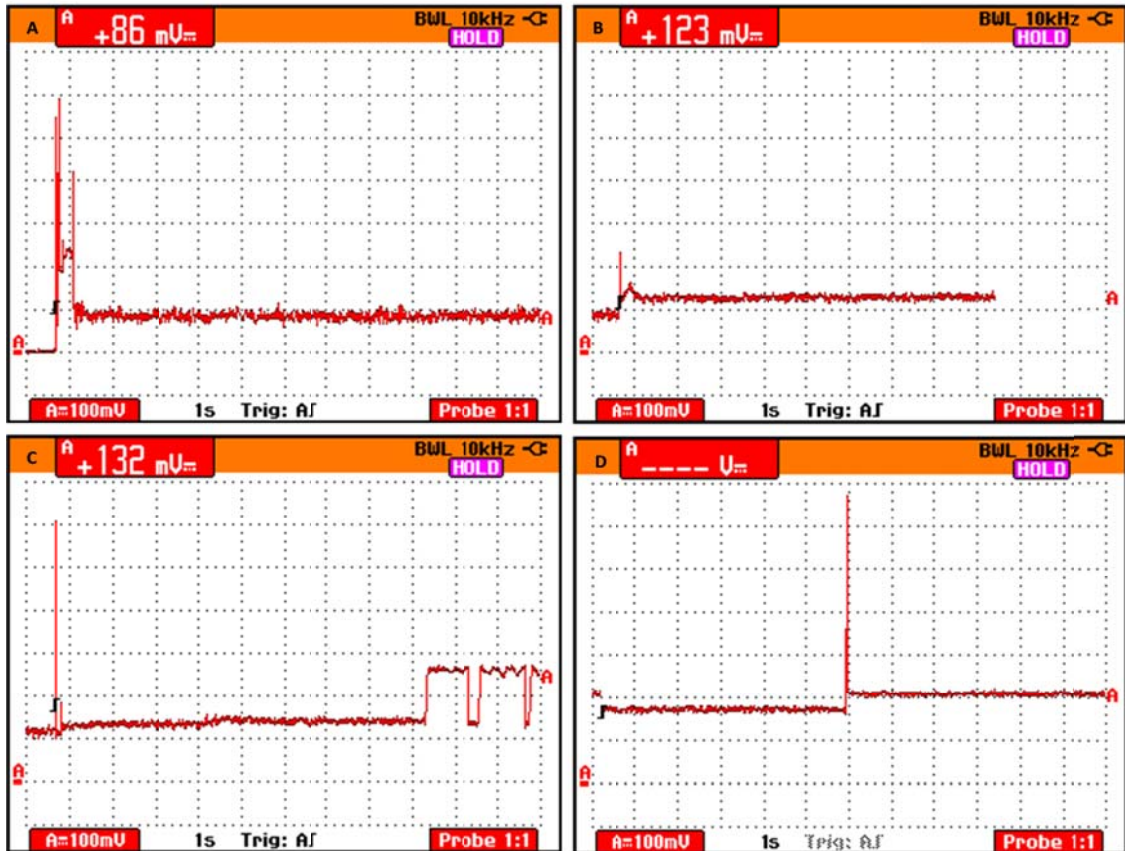


Figure 1.21: A) Initial start-up of the power-distribution board for 400 ms. An instantaneous current draw of ~6 A occurred when the instrument was first plugged in, consuming ~144 W during this short period of time. The power then settled to a baseline power draw of ~24 W. B) Current spike upon turning on the rough pump. C) Power draw upon enabling the turbo pump. Note the current draw during this period is similar to that upon initially plugging in the battery indicating that most of the initial power draw is due to the turbo. D) Power draw upon enabling the on-board LTP supply in negative mode; instantaneous power exceeds 150 W. Note: the current probe produces a 100 mV signal per Ampere consumed and the instrument has an input voltage of 24 V.

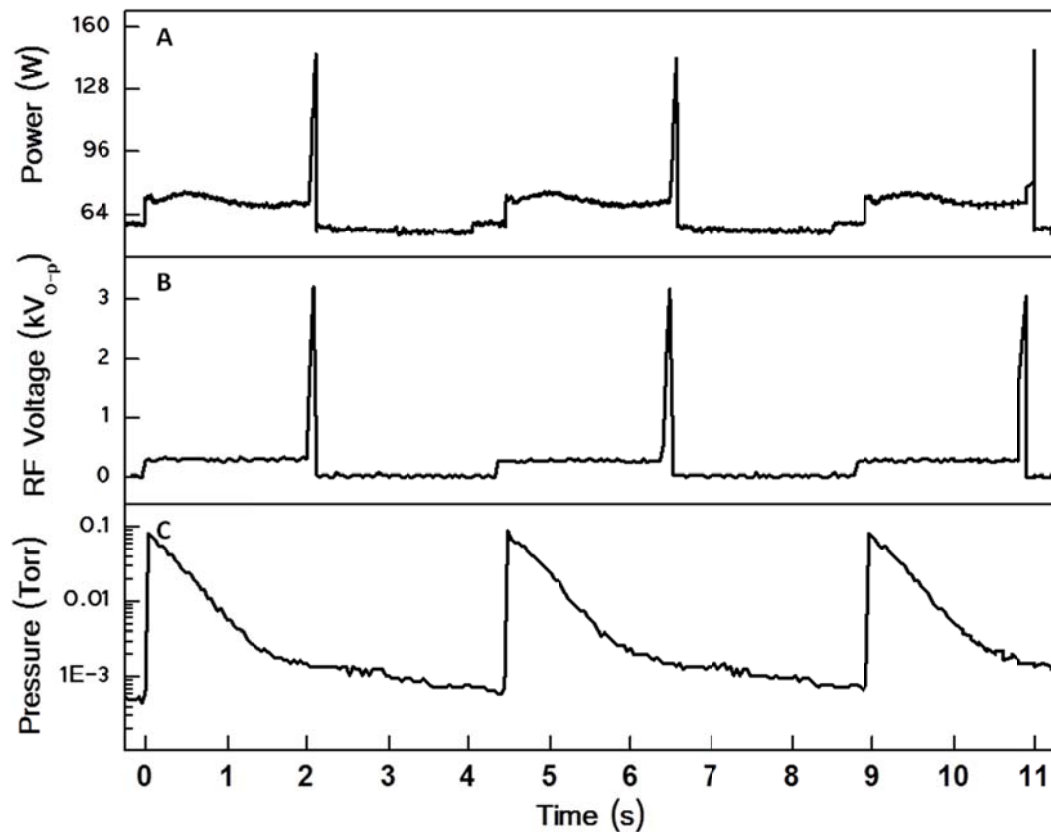


Figure 1.22: Side-by-side plots of the power consumption, RF voltage amplitude, and operating pressures for the Mini-S (A) cumulative instrument power consumption, (B), main RF voltage amplitude, and (C) manifold pressure curves for three consecutive scans. Manifold pressure increase is due to actuation of the DAPI valve (15 – 25 ms) during ion injection into the mass analyzer. Ramp in RF voltage amplitude is due to mass-selective instability scan during mass analysis.

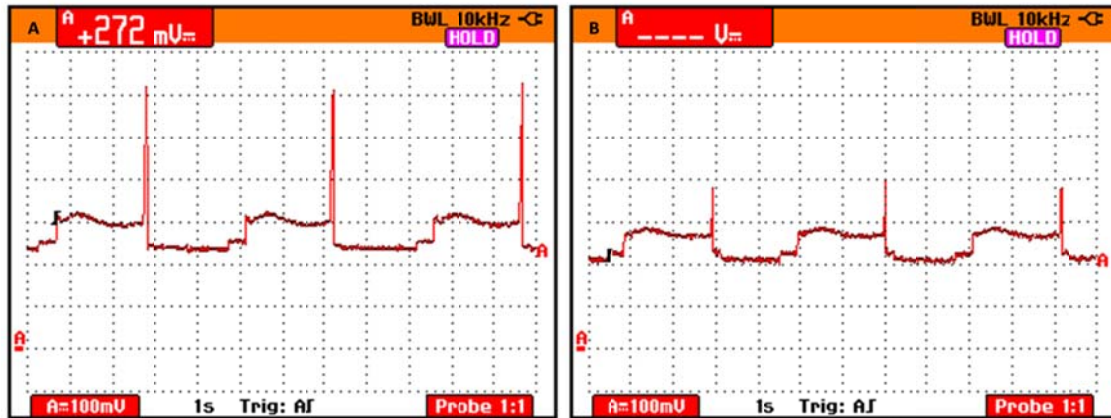


Figure 1.23: A) Power profile during an analytical scan, maximum available RF is used to analyze ions up to m/z 930. B) Power profile during an analytical scan with RF amplitude limited to analyzing ions up to m/z 550. The source voltage is not on during this time. Although the difference in peak-power draw between the two scan functions was 58 W (156 W versus 98 W) the battery life for each mode of operation was approximately the same (~90 min).

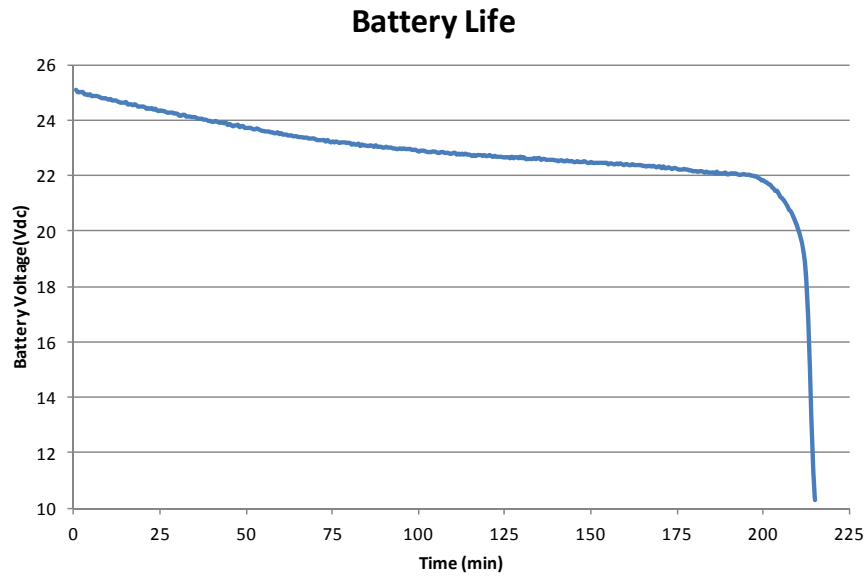


Figure 1.24: Battery-life profile for lithium polymer (Li-Po) batteries obtained from Tenergy (Fremont, Ca, US) (725g, 5000 mAh, item no. 31428). Instrument could be operated for approximately 200 minutes, battery charge < 22 V.

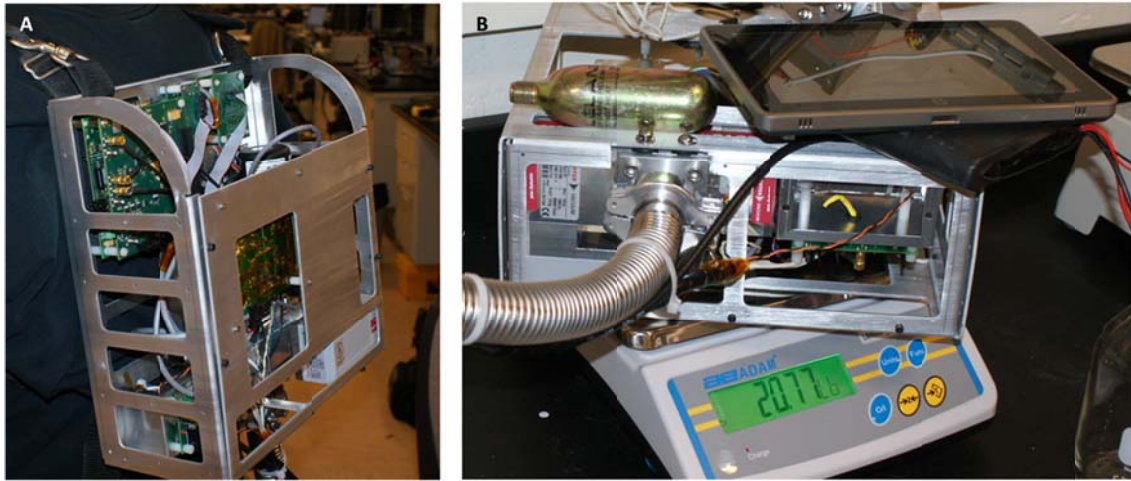


Figure 1.25: A & B) Images of the fully assembled backpack case and the weight of all the components; 20.77 lbs. The backpack is made of two components providing access to the electronics and vacuum system. Table 2 contains the full list of instrument systems contained in the backpack unit and additional details related to the components.

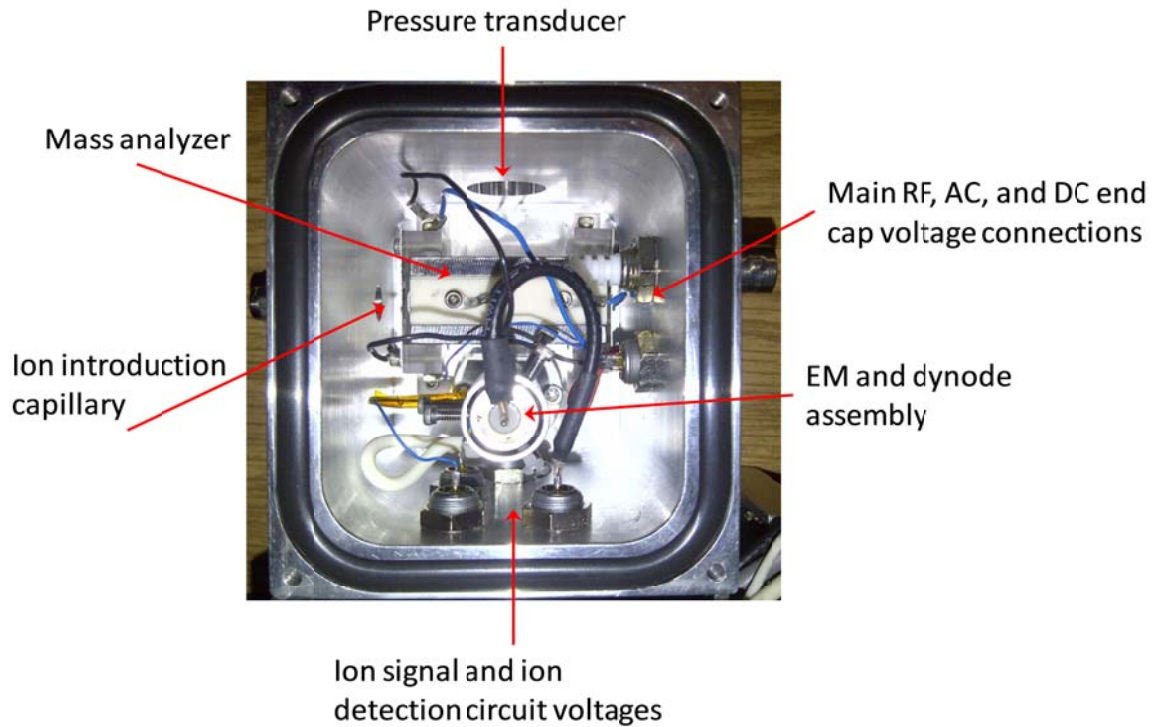


Figure 1.26: Hand-held head unit containing the mass analyzer, ion detector assembly, electrical connections, ion introduction, and pressure transducer.

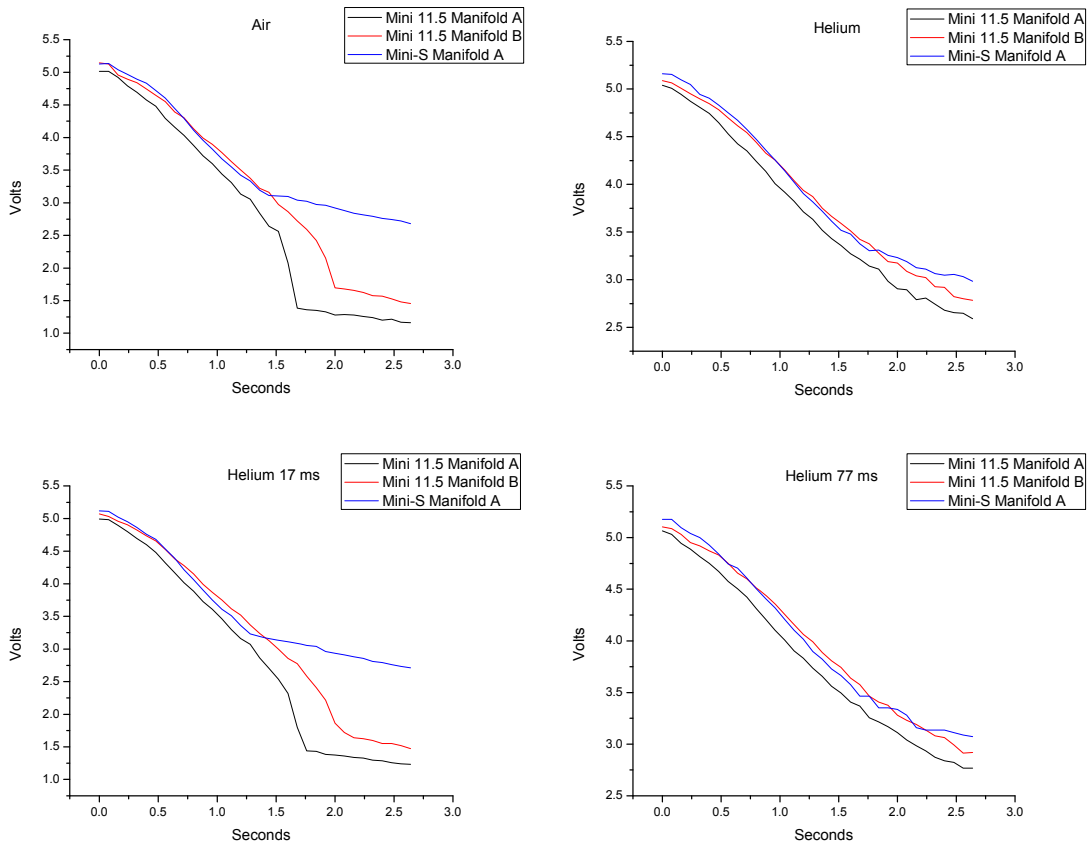


Figure 1.27: Pressure profiles of the vacuum manifold recorded directly from the pressure transducer demonstrate the pumping performance of two Mini 11.5 and the Mini-S manifold A under conditions of air, continuous helium, 17 ms pulse of Helium, and 77 ms pulse of Helium. Each pressure trace is an average of the pressure recordings for 5 consecutive 17ms DAPI pulses.

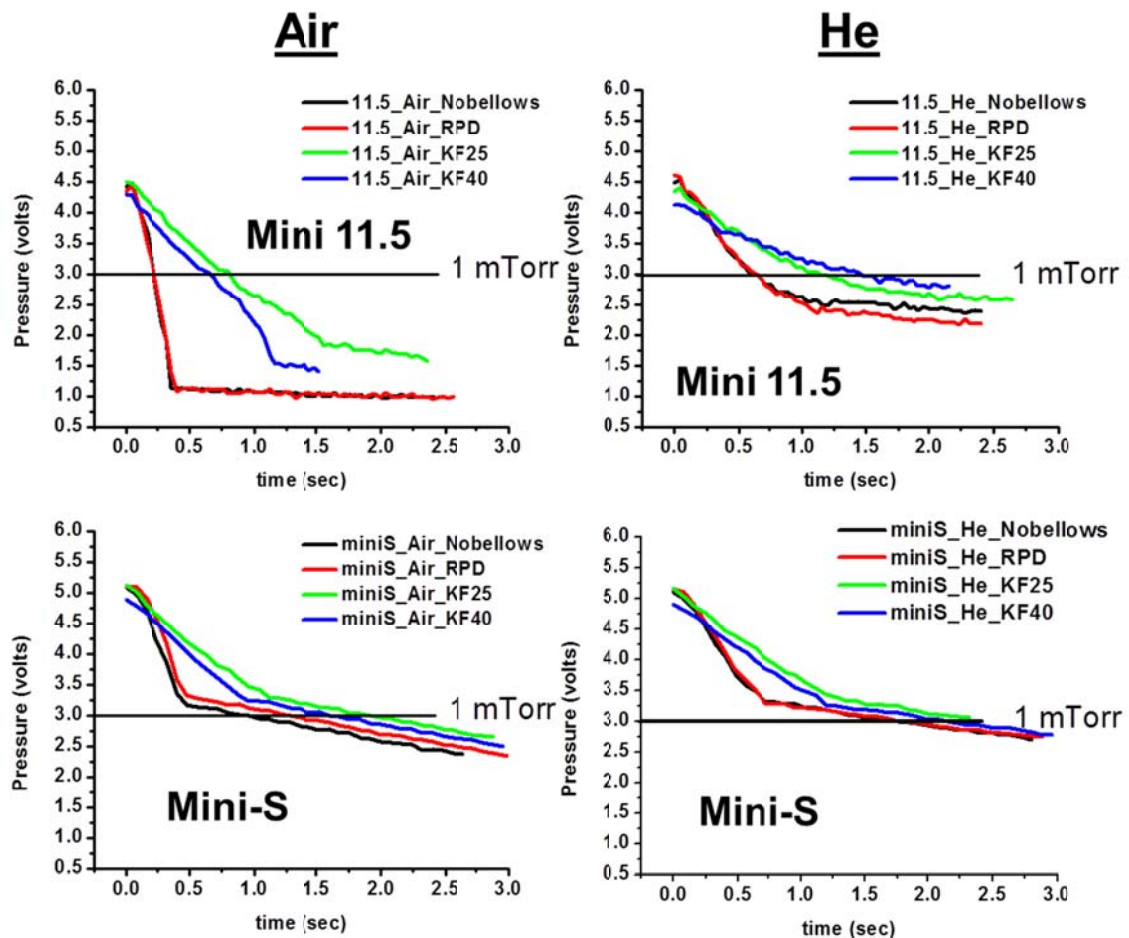


Figure 1.28: Pressure-time profiles for the Mini 11.5 and Mini-S manifold B for four configurations and in the presence of helium and air as the buffering gas.

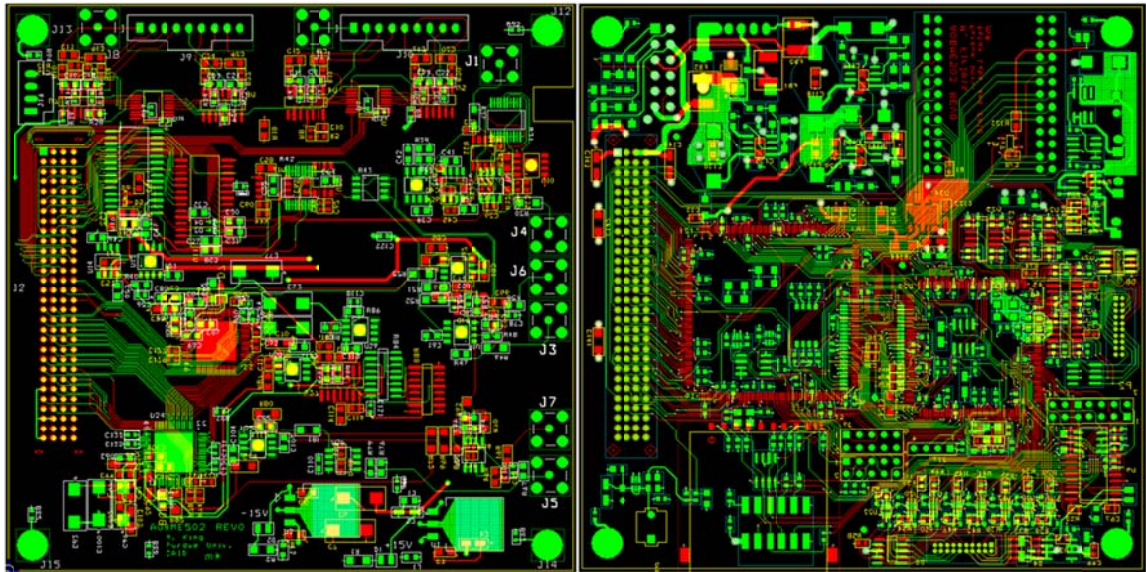


Figure 1.29: Image adapted from reference 4, fabrication layout images of the analogy board (left) and the digital board (right). The digital board contains 8 layers and 457 individual components. Tables 2 and 3 details the other boards used on the Mini-S instrument.

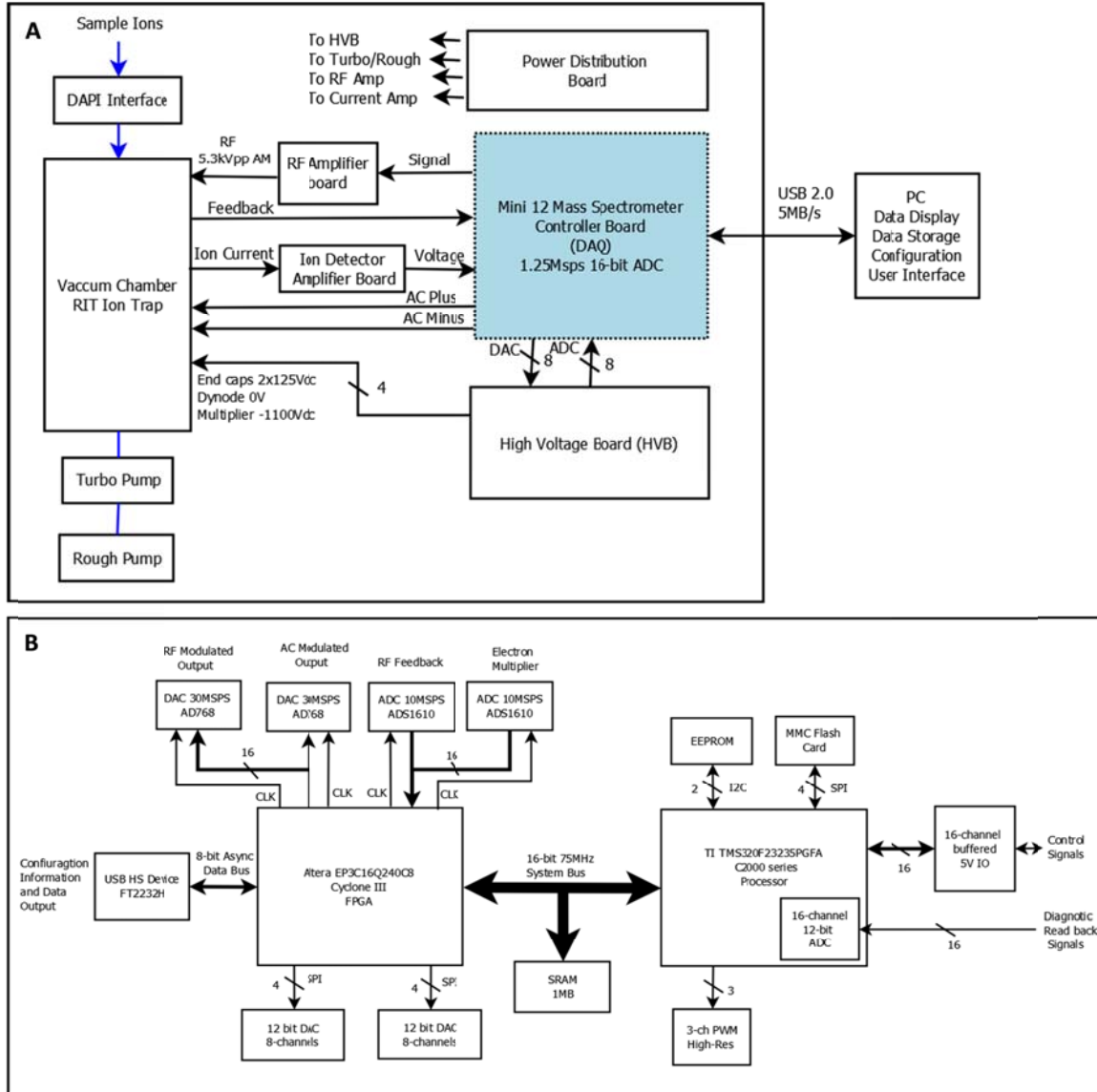


Figure 1.30: Images adapted from reference 4. A) Block diagram of the Mini-S and Mini 12 instrument systems and high level interpretation of the electronic signal connections. B) Details of the electronic signal paths for the FPGA, DSP, and shared random access memory (SRAM).

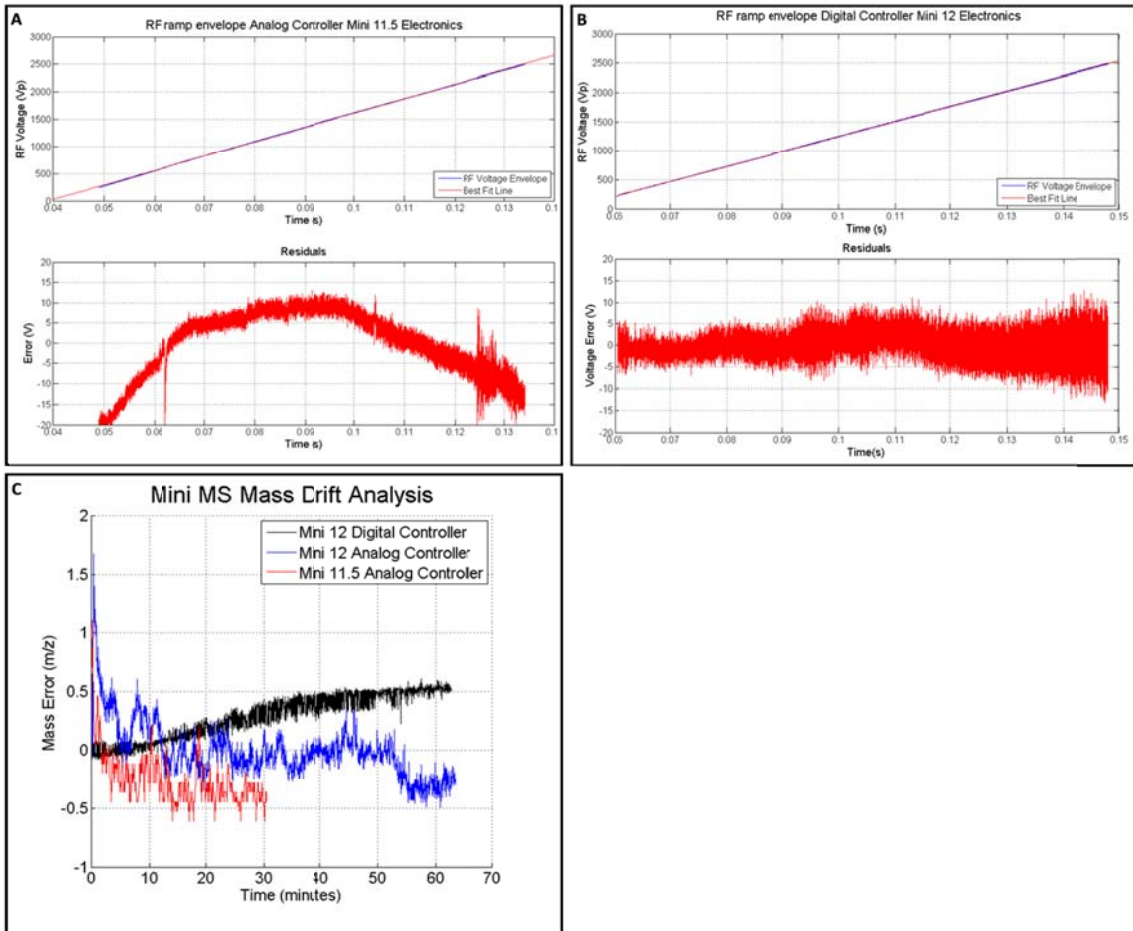


Figure 1.31: Images adapted from reference 4. A) Error associated with the RF amplitude ramp during mass analysis for the analog feedback control used on the Mini 11.5 instrument. B) Same plot as A, but with the Mini 12 digital controller. Notice that the magnitude of the RF error is substantially smaller over the entire RF ramp as compared to the analog control. C) Mass drift over time for the digital controller implemented on the Mini 12 compared to the analog implementation on the 11.5.

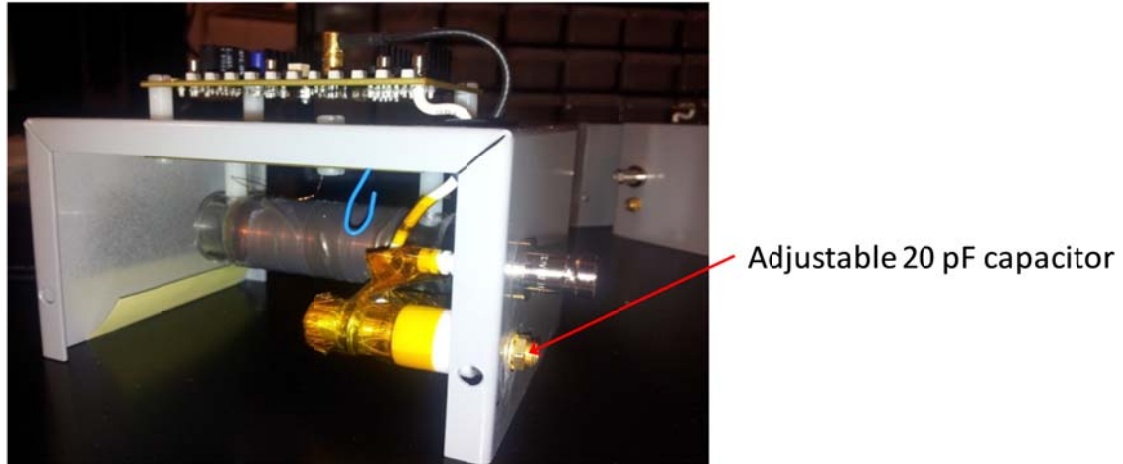


Figure 1.32: Open view of the RF coil box used to amplify the RF voltage amplitude. Note the use of a 20pF tuning capacitor in parallel with the RF resonant circuit. The tuning capacitor was used to manually adjust the resonate frequency of the circuit to 1 MHz by adding or removing capacitance.

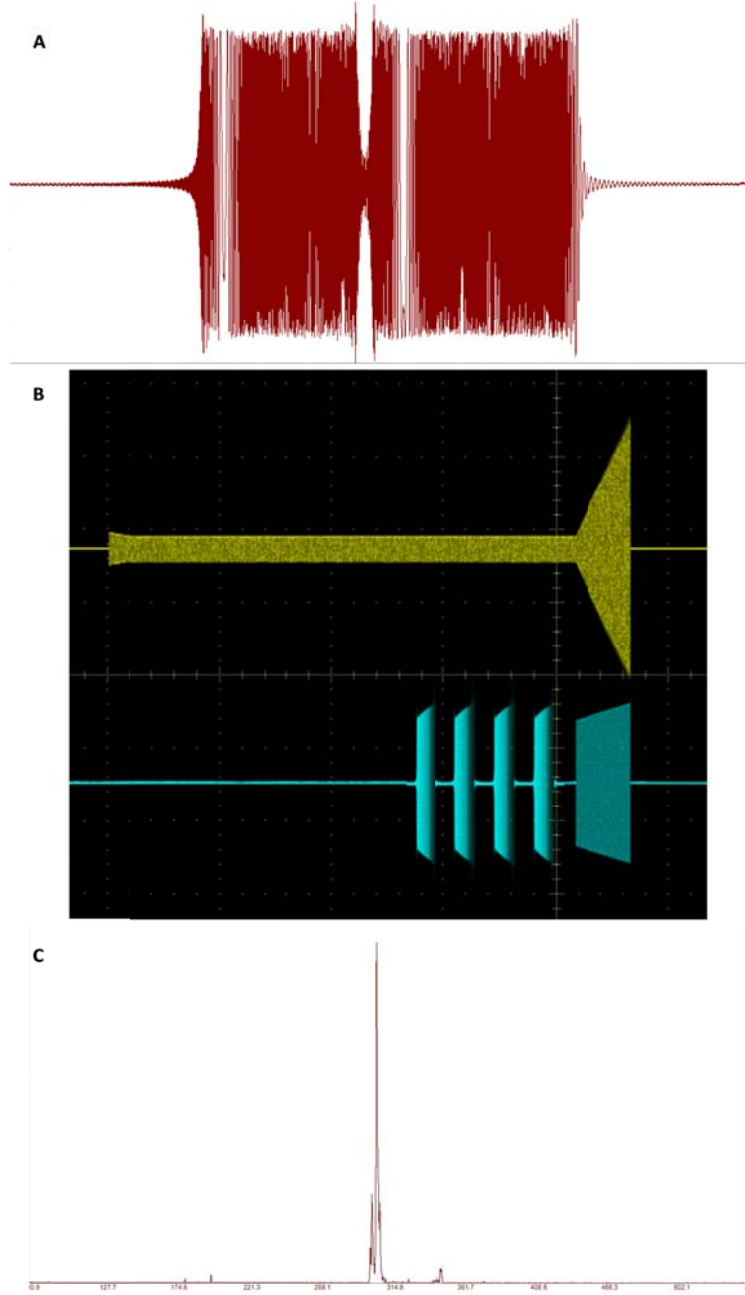


Figure 1.33: Application of SWIFT for ion isolation. A) Time domain SWIFT waveform calculated by the software based on the specified frequency notch. Waveform is applied to the X-electrodes a total of 4 times while the ions are stored inside the ion trap. Frequency notch is 277 to 292 kHz which corresponds to a mass isolation notch of m/z 301 – 310. B) Yellow trace is the RF waveform acquired from the RF amplifier board. Blue trace is the AC voltage applied to the X-electrodes acquired from the AC amplifier board. C) Mass spectrum after the isolation waveform has been applied; inside the notch cocaine (10ppb) m/z 304 $[M+H]^+$ and cocaine-d3 (50ppb) m/z 307 $[M+H]^+$ are isolated.

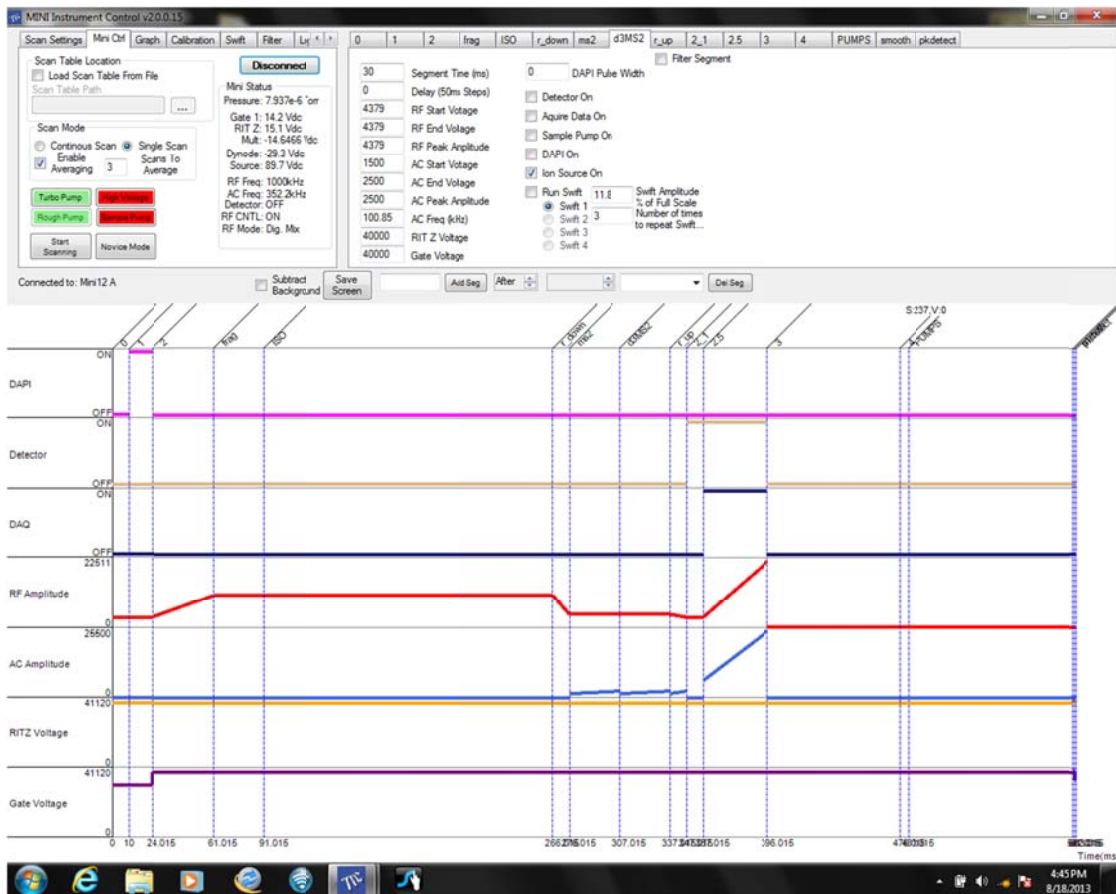
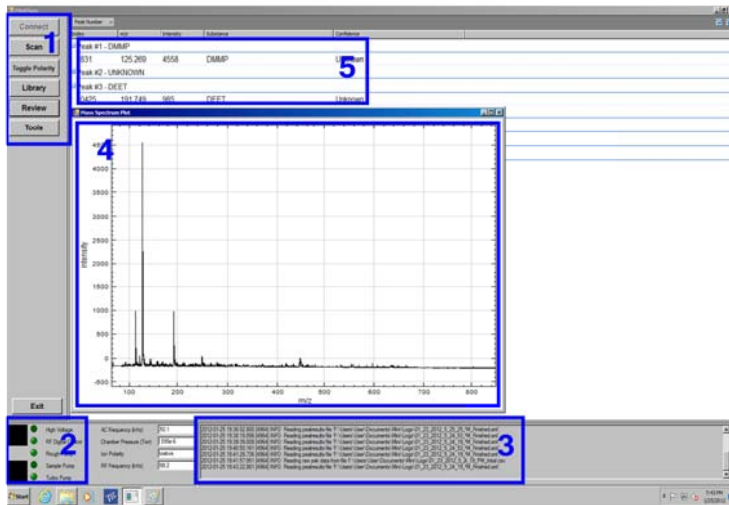


Figure 1.34: Advanced user interface for the Mini-S and Mini 12 instruments adapted from reference 4. This interface is used for setting the voltage control operation and timing for all of the instrument devices which includes the mass analyzer, ion detection circuit, source voltage, ion introduction, and data acquisition. In addition all of the instrument ADCs, the RF frequency, and the RF PID controller are also tuned through this interface. The central display allows for the viewing of acquired data, a graphical view of the instrument method, i.e. voltage amplitudes with respect to time, and the visualization of the SWIFT notch in both frequency and time domains.



1. Instrument operation tool bar
2. Instrument status and compound identification LEDs
3. System read- backs
4. Data visualization
5. Library search results

Additional features:

- RF frequency auto tune
- Automated startup and shutdown sequences
- Positive/ negative switching
- Specific m/z triggers for MSMS analysis

Figure 1.35: Novice user interface (NUI) that allows control of the Mini-S instrument. This interface was developed with research partners at JHU/APL and was designed to work on top of the advanced user interface by executing previously generated scan tables. The NUI is designed to be used with the library search feature however, other functionality necessary for instrument operation such as control of the vacuum system during start up and shutdown, data review, manual switch of polarities, and the ability sweep the RF frequency are also available.

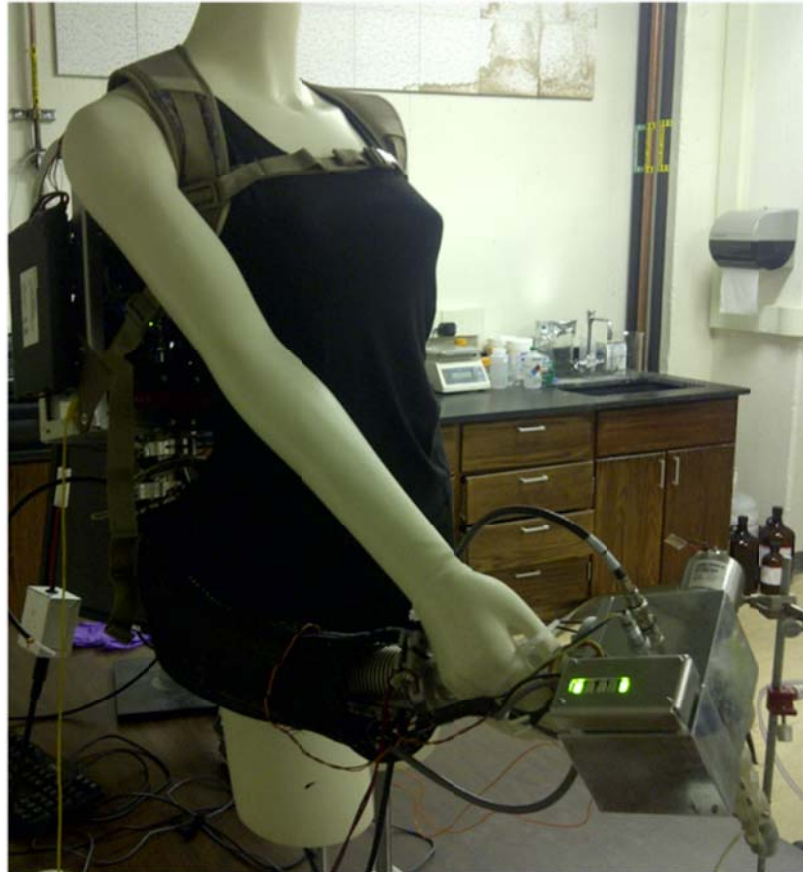


Figure 1.36: Fully assembled Mini-S instrument installed on a mannequin with active LEDs (green) on the hand-held unit indicating the instrument system status as ‘ready for analysis’.

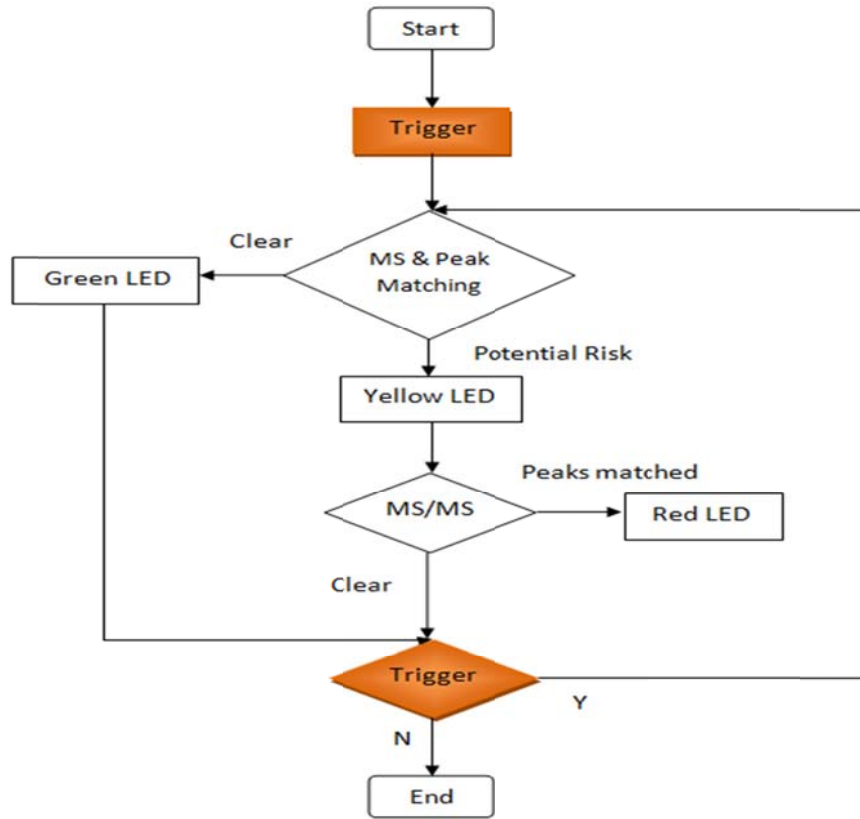


Figure 1.37: Decision flow chart for data acquisition results reporting for the color LEDs.

CHAPTER 2. APPLICATION OF MINIATURE MASS SPECTROMETERS FOR THE CHARACTERIZATION OF TISSUE TYPES VIA LIPID PROFILES

2.1 Introduction

Chapter 1 discusses the development of a backpack portable mass spectrometer; the Mini-S. This instrument is well suited for applications that require a high degree of mobility and the ability to directly sample surfaces that contain matrices and have complex geometries. However, monitoring of environmental contaminants, food, and therapeutic drugs, to name only a few applications, benefit from portable mass spectrometers, but do not require the degree of mobility nor do they require the surface sampling capabilities of the Mini-S. For these applications a desktop portable instrument, the Mini 12, has been developed, Fig. 2.1. The Mini 12 is discussed in detail by Li et al.[1], however, briefly this instrument uses the same electronic components and control software as the Mini-S, has dimensions of 57.15 x 31.75 x 40.64 cm (22.5 x 12.5 x 16.0 in), weights approximately 17.2 kg (38 lbs), and consumes an average of 65 W of power. The Mini 12 also uses the same mass analyzer, a rectilinear ion trap (RIT)[2] X₀ x Y₀ dimensions of 5 x 4 mm, and has an electron multiplier (EM) / conversion dynode assembly for the detection of ions that are positively and negatively charged.[3]

Designed to operate with paper spray as the primary ionization source,[4, 5] the Mini 12 has provisions for two onboard solvent pumps that dispense solvent to the paper spray cartridge. The PS cartridge is held by a specialized tray that establishes the

optimal distance between the paper spray cartridge, mass spectrometer inlet, high voltage electrode, and the solvent dispensing system. Similar to previous Mini instruments, the Mini 12 utilizes a KNF Neuberger (Trenton, NJ) mechanical pump (5 L/min) and a Pfeiffer Vacuum HiPace10 (Nashua, NH) turbo molecular pump (10 L/s) which comprise the vacuum system. A discontinuous atmospheric pressure interface (DAPI)[6, 7] is used to sample externally generated ions at atmospheric pressure.

The ability to sample from atmospheric pressures allows the Mini 12 to be compatible with ambient ionization sources and because the position of the mass spectrometer inlet with respect to the sample and ionization source has been designed to be relatively static multiple, different, types of ambient ionization sources can be interfaced with the Mini 12. This versatility is the focus of the work contained in this chapter. Here it is discussed how the new ambient desorption ionization (ADI) probe, touch spray (TS), is used with a modified Mini 12 to complete analysis of biological lipids directly from tissue samples. In the sections below it is demonstrated that the analysis of lipids directly from tissue, and the characterization of those sections of tissues, is possible and relevant for diagnostic and surgical applications. This initial work demonstrates utility for the combination of ambient ionization and portable mass spectrometers in a field that does not currently utilize miniaturized or portable instrumentation.

2.2 Lipid Analysis and Biological Tissue Characterization

It is well known that the lipid composition of cellular membranes is different across cell types and is dynamic within the same cell type. Differences in the lipid

composition of different cell types is conceptually easy to understand as differentiated cells have different functional roles inside the organism, although they may be present in adjacent sections of the same organ tissue. Conceptually more difficult to understand are the specific factors that promote physiological changes in lipid composition of the cell during its life cycle as well as, or in response to, metabolic, environmental, and disease related stress. Imaging mass spectrometry has been a key technology in this area of research as surgically-excised tissues are analyzed and a false-color image that pertains to the abundance of ions that are indicative of key lipids and, or, proteins can be produced.[8-10] The false-color image, maps the spatial distribution of lipids or proteins within the tissue section which have function-specific roles inside the tissue or pertain to diseased locations.

Ambient mass spectrometry coupled with commercial instrumentation has been widely used to conduct imaging analysis of tissues because individual tissue sections require little or no preparation. In particular, desorption electrospray ionization (DESI)[11] has become a prominent method due to (i) the ability to generate small spot sizes (30 - 100 μm), (ii) compatibility with nondestructive solvents, (iii) reproducibility of the method, and (iv) relatively short data acquisition times.[12-14] With DESI, three dimensional mapping of entire organs has been accomplished as well as the identification and, correct, classification of tumor stages which were based on the detected lipid profile(s).[15, 16] Being able to determine the tumor margin (region of the tumor tissue that is adjacent to healthy tissue) is of considerable importance during surgery where it is difficult to distinguish healthy from diseased tissue through visual or tactile means.

Recent work pursued by Takats, Z. et al. has focused on the ability to determine tumor margins, in-real time, and during a surgical procedure. Rapid evaporative ionization mass spectrometry (REIMS)[17] and direct combination of ultrasonic surgical aspiration and sonic spray mass spectrometry (CUSA / SSI)[18] have been proposed as methods that allow for (i) the ability to surgically excise tissue (ii) release of lipids and proteins from the cellular structure, and (iii) the lipid or protein analyte released to the gas or condensed phase to be directly sampled by the mass spectrometer. MS data is reduced via post processing methods that categorize the tissue type and diseased / not diseased state of the tissue sample.

Both REIMS and CUSA / SSI have excellent figures of merit that include (i) analysis times of ~ 2 - 3 s, (ii) limits of detection that are on the order of 100 ng/ml, (iii) reliable MS information can be obtained with 50 - 500 µg of tissue (iv) negligible carryover and memory effects, and (v) low false positive and false negative rates. Furthermore, these techniques appear to be somewhat universal in that there are no specialized requirements for the surgical facility. Both of the previously discussed surgical sampling methods utilize a continuous sampling source and full size commercial MS instrumentation to complete mass analysis. Limits of detection and duty cycles of the Mini-S and Mini 12 instrument are inside the range of what is required by direct analysis of surgical tissue. So, the question that was asked in the pursuit of this work was if the limitations typically associated with miniaturized instruments (i) available mass range, (ii) mass resolution, (iii) sampling capabilities, and (iv) carryover or excessive memory effects would preclude miniaturized instruments from being used for tissue analysis during intraoperative surgical procedures.

2.3 Materials and Methods

Mouse brain was obtained from JAX Mice and Services (Bar Harbor, ME) which was surgically removed and flash frozen. Once frozen the mouse brain was sectioned with a cryotome (Thermo Scientific, Waltham, MA) at 15 μm intervals and placed on a glass slide. Coronal sections of the mouse brain, bragma 8 - 10 (approximately the middle three slices of the brain) were sampled from the glass slide with a TS probe. Briefly, the TS probe is an aluminum, teasing needle with a roughened tip that has a 120 deg bend and a 20-30 μm tip size. Approximately 100 μg of tissue is sampled from the slide onto the touch spray probe. The TS probe with sample was placed directly in front of the mass spectrometer inlet with approximately 1 cm between the end of the TS probe and the front capillary. 4.5 kV_{dc} was applied to the TS probe. 1 μl of methanol was used as the elution solvent which was applied directly to the TS probe just after starting data acquisition. This was done to be sure that the spray plume would be sampled by the DAPI valve during sample introduction; spray flow rate from the TS is 6 $\mu\text{l}/\text{min}$. Analysis time for the instrument was 2.5s which only allowed for one to two scans to be acquired for each tissue sample.

2.4 Results and Discussion

The inability of the Mini 12 to continuously sample ions at atmospheric pressure makes TS an elegant method for acquiring a tissue sample from a region of an organ that is of surgical interest because TS does not require continuous solvent flow or high frequency / amplitude RF. A subtle yet important distinction between TS and REIMS or CUSA / SSI is that the cellular material used for analysis is ablated or disintegrated

during the cutting action. Thus, parts of the organ tissue are necessarily excised before they can be analyzed. In contrast, the TS probe can be used to sample and analyze tissues (repeatedly if necessary) prior to excising any piece of that tissue from the organ.

In practice, the process of sample collection and mass analysis with TS took little more than 10 - 20 s and allowed for high spatial precision sampling from the organ. Additionally, this method requires very small tissue samples and solvent volumes, and there is no possibility of a mechanical malfunction during the experiment because the TS probe does not contain any moving parts. Should a probe become contaminated it can be replaced during the surgery and subsequently cleaned with typical sterilization protocols.

The Mini 12 instrument used in these experiments used a modified RF circuit to produce 7.8 kV_{p-p} (at 1 MHz) as the maximum voltage amplitude output, Fig. 2.2. This voltage is enough to detect ions of *m/z* up to 1300 Th, Fig 2.3, more than enough for the detection of the most abundant phospholipids, sulfatides, and proteins present in brain-tissue. Mass resolution is critically important for the analysis of biological compounds. The main RF was scanned at a rate of 9500 Th / s, resonance ejection was used during mass analysis where the supplementary RF was ramped from 2 to 7 V_{p-p} (maximum) at 369 kHz ($q_z = 0.81$). Under these conditions peak widths of 1 – 2.5 Th (FWHM) were achieved across the full mass range which allowed for the separation of ion species that were 3 Th apart and inside the target mass range of 700 to 900 Th. In particular, the most abundant phospholipids and sulfatides which were used to characterize tissue sections are clearly visible from the mass spectrum, Fig 2.4.

The combination of TS and a Mini 12 mass spectrometer for the detection of lipids from mouse brain was inspired by previous work in this lab in which an entire

brain organ was imaged via 2D imaging of consecutive tissue slices which were then reconstructed into a 3D image of the brain organ.[15] In this work the major sections of the mouse brain, gray and white matter, were classified based upon presence and relative intensities of phosphatidylserine (PS 18:0 / 22:6), phosphatidylinositol (PI 18:0 / 20:4), and the sulfatide (ST 24:1) inside the full scan mass spectrum, Fig .2.5. For these experiments, it was not only important to detect the relevant phospholipids, but the data quality needed to be consistent from sample to sample such that the raw mass spectral data could be processed in a manner that allowed for clear differentiation between adjacent tissue types. Typically discriminant analysis techniques are used such that individual mass spectra, i.e. regions of tissue, can be classified as being a part of a group or subset of a group.

Three different coronal sections, bragma 8-10, of the same mouse brain were analyzed from a total of 16 different samples from the cerebral cortex and hippocampus which are compromised of gray and white matter respectively. Data was exported from the Mini 12 and the mass range was re-aligned to account for 0.5 to 1.0 amu shifts in the data. This adjustment was necessary due to very minor instabilities in the RF amplitude during mass analysis, which would be anticipated for a prototype instrument. The MS data was then truncated between the mass range of 700 and 900 Th, the target mass range for this analysis, and processed by an online application, MetaboAnalyst 2.0[19] that offered a suite of statistical processing tools. It should be noted that this online tool is a third party application that has been independently verified for the integrity of the statistical results. Furthermore, the statistical tool used was designed to accept data acquired from commercial instruments that produce low and high resolution data. The

results showed excellent 2 and 3 dimensional separation of the white and gray matter tissue. The largest contributors to the variation between the two tissue samples were the ions of mass-to-charge 888.8 (ST 24:1) and 885.6 (PI 18:0 / 20:4), Fig 2.6. These results match the anticipated physiology as the difference in major lipid components between white and grey tissue types is the presence of ST 24:1 and lower abundances of PI 18:0/20:4.

2.5 Conclusion

The ability to differentiate tissue types in real-time, or, near real-time is of importance for intraoperative surgical applications where the operating surgeon needs to quickly determine the margin of the diseased tissue. Here it is demonstrated that TS, a technique that is less invasive than REIMS or CUSA / SSI, can be coupled to a miniaturized mass spectrometer. It is also demonstrated that the performance of the Mini 12 miniature mass spectrometer can provide data analysis on time scales of 2 - 4s, which is relevant for surgical operations, and can produce data that is of sufficient quality and reproducibility that it can be used to successfully characterize tissue types with standard statistical processing methods. Although much work is still required to improve the mass resolution and atmospheric pressure sampling of portable instruments, this demonstration suggests that miniature mass spectrometers have the potential to be used in place of larger commercial instruments for procedures that require tissue analysis.

2.6 References

1. L. Li, T. Chen, Y. Ren, P.I. Hendricks, R. Cooks, Z. Ouyang, Miniature Ambient Mass Analysis System, *Anal Chem - Submitted*, (2013).
2. Z. Ouyang, G. Wu, Y. Song, H. Li, W.R. Plass, R.G. Cooks, Rectilinear Ion Trap: Concepts, Calculations, and Analytical Performance of a New Mass Analyzer, *Analytical Chemistry*, 76 (2004) 4595-4605.
3. N.L. Sanders, S. Kothari, G.M. Huang, G. Salazar, R.G. Cooks, Detection of Explosives as Negative Ions Directly from Surfaces Using a Miniature Mass Spectrometer, *Analytical Chemistry*, 82 (2010) 5313-5316.
4. J. Liu, H. Wang, N.E. Manicke, J.-M. Lin, R.G. Cooks, Z. Ouyang, Development, Characterization, and Application of Paper Spray Ionization, *Analytical Chemistry*, 82 (2010) 2463-2471.
5. H. Wang, J.J. Liu, R.G. Cooks, Z. Ouyang, Paper Spray for Direct Analysis of Complex Mixtures Using Mass Spectrometry, *Angew. Chem.-Int. Edit.*, 49 (2010) 877-880.
6. L. Gao, R.G. Cooks, Z. Ouyang, Breaking the Pumping Speed Barrier in Mass Spectrometry: Discontinuous Atmospheric Pressure Interface, *Analytical Chemistry*, 80 (2008) 4026-4032.
7. L. Gao, G. Li, Z. Nie, J. Duncan, Z. Ouyang, R.G. Cooks, Characterization of a discontinuous atmospheric pressure interface. Multiple ion introduction pulses for improved performance, *International Journal of Mass Spectrometry*, 283 (2009) 30-34.
8. R.M. Caprioli, T.B. Farmer, J. Gile, Molecular imaging of biological samples: Localization of peptides and proteins using MALDI-TOF MS, *Analytical Chemistry*, 69 (1997) 4751-4760.
9. L.A. McDonnell, R.M.A. Heeren, Imaging mass spectrometry, *Mass Spectrometry Reviews*, 26 (2007) 606-643.
10. R.G. Cooks, Z. Ouyang, Z. Takats, J.M. Wiseman, Ambient mass spectrometry, *Science*, 311 (2006) 1566-1570.
11. Z. Takats, J.M. Wiseman, R.G. Cooks, Ambient mass spectrometry using desorption electrospray ionization (DESI): instrumentation, mechanisms and applications in forensics, chemistry, and biology, *Journal of Mass Spectrometry*, 40 (2005) 1261-1275.

12. D.I. Campbell, C.R. Ferreira, L.S. Eberlin, R.G. Cooks, Improved spatial resolution in the imaging of biological tissue using desorption electrospray ionization, *Analytical and Bioanalytical Chemistry*, 404 (2012) 389-398.
13. A.L. Dill, L.S. Eberlin, A.B. Costa, D.R. Ifa, R.G. Cooks, Data quality in tissue analysis using desorption electrospray ionization, *Analytical and Bioanalytical Chemistry*, 401 (2011) 1949-1961.
14. L.S. Eberlin, C.R. Ferreira, A.L. Dill, D.R. Ifa, L. Cheng, R.G. Cooks, Nondestructive, Histologically Compatible Tissue Imaging by Desorption Electrospray Ionization Mass Spectrometry, *Chembiochem*, 12 (2011) 2129-2132.
15. L.S. Eberlin, D.R. Ifa, C. Wu, R.G. Cooks, Three-Dimensional Vizualization of Mouse Brain by Lipid Analysis Using Ambient Ionization Mass Spectrometry, *Angew. Chem.-Int. Edit.*, 49 (2010) 873-876.
16. L.S. Eberlin, I. Norton, A.L. Dill, A.J. Golby, K.L. Ligon, S. Santagata, R.G. Cooks, N.Y.R. Agar, Classifying Human Brain Tumors by Lipid Imaging with Mass Spectrometry, *Cancer Research*, 72 (2012) 645-654.
17. K.-C. Schaefer, J. Denes, K. Albrecht, T. Szaniszlo, J. Balog, R. Skoumal, M. Katona, M. Toth, L. Balogh, Z. Takats, In Vivo, In Situ Tissue Analysis Using Rapid Evaporative Ionization Mass Spectrometry, *Angew. Chem.-Int. Edit.*, 48 (2009) 8240-8242.
18. K.C. Schafer, J. Balog, T. Szaniszlo, D. Szalay, G. Mezey, J. Denes, L. Bognar, M. Oertel, Z. Takats, Real Time Analysis of Brain Tissue by Direct Combination of Ultrasonic Surgical Aspiration and Sonic Spray Mass Spectrometry, *Analytical Chemistry*, 83 (2011) 7729-7735.
19. J. Xia, R. Mandal, I.V. Sinelnikov, D. Broadhurst, D.S. Wishart, MetaboAnalyst 2.0-a comprehensive server for metabolomic data analysis, *Nucleic Acids Research*, 40 (2012) W127-W133.

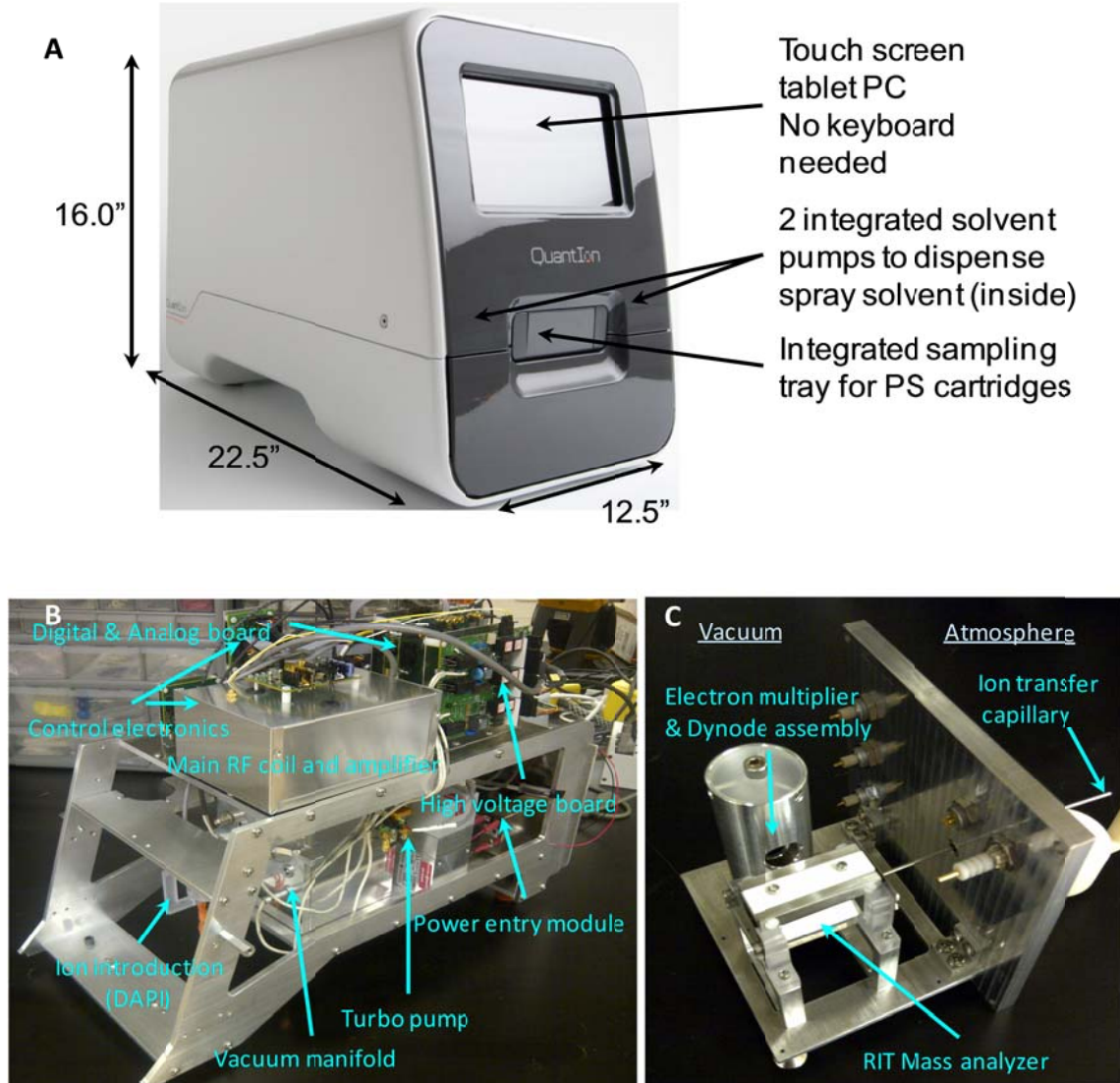


Figure 2.1: A) Image and dimensions of the Mini 12 mass spectrometer fully assembled with the touch screen PC computer and the paper spray cartridge tray installed. B) Mini 12 instrument chassis. The placement of the electronics is visible on the top half of the instrument and the vacuum system, manifold and inlet to the mass spectrometer is on the bottom. C) Details of the mass analyzer, 5 x 4 mm rectilinear ion trap (RIT) and the electron multiplier / dynode assemble which comprise the ion detection system.

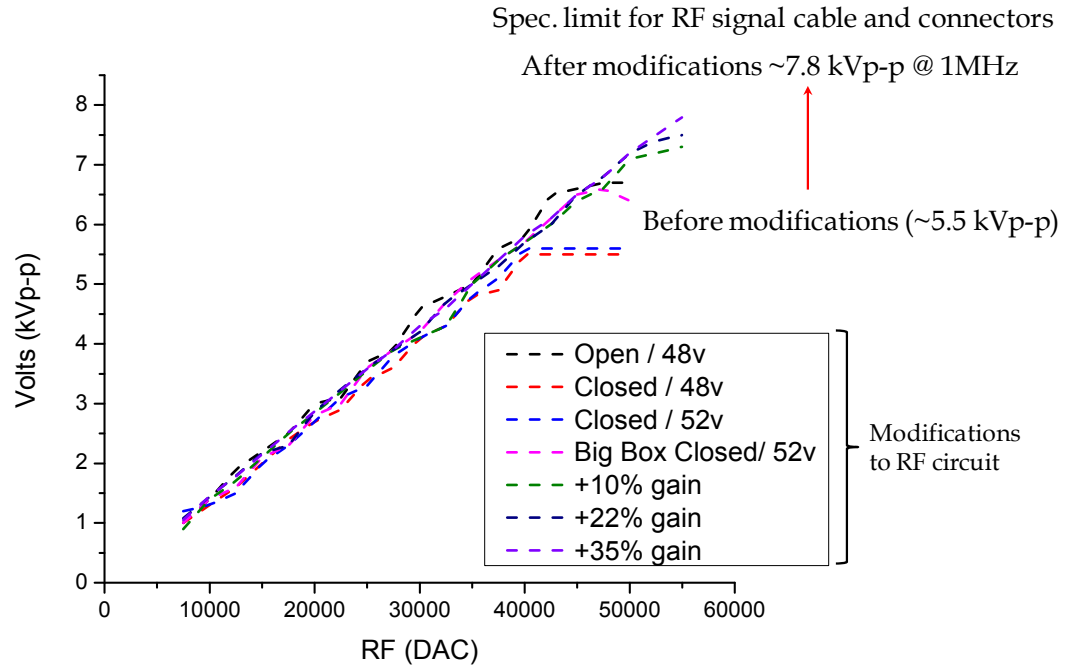


Figure 2.2: Modifications to the Mini 12 RF circuit which increased the voltage from 5.5 kV_{p-p} to 7.8 kV_{p-p}. The anticipated maximum detectable mass-to-charge at the increased voltage amplitude was 1300 amu. The voltage rating of the RF cable and connections were the limiting factor in extending the voltage amplitude further.

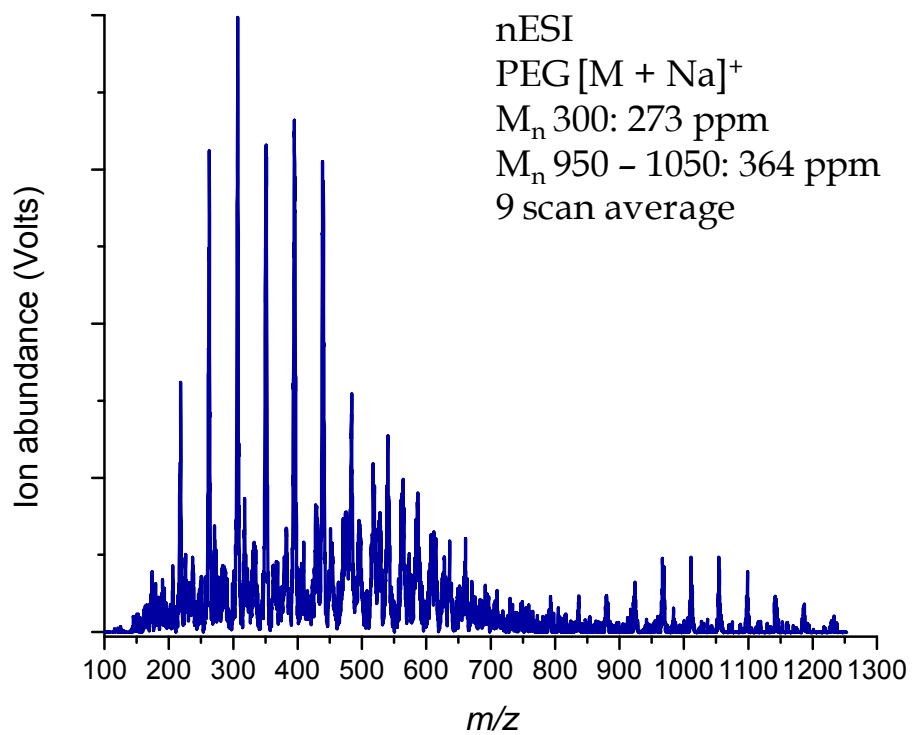


Figure 2.3: nESI mass spectrum of PEG oligomers obtained on the Mini 12 instrument as demonstration of the increased mass range.

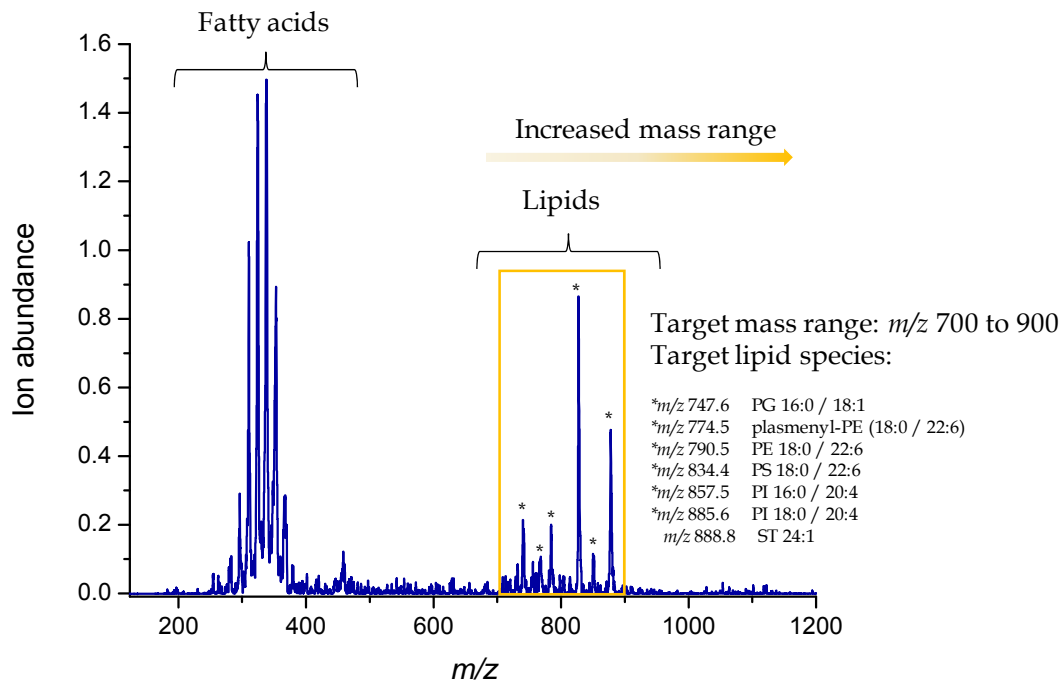


Figure 2.4: Full scan mass spectrum of gray matter ($\sim 100 \mu\text{g}$) sampled directly from mouse brain tissue with TS and analyzed on a Mini 12 mass spectrometer. The mass range m/z 700 to 900 is the target range for biological lipid analysis. Inside this mass range the relevant phospholipids used in tissue characterization can be clearly identified. Common lipids are listed in the figure and are designated in the mass spectrum with an asterisks.

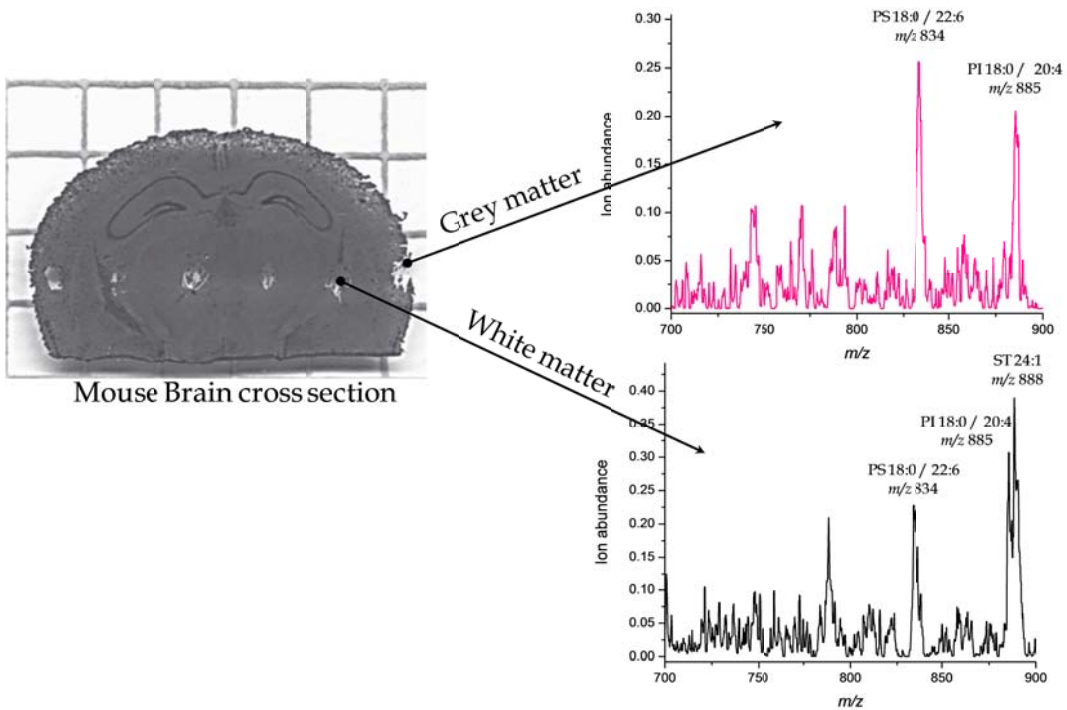


Figure 2.5: Left) Optical image of mouse brain tissue slice, grid spacing is 2 mm. The small circles across the mouse brain tissue are regions that have been sampled with the TS probe is spot represents $\sim 100 \mu\text{g}$ of material that has been removed. Right top) grey matter sampled from the cerebral cortex Right bottom) White matter sampled from the hippocampus. Notice that for the two regions the relative intensity of PS 18:0 / 22:6 is lower for white matter relative to grey matter and also the occurrence of ST 24:1. Both of these differences are expected physiologically and are measured here with a Mini 12 mass spectrometer.

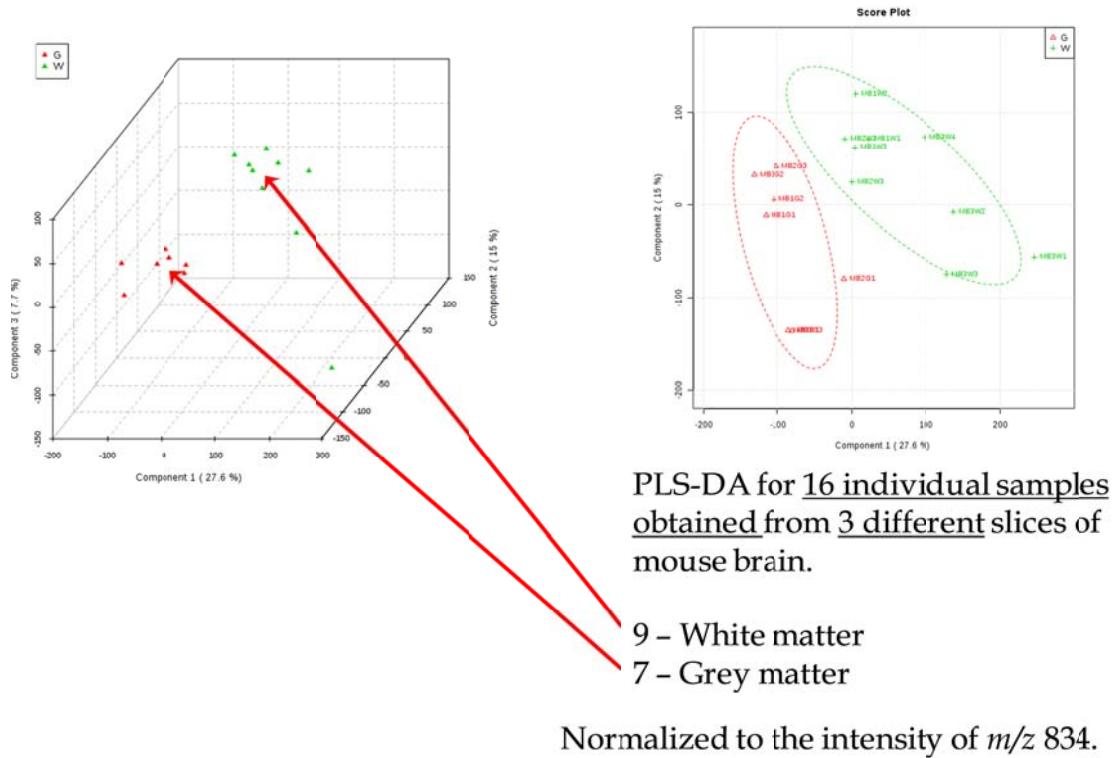


Figure 2.6: PLS-DA analysis of the grey and white matter mass spectra acquired with a Mini 12 MS. The statistical tool used to complete the processing was a 3rd party online application <http://www.metaboanalyst.ca/MetaboAnalyst/faces/Home.jsp>. Largest sources of difference between the two samples were for m/z 888.5 corresponding to ST 24: 1 and m/z 885 corresponding to PI 18:0 / 20:4, fitting well with the physiological differences between white and grey matter of brain tissue.

CHAPTER 3. PERFORMANCE OF A LOW VOLTAGE ION TRAP AND ALTERNATIVE MATERIALS FOR ION TRAP FABRICATION

3.1 Introduction

Demand for *in situ* detection of specific compounds at the parts-per-billion (ppb) and parts-per-million (ppm) levels is one of the factors driving the development of portable mass spectrometers[1-5]. The ability to successfully miniaturize and / or simplify the geometry of instrument components, particularly the electronics, vacuum system, and mass analyzer[6, 7] is the key to this development. Quadrupole ion trap mass analyzers are well suited for use in portable instruments due to their ability to operate at elevated pressures (10^{-2} to 10^{-3} torr), relaxing the vacuum system requirements, and the ability to use a single mass analyzer for tandem MS experiments. Additionally, ion traps, especially those with electrodes of simple geometry such as the cylindrical ion trap[8] (CIT) and the rectilinear ion trap[7] (RIT), are more easily scaled to mini[9-11] and micro[12-15] dimensions than other mass analyzer types. Furthermore, the simplified shape of the electrodes allows for fabrication of these mass analyzers with non-traditional manufacturing techniques and materials.[16]

RITs are simplified linear ion trap mass analyzers consisting of planar electrodes, viz. two end caps, and pairs of Y-electrodes and X-electrodes, respectively. At the usual size scale the optimized dimensions are 5x4 mm nominally (one-half the distance

between opposing X and Y-electrodes)[7]. Details related to the dimensions, mechanical tolerances, and assembly of the 5 x 4 RIT can be found in appendix A. This device has been well characterized and utilized as the mass analyzer in portable instruments for in-field applications[17-20]. Since the operating voltage scales as the square of the distance between the trapping electrodes, and power scales to the square of the RF amplitude, greatly reduced power requirements needed for portable instruments can be achieved by size reduction[10]. RIT mass analyzers have previously been fabricated with nearly the same geometry as used in this work and they have given peak widths of approximately 1.5 - 2 Th (FWHM)[21, 22]. However, these earlier experiments did not employ small total MS systems, and notably they did not suffer from the limited pumping capabilities characteristic of handheld MS systems. In this work a miniaturized, steel, RIT and a full size RIT fabricated with industrial printed circuit board (PCB) manufacturing methods were characterized in a single stage manifold, without ion optics or specialized buffer gas, and under pressure conditions comparable to those of a portable mass spectrometer. Both systems utilized a discontinuous atmospheric pressure interface (DAPI) to sample externally generated ions[23-25]. Performance of the miniaturized, steel, RIT analyzer (1.66x1.43 mm for X_0 and Y_0 respectively; 1/3rd the scale of the usual RIT dimensions) and the PCB RIT (5x4 mm for X_0 and Y_0 respectively) when operated at pressures expected for a portable instrument is characterized and evaluated in this study.

3.2 1/3 Size Stainless Steel RIT

3.2.1 Materials and Method

Machining of the electrodes (304 stainless steel) was executed using computer numerical control (CNC) followed by hand polishing of the inner electrode surfaces to a mirror finish. Precision cut Macor ceramic established the inter-electrode distances and formed the insulating spacers between adjacent electrodes (Fig. 3.1 and 3.2). Analyzer assembly was completed by hand. Upon final assembly the average gap spacing (distance between adjacent X and Y-electrodes) was 0.590 mm, and the trapping dimensions (distance between opposing X and Y-electrode pairs) were 1.66 mm and 1.43 mm respectively. These measurements were made using an optical microscope (SmartScope MVP 300, Optical Gauging Products, Inc.) and are accurate to $\pm 1 \mu\text{m}$. The length of the ion trap (z-dimension) and the dimensions of the ion ejection slits in the X-electrodes were measured to be 40 mm and 0.33 x 25 mm, respectively, as measured with a micrometer (Mitutoyo, CD-6 BS) additional details can be found in appendix A. As in all linear ion traps, the z dimension of this device controls the ion trapping volume but does not impact the generation of a quadrupolar field in the x-y plane.[26] A confining force is however, established in the z-dimension by applying a DC potential to the end cap electrodes.

Mass calibration and experimental determination of the upper limit of the mass range was determined using polyethylene glycol (PEG) in methanol/water (1:1 by vol.) at concentrations ranging from 10 μM to 100 μM . The PEG mix was prepared from seven oligomers with average molecular weights ranging from approximately 100 to 600

(Sigma-Aldrich, Inc.) all used without further purification or modification. PEG was selected for its ability to produce singly-charged, sodiated adducts in the presence of sodium salts.

Ions generated by nano-ESI were pulsed into the vacuum manifold using a discontinuous atmospheric pressure interface (DAPI)[23-25]. This ion introduction interface is comprised of a controllable, short duration valve (ASCO Scientific, Florham Park NJ) with a conductive rubber capillary as the seating material (Simolex Rubber Corp., Plymouth MI). When the DAPI valve is open, gas phase neutrals and the ions generated in the ambient environment are passed to the low pressure (base pressure $\sim 10^{-4}$ to 10^{-6} torr) vacuum manifold that contains the mass analyzer. Once the DAPI valve is closed, the introduced ions are trapped while neutral gas-phase molecules are pumped away. This decreases the operating pressure of the ion trap, and allows the electron multiplier (Photonics, Magnum 5903) to be turned on. In the scan function implemented for these experiments (Fig. 3.3), the DAPI valve was opened to the atmosphere for 50 ms and then closed for the duration of the pump down and mass scan period, which was approximately 2000 ms. The stainless steel ion introduction capillary was aligned coaxially with the aperture in the ion trap front end cap and positioned such that there was a 1 mm gap between the two. This allowed gating of the ions into the trap using the front end cap voltage and it avoided perturbation of the quadrupolar field by inserting the capillary directly between the X and Y electrodes.

A laboratory built system that utilized LCQ Duo (Thermo Fisher Scientific, San Jose CA) electronics and LCQ Duo Tune 1.0 software/Ion Trap Control Language interface was used for electronic timing and control. The vacuum system consisted of a

TSQ7000 manifold with single stage pumping. A BocEdwards E2M30 (30 m³/hr) rotary vane pump at the front and a Pfeifer 260 turbo molecular pump (210 L/s) backed by a second BocEdwards E2M40 (40 m³/hr) was necessary to accommodate the large vacuum manifold. The performance of the vacuum system was specifically de-tuned to achieve pressures in the ion trap similar to those given by miniature systems.

After the DAPI valve was closed, ending the 50 ms ion sampling pulse, the front end cap was held at 1.8 V for 150 ms to allow the ions in the sample volume to transfer completely out of the 200 mm introduction capillary and into the ion trap. The front end cap was then raised to 15 V, and the rear end cap continued to be held at 25 V. Ions were allowed to cool for 500 ms while the manifold pressure dropped from its peak pressure of ~75 mtorr to ~15 mtorr, at which point the RF (drive frequency 1.105MHz) amplitude was scanned from 68 V_{0-p} to 610 V_{0-p} at a rate of 833.3 Th/s, thus completing the analytical mass scan. Mass analysis was completed with a mass selective instability scan with resonance ejection by applying a dipolar, supplementary, RF to the x-electrodes at a frequency of 358 kHz ($q_z = 0.77$). Amplitude of the supplementary AC was ramped linearly from 340 mV_{p-p} to 1.1 V_{p-p} throughout the analytical scan. In this work the scan rate is slower than that used in typical operation of full size RITs (10,000 Th/s) which was necessary to maximize mass spectral resolution.

3.2.2 Results and Discussion

3.2.2.1 MS Performance

Mass resolution performance, ion capacity, mass accuracy, and scan speed of the analyzer depend upon the electronic field structure that is used to trap gas-phase ions which is established by the electrode geometry. Calculations to determine the expansion coefficients from the electric field were completed for the 1/3 size stainless steel RIT by modeling the electrode geometry in SIMION (SIMION 8.0, Scientific Instrument Services, Inc.), Fig. 3.4, and exporting the potential array to an electric field calculator coded with MathCAD (MathCAD v14, Parametric Technology Corporation), Fig. 3.5 and 3.6. The calculated value for the quadrupole (A2) expansion term for the electric filed was 0.673 which was in agreement to the reported values for the full size RIT (0.654)[7] within 5% and was considered to be accurate and acceptable, Fig. 3.6. Additional details related to the MathCAD program used to process the potential array export from SIMION and calculation of the expansion coefficients can be found in appendix A.

The trapping voltage (depth of the effective potential well) for the miniature RIT was optimized by increasing the RF amplitude several volts at a time until the m/z distribution of the PEG sample was detected. A trapping voltage of 68 V_{0-p} (low mass cutoff $\sim m/z$ 140) was determined experimentally to be the minimum voltage necessary to detect ions of up to m/z 1250. The PEG ions covered the entire mass range and were separated by intervals of 44 Th (Fig. 3.7). The peak RF voltage necessary for completing

an analytical scan over this mass range was 610 V_{0-p} and spectral resolution was on the order of 2 Th FWHM at *m/z* 305, which increased with, *m/z* (Fig. 3.8).

By way of comparison the Mini 11, a portable mass spectrometer that uses a full size RIT as the mass analyzer, is limited by the available RF voltage (2250 V_{0-p}) to a maximum *m/z* of 700 when operated at ~1 MHz[27]. Under the operating conditions described in materials and methods, the miniaturized RIT is capable of detecting *m/z* of 900 at 448 V_{0-p}. The two systems give comparable mass resolution. The miniaturized RIT mass analyzer, as evaluated on a laboratory scale instrument, exhibits analytical performance in terms of mass resolution, mass range, and operating voltage that is adequate for affirmative detection of small organic molecules, e.g. explosives, chemical warfare agents, drugs of abuse, and most pharmaceuticals, that have mass-to-charge values below 500. Thus, implementation of such a mass analyzer on a portable instrument is highly attractive. To further support the feasibility of using a 1/3 size RIT in a portable instrument the method of ion introduction in the present study is similar to that expected for a portable instrument also utilizing a DAPI source. It is anticipated that operational pressure for the detuned laboratory scale instrument and the portable instrument will be sufficiently similar to avoid a significant decrease in performance.

The DAPI source provides a method for sampling charged analytes at atmospheric pressure while satisfying the vacuum requirements of the mass spectrometer. We note, however, the somewhat inefficient use of the sample since the duty cycle (open time vs. overall cycle period) of the DAPI is just a few percent. Another drawback is that the mass analyzer is operated at pressures that are an order of magnitude or more above the optimal working pressure of 10⁻³ torr and there is no control over the number of ions

introduced to the ion trap. These factors together with mechanical imperfections in the electrode alignment and the surfaces of the electrodes contribute to peak broadening. The results obtained here are consistent with the performance anticipated for a device of this geometry, scale, and operation inside the pressure range achieved with a DAPI source.

3.2.2.2 Mass Selective Ion Ejection

Frequencies which correlate with effective ion ejection were measured by applying a low amplitude AC signal to the X-electrodes during the ion trapping phase of the scan function. Ions of a selected m/z were resonantly excited and ejected from the ion trap by controlling the frequency, amplitude, and duration of the applied AC signal. Typical time and amplitude values ranged from 50 to 100 ms and 100 to 200 mV_{p-p}.

An approximate determination of the ejection frequency for an ion of a particular m/z ratio can be made by monitoring the frequency at which the ion disappears from the mass spectrum (Fig. 3.9). Repeating this experiment for the most abundant ions in the sample, allows a plot of the ejection frequency versus m/z to be constructed. The results (Fig. 3.10) demonstrate that the ejection frequencies for a given m/z are in close agreement with the calculated secular frequency and follow the theoretical trend attributable to the inverse relationship between q_z and m/z .

3.2.2.3 Tandem MS Performance

The protonated cocaine molecule, m/z 304, fragments to give m/z 182 by elimination of benzoic acid[28, 29]. Also observable, although in lower abundance, is a

competing fragmentation pathway in which benzaldehyde is lost from the protonated molecule, forming an ion of *m/z* 198. Conditions under which both fragmentation pathways are observed can be particularly useful for chemical profiling experiments used to identify pure compounds and/or compound metabolites using known fragmentations[30]. Cocaine was isolated through the application of a stored waveform inverse Fourier transform (SWIFT)[31] function for 450 ms, followed by activation at $q_z = 0.36$ (~ 147 kHz) for 30 ms at amplitudes of approximately 200 mV_{p-p}. DAPI, as previously described, allows introduction of both analyte ions and neutral molecules into the vacuum manifold and mass analyzer. The manifold pressure for CID was optimized at 20 mtorr (as measured from the mini-convectron gauge on the vacuum manifold), where the neutral molecules introduced during the DAPI pulse serve as the buffer gas during these experiments.

To optimize the voltage used during MS/MS experiments, the AC amplitude was varied from 200 to 250 mV_{p-p} by increments of approximately 10 mV_{p-p} (Fig. 3.11 and 3.12). The maximum fragmentation efficiency for cocaine was found to be 9.1% (Fig. 3.13). In this experiment over 90% of the precursor ions are lost prior to dissociation. Fragmentation of the small peptide Bradykinin was also obtained under the optimized pressure and CID energy conditions, where characteristic fragments for y₈, y₇, y₆, y₅, b₅, and b₈ were observed, Fig. 3.14. Demonstration of the ability to perform tandem MS experiments for peptide species suggest that this reduced scale mass analyzer, could be used for the detection of biologically relevant species, an area where portable or instruments with miniaturized systems are not being heavily utilized.

The mechanism by which ions are activated in CID and by which they are resonantly ejected from the ion trap are similar. Excitation energy is supplied using an AC waveform applied in resonance with the ion secular frequency. Considering that the pseudopotential well depth is proportional to the magnitude of the applied RF, the well for a miniaturized RIT is shallower than its full-size counterpart by approximately a factor of nine (due to the three-fold reduction in physical size). Under these conditions resonance ejection increasingly competes with activation and results in poor fragmentation efficiency. Figure 3.15 is a composite image indicating full scan and tandem MS performance as well as mechanical dimensions, operational voltages, and pressures.

3.3 1/2 Size PCB RIT

Parallel to the characterization of the miniaturized stainless steel RIT was the brief investigation and characterization of RIT mass analyzers at both the full size and miniaturized geometries. These mass analyzers were fabricated with industrial printed circuit board (PCB) technology and materials. There have been previous reports of using PCB material to fabricate ion traps intended for chemical analysis[32, 33] however, this investigation was undertaken as a practical exercise for field-portable instruments to assess the effect of replacing the steel mass analyzer. Here, PCB was selected because fabrication could be completed with the same mechanical precision as stainless steel machining (i.e., electrode dimensions and surfaces roughness), cost of fabrication is more than ten times less expensive (\$100 – 160), fabrication time is approximately 4-7 of days, and this technology is scaleable to produce miniaturized RITs such as those previously

discussed. Altogether, these factors make the concept of a disposable mass analyzer practical and potentially necessary for portable instruments that have sample introduction strategies in which the mass analyzer can become contaminated via direct exposure to the ambient atmosphere.

3.3.1 PCB Fabrication

FR-4 was used as the fabrication material for the PCB electrodes (X- electrode, Y-electrode, and end caps) and the ion trap assembly support used to mount the device inside the vacuum manifold. RF-4 is an industry standard, non-conducting, fiberglass material with an epoxy binder. It features high mechanical stability, is chemically inert, has extremely low water absorptivity, and has strong adhesion to successive laminate layers, i.e. the gold metal which is used to form the electrode. Full size (Fig. 3.16) or 1/3rd size RIT (Fig. 3.17) fabrication is well within the capability of the current tooling used in the manufacture of PCBs which produce electrical traces and through-hole vias at sizes of 0.1524 mm (0.006 in) as a standard dimension. The critical trapping dimensions for this device continue to be 5 x 4mm in the X₀ and Y₀ dimensions, except for the 1/3rd size RIT which was 1.66 x 1.33 mm, and in both cases gold plating (0.1778mm (0.007in) thick) was used on one side of the FR-4 substrate to define the trapping electrodes. Mechanical schematics for the full size and miniature RIT (both stainless steel and PCB) can be found in appendix A.

3.3.2 Characterization

Capacitance of the full size PCB RIT was measured to be approximately 7 pF whereas the stainless steel RIT of the same dimension was measured to be 18.7 pF under the same conditions (Table 3.1). If the ion trap is considered to be a generalized form of a parallel plate capacitor then the lower capacitance for the PCB RIT can be explained by a reduction in the electrode size which can be limited, due to the fabrication technology, to only the area responsible for setting up the electric field to trap gas-phase ions while still maintaining the optimized 5 x 4 mm geometry. This reduction in capacitance has a twofold benefit (i) a slightly larger inductor can be used in the LC-Tank circuit which translates to increased voltage amplitude output and therefore increased mass range, (ii) less current is necessary to charge up the capacitor allowing the RF and supplementary RF circuits to obtain their maximum voltages while driving less current, allowing for faster response times and less distortion to the electrical signal(s).

The PCB RIT was operated with a main RF frequency tuned to 942 kHz and was operated in the mass selective instability scan mode with resonance ejection 409 kHz ($q_z = 0.887$). As previously discussed $[PEG+Na]^+$ was used to characterize this instrument for spectral resolution and mass range. A Mini 11.5 was used as the instrument to perform all of the characterization work for the PCB RIT. Under these conditions the maximum detectable mass-to-charge was 921 ($n = 20$) and FWHM values for low mass ions were measured to be just under 1 Th and increased to approximately 2 Th across the mass range (Fig. 3.18). This performance was nearly identical to the stainless steel RIT in terms of mass range, spectral resolution, and MS² capabilities (Fig. 3.19) when operated on Mini 11.5 under the same conditions.

It has been demonstrated that the regions of ion stability can be influenced by operational conditions such as space charge, pressure, and electrode structure.[7, 34, 35] To verify that the PCB RIT had the same region of stability as that reported for the stainless steel RIT with the same X_0 and Y_0 dimensions, region 1 of the ion stability map was mapped with a Mini 11.5 modified to allow for a DC potential to be placed on the X-electrodes. These changes were completed in a way that allowed for the timing and voltage control of the DC and RF circuits to be made with the on-board Mini 11.5 power supplies and method editor software, i.e. no external power supplies or pulse generators were used, Fig. 3.20.

It was observed that the base peak for methamphetamine was m/z 91 instead of m/z 150, $[M+H]^+$, which is a fragment of the protonated molecular ion that is formed as a result of a nitrogen beta-cleavage. This fragmentation occurred prior to any modulation of the RF or DC voltages and, so far, has only been witnessed on Mini instruments which use a discontinuous atmospheric pressure interface to inject externally generated ions into the mass analyzer. As a consequence the stability region was mapped with m/z 91.

Mapping of the stability region was completed in two parts, the top half of the diagram was mapped by modulating the RF from $110V_{0-p}$ to $440V_{0-p}$ in 4.5V steps and DC from 0V to -50V in 1.5V steps. The bottom half was completed by first isolating m/z 91 using RF DC isolation, $340V_{0-p}$ and -42V for 20ms, followed by RF modulation from $110V_{0-p}$ to $440V_{0-p}$ in 4.5V steps and DC from 0V to 50V in 1.5V steps. Data were recorded by setting the RF Voltage and then increasing the DC DAC values until the signal to noise ratio was approximately 1 for m/z 91 indicating that the threshold of the

stability boundary had been reached, at this point the RF DAC value was incremented, the DC DAC was reset to 0V and the process was repeated, Fig. 3.21.

Of the four types of RITs discussed in this work the 1/3 size RIT fabricated from PCB material appears to offer the most promise because it combines all the benefits of PCB fabrication with that of a miniaturized RIT, Table 3.1. Despite the fact that the 1/3 size RIT exhibits reduced performance for tandem MS and mass resolution it could be of use for applications that tolerate these limitations as a trade off for an overall reduction in instrument size, weight, and low power operation. While this device has been constructed and signal has been obtained when used as the mass analyzer on a miniature mass spectrometer, it was not fully characterized.

3.4 Conclusions

The mass range, spectral quality, tandem MS capabilities, and operating voltages of a miniaturized RIT or a full size RIT fabricated with PCB material demonstrate attractive mass analyzer options for use in portable mass spectrometers. This study also serves as a method for evaluation of ion traps in other areas of research namely, devices with further miniaturized dimensions, ion traps made of electrodes fabricated using new technologies/materials, ion traps with novel electrode geometries, and ion trap arrays[9, 22, 36-38]. In addition, at this scale (and smaller) the RF amplitude necessary to complete mass analysis over a range of approximately 100-500 Th, suitable for the detection of most standard organic compounds, is within the range of commercially available operational amplifiers. A “direct drive” approach to RF control would offer the benefit of ion trap operation without the use of specially designed inductance coils, thus

simplifying the design and construction of field portable mass spectrometers through elimination of a tuned resonance circuit for the main RF.

3.5 References

1. Keil, A., et al., *Monitoring of Toxic Compounds in Air Using a Handheld Rectilinear Ion Trap Mass Spectrometer*. Analytical Chemistry, 2008. **80**(3): p. 734-741.
2. Mulligan, C.C., et al., *Direct monitoring of toxic compounds in air using a portable mass spectrometer*. Analyst, 2006. **131**(4): p. 556-567.
3. Riter, L.S., et al., *Analytical Performance of a Miniature Cylindrical Ion Trap Mass Spectrometer*. Analytical Chemistry, 2002. **74**(24): p. 6154-6162.
4. Smith, J.N., et al., *Facility monitoring of toxic industrial compounds in air using an automated, fieldable, miniature mass spectrometer*. Analyst, 2011. **135**(5): p. 994-1003.
5. Smith, J.N., et al., *Ion/molecule reactions for detecting ammonia using miniature cylindrical ion trap mass spectrometers*. Analyst. **136**(1): p. 120-7.
6. Badman, E.R. and R. Graham Cooks, *Miniature mass analyzers*. Journal of Mass Spectrometry, 2000. **35**(6): p. 659-671.
7. Ouyang, Z., et al., *Rectilinear Ion Trap: Concepts, Calculations, and Analytical Performance of a New Mass Analyzer*. Analytical Chemistry, 2004. **76**(16): p. 4595-4605.
8. Bonner, R.F., et al., *The cylindrical ion trap. Part I. General introduction*. International Journal or Mass Spectrometry and Ion Physics, 1977. **24**(3): p. 255-269.
9. Austin, D.E., et al., *Novel Ion Traps Using Planar Resistive Electrodes: Implications for Miniaturized Mass Analyzers*. Journal of the American Society for Mass Spectrometry, 2008. **19**(10): p. 1435-1441.
10. Patterson, G.E., et al., *Miniature Cylindrical Ion Trap Mass Spectrometer*. Analytical Chemistry, 2002. **74**(24): p. 6145-6153.
11. Zhu, Z., et al., *Characterization of bioparticles using a miniature cylindrical ion trap mass spectrometer operated at rough vacuum*. Analyst.
12. Blain, M.G., et al., *Towards the hand-held mass spectrometer: design considerations, simulation, and fabrication of micrometer-scaled cylindrical ion traps*. International Journal of Mass Spectrometry, 2004. **236**(1-3): p. 91-104.

13. Chaudhary, A., F. van Amerom, and R.T. Short, *Development of Microfabricated Cylindrical Ion Trap Mass Spectrometer Arrays*. Microelectromechanical Systems, Journal of, 2009. **18**(2): p. 442-448.
14. Cruz, D., et al., *Design, microfabrication, and analysis of micrometer-sized cylindrical ion trap arrays*. Review of Scientific Instruments, 2007. **78**(1): p. 015107-015107.
15. Moxom, J., et al., *Analysis of Volatile Organic Compounds in Air with a Micro Ion Trap Mass Analyzer*. Analytical Chemistry, 2003. **75**(15): p. 3739-3743.
16. Peng, Y. and D.E. Austin, *New approaches to miniaturizing ion trap mass analyzers*. TrAC Trends in Analytical Chemistry, 2011. **30**(10): p. 1560-1567.
17. Huang, G., et al., *Direct analysis of melamine in complex matrices using a handheld mass spectrometer*. Analyst. **135**(4): p. 705-711.
18. Keil, A., et al., *Ambient Mass Spectrometry with a Handheld Mass Spectrometer at High Pressure*. Analytical Chemistry, 2007. **79**(20): p. 7734-7739.
19. Nathaniel L. Sanders, E.S., *Hand-held mass spectrometer for environmentally relevant analytes using a variety of sampling and ionization methods*. European Journal of Mass Spectrometry. **16**(1): p. 11-20.
20. Sokol, E., et al., *Rapid hydrocarbon analysis using a miniature rectilinear ion trap mass spectrometer*. Analyst, 2008. **133**(8): p. 1064-1071.
21. Fico, M., et al., *Circular arrays of polymer-based miniature rectilinear ion traps*. Analyst, 2009. **134**(7): p. 1338-1347.
22. Fico, M., et al., *Miniaturization and Geometry Optimization of a Polymer-Based Rectilinear Ion Trap*. Analytical Chemistry, 2007. **79**(21): p. 8076-8082.
23. Gao, L., R.G. Cooks, and Z. Ouyang, *Breaking the Pumping Speed Barrier in Mass Spectrometry: Discontinuous Atmospheric Pressure Interface*. Analytical Chemistry, 2008. **80**(11): p. 4026-4032.
24. Gao, L., et al., *Characterization of a discontinuous atmospheric pressure interface. Multiple ion introduction pulses for improved performance*. International Journal of Mass Spectrometry, 2009. **283**(1-3): p. 30-34.
25. Xu, W., et al., *Study of Discontinuous Atmospheric Pressure Interfaces for Mass Spectrometry Instrumentation Development*. Analytical Chemistry. **82**(15): p. 6584-6592.

26. Schwartz, J.C., M.W. Senko, and J.E.P. Syka, *A two-dimensional quadrupole ion trap mass spectrometer*. Journal of the American Society for Mass Spectrometry, 2002. **13**(6): p. 659-669.
27. Gao, L., et al., *Handheld Rectilinear Ion Trap Mass Spectrometer*. Analytical Chemistry, 2006. **78**(17): p. 5994-6002.
28. Wang, P. and M.G. Bartlett, *Collision-induced dissociation mass spectra of cocaine, and its metabolites and pyrolysis products*. Journal of Mass Spectrometry, 1998. **33**(10): p. 961-967.
29. McLuckey, S.A., D.E. Goeringer, and G.L. Glish, *Collisional Activation with Random Noise in Ion Trap Mass-Spectrometry*. Analytical Chemistry, 1992. **64**(13): p. 1455-1460.
30. Kondrat, R.W., G.A. McClusky, and R.G. Cooks, *Multiple reaction monitoring in mass spectrometry/mass spectrometry for direct analysis of complex mixtures*. Analytical Chemistry, 1978. **50**(14): p. 2017-2021.
31. Guan, S. and A.G. Marshall, *Stored waveform inverse Fourier transform (SWIFT) ion excitation in trapped-ion mass spectrometry: Theory and applications*. International Journal of Mass Spectrometry and Ion Processes, 1996. **157-158**: p. 5-37.
32. Jiang, D., et al., *Printed Circuit Board Ion Trap Mass Analyzer: Its Structure and Performance*. Analytical Chemistry, 2013. **85**(12): p. 6041-6046.
33. Li, X.X., et al., *Ion Trap Array Mass Analyzer: Structure and Performance*. Analytical Chemistry, 2009. **81**(12): p. 4840-4846.
34. Todd, J.F.J., et al., *Relative Efficiencies of Confinement of Ar⁺ and Ar²⁺ Ions in a Quadrupole Ion Storage Trap (Quistor)*. International Journal of Mass Spectrometry and Ion Processes, 1978. **28**(2): p. 141-151.
35. Whitten, W.B., P.T.A. Reilly, and J.M. Ramsey, *High-pressure ion trap mass spectrometry*. Rapid Communications in Mass Spectrometry, 2004. **18**(15): p. 1749-1752.
36. Clare, A.T., et al., *Linear Ion Trap Fabricated Using Rapid Manufacturing Technology*. Journal of the American Society for Mass Spectrometry. **21**(2): p. 317-322.
37. Maas, J.D., et al., *Miniature Monolithic Rectilinear Ion Trap Arrays by Stereolithography on Printed Circuit Board*. Microelectromechanical Systems, Journal of, 2010. **19**(4): p. 951-960.

38. Yang, M., et al., *Development of a Palm Portable Mass Spectrometer*. Journal of the American Society for Mass Spectrometry, 2008. **19**(10): p. 1442-1448.

Table 3.1: Comparison of RIT mass analyzers constructed at different dimensions and with different materials

RIT comparison					
Material	Dimensions (X ₀ x Y ₀ x Z mm)	Capacitance (pF)	Inductance (μ H)	Voltage (V _{op}) to obtain m/z 2000 (boundary ejection)	Voltage (V _{op}) to obtain m/z 2000 (resep. $q_z = 0.78$)
Stainless Steel (316)	5 x 4 x 40	18.7	398	7101	6102
PCB (FR-4)	5 x 4 x 40	6.3	494	7101	6102
Stainless Steel (304)	1.66 x 1.33 x 40	22.1	378	789	678
PCB (FR-4)	1.66 x 1.33 x 40	8.2	476	789	678

* Inductance calculations assume 45 pF is included in the cable and cable connections from the vacuum manifold to the inductor

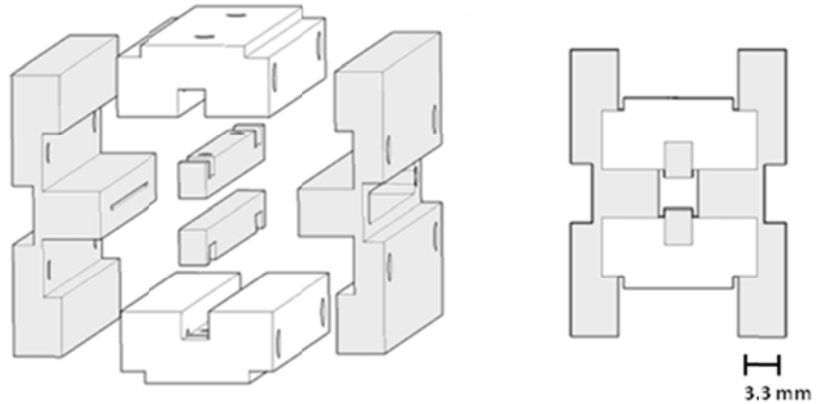


Figure 3.1: Computer aided design (CAD) model of the miniature RIT trapping electrodes and ceramic spacers. The ceramic spacers (white) ensure proper alignment of the trapping electrodes (gray) and act as electrical insulators.

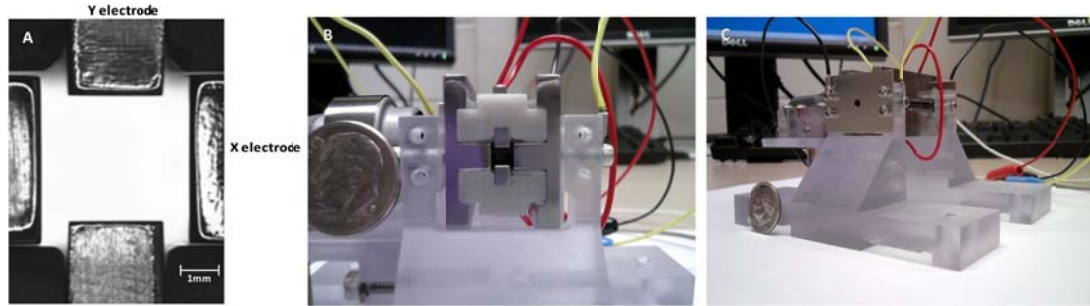


Figure 3.2: A) Optical image of the X-Y plane of the $1/3^{\text{rd}}$ scaled ion trap note the position of the X and Y- electrodes which have X_0 and Y_0 dimensions of 1.66 and 1.33mm respectively. B & C) Images of the fully assembled ion trap mounted to its holder and positioning of the electron multiplier along the ion ejection slit on the X-axis; A US dime (17.91 mm) is used for scale.

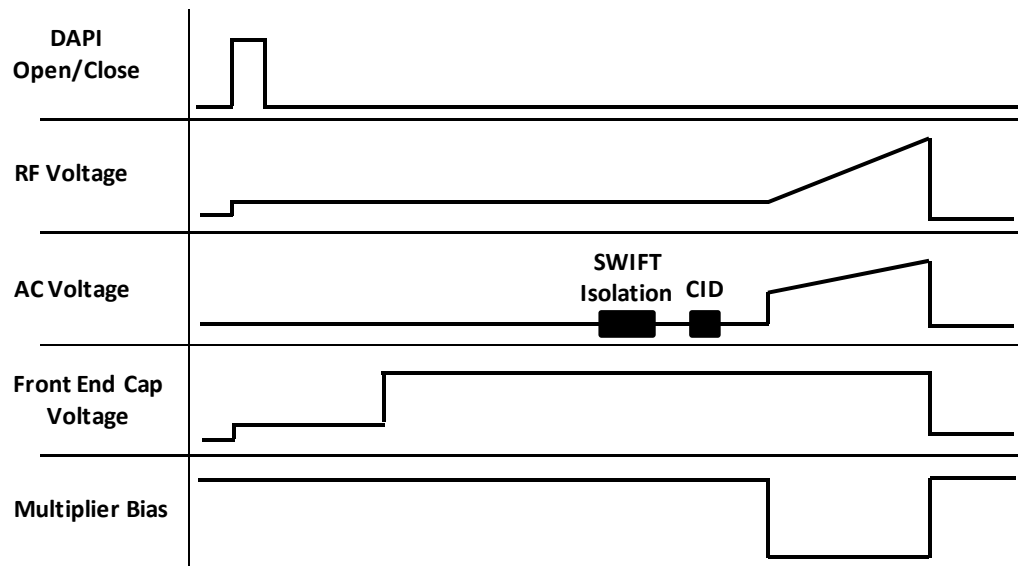


Figure 3.3: Scan function used to operate the miniaturized RIT. During experiments in which no ion isolation or activation were conducted amplitudes and time segments for SWIFT and CID were set to zero.

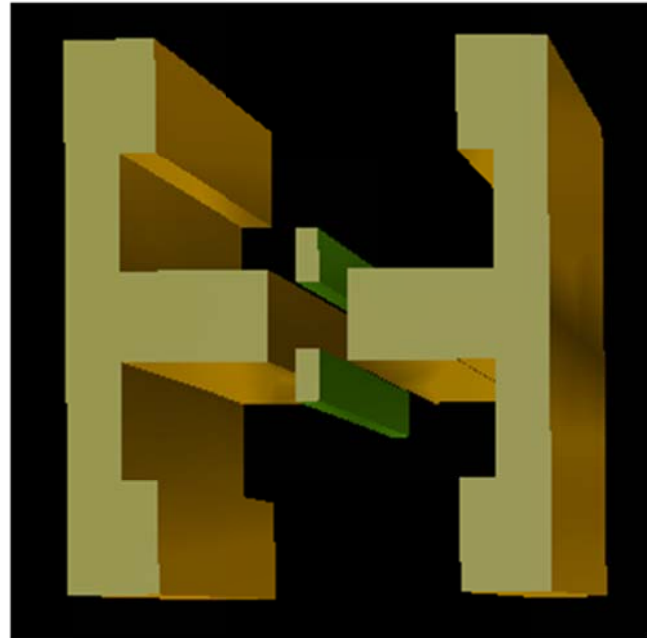


Figure 3.4: SIMION modeling of 1/3rd size stainless steel ion trap. Electrode structures were used to calculate the expansion coefficient for the quadrupole (A2) component of the electric field.

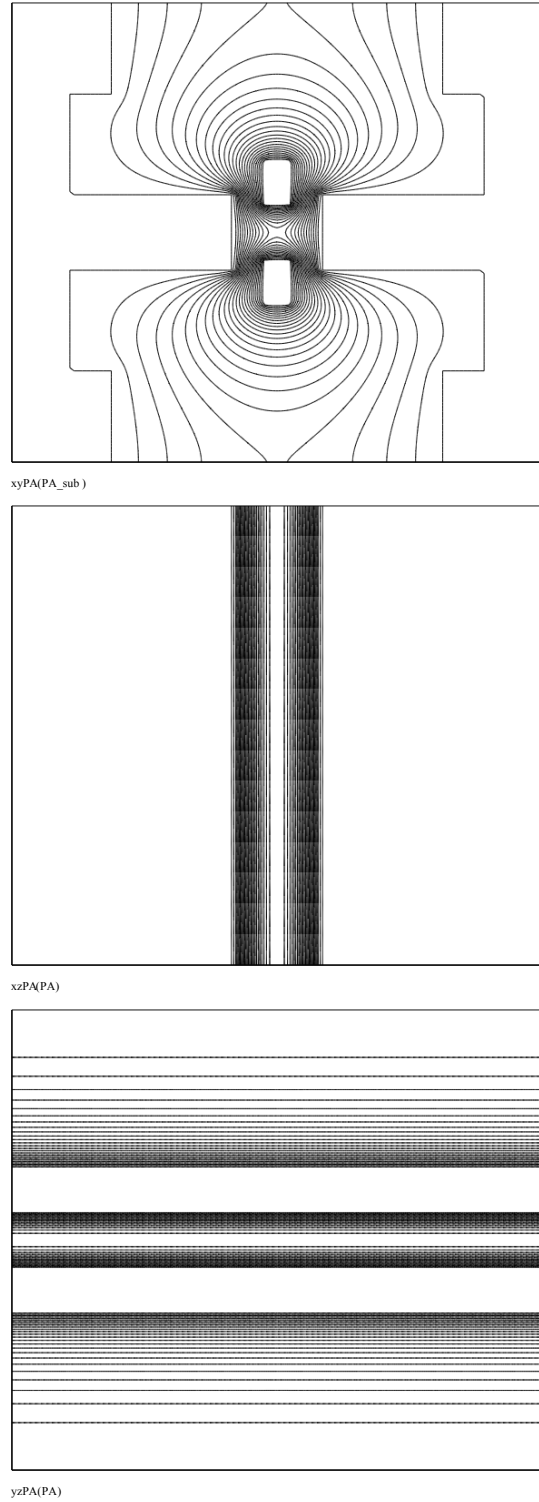
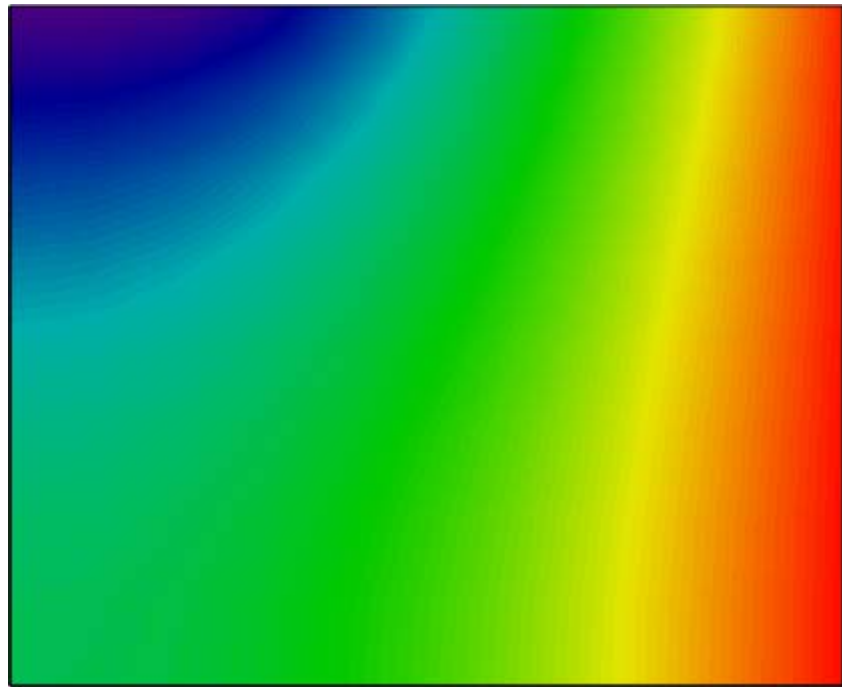


Figure 3.5: Visualization of the electric fields for 1/3rd size RIT calculated from the SIMION potential array. Top) Field in the X-Y plane; Middle) Field in the X-Z plane; Bottom) Field in the Y-Z plane.



grid(PA_sub)

Figure 3.6: Electric field in the X-Y plane; Note: due to symmetry only $\frac{1}{4}$ of the entire field (represented by this grid) is required for the calculation of the expansion coefficients.

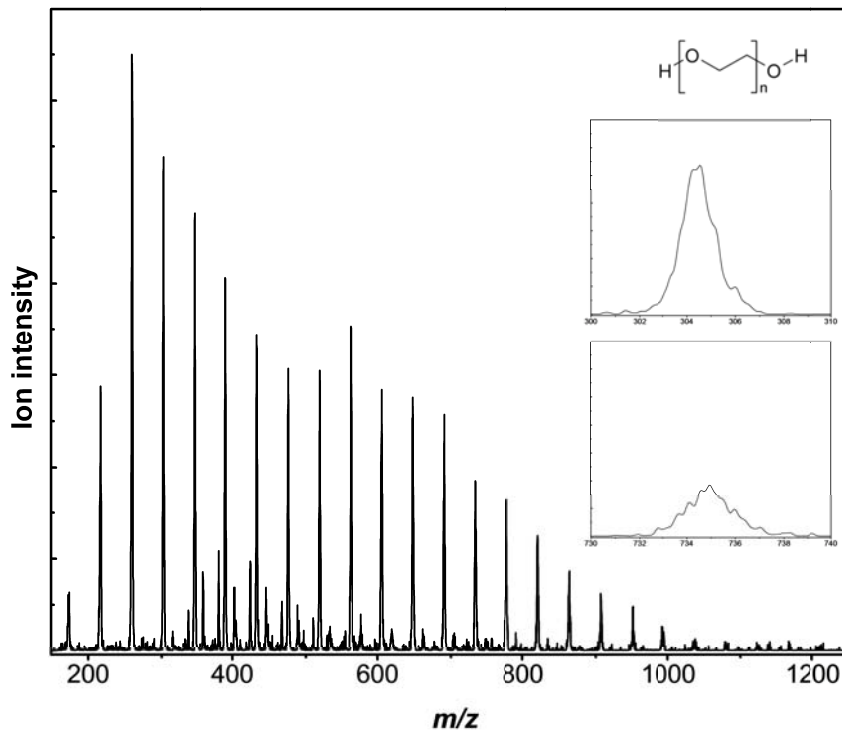


Figure 3.7: Nano-electrospray ionization of PEG oligomers 1-2 Th (FWHM) at concentrations of $10 \mu\text{M}$ to $100 \mu\text{M}$ in $1 \times 10^{-3} \text{ M NaOH}$. RF voltage amplitude scan from $68 \text{ V}_{0-\text{p}}$ to $610 \text{ V}_{0-\text{p}}$, using resonance ejection at 358 kHz with the AC amplitude ramped from $340 \text{ mV}_{\text{p-p}}$ to $1.1 \text{ V}_{\text{p-p}}$ throughout the analytical scan.

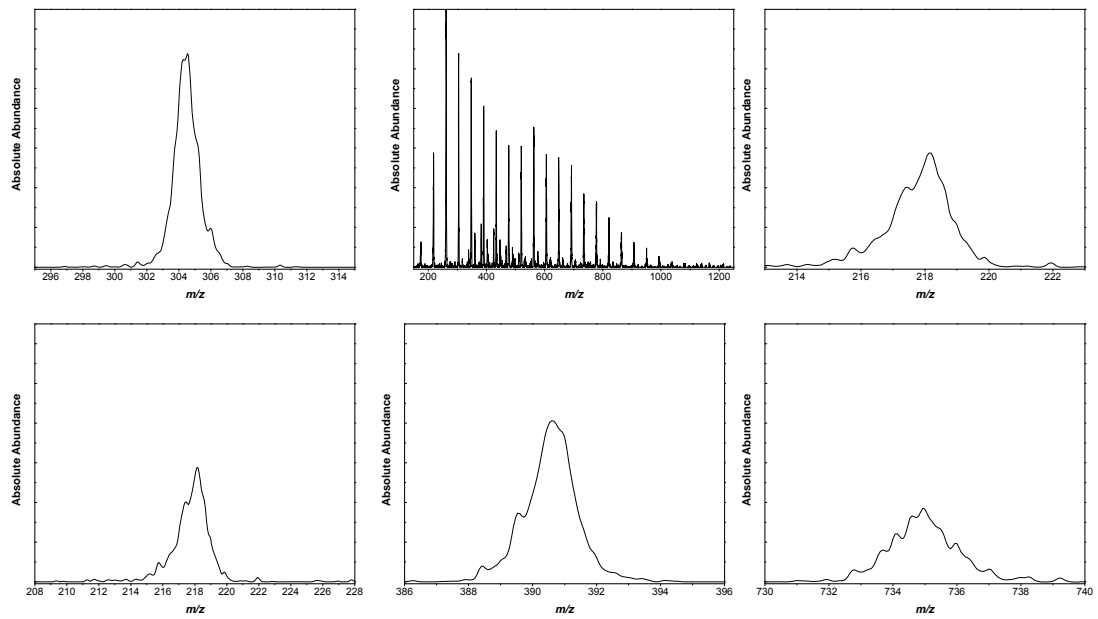


Figure 3.8: Full scan performance of the 1/3rd size RIT for PEG oligomers across the mass range. Note that FWHM values are approximately 1-2 amu across the mass range.

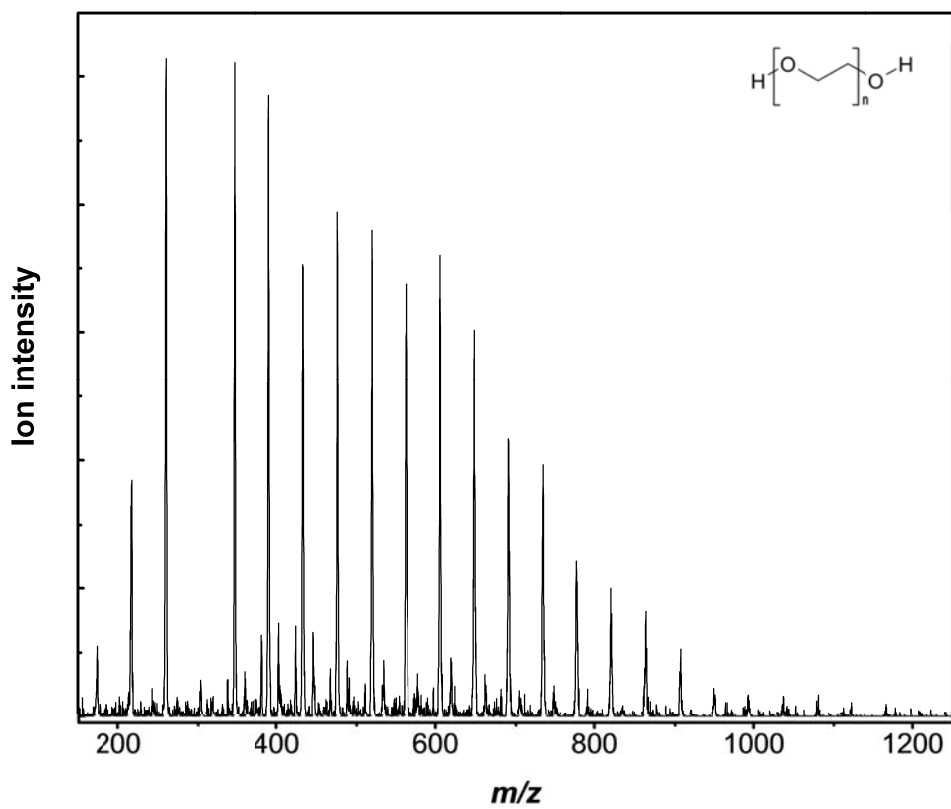


Figure 3.9: Selective ejection of m/z 305 ($n = 6$) by application of dipolar supplementary AC excitation voltage applied to the X-electrodes; freq 142 kHz, 130 mV_{p-p}, 50 ms.

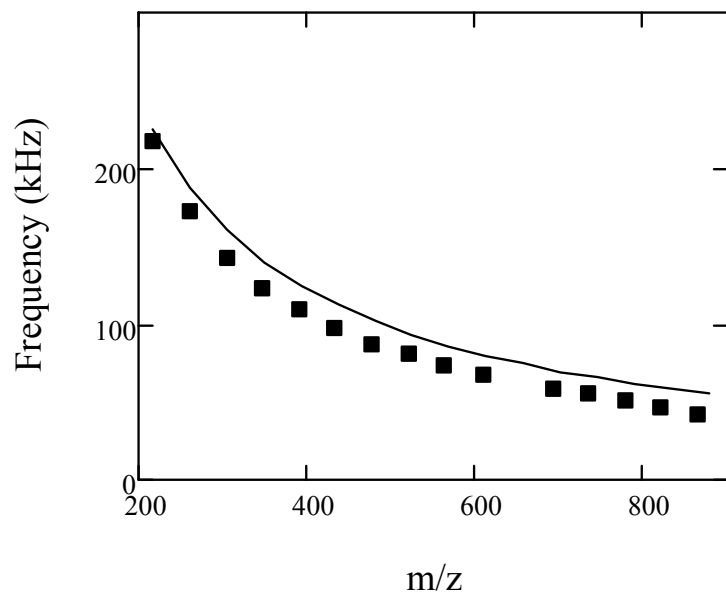


Figure 3.10: Ion frequency map: Solid line indicates the calculated secular ion frequencies. Points indicate frequencies determined experimentally through selective ion resonant ejection.

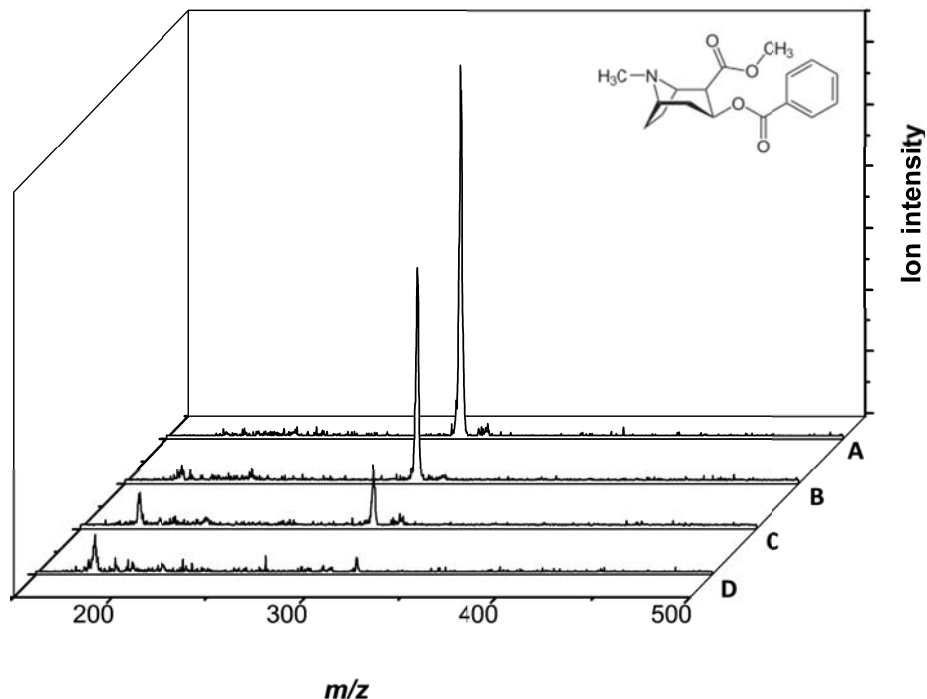


Figure 3.11: Cocaine after A) $200\text{ mV}_{\text{p-p}}$ activation B) $220\text{ mV}_{\text{p-p}}$ activation C) $230\text{ mV}_{\text{p-p}}$ activation D) $250\text{ mV}_{\text{p-p}}$ activation. All activation experiments were initiated at a pressure of 20 mtorr and at $10\mu\text{g/ml}$ concentration.

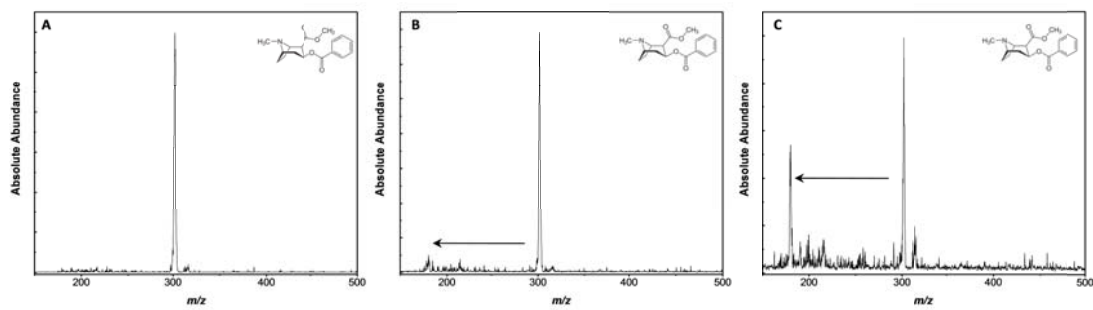


Figure 3.12: Figures A – C show the conversion of the production m/z 182 from the parent m/z 304 as the collision energy is increased.

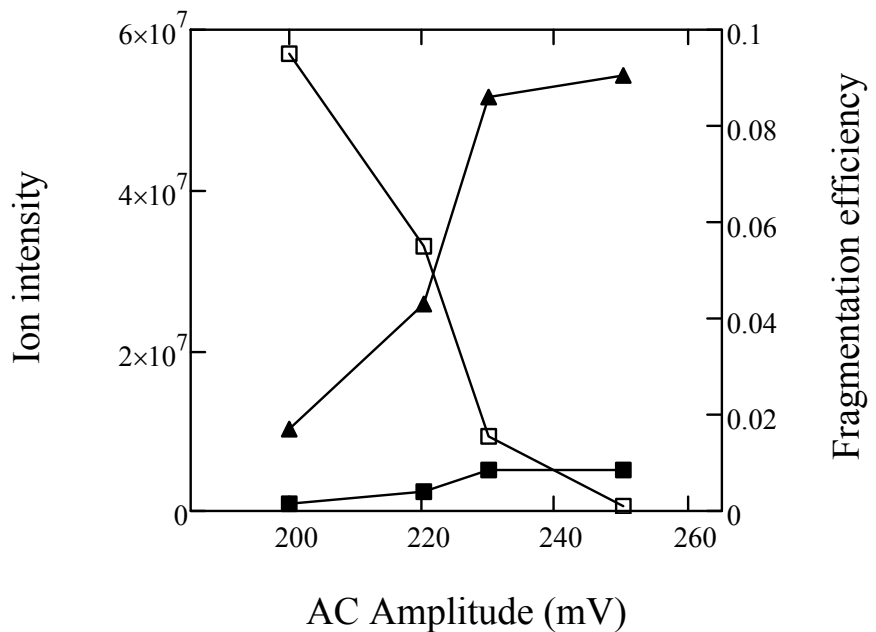


Figure 3.13: Precursor m/z 304, \square , and product ion m/z 182, \blacksquare , intensity vs. AC amplitude; Right axis) Fragmentation efficiency, \blacktriangle ,(Fragment ion intensity/ Total intensity).

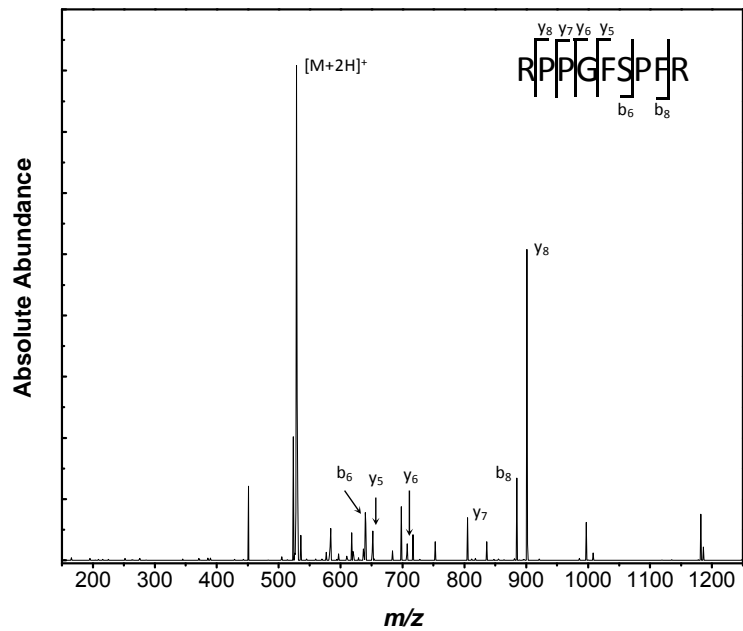


Figure 3.14: Collisional induced dissociation (CID) mass spectrum of Bradykinin obtained on the 1/3rd RIT; activation $q_z = 0.206$, AC amplitude 220 mV, manifold pressure 15 mTorr, activation 30 ms.

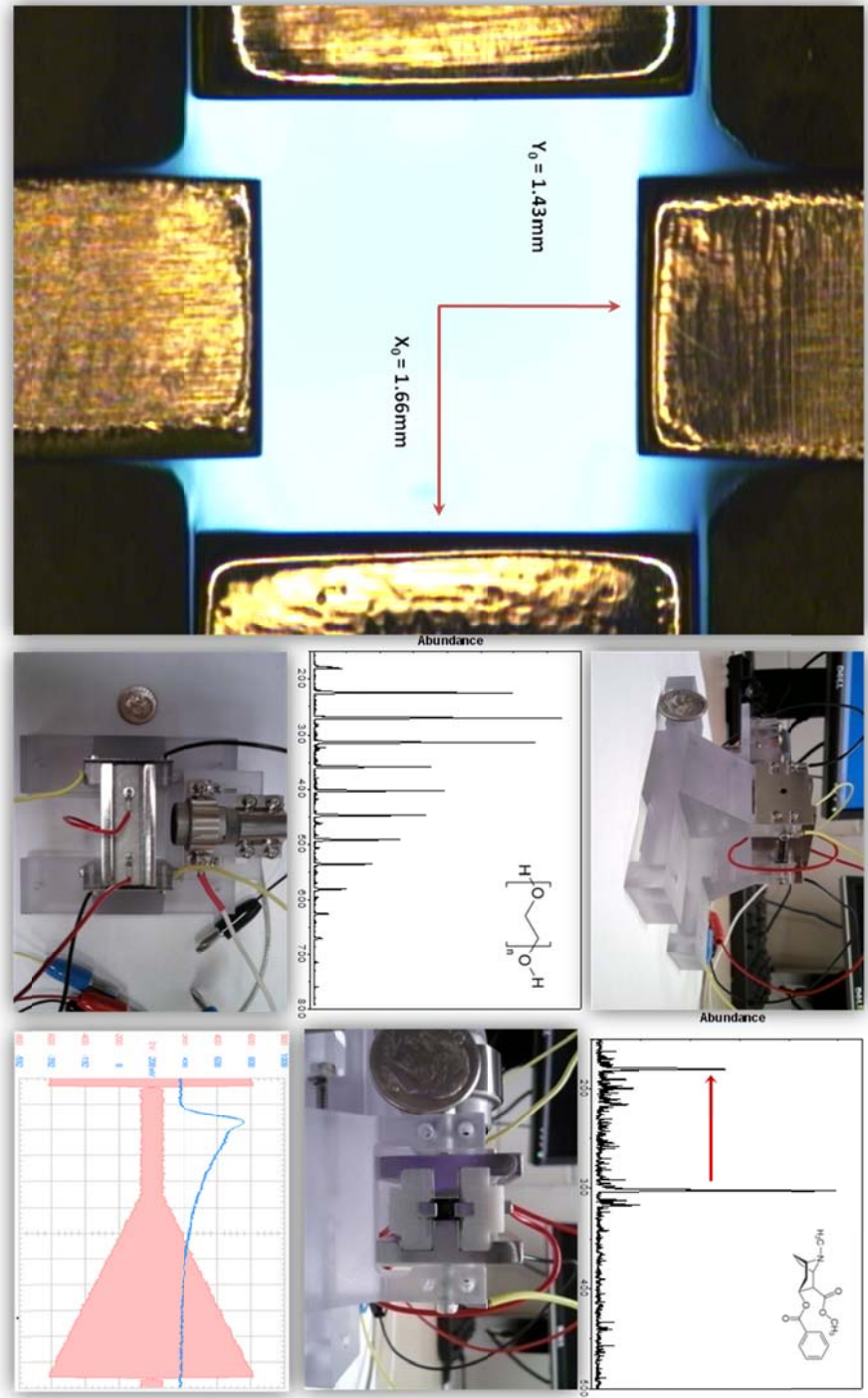


Figure 3.15: Composite figure of the 1/3rd stainless steel RIT demonstrating the X_0 and Y_0 dimensions, PEG spectrum, position of the detector, operating voltages and pressures, as well as tandem MS capability.

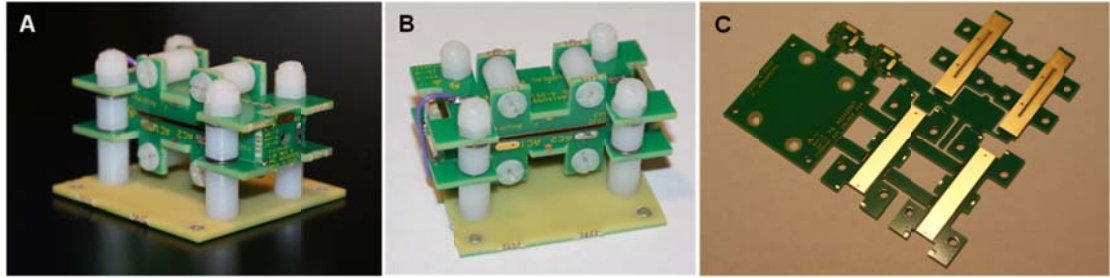


Figure 3.16: Full size (5 x 4 mm) RIT fabricated with FR-4. A) Aspect image of a fully assembled RIT. Note the entrance aperture on the right side of the image which is used for axial injection of ions and the ion ejection slit on the left which is used for radial ejection of ions during mass analysis. B) Side view of the 5 x 4 mm RIT with a clearer image of the ion ejection slit. C) Monolithic construction of the PCB RIT. all six electrodes and the support base are fabricated simultaneously.

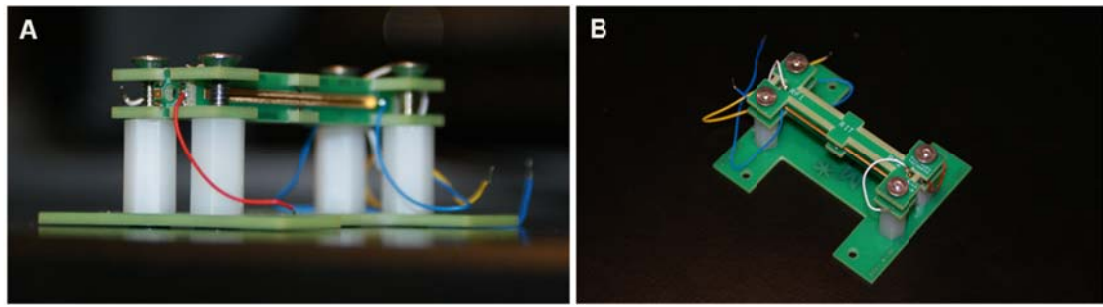


Figure 3.17: 1/3rd scaled RIT PCB. A & B) Aspect and top, respectively, images of the miniaturized PCB RIT; this mass analyzer has the same X₀ x Y₀ x Z dimensions as the 1/3rd scaled stainless steel RIT.

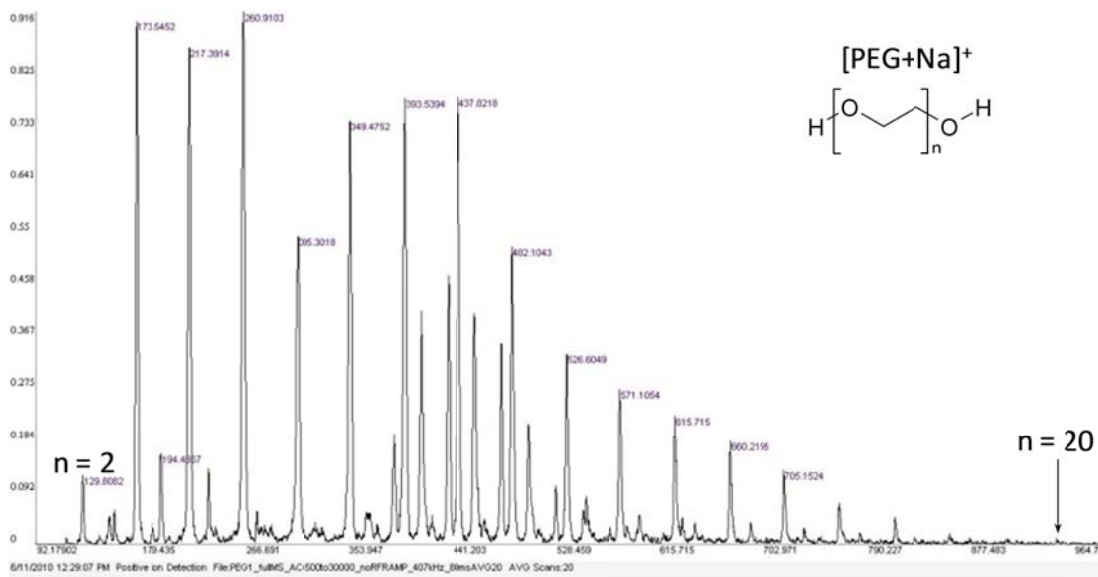


Figure 3.18: Nano-electrospray ionization of $[\text{PEG}+\text{Na}]^+$ oligomers ~ 1 Th (FWHM) for low mass ion and increases to ~ 2 Th for high mass ions. Concentrations of $10 \mu\text{M}$ to $100 \mu\text{M}$ in 1×10^{-3} M NaOH. RF voltage amplitude scan from $312 \text{ V}_{0-\text{p}}$ to $3345 \text{ V}_{0-\text{p}}$, using resonance ejection at 409 kHz ($q_z = 0.887$) with the AC amplitude $2 \text{ V}_{\text{p-p}}$ to $18 \text{ V}_{\text{p-p}}$ throughout the analytical scan.

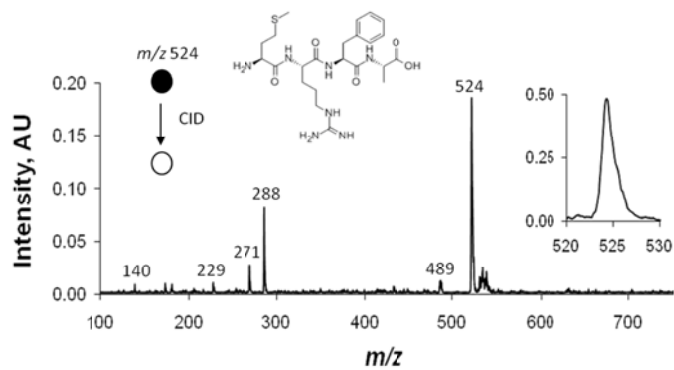


Figure 3.19: Tandem MS of MRFA acquired using full size PCB RIT

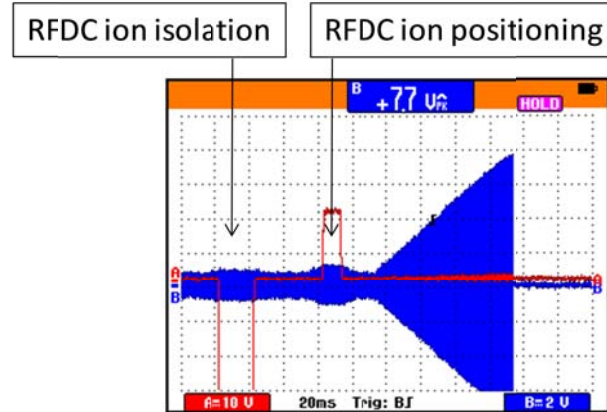


Figure 3.20: RF and DC waveforms used to complete mapping of the first region of ion stability for the PCB RIT. Notice there are two pairs of RF and DC waveforms applied. The first is used to isolate m/z 91 at the stability region apex and the second is used to reposition the ion packet corresponding to m/z 91 to determine boundaries of the stability region.

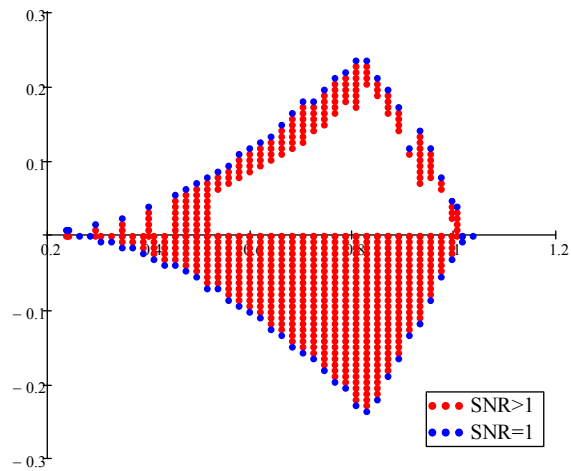


Figure 3.21: Map of the first region of stability as acquired with the PCB RIT. The boundary of the stability region was determined to be when the s/n of m/z 91 was equal to 1

CHAPTER 4. DEVELOPMENT OF A MINIATURE RECTILINEAR ION TRAP ARRAY WITH INDEPENDENTLY CONTROLLED CHANNELS

4.1 Introduction

Desire to improve the utility of field portable and handheld mass spectrometers for *in-situ* chemical detection has inspired new developments in instrumentation design. Arguably, the most important consideration is the operational power consumption which directly limits the effectiveness of portable instruments in the field. Miniature instrument systems such as control electronics,[1, 2] vacuum systems,[3-5] and mass analyzers[6-8] has therefore become the subject of recent investigation due to its effect on power consumption, physical size, and weight. The accomplishments in these areas have dramatically narrowed the performance gap between laboratory based and portable instruments. Of continuing importance, and the subject of the work presented here, is research focused on reducing mass analyzer size.

The list of miniaturized mass analyzers includes ion cyclotron resonance (ICR) cells, time of flight (TOFs), sector instruments, quadrupole mass filters (QMF), quadrupole ion traps (QIT or ITMS), and toroidal ion traps. All have demonstrated mass ranges and resolutions that are analytically useful for field portable instruments.[6, 7, 9] However, the following attributes are unique to ion traps which makes them attractive as

the mass analyzer in portable instruments: (i) Optimal operating pressures are in the mTorr range,[10] relatively high compared to other mass analyzers, which directly benefits portable mass spectrometers because it allows miniaturized vacuum systems to be used which reduce instrument weight and power consumption. (ii) Multiple stages of collisionally induced disassociation (CID) can be executed within the same analyzer[11] thereby improving the specificity and the signal to noise of ratio of the chemical measurement. (iii) The electric field strength necessary for operation is inversely proportional to the square of r_0 ; where r_0 is defined as the dimension of the inscribed radius of the electric field generated by the electrodes of the mass analyzer. Ion traps with reduced physical dimensions, therefore require comparatively lower voltage amplitudes than their full size counterparts to trap gas phase ions and complete mass analysis.[12-14]

Although ion trap miniaturization offers a solution to reducing the operating voltage requirements for conducting mass analysis, sensitivity, limits of detection, and signal-to-noise are negatively impacted due to reduced ion storage capacity. Furthermore, mass resolution is also negatively affected as lower voltages generate shallower pseudopotential well depths.[15] To offset this drawback strategies such as increasing the operating frequency of the main RF[16] and parallel operation of ion trap arrays with various numbers of ion trap elements, electrode geometries, and dimensions have been explored.[9, 17-23] Interestingly, materials science now plays a large role in the development of array based mass analyzers due to the dimensional scale and number of individual mass analyzers that can be constructed using integrated circuit manufacturing technology. Operation of ion trap arrays with r_0 dimensions between 40 to 500 μm have been demonstrated[16, 20, 24] and the analytical merits of still smaller devices ($r_0 = 1 \mu\text{m}$)

and arrays containing 10^6 - 10^7 individual traps have been discussed.[9] While few ion traps or ion trap arrays have been built at micron scales, fabrication technologies that offer an alternative to steel machining such as metalized plastic polymer, printed circuit board, and ceramic are attractive because they allow analyzers to be constructed with a high degree of complexity, at lower cost, and are manufactured on time scales of days rather than weeks.[7, 8, 25]

Despite advances made toward reduced operating voltages through mass analyzer miniaturization and adaptation of non-traditional fabrication techniques to create ion trap arrays, errors in fabrication compromise the integrity of the physical electrodes, surface roughness, and, or, electrode alignment. The effects of these physical defects are manifest in the resulting mass spectrum. For example and ion trap array that has adjacent ion traps with slightly different r_0 values will cause ions of the same m/z to eject at different time points during the amplitude scan of the main RF. The result is a broadening of the mass spectral peak attributed to that ion due to contributions from each ion trap. In situations where the r_0 value for adjacent traps is substantially different from each other the mass-to-charge value for that ion may be completely miss assigned in the mass spectrum. This phenomenon is not limited to miniaturized ion traps fabricated with alternative technologies and has been reported for array instruments that utilize ion traps fabricated from stainless steel with millimeter r_0 dimensions.[26-29] Even though utilization of highly miniaturized ion traps and ion trap arrays as mass analyzers for portable mass spectrometers has been anticipated, little discussion has been made on methods to control ion trap arrays or compensate for physical defects in the electrode structure to improve the overall analytical signal. In this investigation two types of control are investigated for

an ion trap array (i) the ability to enable or disable any ion trap channel inside the array structure at any point in time, (ii) the ability apply calibrated RF waveforms during mass analysis to compensate for differences in r_0 , and (iii) demonstration of the ability to selectively scan any ion trap channel at any time point without affecting the ions trapped in other ion trap channels.

An eight-channel array of miniaturized rectilinear ion traps (RIT) with ion trap dimensions of 1.33 x 1.66 x 16.66 mm for X₀, Y₀, and Z respectively has been constructed using a Stereolithography apparatus (SLA). Ion trap “on/off” control is established using a bias tee circuit in which a switch that toggles between 0 and -21 V_{DC} applies a potential difference between the x and y-electrodes of the mass analyzer allowing for the Mathieu a parameter to be changed. At 0 V_{DC} there is no potential bias between the x and y-electrodes (Mathieu parameter $a = 0$) and the ions undergo stable trajectories and the ion trap is referred to as being ‘on’ because it contributes to the total ion signal during mass analysis. At -21 V_{DC} a bias between the electrode pairs exists (Mathieu parameter $a \neq 0$) which destabilizes the ion trajectories. Under this operating condition the mass analyzer is referred to as being “off” because it does not contribute to the total ion signal during mass analysis.

Mass analysis is completed with a mass selective instability scan. In this method of mass analysis the amplitude of the RF is scanned from low to high causing ions to become unstable and eject from the trap in order of low to high mass-to-charge. It is ideal for each ion of the same mass-to-charge eject from each ion trap in the array at the same time during the RF ramp. However, due to differences in r_0 between adjacent ion traps this is does not always occur. To compensate for differences in r_0 individual RF

waveforms were applied per ion trap channel to achieve simultaneous ejection from all ion trap channels for an ion(s) of a given mass-to-charge. RF amplitude compensation is established by using an eight channel circuit in which each ion trap in the array has a dedicated operational amplifier[30] that amplifies a trap-specific calibrated waveform generated by two arbitrary waveform generators. Each ion trap is electrically isolated such that it can be independently controlled without impact on any other element in the array.

4.2 Materials and Methods

4.2.1 Fabrication: PCB-Stereolithography Apparatus Technology, Metallization, Channel Isolation

The Stereolithography apparatus on printed circuit board (PCB) fabrication technique and circular architecture of the electrodes used to construct the array of miniaturized RITs has been previously described[21, 31] and was completed in collaboration with Prof Chappell, Electrical and Computer Engineering, Purdue University. Additional information related to the fabrication methodologies can be found in the thesis of Jeffery D. Maas titled *3D Integration of Geometry Optimized Single and Multichannel Miniature Ion Trap Chemical Sensor*.[32] The steps in the build process are schematically outlined in figure 4.1. PCB is an excellent substrate for attaching the SLA electrodes that form the ion trap array because the surface can be milled to form the necessary electrical traces and the pads from which are cut into the PCB and form the base of the trapping electrodes adhere strongly to the SLA polymer resin. Briefly,

NanoForm™ 15120 (DMS Somos®, New Castle DE) was used as the photoactive resin to grow the electrodes on top of a PCB substrate that had been previously milled to create the RF, AC, and DC electrical traces. A Viper Si2 SLA build instrument (3D Systems, Rock Hill SC) was used. This instrument has a laser spot size of $75 \mu\text{m} \pm 15 \mu\text{m}$, in high resolution mode, and a minimum distance of $50 \mu\text{m}$ between successive build layers. When completed, the array consists of 8 individual miniaturized RITs circularly arranged around a single Magnum 5903 electron multiplier detector (BURLE Industries Inc., Lancaster PA). Each ion trap channel has the nominal trapping dimensions of $1.66 \times 1.33 \times 16.66 \text{ mm}$ for X₀, Y₀, and Z respectively and the entire array volume measures $77 \times 90 \times 32 \text{ mm}$ (Fig. 4.2).

Metallization of the ion trap array has been slightly changed to improve adherence of the metal plating to the polymer substrate and to allow for physically smoother surfaces and even metal deposition. All chemicals were obtained from Electrochemicals, Inc. (Maple Plain, MN) and were used as recommended by the manufacturer. Following a thermal post-cure the completed array was submerged in hydrochloric acid (5:1, H₂O:HCl) for 30 seconds to remove excess solvent residue and this was followed by a sulfuric acid rinse (10:1, H₂O: H₂SO₄) for 1 minute to slightly etch the copper traces. The entire array was then placed in an agitating solution of palladium-tin catalyst for 5 minutes to establish a seed layer of copper, removed, and placed in the copper 4000 chemical bath for approximately 45 seconds to form a Cu layer approximately 50 nm in thickness. Once the Cu layer is established the entire array was immediately placed into the nickel plating solution (Uyemura KPR-11) for 30 min in order to plate the entire array

with a 5 μm thick layer of nickel. Finally, the array is placed into the gold plating bath (TAM-55 Au) for 5 to 10 minutes, forming a gold layer approximately 50 nm thick.

Electrical isolation for each of the ion trap electrodes was completed using a laser with a 6 μm focal point to ablate excess metal deposited during the metallization process. Use of this laser allowed for metal ablation to be completed close to the electrode base without ablating the sidewalls or top of the electrode. A pattern is needed for every 500 μm variation in height across the array, 8 distinct patterns were necessary to complete the electrical isolation. The smallest distances between individual electrodes inside the array structure is approximately 550 μm (adjacent X and Y-electrodes along the interior of the ion trap) which is an air gap, the narrowest isolation completed by the ablation laser is approximately 1.5 mm (adjacent X and Y-electrodes along the exterior of the ion trap).

4.2.2 Instrumentation: Control Electronics (LCQ), Pumping System, Operational Pressure, and Voltage Amplitudes

LCQ Duo (Thermo Fisher Scientific, San Jose CA) electronics and LCQ Duo Tune 1.0 software/Ion Trap Control Language software were used for system electronics timing and control. The vacuum system consisted of a TSQ 7000 manifold, a front mounted Pfeifer 260 turbo molecular pump (210 L/s) operated at $\frac{2}{3}$ power, and a second Pfeifer 260 turbo molecular pump (210 L/s) backed by a BocEdwards E2M40 (40 m³/hr) mounted at the rear. The vacuum system for this instrument was specifically de-tuned to achieve similar operational pressures, as measured from a mini-convectron gauge connected to the vacuum manifold (Brooks Granville-Phillips, Chelmsford, MA, US), as portable mass spectrometers also utilizing single stage vacuum system and direct

injection of externally generated ions via a discontinuous or continuous atmospheric pressure interface (DAPI).[4, 33-36]

Ions were generated at ambient pressure via atmospheric pressure ionization (APCI) or nano-electrospray ionization (nESI). All chemical samples were obtained from Sigma-Aldrich (St. Louis, MO) and were used without further purification or modification. Analyte ions were introduced to the vacuum manifold using a discontinuous atmospheric pressure interface (DAPI).[4, 34, 35] Typical DAPI pulse durations are on time scales of tens of milliseconds (ms). During this time interval the gas conductance of ion and neutrals is high enough that a sufficient number of analyte ions are drawn into the ion trap and fall under the influence of the RF field where they undergo stable trajectories. Once the DAPI valve is closed, neutral molecules are pumped away while ions remain confined inside the ion trap. Unless otherwise noted the DAPI valve was open to the atmosphere for 15 to 50 ms and then closed for the duration of the scan, which was approximately 1000 to 2000 ms depending upon the scan function and mass range analyzed. Typical pressures experienced by the array mass analyzer under these operating conditions was approximately 7.0×10^{-2} Torr during ion introduction and 1.5×10^{-2} Torr at the start of the mass analysis scan.

Once inside the vacuum chamber ions were transferred to the RIT array via a 20 cm long stainless steel capillary which was co-axially aligned with the center of the ion trap array and separated from the front end cap of the array by a 10 mm gap. No guiding or focusing lenses were used to aid in the injection of ions into individual traps.[21, 31] Ion dispersion and injection into each trap depended entirely on the gas expansion generated by the difference between manifold and ambient pressures.[37, 38] The RF

drive frequency was tuned to 950 kHz for experiments utilizing an LC tank circuit or Apex 85 operational amplifier (Cirrus Logic, Austin TX). A mass selective instability scan in which the RF amplitude was scanned from 50 V_{0-p} to 200 V_{0-p} at a rate of 833.3 Th/s was used for mass analysis except for analysis of intact proteins. Due to the number of available basic sites on an intact protein, they typically have large charge state envelopes that can range from *m/z* 600 to 1200. For these experiments the RF amplitude was scanned to a maximum voltage of 600 V_{0-p}, using the LC tank circuit exclusively. Resonance ejection was also utilized to improve spectral resolution and extend the mass range.[39] Here, a dipolar supplementary RF was applied to the x-electrodes at a frequency of 307 kHz ($q_z = 0.77$) and was ramped linearly in amplitude from several hundred millivolts to several volts during mass analysis.

4.3 Results and Discussion

4.3.1 Channel Control

4.3.1.1 Bias Tee & Operational Amplifiers

Problems unique to mass analyzer arrays arise in the manufacturing process and are due primarily to dimensional variation between individual ion traps and mal-formed electrode structures within the array. As fabrication techniques such as deep reactive ion etching (DIRE) and SLA are utilized to achieve the desired r_0 dimensions, the fabrication process becomes more complex because multiple steps are required to construct and assemble the three dimensional trapping structure. For processes that utilize two or more

different material substrates in the build process, differences in thermal expansion coefficients and relaxation due to mechanical stress play large roles in the final geometry of individual ion traps and also affect how uniform ion trap dimensions are across the entire array. While large defects may be localized to only a few of the ion traps, they have a significant effect on the resulting mass spectrum that compromises the performance of the entire device through peak broadening, misshapen / split peaks, and in the most severe cases miss assigned m/z values.

A bias tee electrical circuit was constructed from a $1\text{ M}\Omega$ resistor and 10 nF capacitor (Fig. 4.3a) and inserted between the Y electrodes and the RF drive (inductance coil or operational amplifier) to allow for control of the DC bias on the drive RF and thereby modifying the Mathieu operational parameter ' a '.[15] When the DC voltage applied to the Y electrodes matches that applied to the X-electrodes (set through the LCQ control electronics) zero DC potential exists between the X and Y electrode pairs, effectively setting the operation point of the Mathieu a parameter equal to zero (Fig 4.3b). Under this condition, ions under the influence of the RF field undergo stable trajectories and are trapped prior to the mass selective instability scan for mass analysis.[10] A two way switch for each ion trap was located outside the vacuum manifold. The DC offset applied to the Y electrodes could be toggled between the previously described $a = 0$ or 'on' state and $a \neq 0$ or 'off' state in which the applied DC bias creates a non-zero potential between the X and Y-electrode pairs. The potential is of sufficient magnitude that the operation point for a is outside the first stability region (Fig 4.3c). Under this set of conditions ions do not undergo stable trajectories, are not trapped, and do not contribute to the total ion signal.

Furthermore, because no physical obstruction was used to block ion injection, ejection, or detection of the ions, the performance of individual channels can be accurately and clearly demonstrated. Figure 4.4 shows the performance for each channel in the array which was interrogated with 50 ppm MRFA m/z 524, $[M+H]^+$. With the exception of the DC bias applied to the Y-electrodes, all ion trap channels are subject to the same voltages over the same time intervals, and thus the cause for mass shifts and differences in resolution between channels for the same m/z ion is attributed primarily to dimensional variation in r_0 for ion traps inside the array. This is further supported by the fact that the signal for individual channels, when summed, yields the same profile and intensity as measured when all channels are operated in parallel, an indication that turning individual traps ‘on’ and ‘off’ does not substantially interfere with the voltage magnitudes or frequencies each ion trap experiences during operation. Thus ion signal from each channel represents a fraction of the composite array ion signal. Importantly, the bias tee circuit allows the performance of the entire array to be evaluated, trap by trap. With such information individual channels which have poor performance can be identified and then disabled such that their effect on the total ion signal is eliminated (Fig. 4.5 and 4.6). This idea is analogous to disabled sectors on a computer hard disk because they were bad.

The effects of dimensional variation on mass analyzer performance have been well discussed in the literature.[40-43] Due to differences in geometry between ion traps, ions of the same m/z value will eject at different time points during the RF amplitude scan. If not compensated for, this artifact will be recorded in the mass spectrum in the form of peak broadening or incorrect mass assignments that correlate to the magnitude of Δr_0 .

between ion traps in the array. In this study, channel 4 was tuned for optimal performance and the remaining seven channels were evaluated against it. Using the apparent mass-to-charge ratio for the singly charged MRFA, m/z 524.3, in combination with the voltage amplitude of the RF scan, the dimensional variation between individual channels was experimentally determined to be on the order of tens of microns, which is in agreement with physical measurements taken in 2010 (Table 4.1). It should be noted that these experiments were of the first to be completed on this device and it is speculated that the actual dimensions for each trap are closer to the 2010 values than those of 2011 performed using the same optical microscope and measurement methods.

What is not explained by the dimensional analysis is the difference in performance between ion trap channels that have nearly the same dimensions. For example ion trap 4 and 6 are both reported to have the same deviation from theoretical dimensions, but ion trap 4 was consistently the best performer and 6 was of the worst. Similarly, ion traps 3 and 7 may both be expected to be equally bad based upon the dimensional measurement alone. However, ion trap 3 was among the best in terms of resolution, second to trap 4, and 7 was the worst. It is known that deviation from the optimized ion trap dimensions by way of damage to the electrode structure, surface roughness, nonparallel, or skewed electrodes results in a loss of performance.[8, 16, 29] This suggest that measurements from the top X-Y plane of the ion trap electrodes is not sufficient to fully characterize the electrode structure and that physical aberrations, along the z axis, which reside outside the field of view of the optical microscope quite possibly have a significant effect and remain uncharacterized. Furthermore, the ion trap dimensions are not static over time, the X and Y dimensions taken in 2010 and then again

in 2011 show differences of over 100 μm for almost every ion trap channel. RF heating has been previously investigated as a cause for time dependent deformation of the electrode structures[44] and the results here suggest that this factor, possibly in combination with others such as a mechanical relaxation of the electrodes structures continues to exist.

To compensate for some aspects of the mechanical deviations between ion trap channels, an eight channel circuit that utilized Apex PA85 operational amplifiers (Cirrius Logic, Austin TX) with a gain of 100:1 was developed to supply the drive RF for each ion trap (Fig.4.7). This device allows for RF waveforms to be calibrated to a specific ion trap in the array. The RF waveform supplied to the multi-channel RF circuit was created using two Agilent 33259 (Agilent, Santa Clara CA) arbitrary waveform generators per channel. One waveform generator was used to synchronize with the LCQ instrument at the start of the acquisition and setup the RF modulation envelope, the second waveform generator mixed the RF modulation with the carrier frequency of 950 kHz (same frequency that was used in the experiments with the inductance coil). Because two waveform generators were required to operate a single channel of the array, only 4 channels were operated due to availability of the waveform generators. The results for these experiments are discussed in the section titled '*Multi-channel signal response*'.

4.3.2 Performance

4.3.2.1 Mass Resolution and Mass Range

The ability to selectively turn individual channels ‘on’ and ‘off’ allowed for tuning and performance characterization of the single best channel inside the array; establishing criteria by which a comparison could be made to other ion traps in the array and analyzers of similar dimensions, but fabricated using different materials or techniques, such as stainless steel. Channel 4 of the SLA array demonstrated superior performance in terms of resolution and peak shape and was therefore used to collect data demonstrating mass range, resolution, and MS^2 performance for a single ion trap.

Control of the number of ions injected into the ion trap has a critical impact on the data quality and performance of the mass analyzer. So much so that commercial systems have implemented autonomous, dynamic, controls such as automatic gain control (AGC)[45] and Ion charge control (ICC)[46] to aid in avoiding space charge conditions that result from the injection of too many ions. Excessive space charge results in broadened spectral peaks and shifts in the mass assignment, both degrade the analytical quality of the mass spectrum and thus the utility of the mass analyzer. Further effects of space charge, while not witnessed here, are ion/ion and ion/molecule reactions that change the composition of the chemical species available for mass analysis. Because no ion optics are used to focus or in any other way control the introduction of ions into the array, the pulse duration of the DAPI served a dual purpose of controlling the pressure inside the manifold and the ion population injected into the mass analyzer (Fig. 4.8). Under the best conditions, in which the DAPI pulse duration was finely tuned along with

the position and voltage of the nESI emitter (with respect to the ion introduction capillary), resolution of approximately 1 amu (FWHM) was recorded for both $^{+1}$ and $^{+2}$ charge states of MRFA, m/z 524.3 ($[M+H]^+$) and 262.7 ($[M+2H]^{++}$) respectively (Fig. 4.9). More typical resolutions were between 2 and 2.5 Th (FWHM).

While the ion trap channels of this array demonstrated the same performance as those with similar dimensions,[14] it was anticipated that individually, each ion trap would have resolution performance at or near unit resolution, similar to their full size (5 x 4 mm) counterparts. This however, was not observed and it is suspected that this difference in performance is related to one or more of the following: deviations from the optimized electrode distances, low pseudo potential well depth, space charge effects, and the pressure / composition of the buffer gas. All of these factors degrade mass spectral resolution because they cause physical dispersion of the ion cloud and a wider distribution of ion kinetic energies prior to ejection.

The mass range was determined to be approximately 800 amu (*m/z* 200 to 1000) as demonstrated using a single channel with a mixture of sodiated PEG oligimers, 50 to 100 μ M, $(M+Na)^+$ having monomer repeats of 44 amu across the mass range (Fig. 4.10). Furthermore, intact protein analysis was also demonstrated using 56 μ M equine myoglobin (17 kDa) in which the charge state envelope from $^{+26}$ to $^{+14}$ required maximum RF amplitudes of 1.2 kV_{p-p}. By way of comparison, the spray voltage at 1.6 KV_{DC} was greater in magnitude than the maximum peak-to-peak RF voltage necessary for mass analysis, which supports the possibility that mass analyzers of this size and scale have utility in the detection and analysis of large biological molecules in non-laboratory settings. While the concentration range used in the analysis of PEG and Myoglobin

(present as apomyoglobin under denaturing conditions) were high, this was necessary due to the turbulent and unpredictable nature of using a high velocity gas expansion to support off-axis ion injection and is most likely a primary source of ion loss.

4.3.2.2 Tandem MS- Single Channel Data

As previously stated, one of the key arguments for using an ion trap mass analyzer is the ability to use a single device to complete tandem mass spectrometry, i.e. multiple stages of fragmentation and mass analysis. Miniaturized ion traps, while capable of producing tandem MS spectra, require consideration of additional factors that are less necessary for larger devices. The first of these has been previously stated; smaller ion trap mass analyzers necessarily have reduced ion trapping capability impacting sensitivity and signal to noise. Second, while reduced physical dimensions help to lower the necessary operational voltage, reduction in RF voltage also reduces the depth of the pseudopotential well. This has an impact on both the mass resolution and allows ejection of ions from the trap, by way of resonance excitation, to compete more strongly with collisionally induced dissociation (CID) during tandem MS experiments.[13, 47] While increasing the operating frequency may be viewed as a solution for improving mass resolution and fragmentation efficiency it would also require increased voltage, and therefore power, for mass analysis over the same mass to charge range.

In order to increase the potential well depth during CID experiments for the miniature RIT array the RF voltage was increased during the activation period and then restored to its original value prior to mass analysis. While repositioning the working point of the ions to an increased q_z value allowed for increased well depth, it also increases the

low mass cutoff (LMCO) whereby low m/z ions generated by CID do not undergo stable trajectories and are lost, limiting the information obtained by completing the experiment. Tandem MS was demonstrated using the $\text{M}+\text{H}^+$ ion for the beta blocker atenolol, m/z 267 and required a complex scan function that utilized stored waveform inverse Fourier transform (SWIFT) for isolation and a second DAPI pulse to increase the manifold pressure during activation (Fig 4.12). During the 30 ms activation time the ion was repositioned and held at $q_z = 0.655$, subjected to an increase in manifold pressure to 25 mTorr necessary for increasing the number of collision events, and a supplementary RF at 241 kHz, 1 V_{0-p}, to resonantly excite the ions. The results of this experiment show generation of fragment ions at m/z 250 and m/z 225 indicative of ammonia and propene losses from the protonated molecule. The commonly expected fragment ions at m/z 190 (concerted loss of propylamine and H₂O) and m/z 116 (loss of *p*-hydroxylphenyl acetamide) were not observed due to the increased LMCO (Fig. 4.13). It is also noteworthy that over the same pressures and activation amplitudes, q_z values below 0.655 resulted in ion ejection prior to the onset of fragmentation. At $q_z = 0.655$ the potential well depth was calculated to be 5.5 eV using the Dehmelt approximation. Fragmentation may be improved at increased q_z values however, this would also further increase the LMCO and the fragments generated would be lost due to unstable trajectories.

4.3.2.3 Multi-channel Signal Response

The ability to use multiple mass analyzers in parallel to improve analytical signal requires stringent physical requirements on the fabrication of the device so that all of the array elements perform nearly identically. Physical differences between individual ion

traps due to errors in the fabrication process and tolerances of the fabrication technique have an adverse affect on the overall performance of the device as changes to the geometry degrade mass resolution.[42, 43] Additionally, as the trapping dimensions of the device become smaller, mechanical imperfections have a greater effect on the analytical signal. While dimensional variation of r_0 compromises the quality of the mass spectrum (Fig. 4.6) the differences in voltage at which ions of the same m/z are ejected from the ion trap are small enough that waveforms can be uniquely calibrated to individual channels in the array and used as a compensation method to recover an improved mass spectrum (Fig. 4.14 & 4.15). This approach represents a departure from previous operations of array devices in which a common RF drive was linked to the y-electrode(s) for all ion traps. By operating each ion trap channel with an independent main RF drive signal, the spectral resolution obtained from operating multiple channels in parallel is dependent upon the accuracy of individual mass calibrations, stability of the RF signal, as well as the inherent resolution obtainable for individual channels.

Limited by the number of available waveform generators, only 4 of the available 8 channels in the array were used with RF calibration with individual channels. Signal response was obtained by fitting the $[M+H]^+$ peak for propranolol to a Gaussian curve and then integrating over the m/z range that corresponded to 95% of the area. Because addition of multiple channels caused the propranolol peak to broaden by approximately 13%, the Gaussian fit was completed for both single and mult-channel data sets (Fig. 4.16). A calibration curve showing the signal response for one to four channels was constructed by analyzing propranolol at concentrations from 0.1 $\mu\text{g/ml}$ to 4 $\mu\text{g/ml}$ (three

replicates for each concentration) and atenolol at 10 µg/ml, used as a diagnostic analyte signal during execution of the experiments (Fig. 4.17).

The improvement in sensitivity using 4 channels versus 1 was a factor of 2.7, in close agreement with the relative contributions from each channel when the area for each channel is measured individually. Not all channels contribute equally to the total analytical signal, this is likely due to a combination of the off-axis method of ion injection and the ability of an ion trap with compromised geometry to effectively disperse ions, i.e. ions of a given m/z eject over a wide range instead of a narrow range of RF amplitude voltages, during the analytical scan (Fig. 4.18). Additionally, no improvement to the limit of detection was observed through the operation of multiple channels. While increased signal was observed, so was the level of chemical noise. It is anticipated that the performance of this experiment would be improved by any experiment that exhibits improved selectivity for the target analyte and reduces chemical noise, thereby improving the signal-to-noise ratio of the measurement, e.g. the ion(s) of interest are selectively isolated in the ion trap, all other ions are ejected, and the isolated ion(s) are scanned or fragmented and then scanned.

4.4 Conclusions

As ion traps and ion trap arrays are fabricated at smaller dimensions the accuracy and reproducibility of the fabrication technology is critical to the overall performance of the device. The controls discussed in this work were, straightforward to design and implement. Using such controls greatly improves the utility of parallel miniature ion trap arrays, by mitigating physical differences in r_0 between array elements, thereby

improving overall array performance. Additionally, the controls are scalable to arrays of smaller ion traps. For example arrays of ion traps fabricates with r_0 dimensions at micron scales could have provisions for these circuits to be implemented as a part of the analyzer architecture. This would allow for multiple levels of device sensitivity to be obtained or, individual ion traps that may have been damaged to be switched off.

Similarly, individual ion traps or, groups of ion traps in the case of large arrays, could be operated with unique waveforms to compensate for geometric variability. Improvement to both sensitivity and spectral quality or amplification of signals due to particular ions or ions in a range of mass-to-charge values – separate sections of the array analyzer tuned to detect different target analytes could be afforded by such a control. As a side note the scalability of these controls does not need to be limited by the use of expensive arbitrary waveform generators. Instead, advances in the digital synthesis of electronic signals, such as the use of a field programmable gate array (FPGA) would allow a single chip to generate multiple low-amplitude, frequency-modulated, waveforms to drive the ion trap channels.

An unintended consequence of the flexibility afforded by these controls is the possibility of performing different kinds of experiments not available with single channel mass analyzers or arrays of mass analyzers that utilize a common drive RF. For example, the ability to selectively scan any ion trap channel at any arbitrary time point and collect mass spectral information (Fig 4.19). Considering that each ion trap in the array is a vessel for completing gas phase reactions, then the ability to preselect ions per channel on the basis of mass-to-charge and then selectively scan individual channels at arbitrary time

points may find utility in the study of gas phase ion/ion, ion/molecule reactions, or even spectroscopic experiments.

4.5 References

1. Kirleis, M., *FPGA RF Control for a Portable Mass Spectrometer*, in ECET. 2011, Purdue University.
2. Rafferty, D., *Driving a mass spectrometer ion trap or mass filter*. 2011, 1ST Detect Corporation: US.
3. Kline-Schoder, R., *Miniature High Vacuum Pumps for Analytical Instruments*, in *Workshop on Harsh-Environment Mass Spectrometry*. 2007: Cocoa Beach, Fl.
4. Gao, L., et al., *Design and characterization of a multisource hand-held tandem mass spectrometer*. Anal Chem, 2008. **80**(19): p. 7198-205.
5. Yang, M., et al., *Development of a Palm Portable Mass Spectrometer*. Journal of the American Society for Mass Spectrometry, 2008. **19**(10): p. 1442-1448.
6. Badman, E.R. and R. Graham Cooks, *Miniature mass analyzers*. Journal of Mass Spectrometry, 2000. **35**(6): p. 659-671.
7. Ouyang, Z. and R.G. Cooks, *Miniature Mass Spectrometers*. Annual Review of Analytical Chemistry, 2009. **2**(1): p. 187-214.
8. Peng, Y. and D.E. Austin, *New approaches to miniaturizing ion trap mass analyzers*. TrAC Trends in Analytical Chemistry. **30**(10): p. 1560-1567.
9. Blain, M.G., et al., *Towards the hand-held mass spectrometer: design considerations, simulation, and fabrication of micrometer-scaled cylindrical ion traps*. International Journal of Mass Spectrometry, 2004. **236**(1-3): p. 91-104.
10. Stafford Jr, G.C., et al., *Recent improvements in and analytical applications of advanced ion trap technology*. International Journal of Mass Spectrometry and Ion Processes, 1984. **60**(1): p. 85-98.
11. Louris, J.N., et al., *Instrumentation, applications, and energy deposition in quadrupole ion-trap tandem mass spectrometry*. Analytical Chemistry, 1987. **59**(13): p. 1677-1685.
12. Badman, E.R., et al., *A miniature cylindrical quadrupole ion trap: Simulation and experiment*. Analytical Chemistry, 1998. **70**(23): p. 4896-4901.
13. Patterson, G.E., et al., *Miniature Cylindrical Ion Trap Mass Spectrometer*. Analytical Chemistry, 2002. **74**(24): p. 6145-6153.

14. Hendricks, P., et al., *Performance of a low voltage ion trap*. International Journal of Mass Spectrometry. **305**(1): p. 69-73.
15. March, R.E. and J.F.J. Todd, *Quadrupole Ion Trap Mass Spectrometry*. Chemical Analysis: A Series of Monographs on Analytical Chemistry and Its Applications. 2005, Hoboken, New Jersey: John Wiley & Sons, Inc.
16. Pau, S., et al., *Microfabricated quadrupole ion trap for mass spectrometer applications*. Physical Review Letters, 2006. **96**(12).
17. Boumsellek, S. and R. Ferran, *Trade-offs in miniature quadrupole designs*. Journal of The American Society for Mass Spectrometry, 2001. **12**(6): p. 633-640.
18. Chaudhary, A., F.H.W. van Amerom, and R.T. Short, *Development of Microfabricated Cylindrical Ion Trap Mass Spectrometer Arrays*. Journal of Microelectromechanical Systems, 2009. **18**(2): p. 442-448.
19. Van Amerom, F.H.W., et al., *Microfabrication of cylindrical ion trap mass spectrometer arrays for handheld chemical analyzers*. Chemical Engineering Communications, 2008. **195**(2): p. 98-114.
20. Moxom, J., et al., *Analysis of Volatile Organic Compounds in Air with a Micro Ion Trap Mass Analyzer*. Analytical Chemistry, 2003. **75**(15): p. 3739-3743.
21. Fico, M., et al., *Circular arrays of polymer-based miniature rectilinear ion traps*. Analyst, 2009. **134**(7): p. 1338-1347.
22. Tabert, A.M., et al., *High-Throughput Miniature Cylindrical Ion Trap Array Mass Spectrometer*. Analytical Chemistry, 2003. **75**(21): p. 5656-5664.
23. Chaudhary, A., et al., *Fabrication and testing of a miniature cylindrical ion trap mass spectrometer constructed from low temperature co-fired ceramics*. International Journal of Mass Spectrometry, 2006. **251**(1): p. 32-39.
24. Chaudhary, A., F. van Amerom, and R.T. Short, *Development of Microfabricated Cylindrical Ion Trap Mass Spectrometer Arrays*. Microelectromechanical Systems, Journal of, 2009. **18**(2): p. 442-448.
25. Ouyang, Z. and L. Gao, *Quadrupole ion traps and trap arrays: geometry, material, scale, performance*. European Journal of Mass Spectrometry, 2007. **13**(1): p. 13-18.
26. Moxom, J., et al., *Double resonance ejection in a micro ion trap mass spectrometer*. Rapid Communications in Mass Spectrometry, 2002. **16**(8): p. 755-760.

27. Tabert, A., M. Goodwin, and R. Cooks, *Co-occurrence of boundary and resonance ejection in a multiplexed rectilinear ion trap mass spectrometer*. Journal of The American Society for Mass Spectrometry, 2006. **17**(1): p. 56-59.
28. Kothari, S., et al., *Multiplexed Four-Channel Rectilinear Ion Trap Mass Spectrometer*. Analytical Chemistry, 2009. **81**(4): p. 1570-1579.
29. Xu, W., et al., *Characterization of electrode surface roughness and its impact on ion trap mass analysis*. Journal of Mass Spectrometry, 2009. **44**(3): p. 353-360.
30. Mancini, R., ed. *Op Amps For Everyone*. 2002, Texas Instruments
31. Maas, J.D., et al., *Miniature Monolithic Rectilinear Ion Trap Arrays by Stereolithography on Printed Circuit Board*. Microelectromechanical Systems, Journal of, 2010. **19**(4): p. 951-960.
32. Maas, J.D., *3D Integration of Geometry Optimized Single and Multichannel Miniature Ion Trap Chemical Sensor*, in *Electrical and Computer Engineering*. 2011, Purdue University.
33. Keil, A., et al., *Ambient Mass Spectrometry with a Handheld Mass Spectrometer at High Pressure*. Analytical Chemistry, 2007. **79**(20): p. 7734-7739.
34. Gao, L., R.G. Cooks, and Z. Ouyang, *Breaking the Pumping Speed Barrier in Mass Spectrometry: Discontinuous Atmospheric Pressure Interface*. Analytical Chemistry, 2008. **80**(11): p. 4026-4032.
35. Gao, L., et al., *Characterization of a discontinuous atmospheric pressure interface. Multiple ion introduction pulses for improved performance*. International Journal of Mass Spectrometry, 2009. **283**(1-3): p. 30-34.
36. Sanders, N.L., et al., *Hand-held mass spectrometer for environmentally relevant analytes using a variety of sampling and ionization methods*. European Journal of Mass Spectrometry. **16**(1): p. 11-20.
37. Bruins, A.P., *Mass-Spectrometry with Ion Sources Operating at Atmospheric-Pressure*. Mass Spectrometry Reviews, 1991. **10**(1): p. 53-77.
38. Jugroot, M., et al., *Numerical investigation of interface region flows in mass spectrometers: neutral gas transport*. Journal of Physics D-Applied Physics, 2004. **37**(8): p. 1289-1300.

39. Goeringer, D.E., et al., *Theory of high-resolution mass spectrometry achieved via resonance ejection in the quadrupole ion trap*. Analytical Chemistry, 1992. **64**(13): p. 1434-1439.
40. Badman, E.R. and R.G. Cooks, *Cylindrical Ion Trap Array with Mass Selection by Variation in Trap Dimensions*. Analytical Chemistry, 2000. **72**(20): p. 5079-5086.
41. Gill, L.A., et al., *In situ optimization of the electrode geometry of the quadrupole ion trap*. International Journal of Mass Spectrometry, 1999. **188**(1-2): p. 87-93.
42. Ouyang, Z., et al., *Rectilinear Ion Trap: Concepts, Calculations, and Analytical Performance of a New Mass Analyzer*. Analytical Chemistry, 2004. **76**(16): p. 4595-4605.
43. Wu, G., R.G. Cooks, and Z. Ouyang, *Geometry optimization for the cylindrical ion trap: field calculations, simulations and experiments*. International Journal of Mass Spectrometry, 2005. **241**(2-3): p. 119-132.
44. Meng, Y., et al., *Polymer-Based Ion Trap Chemical Sensor*. Sensors Journal, IEEE, 2006. **6**(6): p. 1429-1434.
45. Stafford, J., George C., D.M. Taylor, and S.C. Bradshaw, *Method of increasing the dynamic range and sensitivity of a quadrupole ion trap mass spectrometer*. 1992, Finnigan Corporation.
46. Hager, J.W., *Method of reducing space charge in a linear ion trap mass spectrometer*, U.S. Patent, Editor. 2003, MDS Inc.
47. Charles, M.J., S.A. McLuckey, and G.L. Glish, *Competition between resonance ejection and ion dissociation during resonant excitation in a quadrupole ion trap*. Journal of the American Society for Mass Spectrometry, 1994. **5**(12): p. 1031-1041.

Table 4.1: Internal distance between X and Y-electrode pairs in the ion trap array. Measurements were taken for all 8 ion traps in the X-Y plane at the top of the ion trap array; NanoForm™ 15120 was used as the SLA resin. Measurements taken in 2010 reflect the dimensions when the device was initially fabricated. ΔX and ΔY are the absolute values of the differences between the design dimension and the measured dimension. 2011 measurements were taken roughly 12 months after the device had been fabricated, under constant vacuum, and subjected to high amplitude RF. It is noteworthy to mention that the magnitude of the dimensional variation between the measurements taken in 2010 and 2011 differ by more than 100 μm for almost all traps and were completed the same microscope and measurement methods.

	Theoretical		2010				2011				Change over 1 year	
	X (mm)	Y (mm)	X (mm)	Y (mm)	ΔX (mm)	ΔY (mm)	X (mm)	Y (mm)	ΔX (mm)	ΔY (mm)	ΔX (mm)	ΔY (mm)
Trap 1	3.32	2.66	3.34	2.73	0.02	0.07	3.16	2.56	0.16	0.1	0.18	0.17
Trap 2	3.32	2.66	3.3	2.76	0.02	0.1	3.2	2.58	0.12	0.08	0.1	0.18
Trap 3	3.32	2.66	3.28	2.82	0.04	0.16	3.13	2.65	0.19	0.01	0.15	0.17
Trap 4	3.32	2.66	3.31	2.77	0.01	0.11	3.09	2.68	0.23	0.02	0.22	0.09
Trap 5	3.32	2.66	3.35	2.72	0.03	0.06	3.23	2.67	0.09	0.01	0.12	0.05
Trap 6	3.32	2.66	3.31	2.77	0.01	0.11	3.22	2.64	0.1	0.02	0.09	0.13
Trap 7	3.32	2.66	3.29	2.81	0.03	0.15	3.14	2.81	0.18	0.15	0.15	0
Trap 8	3.32	2.66	3.31	2.79	0.01	0.13	3.17	2.53	0.15	0.13	0.14	0.26

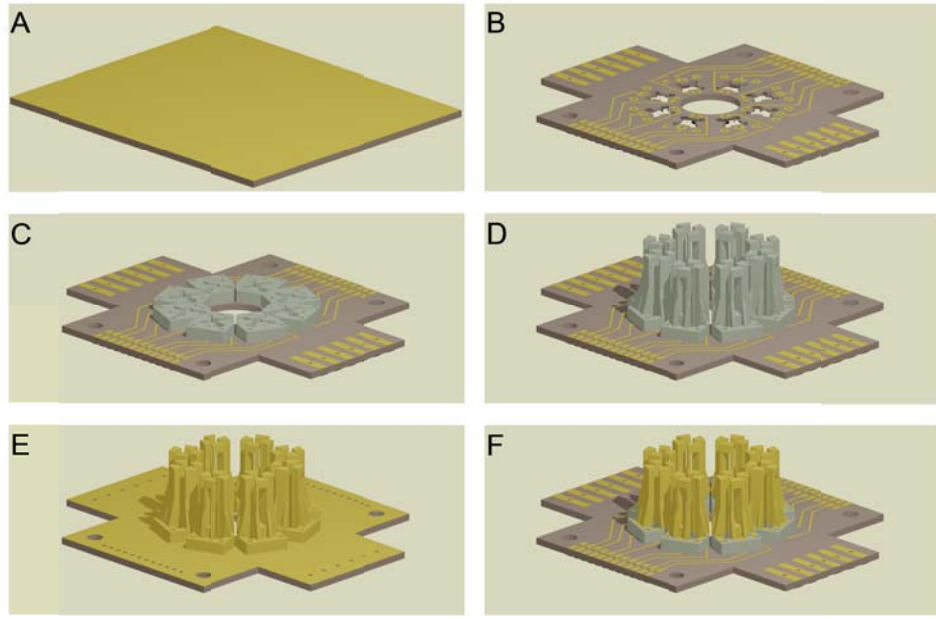


Figure 4.1: A) Base PCB substrate B) Pattered substrate that contains the electrical pads for all RF and DC connections to the array electrodes C) SLA build on PCB surface, gray pillars represent layer by layer construction of the electrodes D) Finished integration of SLA and PCB E) Gold plated array F) Electrode isolation is completed by laser ablation.

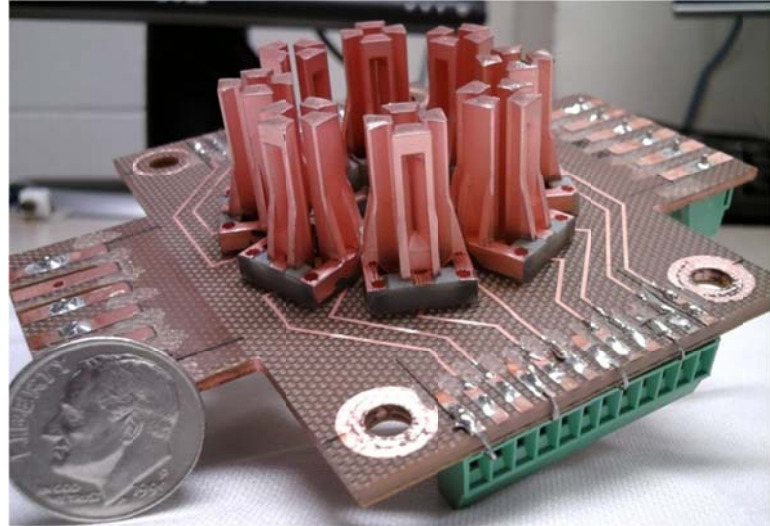


Figure 4.2: Eight channel rectilinear ion trap array with independently isolated electrodes arranged in a circular pattern around a single centralized detector. Electrical connections to each electrode are milled into the PCB substrate. Each channel is designed to be $1.66 \times 1.33 \times 16.66$ mm in the $X_0 Y_0$ and Z directions, entire footprint measures $77 \times 90 \times 32$ mm. Note the US dime (17.91 mm diameter) as a scale reference.

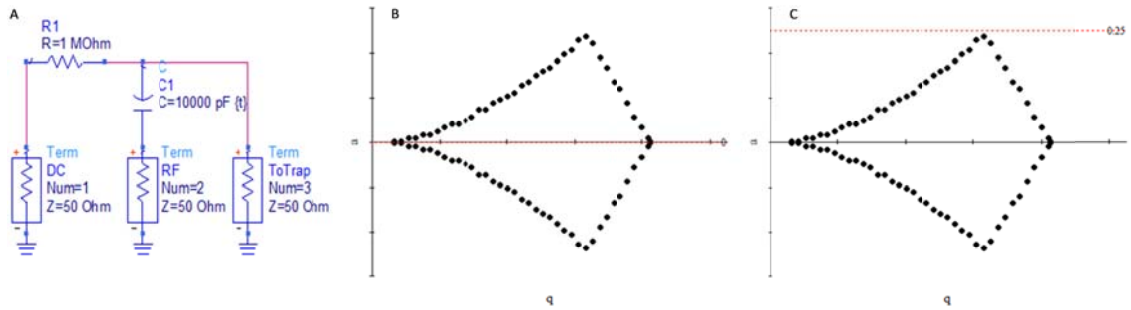


Figure 4.3: A) Bias T circuit schematic used to control the DC voltage applied to the Y-electrodes during operation of the ion trap. B&C) Position of the Mathieu operational parameter ‘ a ’ in relation to the first stability region. Note because of the implementation of an external switch, the ‘ a ’ parameter can be adjusted in real time and without interference to the applied RF.

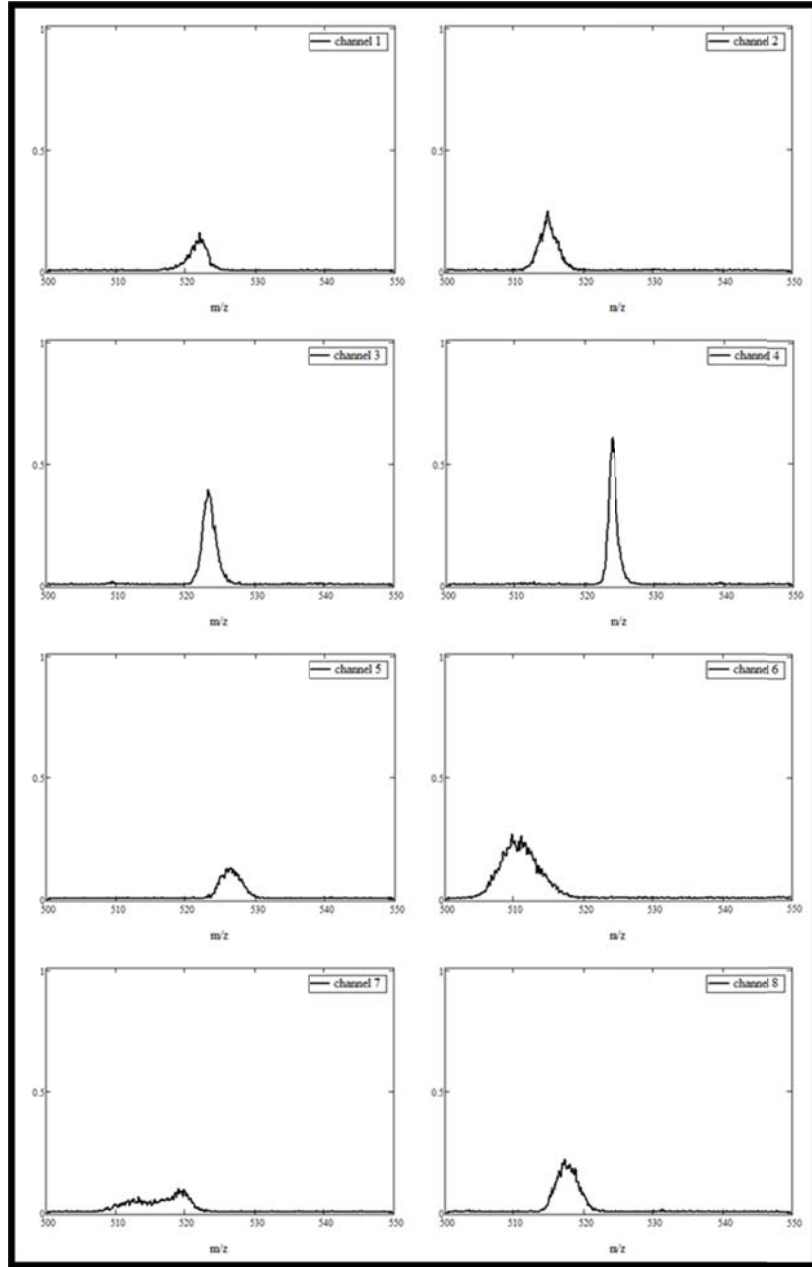


Figure 4.4: Spectra for individual channels, 10 $\mu\text{g}/\text{ml}$ MRFA, m/z 524.3 $[\text{M}+\text{H}]^+$. All spectra have the same normalization to show the relative intensities for each channel. All channels are operated with the same RF and AC waveforms. Special attention should be made to the difference in performance between channel 4 and channel 7 demonstrating the contrast between the best performing and worst performing traps in the array.

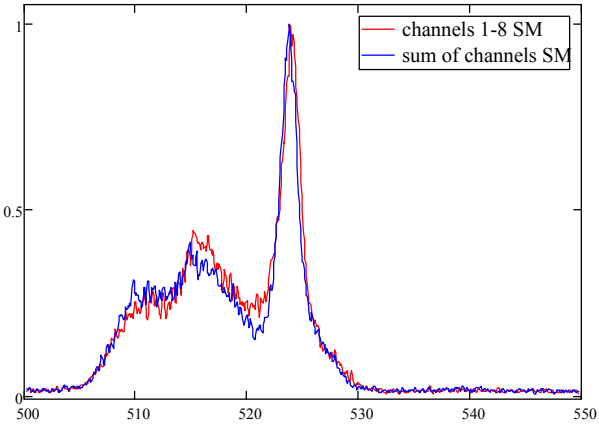


Figure 4.5: 50 $\mu\text{g/ml}$ MRFA, m/z 524.3 $[\text{M}+\text{H}]^+$, Red trace is the spectrum acquired with all channels in the array being acquired simultaneously. Blue trace is the summation of signal acquired from channels 1 through 8 independently and then summed to total trace. Note Red and blue traces are conceptually the same.

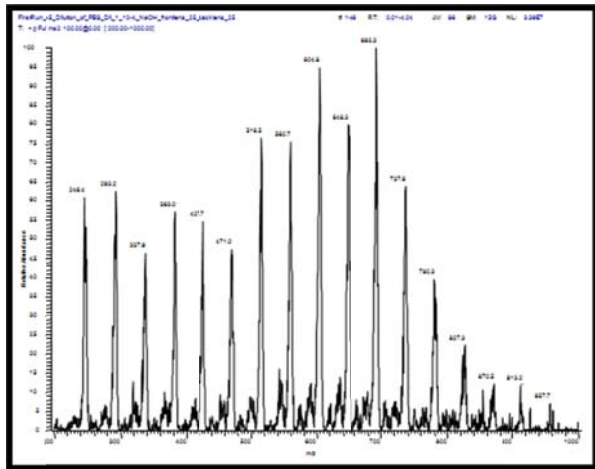


Figure 4.6: Polyethylene glycol (PEG) in concentrated NaOH to form $[M+Na]^+$ adducts. Simultaneous operation of all eight channels in the array, smaller peaks that are reminiscent of a bi and tri modal distribution are due to dimensional variation between ion trap channels.

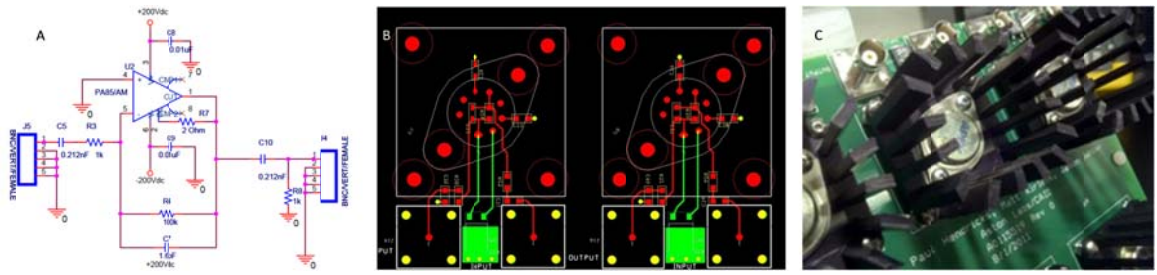


Figure 4.7: A) Circuit schematic of the PA85 operational amplifier used to drive a single channel of the ion trap array. B) OrCAD rendering of the RF circuit, two drive circuits are side by side. C) Assembled multi-channel RF drive circuit for the array.

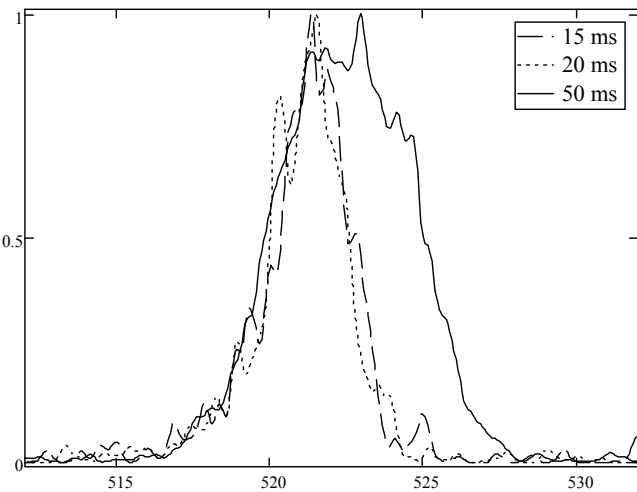


Figure 4.8: Effect of pulse duration on mass assignment and peak resolution for 50 $\mu\text{g/ml}$ MRFA, m/z 524.3 $[\text{M}+\text{H}]^+$. For a 50 ms pulse duration FWHM values are approximately 5 amu while reducing the duration to 20 ms improved the resolution approximately 2 amu. 15 ms was tested to verify that no further improvements were obtained by continuing to reduce the pulse duration.

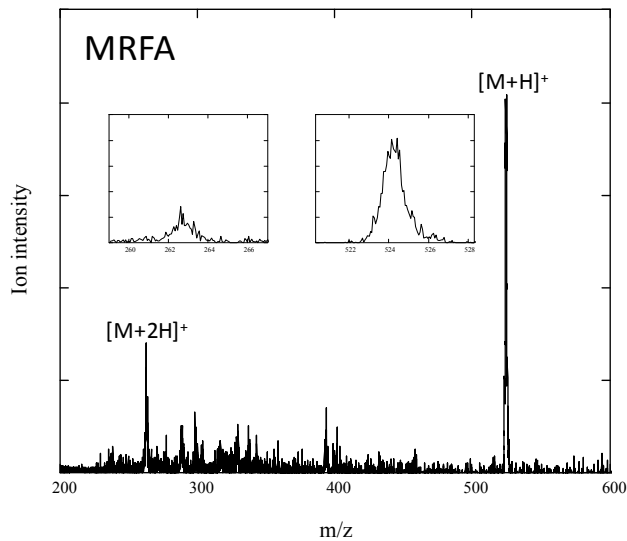


Figure 4.9: 50 $\mu\text{g/ml}$ MRFA, m/z 524.3 $[\text{M}+\text{H}]^+$, fully optimized source conditions resulting in FWHM values on the order of 1 amu for both +1 and +2 charge states.

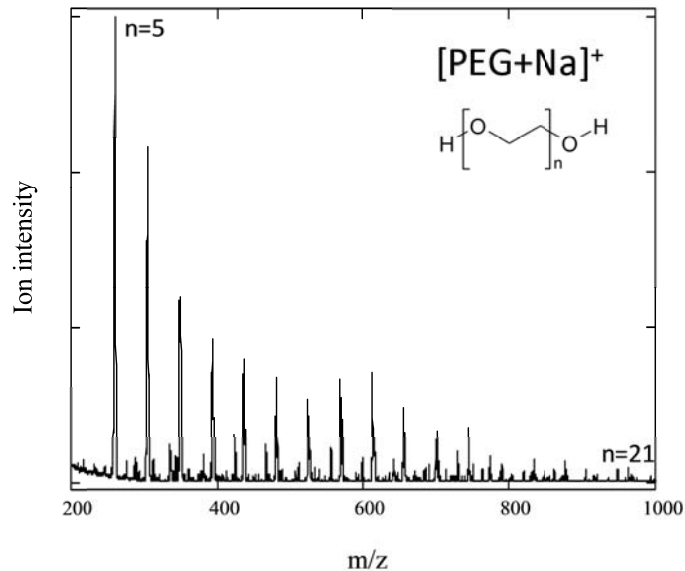


Figure 4.10: PEG oligomers ranging from 50 to 500 μM in solution with concentrated NaOH, $[\text{M}+\text{Na}]^+$, at intervals of 44 amu across the mass range.

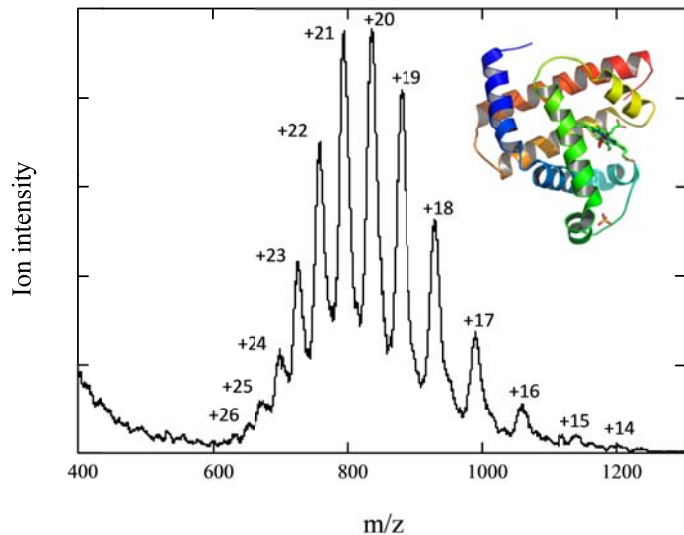


Figure 4.11: $56 \mu\text{M}$ of equine myoglobin (17 kDa), detection of the charge state envelope from +26 to +14 is detectable at RF voltages of $1.2 \text{ kV}_{\text{p-p}}$. By way of comparison the source spray voltage was $1.6 \text{ kV}_{\text{DC}}$.

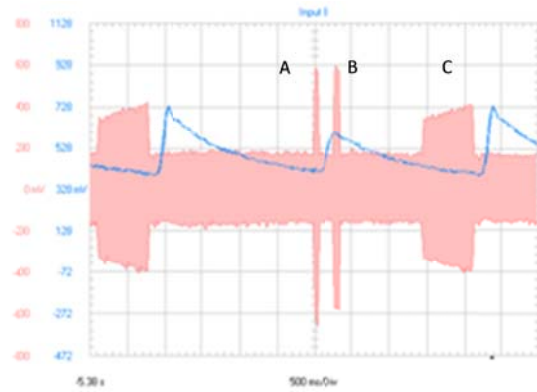


Figure 4.12: Scan function used to execute tandem MS, red trace represents AC and blue trace represents the pressure inside the manifold. A) SWIFT isolation of parent ion at m/z 267 at sub mTorr pressures. B) Excitation for CAD, pressure increase is due to a second DAPI pulse increasing the manifold pressure to 25 mTorr. C) AC ramp during mass analysis.

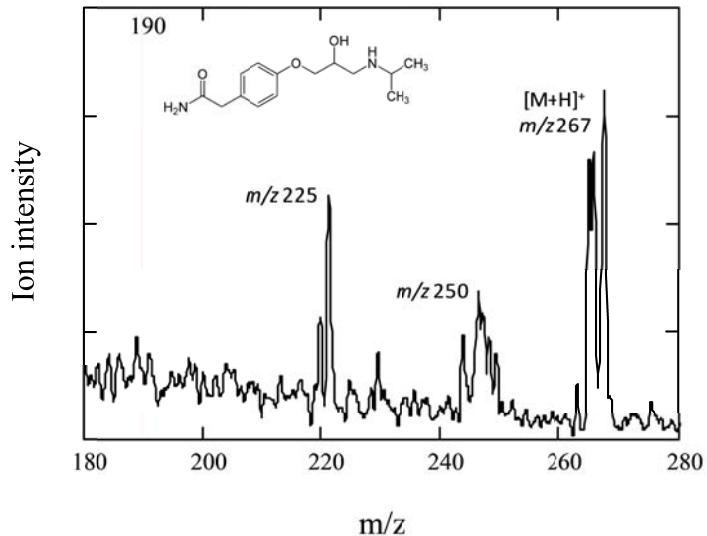


Figure 4.13: Tandem MSMS of atenolol, m/z 267. Fragment ions at m/z 225 and 250 are indicative of propene and NH_3 losses. Red trace at m/z 190 is indicative of the calculated LMCO based upon the amplitude of the applied RF during CAD. Fragment ions below this value are not detected.

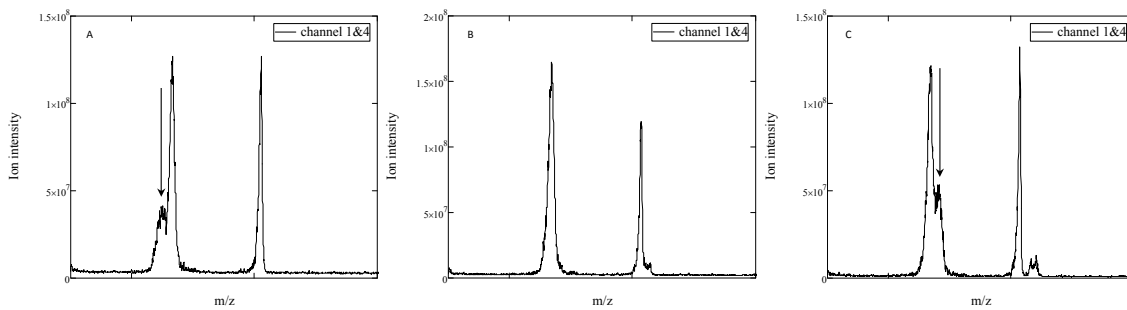


Figure 4.14: *N,N*-Diethyl-meta-toluamide (DEET) fragment m/z 119 and monomer m/z 192 and respectively A) Ion traps 1 and 4 driven independently using the multi-channel operational amplifier circuits described in the text. Most apparent is the DEET monomer ejecting from trap 1 just before trap 4. B) q_z values for all ions in trap 1 have been increased by increasing the amplitude of the RF waveform. Ions eject at roughly the same time for the two channels. C) Further increase of the RF waveform amplitude causes ions from trap 1 to eject after trap 4.

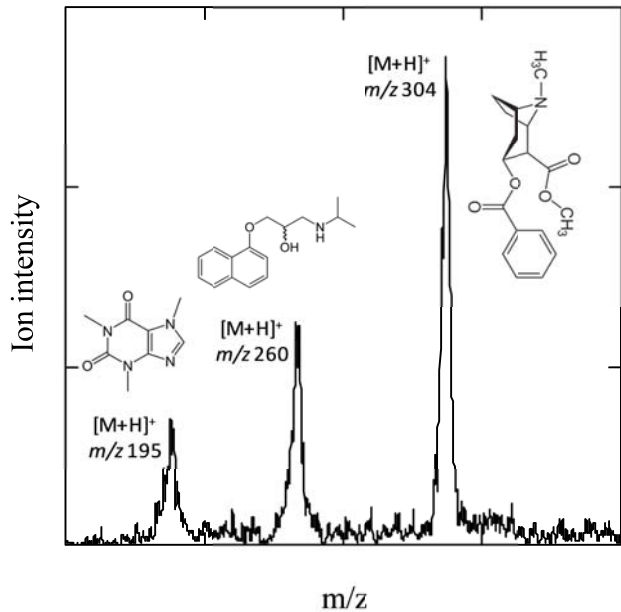


Figure 4.15: 4 ion trap channels operating simultaneously using individually calibrated RF waveforms. nanoESI mass spectrum of caffeine (m/z 195), propranolol (m/z 260), and cocaine (m/z 304) each at 33 $\mu\text{g/ml}$.

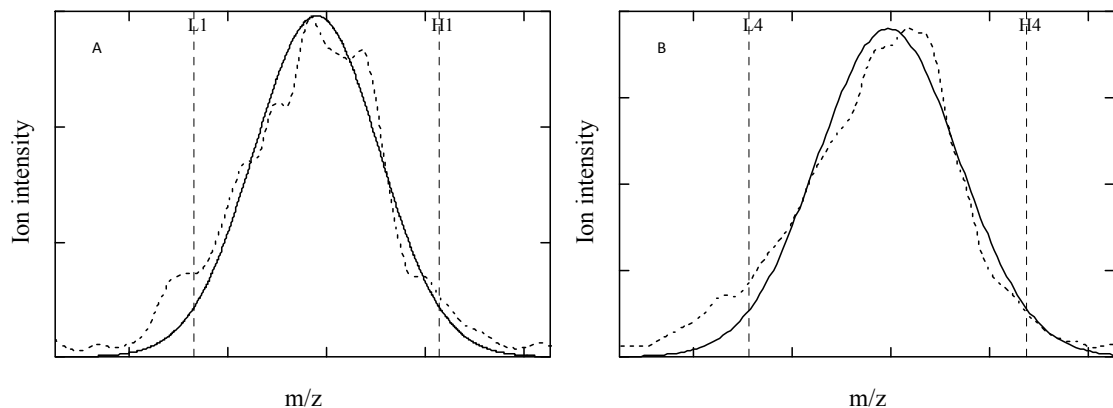


Figure 4.16: A) Single channel B) Multi-channel Gaussian fits to propranolol $[M+H]^+$ signal to define the limits of integration. The area between the low m/z (L1 & L4) and the high m/z (H1& H4) define ~95% of the peak area based upon the fit. m/z values inside this boundary are the limits of integration from which the peak area was calculated.

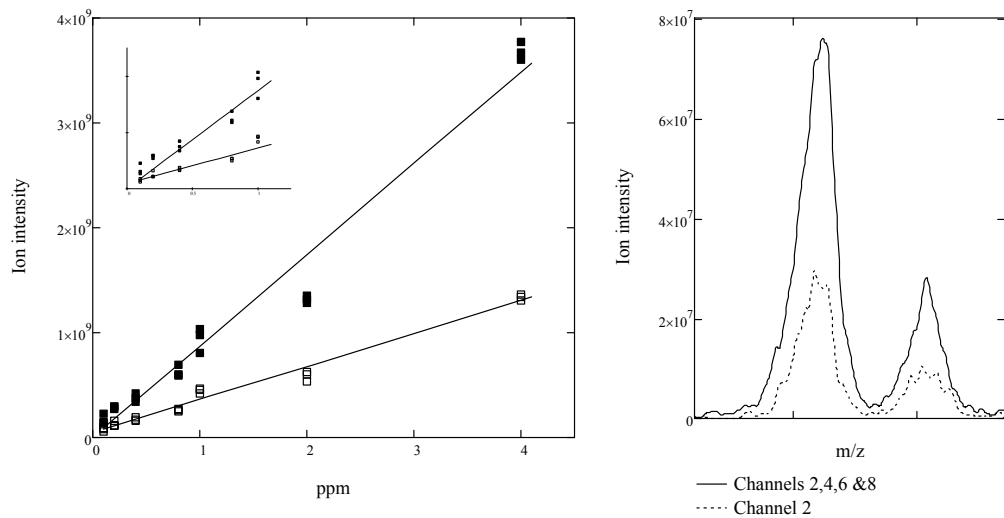


Figure 4.17: Signal response due to one or four channels for propranolol and atenolol. Increased sensitivity obtained by operating multiple channels in parallel. Response was linear from 100 ng/ml to 1400 ng/ml and had good linearity over this range as represented by the R^2 values; 0.982 and 0.97 for one and four channels respectively. Slopes increased from 3.145×10^8 to 8.709×10^8 for one versus four channels.

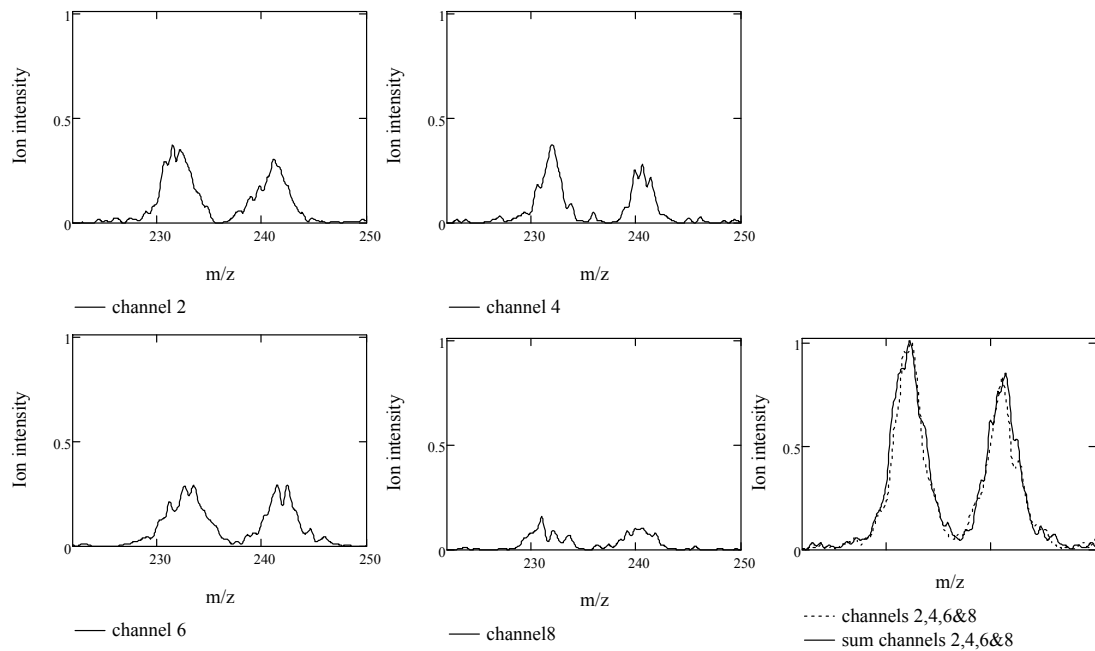


Figure 4.18: Relative contribution for each channel in the array for the composite spectrum. Note that not all channels contribute equally to the analyte response and that not all channels have the same resolution performance. Resonance ejection parameters were tuned for channel 4 and used for all other channels (only one AC signal was available on the LCQ instrument). Recalibrated RF waveforms helped to adjust ion ejection points but did not improve resolution.

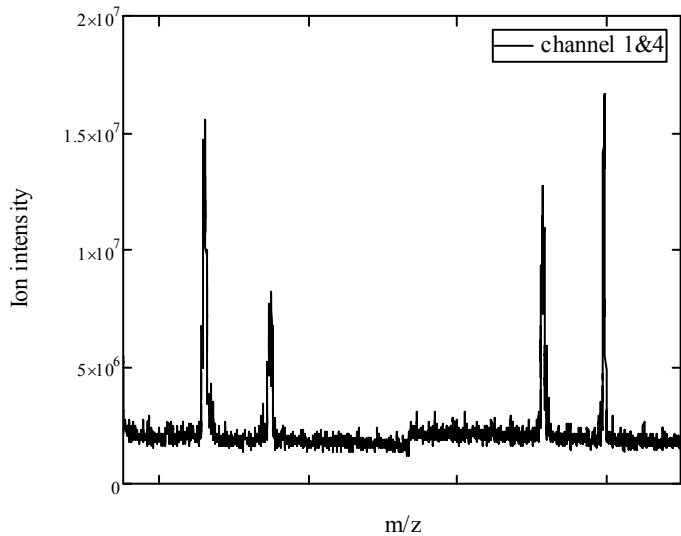


Figure 4.19: Independently controlled RF waveforms allow mass analysis to be completed for any ion trap channel at any time point. The above figure shows an atmospheric pressure chemical ionization (APCI) mass spectrum of DEET from ion trap 1 and 4, but each ion trap channel was scanned at two different time points, i.e. ion trap 1 was scanned first and upon completion the detector was left on to collect the ion signal from trap 4 in which the RF amplitude (from an independent waveform) was scanned. While it was not necessary to scan ion trap 4 following ion trap 1, any element in the array could be scanned in any order, this demonstrated that ions continued to remain trapped in adjacent traps that were not scanned after the first RF ramp. The mass scales from each ion trap are the same and there is no relevance to the difference in peak heights for the m/z 119 and 192 ions.

APPENDIX

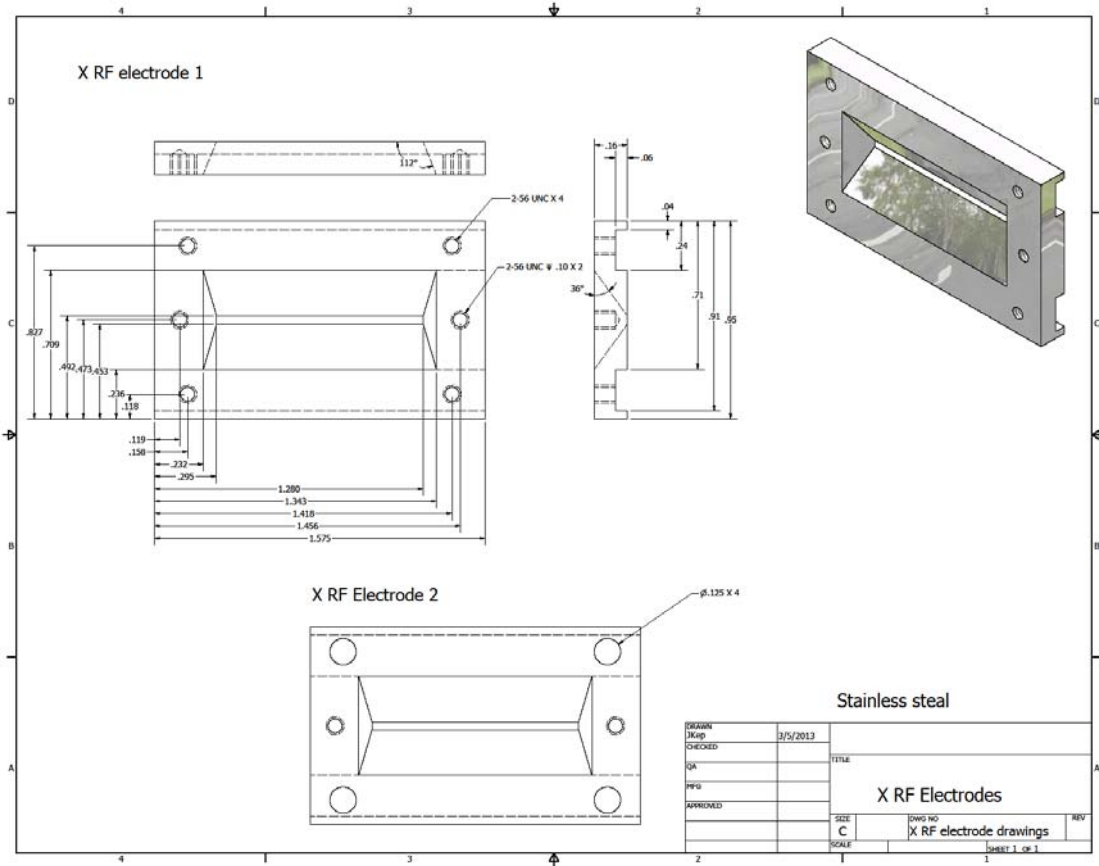
APPENDIX CHAPTER 3

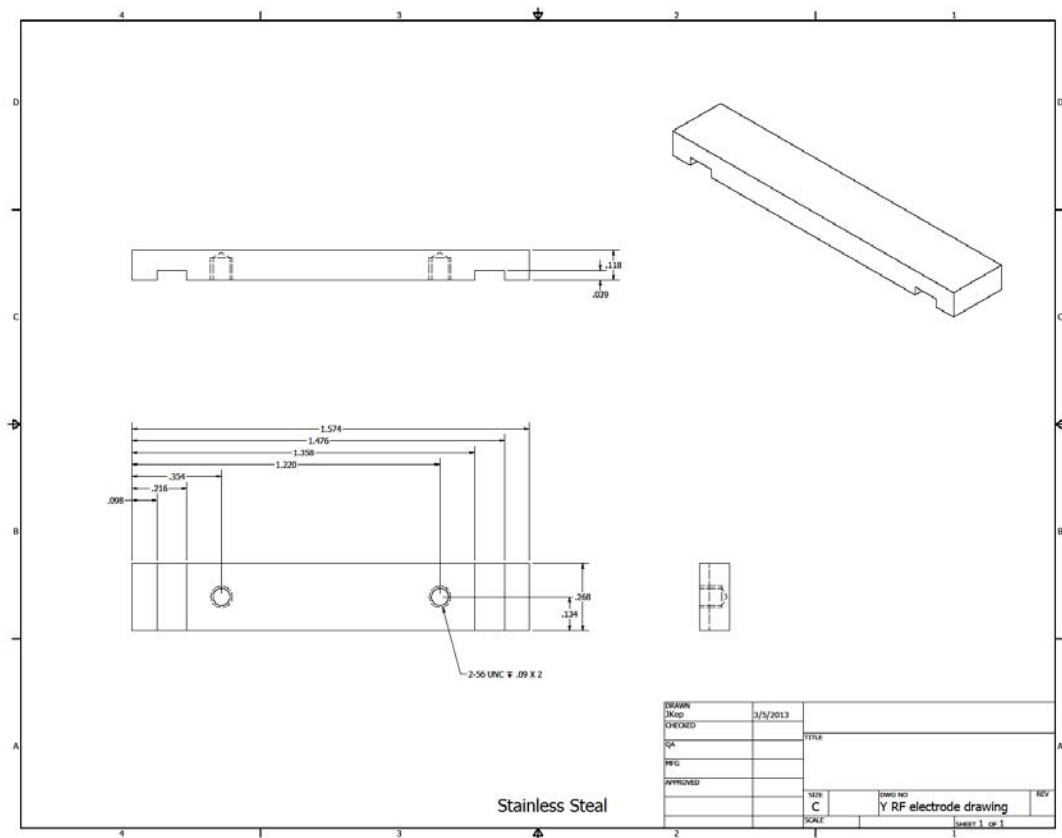
$xPA(x) :=$ <pre> M <- x M1 <- submatrix(M, 0, 64, 4, 4) for i in 1..length(M^{(0)}) - 1 P_i <- submatrix(M, 65*i, 65*i + 64, 4, 4) M1 <- augment(M1, P_i) M2 <- submatrix(M1, 0, length(M1^{(0)}) - 1, 1, 1) for i in 2..cols(M1) - 1 Y_i <- submatrix(M1, 0, length(M1^{(i)}) - 1, i, 1) M2 <- augment(Y_i, M2) M3 <- augment(M2, M1) M4 <- submatrix(M3, 1, 1, 0, cols(M3) - 1) for i in 2..length(M3^{(i)}) - 1 X_i <- submatrix(M3, i, i, 0, cols(M3) - 1) M4 <- stack(X_i, M4) M5 <- stack(M4, M3) out <- M5 </pre>	$yPA(y) :=$ <pre> M <- x M1 <- submatrix(M, 0, 64, 4, 4) for i in 1..length(M^{(0)}) - 1 P_i <- submatrix(M, 65*i, 65*i + 64, 4, 4) M1 <- augment(M1, P_i) M2 <- submatrix(M1, 0, 0, 0, 73) for i in 1..cols(M1) - 1 Z_i <- submatrix(M1, 0, length(M1^{(i)}) - 1, i, i) M2 <- augment(Z_i, M2) M3 <- submatrix(M2, 0, length(M2^{(0)}) - 1, 1, 1) M4 <- submatrix(M3, 1, 1, 0, cols(M3) - 1) for i in 2..length(M3^{(i)}) - 1 X_i <- submatrix(M3, i, i, 0, cols(M3) - 1) M4 <- stack(X_i, M4) M5 <- stack(M4, M3) out <- M5 </pre>	$zPA(z) :=$ <pre> M <- x M1 <- submatrix(M, 0, 64, 4, 4) for i in 1..length(M^{(0)}) - 1 P_i <- submatrix(M, 4810*i, 4810*i + 64, 4, 4) M1 <- augment(M1, P_i) M2 <- submatrix(M1, 0, length(M1^{(0)}) - 1, 1, 1) for i in 2..cols(M1) - 1 Z_i <- submatrix(M1, 0, length(M1^{(i)}) - 1, i, i) M2 <- augment(Z_i, M2) M3 <- submatrix(M2, 0, length(M2^{(0)}) - 1, 1, 1) M4 <- submatrix(M3, 1, 1, 0, cols(M3) - 1) for i in 2..length(M3^{(i)}) - 1 Y_i <- submatrix(M3, i, i, 0, cols(M3) - 1) M4 <- stack(Y_i, M4) M5 <- stack(M4, M3) out <- M5 </pre>
--	---	---

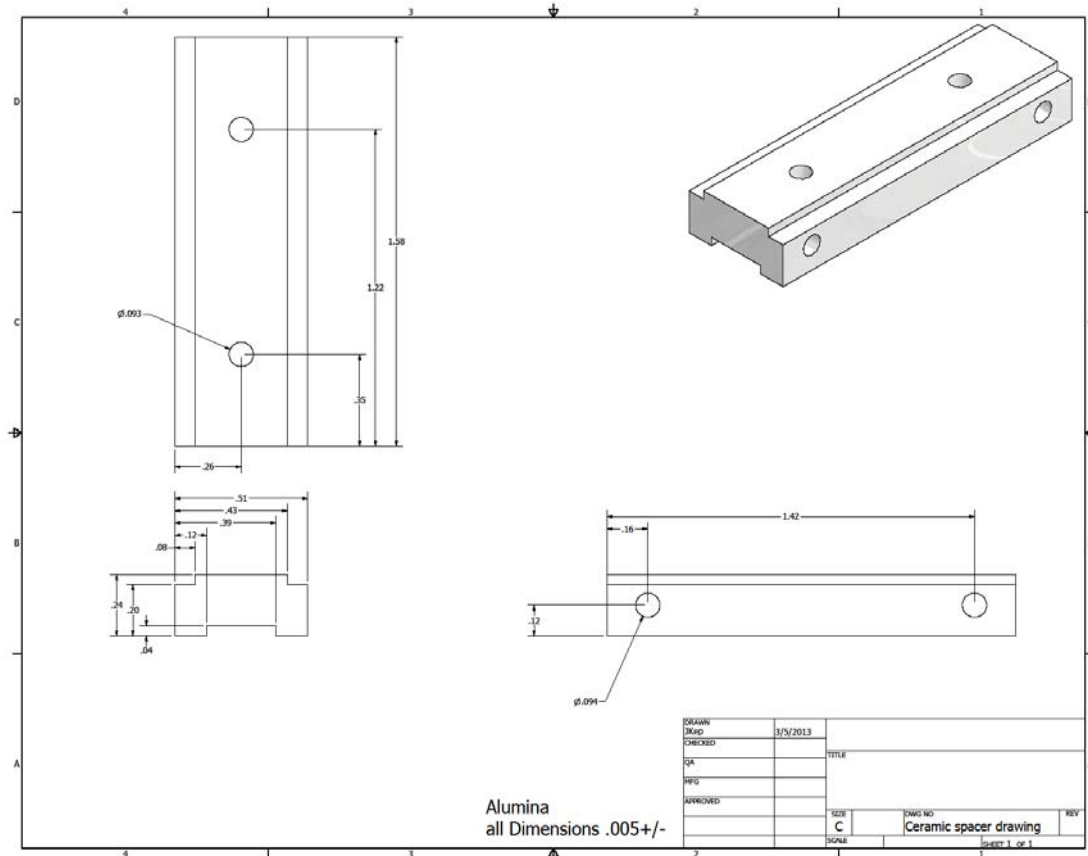
Field calculation for a 1/3rd size RIT from a PA output from SIMION that used dx spacing of 3.25, which was necessary in order to reduce the data size to something manageable by MathCAD.

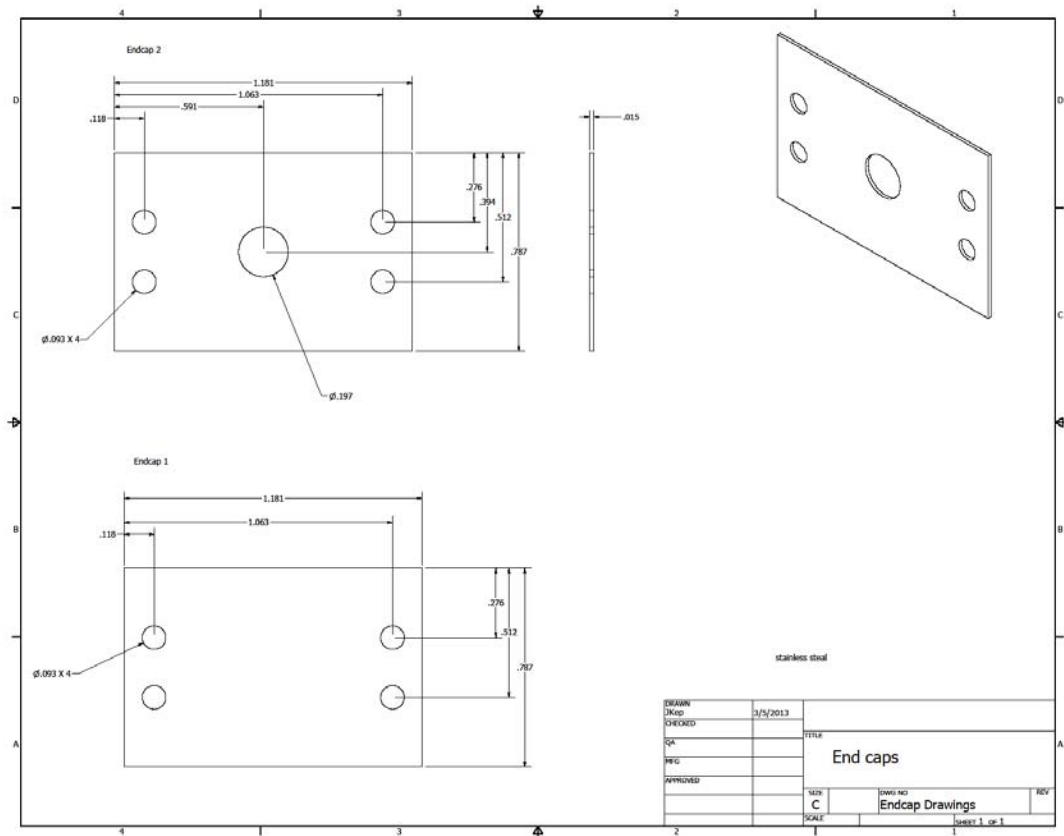
$\text{grid}(x) := \begin{cases} M \leftarrow x \\ M1 \leftarrow \text{submatrix}(M, 0, 64, 4, 4) \\ \text{for } i \in 1.. \frac{\text{length}(M^{(0)})}{65} - 1 \\ \quad P_i \leftarrow \text{submatrix}(M, 65 \cdot i, 65 \cdot i + 64, 4, 4) \\ \quad M1 \leftarrow \text{augment}(M1, P_i) \\ M2 \leftarrow \text{submatrix}(M1, 0, 10, 0, 8) \\ \text{out} \leftarrow M2 \end{cases}$	$\text{expansion}(x, r_0, n) := \begin{cases} \text{for } i \in 0..n - 1 \\ \quad C_i \leftarrow \begin{cases} (n \leftarrow 2 \cdot i + 2) \\ \text{out} \leftarrow \text{cn_solve}(x, r_0, n) \end{cases} \\ S_i \leftarrow \begin{cases} (n \leftarrow 4 \cdot i) \\ \text{out} \leftarrow \text{sm_solve}(x, r_0, n) \end{cases} \\ \text{out} \leftarrow \text{augment}(C, S) \end{cases}$
$\text{cn_solve}(x, r_0, n) := \begin{cases} \Delta \leftarrow 0.166 \\ \text{sum} \leftarrow 0 \\ \text{for } i \in 0.. \text{length}(x^{(0)}) - 1 \\ \quad \text{for } j \in 0.. \text{cols}(x) - 1 \\ \quad \quad r \leftarrow \begin{cases} \sqrt{(0.166i)^2 + (0.166j)^2} & \text{if } r \leq r_0 \\ r = r_0 & \text{otherwise} \end{cases} \\ \quad \quad \Theta \leftarrow \begin{cases} 0 & \text{if } i = 0 \\ \text{atan}\left(\frac{0.166j}{0.166i}\right) - \frac{\pi}{4} & \text{otherwise} \end{cases} \\ \quad \quad \text{sum} \leftarrow \text{sum} + x_{i,j} \cdot \left(\frac{r}{r_0}\right)^n \cdot \cos(n \cdot \Theta) \cdot \Delta^2 \\ \quad \text{out} \leftarrow \frac{8(n+1)}{r_0^2 \cdot \pi} \cdot \text{sum} \end{cases}$	$\text{sm_solve}(x, r_0, n) := \begin{cases} \Delta \leftarrow 0.166 \\ \text{sum} \leftarrow 0 \\ \text{for } i \in 0.. \text{length}(x^{(0)}) - 1 \\ \quad \text{for } j \in 0.. \text{cols}(x) - 1 \\ \quad \quad r \leftarrow \begin{cases} \sqrt{(0.166i)^2 + (0.166j)^2} & \text{if } r \leq r_0 \\ r = r_0 & \text{otherwise} \end{cases} \\ \quad \quad \Theta \leftarrow \begin{cases} 0 & \text{if } i = 0 \\ \text{atan}\left(\frac{0.166j}{0.166i}\right) - \frac{\pi}{4} & \text{otherwise} \end{cases} \\ \quad \quad \text{sum} \leftarrow \text{sum} + x_{i,j} \cdot \left(\frac{r}{r_0}\right)^n \cdot \cos(n \cdot \Theta) \cdot \Delta^2 \\ \quad \text{out} \leftarrow \frac{8(n+1)}{r_0^2 \cdot \pi} \cdot \text{sum} \end{cases}$

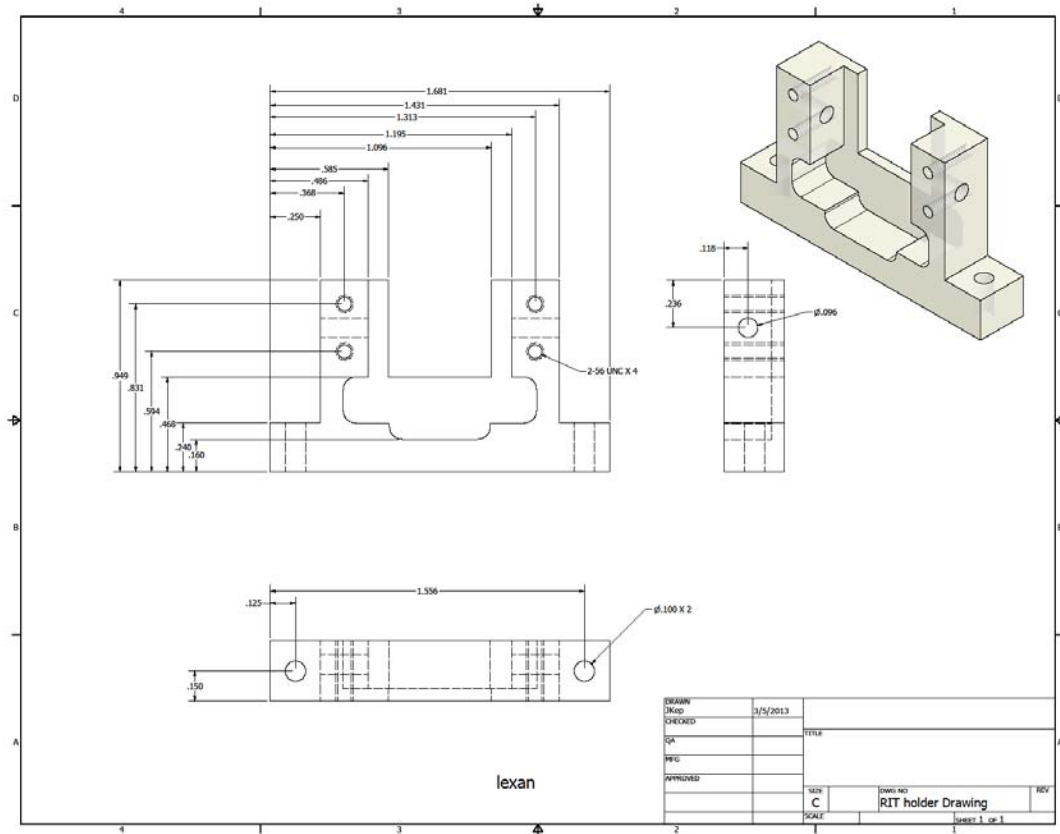
The expansion calculator x = the array of potentials for x and y coordinates; r_0 = the inscribed radius for RIT designs $r_0 = X_0$; n = number of coefficients that will be calculated for C and S . Also note that the current values of 0.673 for the A2 term is very close to the reported values from the RIT AC paper which is 0.654. These calculations are dependent upon the grid spacing units and correct dimensions for X and Y coordinates which are used to calculate 'r'.

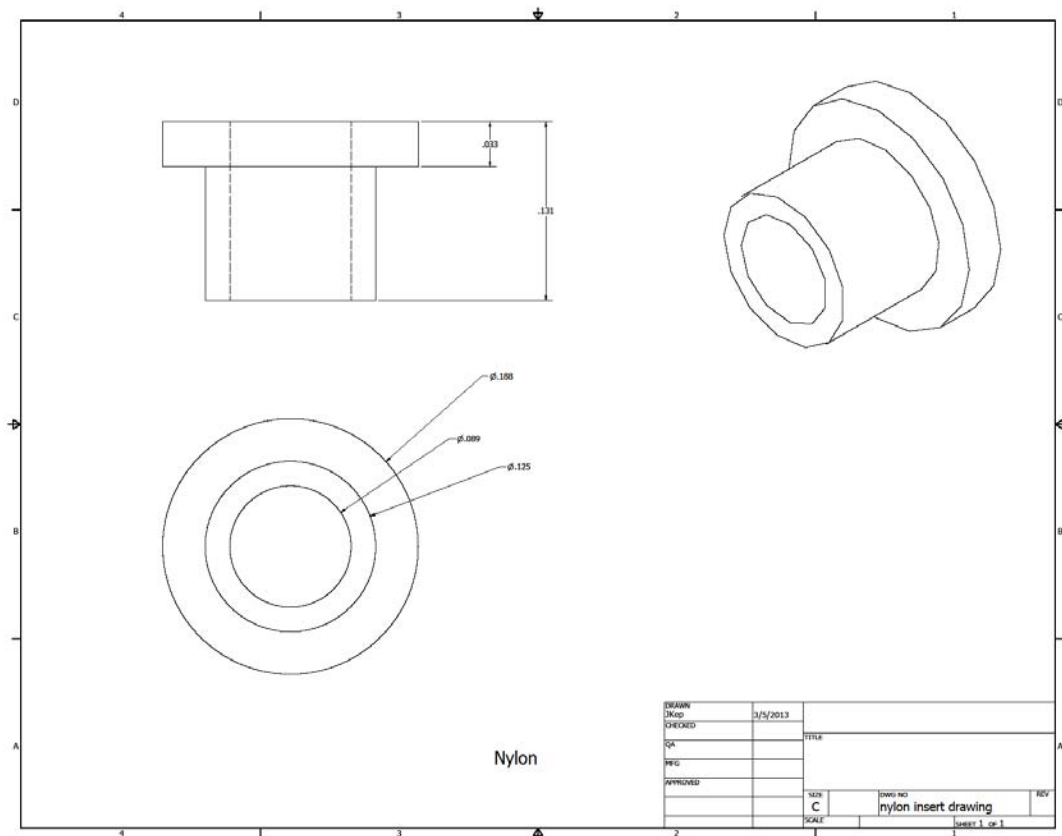






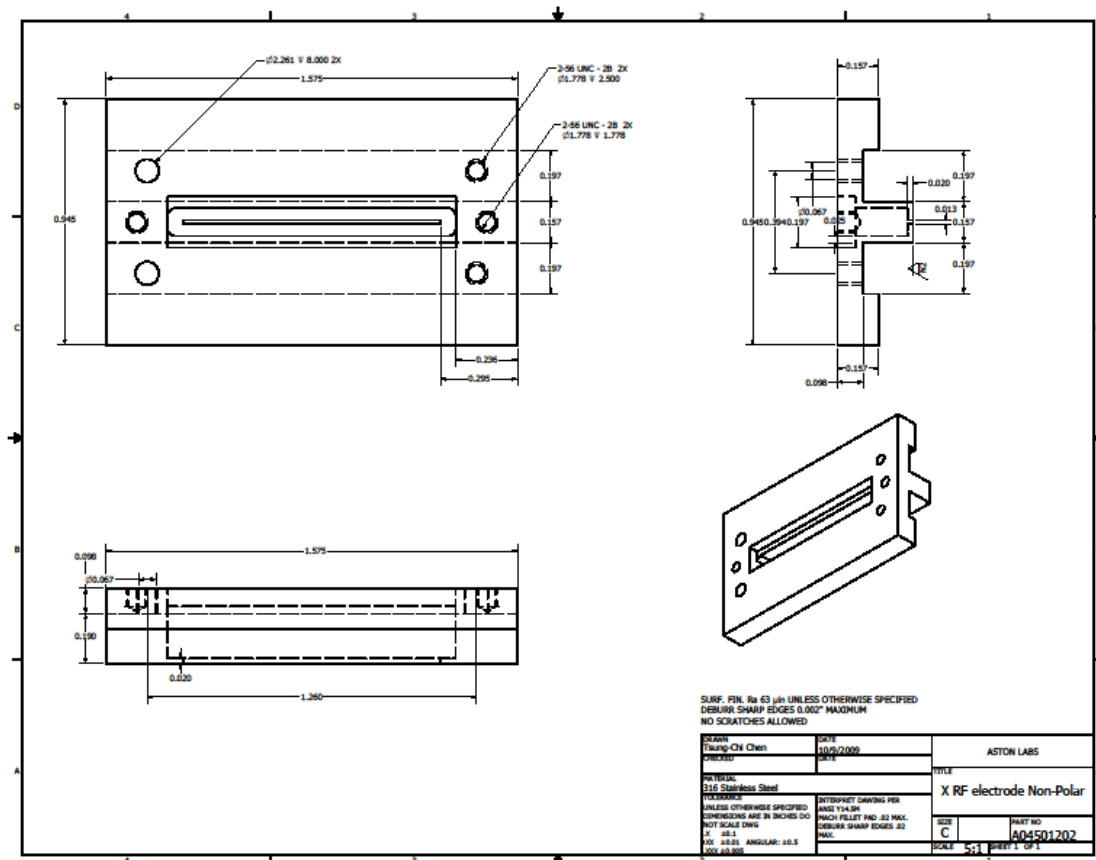


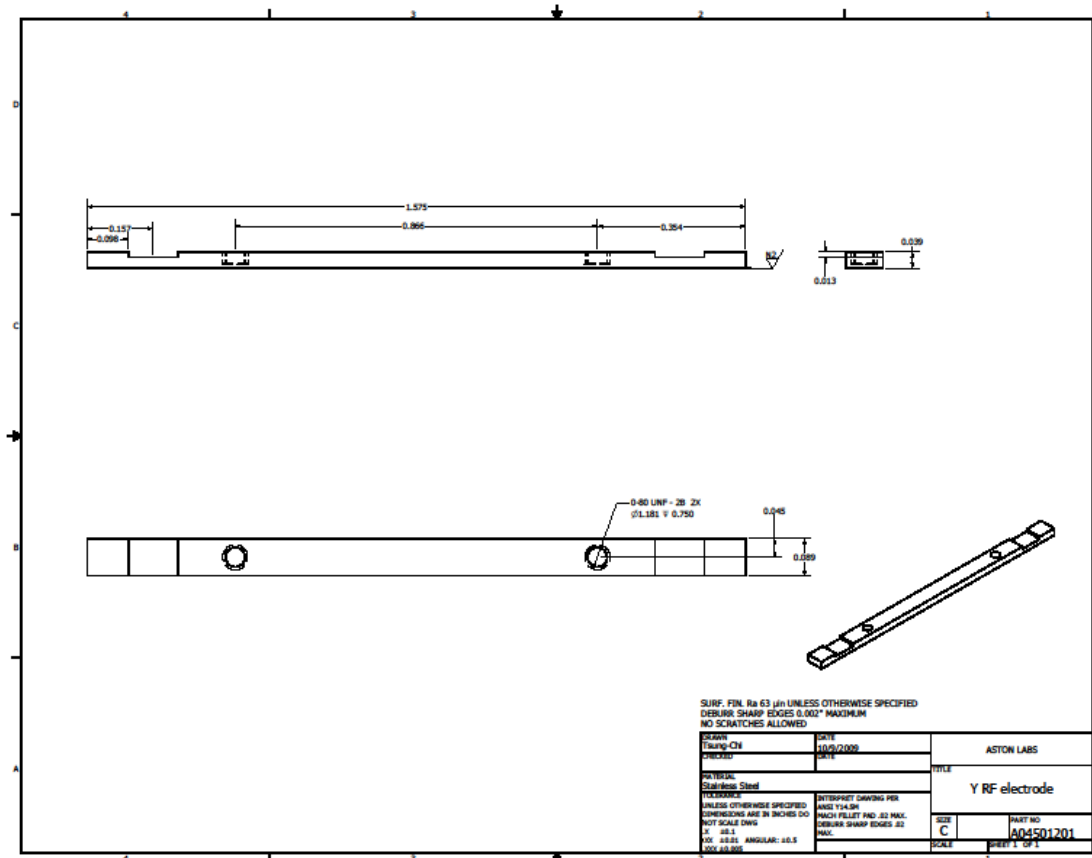


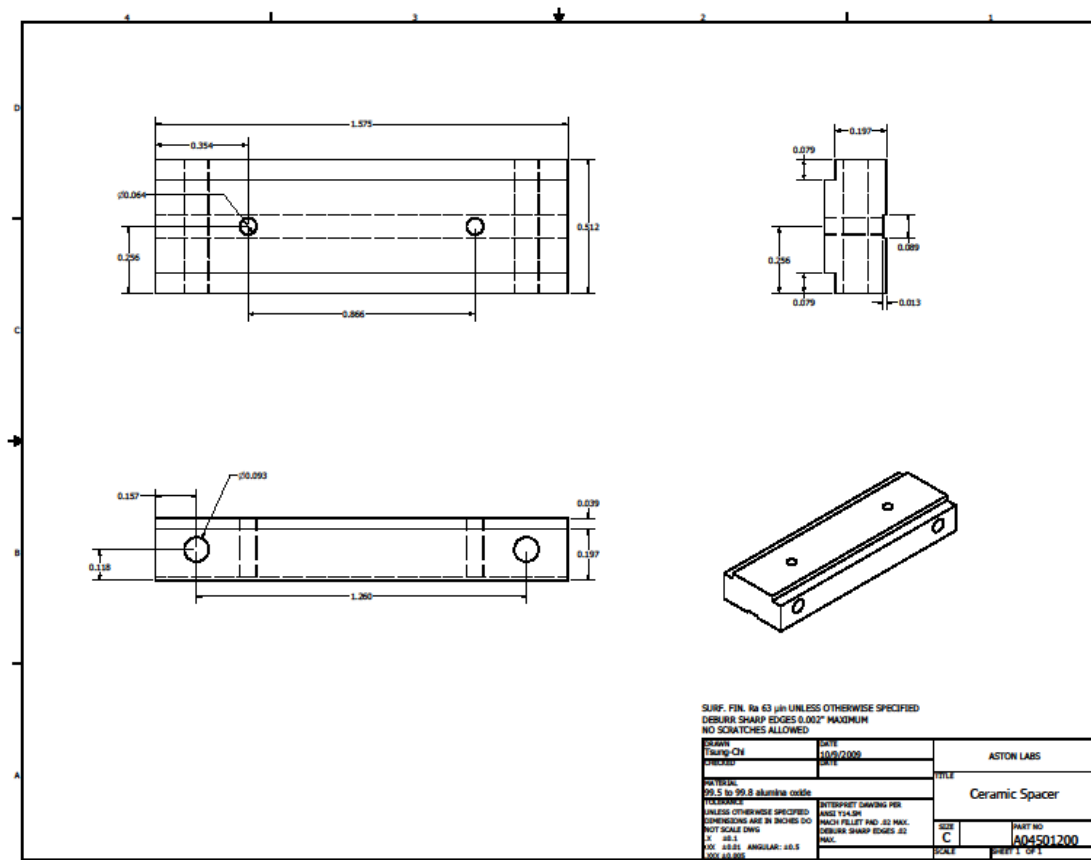


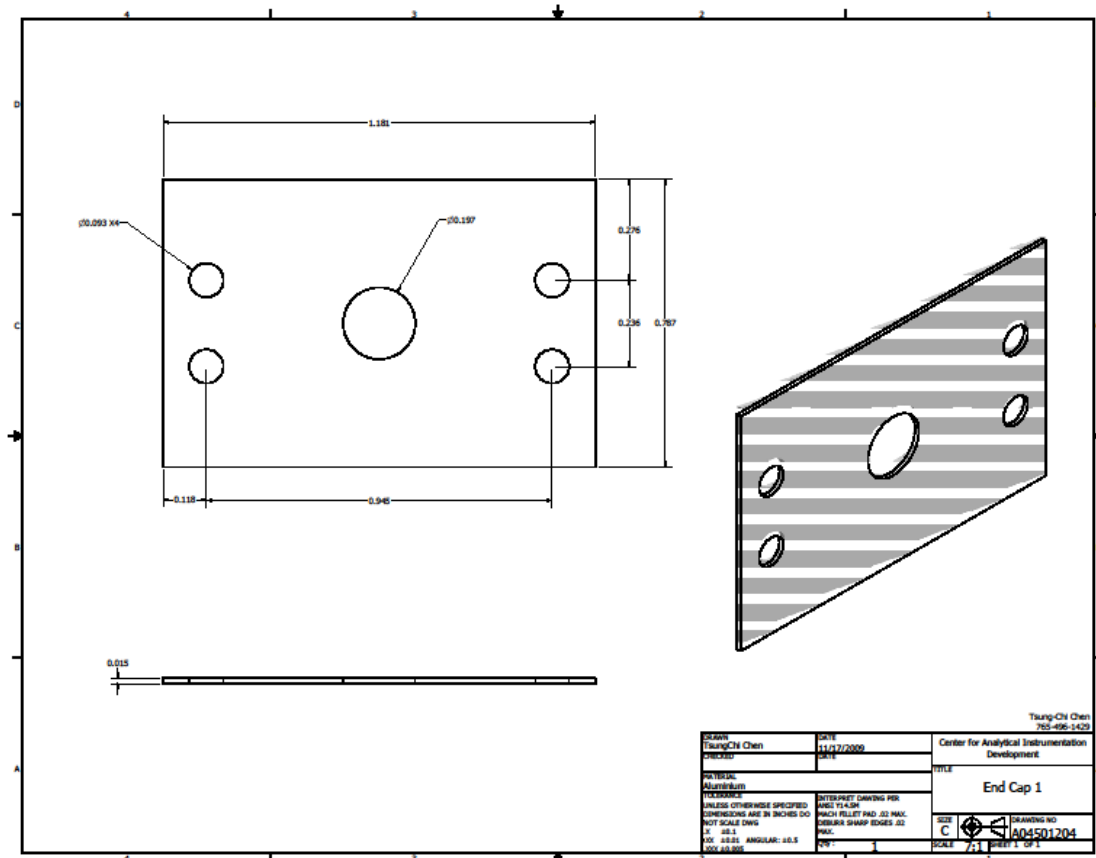
Rectilinear Ion Trap Parts Assembly Parts List		
Part	Material	Count
X-electrodes	316 stainless steel	2
Y-electrodes	316 stainless steel	2
Front end caps	316 stainless steel	1
Rear end caps	316 stainless steel	1
Ceramic spacers	Glass-Mica (Ultra High temp)	2
Trap holders	Polycarbonate (Lexan)	2
nylon inserts	Nylon-66	4
2-56 screws (5/16 in)	Stainless steel	16
2-56 screws (1.0 in)	Stainless steel	4
No. 2 washers	Stainless steel	20

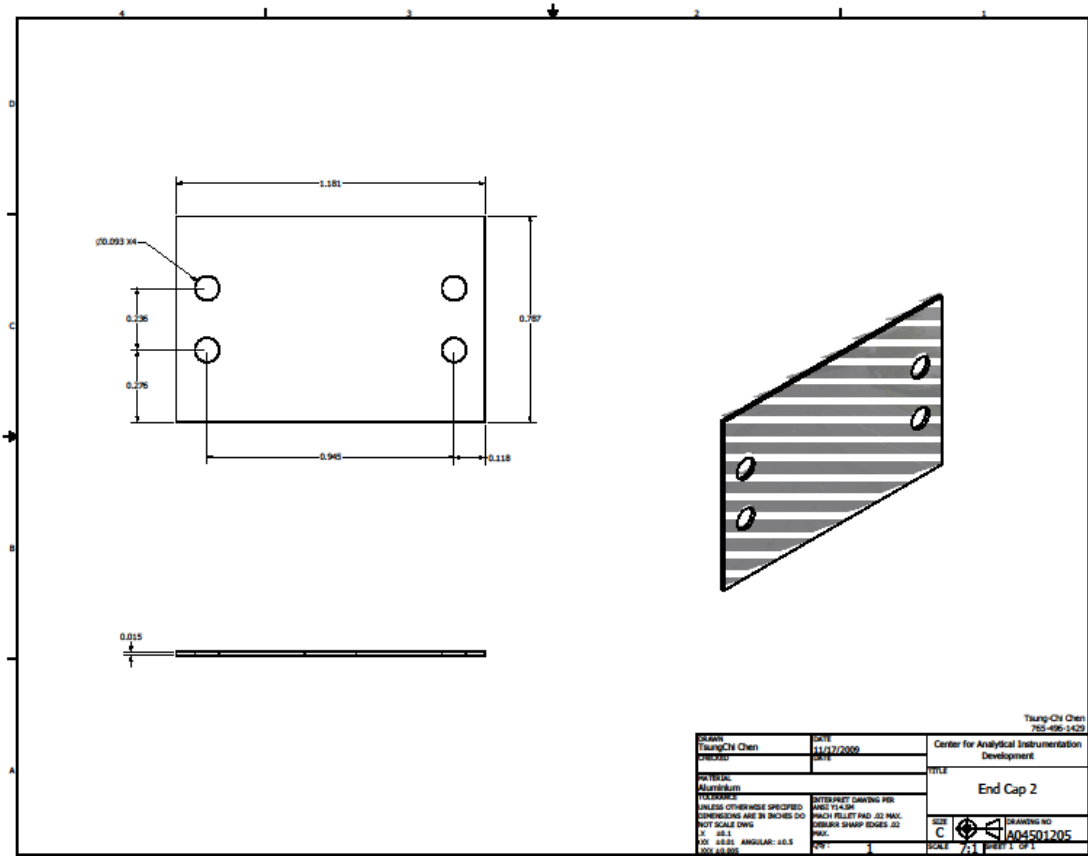
Rectilinear Ion Trap Dimensional Analysis			
Location	RIT DIMENSIONS (in.)	DESIGN DIMENSION (in.)	TOLERANCE (in.)
Gap between ion trap and front endcap	0.061	0.0625	0.005
Gap between ion trap and rear endcap	0.06	0.0625	0.005
Front endcap ion injection aperture	0.197	0.197	0.005
Ion ejection slit: X-electrode (1)	0.039	0.039	0.005
Ion ejection slit: X-electrode (2)	0.039	0.039	0.005
Length X-electrode (1)	1.576	1.575	0.005
Length X-electrode (2)	1.576	1.575	0.005
Length Y-electrode (1)	1.575	1.575	0.005
Length Y-electrode (2)	1.5755	1.575	0.005
Internal distance between X-electrodes (front)	0.3965	0.394	0.005
Internal distance between X-electrodes (rear)	0.3975	0.394	0.005
Internal distance between Y-electrodes (front)	0.312	0.315	0.005
Internal distance between Y-electrodes (rear)	0.3125	0.315	0.005

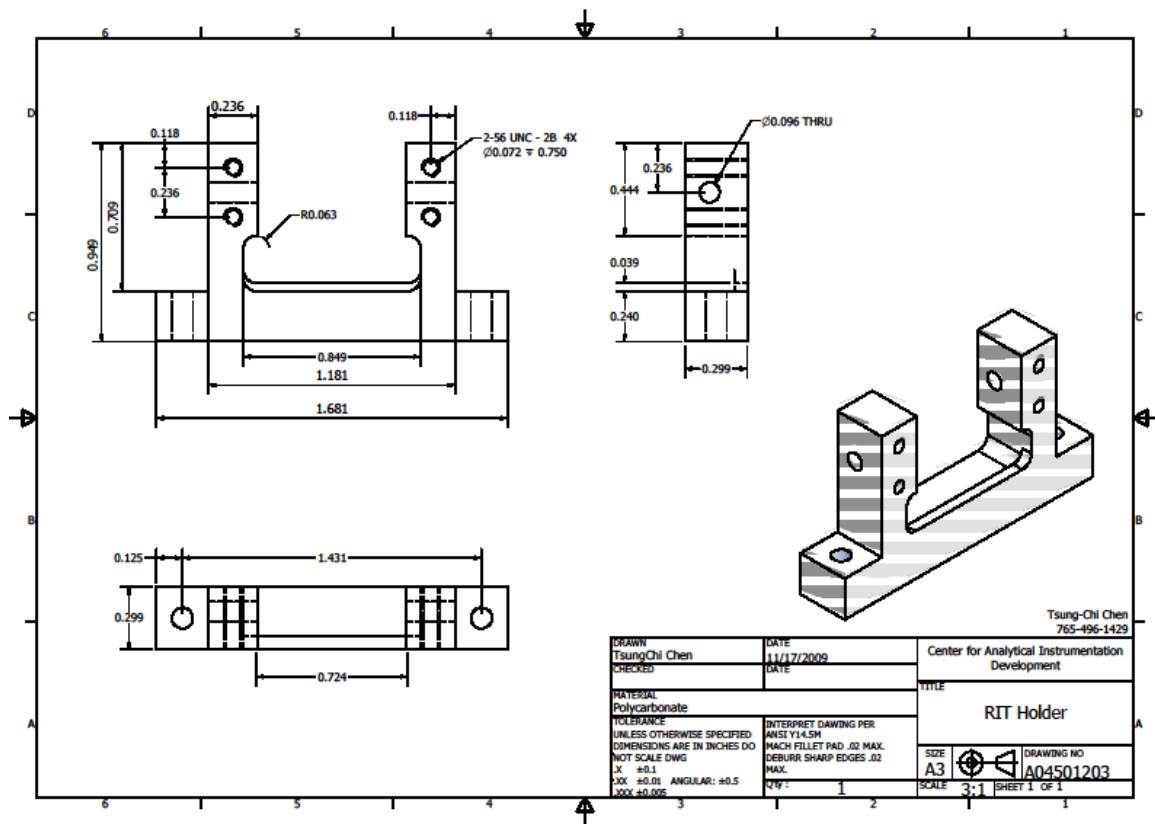


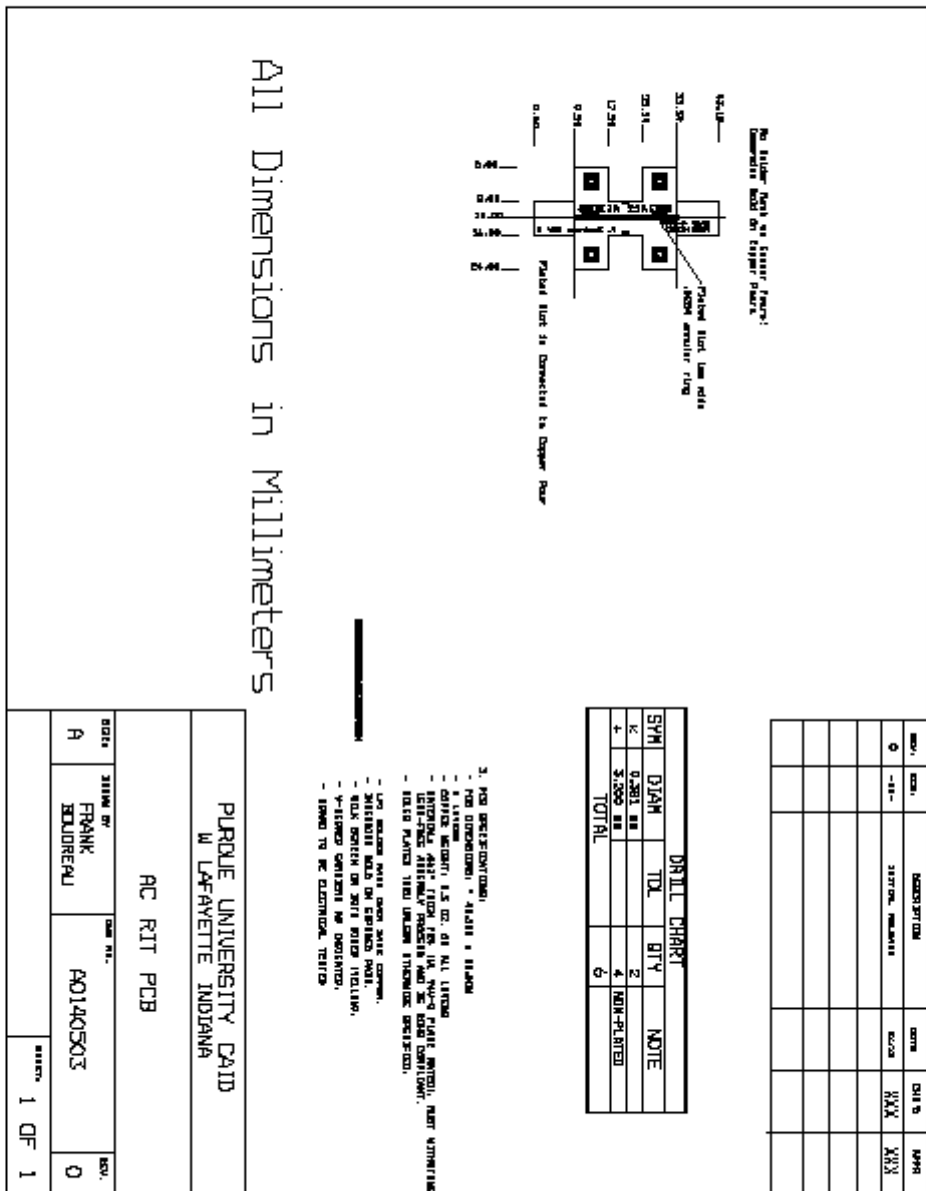


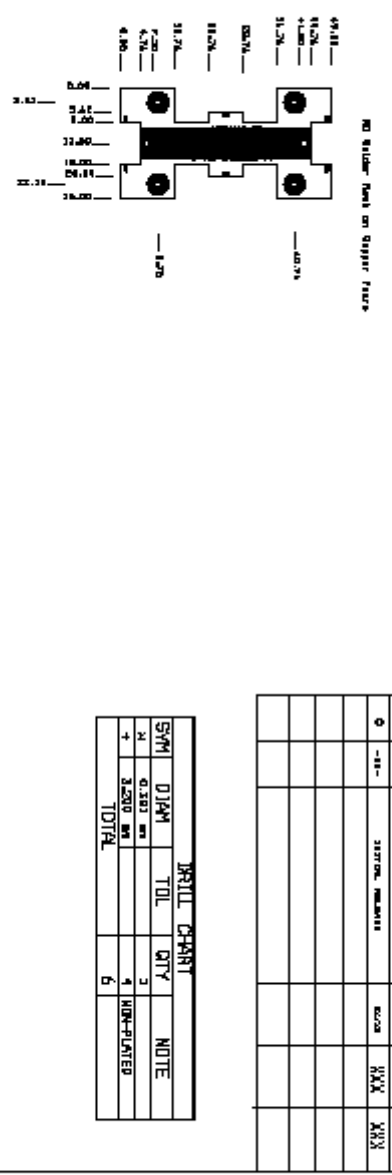










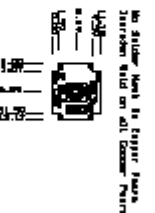


All Dimensions in Millimeters

3. PCB SPECIFICATIONS:
- PCB MATERIALS = FR4/FR5 + THERM
 - LAYUP - 2 LAYUP
 - COUPIC WEIGHT: 1.5 OZ. OR ALL LAYUP
 - INTERNAL HALF-TRACES OR VIAS "WALL PLATE" METHOD. REST MATURED
 - INTERNAL AND EXTERNAL PLATES MUST BE ROUGH SURFACE.
 - VARIOUS PLATES IN ALUMINUM THICKNESS DESCRIBED.
 - NO PLATING ON ALUMINUM
 - NO PLATING ON CERAMIC BASE PLATE.
 - NO PLATING ON TOP BASE PLATE.
 - NO PLATING ON BOTTOM BASE PLATE.
 - PLATING POSITION TO BE DETERMINED.
 - PLATED HIGHLIGHTS TO BE DETERMINED.
 - PLATE TO BE ELECTROPLATE

PURDUE UNIVERSITY CAD W LAFAYETTE INDIANA		
RF RIT PCB		
DATE	DESIGN BY	REV.
A	FRANK JULIOPALU	A0140501 0
PRINTED 1 OF 1		

All Dimensions are In Millimeters



SYN	DIAH	DRILL CHART	QTY	NOTE
2	0.380 mm		3	
4	2.500 mm		3	HORN-PLATED
	TOTAL		3	

3. HORN PLATED (COPPER)
 - TOP SURFACE = 1.0MM ± 0.075
 - A 1.0MM
 - COPPER MIGHT BE ADDED TO ALL LAYERS
 - INTERNAL HORN PLATE FOR VIBRATION PLATE POSITION. MUST MATCH THE
 - HORN PLATE THAT WAS IN THE HORN PLATE POSITION.
 - NO PLATING ON ALUMINUM TRACES OR OVERHANGS.
 - NO PLATING ON THE CONDUCTIVE PASTE.
 - HORN PLATED AS DEFINED.
 - HORN TO BE ELECTRO PLATED.

PURDUE UNIVERSITY CAD
 W LAFAYETTE INDIANA

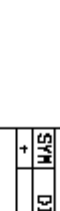
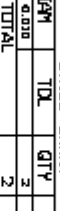
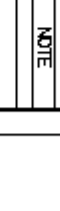
End Cap RIT PCB

DATE	DESIGN REV	CASE REV.	REV.
A	FRANK BELLIRAU	A0140505	0

PRINT 1 OF 1

ALL DIMENSIONS IN MILLIMETERS				
<p>Technical drawing of a PCB component showing various dimensions and assembly notes. The drawing includes a central rectangular area with internal components and several callouts with dimensions like 1.00 mm, 0.50 mm, 0.25 mm, 0.20 mm, and 0.10 mm. There are also notes such as "bottom edge no trim" and "center edge no trim".</p>				
DRILL DATA				
SYM	DIAM	TOL	QTY	NOTE
3	2.500 mm	+ .0050	1	HOT PLATED
			TOTAL	8

3. PCB SPECIFICATIONS:
 - PCB INSIDE DIMENSION = 40.71
 - A 1.00MM TOP EDGE AND A 0.50MM BOTTOM EDGE ARE TO BE LEFT UNTRIMMED.
 - INTERNAL HOLE FLOOR FOR VLSI WIRE PLATE MOUNTS. MUST MATCH FLOOR
 - HOLES PLACED IN ALUMINUM TRACES ARE UNTRIMMED.
 - NO PLATING ON ALUMINUM TRACES.
 - NO PLATING ON THE INSIDE OF HOLES.
 - HOLES POSITION ON PCB MUST FOLLOW.
 - VLSI FLOOR POSITION AS DEFINED.
 - DUE TO THE ELECTROPLATE PROCESS.

PCB RIT AC ELECTRODE THIRD SIZE				
SHEET NO.	DESIGN NO.	DRAWN BY	REV.	
A	FRANK JULIOPAU	A014050RC	O	PRINTED 1 OF 1
PURDUE UNIVERSITY CAD W LAFAYETTE INDIANA				
4. THIS HOLDS THE PREVIOUS PAGE NUMBER REFERENCED SHEET!				
5. NO PREDENT SHEET! - NO DRAFTS! - 2 UNTYPED - COMMON SPACES: 1/8", 1/4", OR 1/2" UNLESS INTERNAL HOLE FLOOR TO U/C. THIN PLATE MATERIAL, MUST MATCH FLOOR - HOLES PLACED THAT USELESS THROUGH DRILLED. - ONE PLACEMENT ON ALUMINUM - FOR MACHINED PARTS USE SOLID CENTER LINE - FULL WALL WELDED ON PARTS USE SOLID CENTER LINE - ALL PARTS HELD/JOINED AND CLASPED IN THERMAL RELAY - IMPOSSIBLE HOLE IS CLOSERD PIERCE - SURE SCAFFOLD IN BOTH AREA HELD/JOINED - VERSATILE WELDING IS JIGGED/JOINED - DEDICATED TO THE ELECTRONIC TRADE				
6. DRILL CHART				
SYM	DIA#	TOL.	QTY	NOTE
+ 	6.000		2	
TOTAL				
				
				
				
				
				

	<table border="1" style="width: 100%; border-collapse: collapse;"> <thead> <tr> <th style="text-align: left;">SYN</th> <th style="text-align: left;">DIA#</th> <th style="text-align: left;">DRILL CHART</th> <th style="text-align: left;">NOTE</th> </tr> </thead> <tbody> <tr> <td style="text-align: center;">Φ</td> <td style="text-align: center;">6.010</td> <td style="text-align: center;">TOL</td> <td style="text-align: center;">2</td> </tr> <tr> <td style="text-align: center;">+</td> <td style="text-align: center;">6.025</td> <td style="text-align: center;">GTY</td> <td style="text-align: center;">4 HOLE-PLATED</td> </tr> <tr> <td></td> <td></td> <td style="text-align: center;">TOTAL</td> <td style="text-align: center;">6</td> </tr> </tbody> </table> <p style="margin-top: 10px;">4. HOLE HELDS THE PLATES FOR HAVING REFERENCE GUY!</p> <p style="margin-top: 10px;">5. NO SPECIFIC COMI - NO INDENTION! - 2 UPTIME - COMMON MOUNT: 3 1/8" OR 4 1/8" LIPLESS - INTERNAL MOLD FLICK FOR IN. THICK PLATE POSITION. MUST WAIT TIME - EXTRUDED ALUMINUM PROBLEMS MAY BE SOLVED BY PLATE. - EXTRUDED PLATE THAT USES TRIMMING OPERATIONS. - ONE PLATING ON ALUMINUM - ONE PLATING ON ALUMINUM - ONE PLATING ON ALUMINUM - FULL MOLD WHEELED AFTER PLATING. DON'T USE IN GUY - ALL PARTS HELDUSING AIR PLACED IN THERMAL RELAX - INSPECT GUY IN COLD AIR FLOW - BULL'S EYE IN BOTH ALUM. PLATES - VERTICAL DIMENSION IS JIGGING - JIGGING TO 10' ELECTRICAL TORQUE</p>	SYN	DIA#	DRILL CHART	NOTE	Φ	6.010	TOL	2	+	6.025	GTY	4 HOLE-PLATED			TOTAL	6
SYN	DIA#	DRILL CHART	NOTE														
Φ	6.010	TOL	2														
+	6.025	GTY	4 HOLE-PLATED														
		TOTAL	6														
PURDUE UNIVERSITY CAD W LAFAYETTE INDIANA																	
RF ELECTRODE THIRD SIZE																	
DATE:	DESIGN BY:	CAM. NO.:	REV.:														
A	FRANK	AC140509A	0														
PRINTED 1 OF 1																	

SYN	DIA/M	TOL.	QTY	NOTE
+	0.010	± .005	2	
%	0.005		1	NOT-APPROVED
TOTAL			3	

◆

4. THIS HOLDS THE PREVIOUS PAGE NUMBER REFERENCED QTY!

5. NO SPECIFICATIONS!
- NO DIMENSIONS!
- NO TOLERANCES!
- COMMON MATERIALS, 3 OR 4 OR ALL, LUMBER
- INTERNAL, EXTERNAL, FLAT, ROUND, TUBE, PLATE, PROFILE, PLASTIC, MASONRY, ETC.
- EXTERIOR, INTERNAL, EXTERIOR, PROFILES THAT ARE NOT COMMON.
- EXTERIOR PLATES THAT USELESS THICKNESS SPECIFIED.
- ONE PLATE OR IN ALUMINUM
- ONE MATERIAL WITH WHICH OTHER MATERIAL IS USED
- FULL, HALF, THREEQUARTER, ETC. PLATES, ETC. AND OTHERS IN USE
- ALL PARTS IDENTIFYING ARE PLACED ON THE DRAWING AS LOCATED
- IDENTIFICATION CALLS IN DIFFERENT PLACES
- BILLETS, SCREWS, IN BOTH ALUMINUM, MASONRY,
- VARIOUS MATERIALS IN IDENTIFICATION
- DESCRIBE TO THE EXTENT OF THE DRAWING

PURDUE UNIVERSITY CAD W LAFAYETTE INDIANA	
RF END CAP THIRD SIZE	
SERIAL NO.	DATE NO.
A FRANK BELLUREAU	AC140509B 0
PRINTED 1 OF 1	

<p style="text-align: center;">Mounting 0.063 on center Mounting 0.254 to top surface</p>																								
<p style="text-align: center;">Mount RIT + PLACES TOP SIDE</p>																								
<p>3. PCB ASSEMBLY NOTES:</p> <ul style="list-style-type: none"> - NO SOLDERING. - 1 LAYER - CERAMIC WAVELET: 3.00 - INTERNAL GND FLICK FOR VLSI WAVE PLATE POSITION. MUST MATCH FAB. - USE 1-POLE ANTENNA PROBE IN MOLD. NO LEAD CANTILEVER. - BOARD PLATES THAT USE THE TRACER LINE MUST BE DESIGNED. - TWO PLATES ARE ACTIVELY COUPLED AND CAN NOT BE SEPARATED. - ANTENNAES ARE COUPLED AND CAN NOT BE SEPARATED. - BACK POSITION OF RIT RIVER IS TYPICAL. - PLACES POSITION AS DIRECTIONAL. - DUE TO THE ELECTROOL TESTED 																								
<table border="1"> <thead> <tr> <th>SYN</th> <th>DIAM</th> <th>TOL</th> <th>CHART</th> <th>NOTE</th> </tr> </thead> <tbody> <tr> <td>S</td> <td>6.000</td> <td></td> <td>1</td> <td>RAT-PLATES</td> </tr> <tr> <td>*</td> <td>4.750</td> <td></td> <td></td> <td>ROT-PLATES</td> </tr> <tr> <td>TOTAL</td> <td></td> <td></td> <td>8</td> <td></td> </tr> </tbody> </table>					SYN	DIAM	TOL	CHART	NOTE	S	6.000		1	RAT-PLATES	*	4.750			ROT-PLATES	TOTAL			8	
SYN	DIAM	TOL	CHART	NOTE																				
S	6.000		1	RAT-PLATES																				
*	4.750			ROT-PLATES																				
TOTAL			8																					
<p>PURDUE UNIVERSITY CAD W LAFAYETTE INDIANA</p> <p>THIRD SIZE RIT HOLDER PCB</p> <table border="1"> <tr> <td>DESIGN BY: A</td> <td>DATE REV. FRANK JULIUREAU</td> <td>REV. A0140509D</td> <td>REV. 0</td> <td>PRINTED 1 OF 1</td> </tr> </table>					DESIGN BY: A	DATE REV. FRANK JULIUREAU	REV. A0140509D	REV. 0	PRINTED 1 OF 1															
DESIGN BY: A	DATE REV. FRANK JULIUREAU	REV. A0140509D	REV. 0	PRINTED 1 OF 1																				

VITA

VITA

Paul Isaac Hendricks graduated from Summerville Union High School (Tuolumne, CA) in 1996. During this time he met and fell in love with his future wife Krista Anne Gold. Although he never excelled at Spanish, it could be argued that the distraction of discussing afterschool and weekend plans with Krista was a more valuable investment of his time. He graduated from the University of California, Santa Cruz (Santa Cruz, CA) in 2001 with a double major in Biochemistry and Molecular Biology and Business Management, Economics. In addition to regular course work Paul served as a residential advisor in the Porter College dormitories and spent three years conducting research toward the total organic synthesis of Diazonamide A under the supervision of Dr. Nhu-Y Stessman (now professor and CSUS) and Prof. Joseph P. Konopelski.

Following graduation from UCSC, Paul began work for Thermo Fisher Scientific (San Jose, CA) as a test engineer for mass spectrometer instrument control software. At Thermo Paul became fascinated by the science and engineering necessary to trap small numbers of gas-phase ions and subsequently complete mass measurements. Ultimately this fascination, with strong motivation from his colleagues, led him to Purdue University (West Lafayette, IN) where he completed his Ph.D. in Chemistry (2013) with Professor R. Graham Cooks. His research included development of field portable mass spectrometers

capable of *in-situ* analysis and strategies for the fabrication and operation of miniaturized ion traps and ion trap arrays.